Dissertation

Cell polarity & sterol-rich membrane domains in fission yeast

Tatyana Makushok

Supervisor: Prof. Dr. Damian Brunner

Ruperto - Carola University of Heidelberg, Germany

2013

Dissertation

submitted to the

Combined Faculties for the Natural Sciences and for Mathematics

of the Ruperto-Carola University of Heidelberg, Germany

for the degree of

Doctor of Natural Sciences

presented by

Tatyana Makushok, M.Sc. in Fundamental and Applied Physics

born in Minsk, Belarus

Oral examination:

Cell polarity & sterol-rich membrane domains in fission yeast

Referees: Dr. François Nédélec

Prof. Dr. Ulrich Schwarz

Summary

Fission yeast (*Schizosaccharomyces pombe*) is a model organism widely used for studying cell polarization. Polarization in fission yeast involves cytoskeleton-mediated positioning of growth sites. A complex consisting of the polarity factors Tea1 and Tea4 is transported on microtubules to the cell end regions. Tea4 interacts with the actin polymerization promoter For3. Selective activation of For3 in the cell end regions makes them rich in F-actin that contributes to localized cell growth. In this study, sterol-rich membrane (SRM) domains present at the growth sites are introduced as a new element in this picture, and their role in cell polarity establishment is analyzed. Since SRMs are absent from the plasma membrane in starved cells, imaging of cells recovering from starvation using the novel SRM marker GFP-Tna1 was performed to follow SRM domain formation *de novo*. Automated image analysis software was developed to analyze and correlate cell growth and SRM dynamics with an unprecedented level of precision. The results show that properly formed SRM domains are essential for fission yeast growth. SRMs, and with them the growth machinery, have to polarize before cell growth initiation. F-actin is required for selective removal of SRM domains in the cell middle region, and thus for polarizing SRMs. Fast removal of SRM domains in the cell middle region is not due to increased endocytic activity (mediated by F-actin). Tea1 controls the localization of polarized growth *via* Tea4 by affecting the positioning of SRM domains. Tea1 and Tea4 are essential for the stability of the SRM domains not associated with active growth sites. The importance of the microtubule cytoskeleton for the stability of SRM positioning stems from its role in the transport of the Tea1-Tea4 complex to the cell end regions. *Tea1*Δ and *tea4*Δ cells, known to grow monopolarly, grow faster at individual cell ends than wild type cells. Tea1 and Tea4 are required for proper timing of growth initiation. The proteins associated with the actin cytoskeleton, For3 and its activator Bud6, are important for the stability of SRM domains at both cell ends. For3 is also important for growth speed stabilization. In conclusion, a complex feedback loop links SRMs and cell growth. SRMs are essential for the polarization of the growth machinery, probably serving as platforms for its recruitment. The growth machinery, in turn, seems to stabilize SRM domains at sites that have initiated growth. Importantly, the results of this study show that SRMs are a critical factor in *de novo* cell polarization, and not merely a player in its maintenance, as was previously thought.

Zusammenfassung

Die Spalthefe *Schizosaccharomyces pombe* ist ein Modellorganismus in der Erforschung der Zellpolarisation. Die zytoskelettgesteuerte Positionierung der Wachstumsregionen spielt eine entscheidende Rolle bei der Polarisierung der Hefezellen. Dabei wird ein Komplex, bestehend aus den Polarisationsfaktoren Tea1 und Tea4, entlang der Mikrotubuli zu den zwei entgegengesetzten Zellenden transportiert. Tea4 interagiert dort mit For3, einem Faktor der die Aktinpolymerisation beschleunigt. Die selektive Aktivierung von For3 an den Zellenden führt zur Anreicherung von F-Aktin in diesen Regionen, was zum lokalisierten Zellwachstum führt. In dieser Studie untersuchen wir die Rolle von sterolreichen Membranregionen (SRM) bei der Polarisierung der Hefezelle und zeigen die wichtige Bedeutung dieser Regionen.

SRMs sind abwesend in Hefezellen, die unter Nährstoffmangel leiden. Neue SRMs werden gebildet sobald man den Zellen Nährstoffe zuführt. Mittels GFP-Tna1, einem neuen SRM-Marker, beobachteten wir die Neubildung der SRMs. Neu entwickelte Bildanalysesoftware erlaubt uns Zellwachstum und SRM-Neubildung mit bisher unerreichter Präzision zu analysieren und miteinander zu Korrelieren. Wir konnten zeigen, dass die korrekte Bildung der SRMs und ihre Lokalisierung an den Zellpolen und damit einhergehend die Lokalisierung der Wachstumsmaschinerie an den Zellpolen essentiell für die Initiierung des Zellwachstums sind. F-Aktin spielt eine wichtige Rolle beim Transport der SRMs von der Zellmitte zum Zellpol. Der schnelle Transport der SRMs ist jedoch nicht abhängig von der gesteigerten, F-Aktin initiierten endozytotischen Aktivität. Tea1 und Tea4 sind essentiell für die Positionierung der SRMs und somit die Polarisierung der Hefezelle. Tea4 koppelt Tea1 mit den SRMs. Da der Tea1/Tea4-Komplex mittels der Microtubuli zum Zellpol transportiert wird, hat das Microtubulizytoskelett eine entscheidende Rolle bei der stabilen Positionierung der SRMs. *Tea1*Δ und *tea4*Δ wachsen monopolar. Sie wachsen schneller an dem einen Ende als Wildtypzellen. Tea1 und Tea4 sind notwendig für den korrekten Zeitpunkt der Wachstumsinitiierung. In *for3*Δ Zellen sind sowohl das Wachstumsgeschwindigkeit als auch die Lokalisierung der SRMs instabil. Das F-Aktin assoziierte Protein For3 und dessen Aktivator Bud6 sind essentiell für die Stabilisierung der SRMs an beiden Zellpolen.

Zusammenfassend lässt sich sagen, dass SRMs und Zellwachstum durch eine komplexe Rückkopplungsschleife verbunden sind. SRMs sind essentiell für die Pollokalisierung der Wachstumsmaschinerie. Es ist anzunehmen, dass sie als Plattform dienen, auf der sich die Maschinerie aufbaut. Die Wachstumsmaschinerie auf der anderen Seite lokalisiert die SRM an Wachstumsstellen stabil. Wir können in dieser Studie erstmals zeigen, dass die SRMs eine kritische Rolle bei der Neubildung der Zellpolarität spielen und nicht nur bei deren Stabilisierung wie bislang angenommen.

To my parents,

my grandmother, and Aleksey,

with all my love

Acknowledgements

I would like to express my deep gratitude to Damian Brunner, my PhD supervisor, for many things. Thank you for accepting me to your great lab. The beautiful day when, set against the background of the magnificent Heidelberg forest covered with snow, I received the envelope saying that I can join the lab, will forever remain in the collection of the happiest days of my life. Thank you for being such an inspirational group leader, for making my eyes shine with excitement during scientific discussions. Thank you for directing my research activity and for teaching me to think like a biologist. Thank you for your patience in bridging the interdisciplinary gap stemming from my background in physics. Thank you for all the time and effort you invested into ameliorating this thesis. Thank you for your kindness and patience in the times when I was questioning myself and the path I was taking. Your wise advice has been most helpful. Thank you for bringing together the amazing group of people that formed Brunner Lab, and for maintaining its great atmosphere. Thank you for the evening spherical Lindt chocolates. Thank you for the great time we all spent together outside the lab. And for that very special badminton match in Switzerland :-) And for so much more!

I am very grateful to the members of my Thesis Advisory Committee: François Nédélec, Jan Ellenberg, Ulrich Schwarz, and Matthieu Piel. Thank you for your involvement in my work over the years. Your advice was very important both for the progress of my research projects and in a broader sense.

I am very grateful to François Nédélec and Dietrich Foethke for our collaboration. It was a very positive experience. François, thank you for all the scientific discussions we had. More globally, thank you for changing my life by organizing the visit to EMBL for the IPB Master program, during which I fell in love with EMBL. Also, thank you for the inspiring lectures you gave us in Paris that year.

I am very grateful to Marko Kaksonen for his kind help during my final months at EMBL. Thank you for all the discussions we had, starting with the great practical you organized during the predoc course.

I am very grateful to Paulo Alves for our close collaboration and for being such a great friend. Our collaboration, that started off as a small practical project designed for students, gave me so much on so many levels. Thank you for the many long

discussions we had about the project, for sharing your knowledge and scientific experience with me. Our interaction was one of the most enjoyable parts of working on this project, with the magic of new ideas being born during discussions. And thank you for being such a great person to talk to (and to row with :-)!

I am very grateful to the people at the Advanced Light Microscopy Facility, and in particular to Yury Belyaev, Kota Miura, Christian Tischer, Stefan Terjung, Arne Seitz, for their amazing work taking care of a variety of microscopes and image analysis software, for organizing great courses, for always being available to help people out, and for most useful discussions. I am also grateful to image analysis *aficionados* at EMBL, for sharing this passion.

I am very grateful to all members of the Brunner Lab I had the chance of interacting with: Andreia, Aynur, Camille, Chieze, Gökçe, Imola, Jérôme, Linda, Lindsay, Mariam, Mikhail, Nadia, Nestor, Paulo, Steve, Tanja, and also to Boryana, Helio, Ioannis, Johanna, and John. Thanks to you, my years at EMBL were years of happiness. I was excited to come to the lab even on the first day after holidays. You were so kindly teaching me lab techniques and reasoning in biology, you advised me on my projects. And, above all, you are amazing friends! I admired each of you, enjoyed our discussions so much, learned so much on the personal level from you, and will never forget your kindness and the fun we had together!

I am very grateful to Hella Baumann for translating the summary of this thesis into German.

I am very grateful to all the amazing people I met at EMBL and had the honor of calling my friends. Thank you, Iryna, for sharing so many experiences and thoughts during our years at EMBL. Thank you for your support and advice, starting from the very beginning: the selection week. Thank you for our laughs at the EMBL cafeteria in the evenings (you prolonged my life, for sure!), for the great parties and trips. Many thanks to all members of the "Russian community" at EMBL: I never felt lonely in Heidelberg thanks to you. Thank you, Vladimir, for sharing your wisdom and always helping me with great advice. Thank you to all the people who shared my passion for rowing, diving, and badminton. It was so great sharing emotions with you! Many thanks to Chaitanya, France, Xavier, Claudia, Anton, Anne-Marie, Shira, Tony, Karla, Hella, Manu, Maria, Sergey, Morgane, Sergey, Fargol, George, Marianne: spending time with you made my life so much richer! Thank you to the people who were working in the neighboring labs, for making me

smile when I met them in the labyrinth of EMBL corridors. Thank you to the great community of the Cell Biology and Biophysics Unit and of EMBL in general, for the vibrant and exciting scientific environment. Thank you to the nice and highly professional people at the cafeteria, in administration, in IT support, to the media kitchen ladies, to the cleaning ladies, to the night guards, for the efficiency of their work and for their unforgettable smiles.

I am very grateful to the amazing scientists I had the pleasure of working with during the years before coming to EMBL. Thank you, Michel Bornens, for giving the exciting talk to IPB students that sparked my interest in the particular set of questions in biology that defined my path in science. Thank you for allowing me to join your lab and work on a project I became passionate about. Thank you, Matthieu Piel, for having been such a great supervisor. I very much enjoyed working with you, discussing ideas and results, and in general talking to you. Thank you for supporting me in many situations. The support from Institut Curie that you arranged was essential for me. Thank you for crossing the border to come to my TAC meetings, for your advice and support. I am also grateful to all the great scientists that were working on the 4th floor of the Institut Curie building at rue Lhomond, for the great atmosphere and for their kindness, and in particular to Anne Paoletti, for introducing me to fission yeast. I am very grateful to Yong Chen for allowing me to join the magic world of microfluidics.

I am very grateful to Phong Tran for giving me the chance to work with fission yeast and thus for developing my tenderness for this cute model organism. Thank you for the thrilling trip to your lab in Philadelphia that allowed me to see how "the opposite side of the planet" looked and how science was done there. Thank you for your contagious passion for science. Thank you for demonstrating me the result- and publication-oriented approach to experimental biology. Thank you for your support on many occasions and for your wise advice. And thank you for organizing great out-of-the-lab activities, and particularly for that open-air concert+dancing on a warm Philadelphia evening. I am very grateful to all members of Tran Lab for the great time we had together. Thank you, Courtney Terenna, for being such a great person to work with and for your patience during the time when I was getting used to the American language :-)

I am very grateful to Didier Chatenay for letting me join his lab to work on my first biology project. Thank you, Luis Alvarez and Philippe Thomen, for having been my great supervisors and friends. Thank you for teaching me my first lessons of

experimental biology and for showing me its beauty. Observing the movement of *E.coli* cells infected with GFP-labeled phages live under the microscope fascinated me to the point that I devoted the following years of my life to studying dynamic processes in cells. Thank you to all members of Chatenay Lab for the great atmosphere. Thank you, Jean-Bernard Zuber, for your active participation in the progress of my scientific career and for your help introducing me to various great scientists working in the best scientific institutions of Paris. These meetings allowed me to figure out the direction I wanted to follow and to join Chatenay Lab.

I am very grateful to Vitali Parkhutik, may he rest in peace. For allowing me to join his lab with the beautiful view on the Alcoy rocks. For introducing me to experimental lab work. For his professionalism in science. For sharing his wisdom on various topics. For teaching me the lesson of extraordinary personal strength and endurance. During the time I spent in his lab, I discovered something I previously thought impossible: that I could dare to follow the path of scientific research, with its beauty, numerous disappointments, and the rare but priceless moments of eureka. Thank you, Ester and Emilio, for having been great lab mates and for helping me in my acquaintance with Spanish culture. I am very grateful to Didier Schmaus for attentively and kindly mentoring me during my stay in Spain and afterwards.

I am very grateful to all the great teachers and professors I had the honor of meeting during my life, for sharing their knowledge and for influencing the development of my personality. Thank you, Valentina Fedorovna Skorobogatova, for your professionalism and your passion for mathematics, for being a person of utmost integrity, and for your priceless friendship. I am grateful to all the teachers of the Lyceum of BSU for sharing not only their knowledge, but also their souls with us. Thank you for creating the unique environment that I was so happy in and that profoundly influenced me. I am very grateful to all the professors of BSU. Thank you, Natalia Grigorjevna Abrashina-Zhadaeva, for the excellent teaching and for having been an inspiring role model of a woman in science for me. I am very grateful to Sergey Nikolaevich Cherenkevich, whose orientation talk showed me the irresistible fascination of biophysics and thus profoundly influenced my scientific interests. I am also grateful to Pavel Bulay, for his patience and for inciting me to radically change my life. I am grateful to all the professors who taught at Paris 7-Denis Diderot and who broadened my horizons. I am also grateful to all the people who administered and taught at the IPB Master program, including Luc Valentin,

Roland Mastrippolito, Benoît Ladoux, Michel Vervoort, Emmanuel Fort, for their professionalism and extraordinary efforts to prepare us for scientific careers.

I am very grateful to Mathilde Bourdat for being such a great friend of the family and for changing the way of thinking and the lives of my parents and myself. Thank you, Mathilde, Jean-Pierre, Kevin, and Corentin, for your hospitality during my first years in France. Your help and support were absolutely essential for the most significant transition of my life. I am very grateful to Denis and Hélène Blech for their friendship, hospitality, warmth of heart, help, and support. Each visit to Anfernel is engraved in my heart.

I am very grateful to all my friends, for giving the essence and color to my life. My dear friends, you know who you are, and I hope that you know how much you matter to me and how very often I think about each of you. Thank you, Sasha Marchenko, for being a dearest friend over the years, for sharing some of the most memorable moments of my life, for your help on numerous occasions, including during the submission of this thesis, and for being such a great father to Luchik :-)

I am infinitely grateful to all members of my family for their love, support, and for believing in me. In particular, I am infinitely grateful to my grandmother, for everything she did for me over the years. Thank you, Babushka, for your great personality, for your sense of humor, your liveliness, for being a passionate traveler, for your patience when dealing with me, for the tasty produce from your garden, for your great cuisine, for the great memories of the time we spent together, for your kind support during the writing of this thesis, and for being a great friend to me over the years.

I am infinitely grateful to my grandfathers, for inspiring me to move forward by the example of their extraordinary academic careers.

I am infinitely grateful to my parents. Thank you for giving me the gift of life, for my perfect childhood, for our great trips, for sharing your wisdom with me. Thank you for implanting the interest in science into me from the early age, for example, by telling me stories about the perfectly black body in front of the campfire. :-) Thank you for your help during each stage of my life, for giving me all the opportunities I had, and for always believing in me.

I am infinitely grateful to Aleksey for being the source of my happiness every day, for his open-mindedness, sense of humor, various talents, for being such an inspiring

person. Thank you for understanding me like no one else and for the amazing amount of support you gave me. Many thanks for all the time and effort you invested into the proofreading and printing of this thesis.

I am infinitely grateful to Sushka, one of the most loved cats on the planet, for her unconditional love and tenderness.

Table of contents

Abbreviations

DMSO	Dimethyl sulfoxide
GAP	GTPase-activating protein
GEF	Guanine exchange factor
GFP	Green fluorescent protein
KW	Ketoconazole washout
MARS	Multivariate adaptive regression splines
MBC	Methyl-2-benzimidazolecarbamate
MTOC	Microtubule-organizing center
NETO	New end take-off
RCP1	Rate change point 1
RCP2	Rate change point 2
RS	Release from starvation
SIN	Septation initiation network
SPB	Spindle pole body
SRM	Sterol-rich membrane
γ-TuC	γ-tubulin complex
+TIP	Microtubule plus end tracking protein

Pour connaître la rose, quelqu'un emploie la géométrie

et un autre emploie le papillon.

Paul Claudel

1 Introduction

The introduction will start with a general overview of the topic of cell polarity. Fission yeast, the organism used in this study, will then be introduced. The organization of the microtubule and actin cytoskeletons, which are important for the establishment and maintenance of fission yeast polarity, will be considered. The focus will then be shifted to the mechanisms of cell polarity control. Finally, the current knowledge on the role of specific plasma membrane regions for cell polarity will be presented.

1.1 Cell polarity

Cell polarity is the basic property of all living cells: archaea, bacteria, and eukaryotes. It manifests itself in cell shape asymmetry and the inhomogeneity of protein distribution within individual cells. Correctly established polarity is essential for cell functioning, performing particular cell functions within a tissue, and correct cell division. Thus, a detailed understanding of the cell polarization process is important both from the perspective of fundamental science and for medical applications. Classic examples of highly polarized cells are: migrating cells, neurons, and epithelial cells (Siegrist & Doe, 2007).

The mechanisms of cell polarity establishment and maintenance are studied in a range of model organisms. Fascinating questions are being addressed, such as what external and internal chemical and mechanical signals govern the process of polarization; what common principles underlie the mechanisms of establishing cell polarity in response to those signals; what is the relationship between the established cell polarity and the function of a particular cell type (Nelson, 2003).

Correct functioning of three general molecular mechanisms is required for establishing protein polarization (Mellman & Nelson, 2008). Proteins are sorted within a cell, and some of them are then transported to special domains within the plasma membrane. Intracellular signaling complexes define these domains. The positioning of these complexes can, in turn, be influenced by a variety of external signals of various types. Firstly, cells can polarize under the influence of asymmetric concentration of external molecular signals, for example, in the case of mating budding yeast cells (Hawkins et al., 2009). Secondly, forces acting on a cell can

induce its polarization, for example, in the case of mammalian cells grown on micropatterned substrates used to model tension exerted on a cell within cell tissue (Fink et al., 2011; Thery & Bornens, 2006). Thirdly, cell polarity can be inherited from the mother cell in the process of cell division. An example of that is the inheritance of the organelle centriole that plays an important role in cell polarity in mammalian cells (Bornens, 2008). Finally, there is spontaneous cell polarization. It can be observed when stochastic variations of protein concentrations are amplified on the cellular level with the help of positive feedback loops, combined with the action of global inhibitors (Gierer & Meinhardt, 1972; Meinhardt & Gierer, 2000; Wedlich-Soldner & Li, 2003).

1.2 Fission yeast

Fission yeast (*Schizosaccharomyces pombe*) was first described in 1893 by P. Lindner, who isolated it from East African millet beer. *S.pombe* was introduced as a model organism in the 1950s by Urs Leupold and Murdoch Mitchison. In 2001, the Nobel Prize in Physiology or Medicine was awarded to Paul Nurse, the prominent researcher in the field of genetics and cell cycle of fission yeast, together with Lee Hartwell and Tim Hunt, for their work on cell cycle regulation (Egel, 2004).

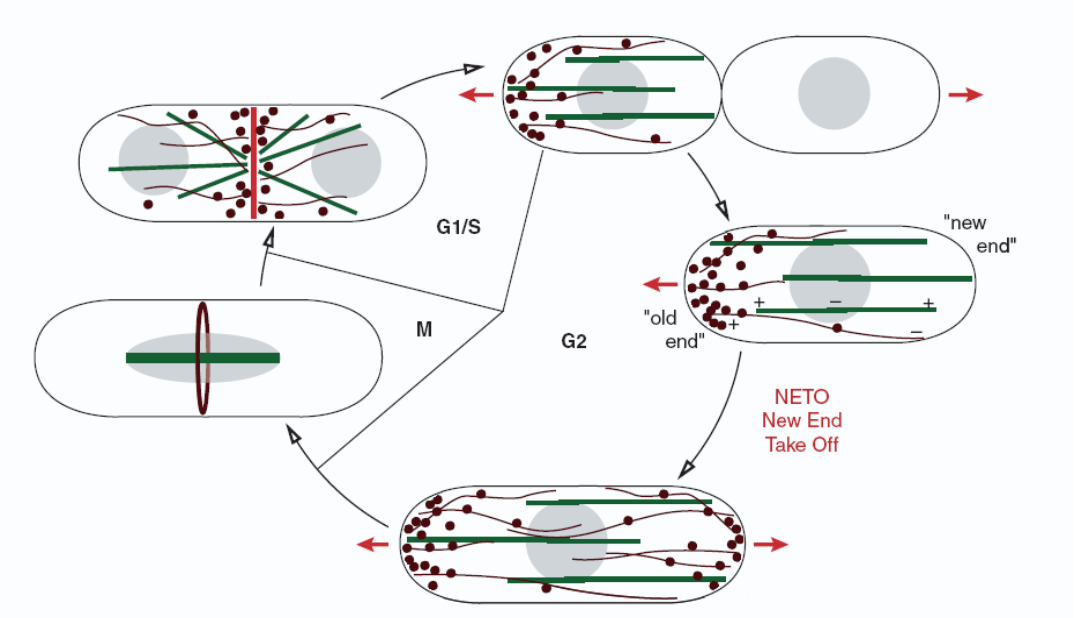

Figure 1.1. Schematic representation of the fission yeast cell cycle. Red line and arrows – location and direction of active cell growth. Green lines – microtubules. Dark red lines – F-actin filaments. Dark red dots – actin patches. Figure adapted from (Chang & Martin, 2009).

Fission yeast is one of the model organisms that has been widely used for the study of cell polarity (Hayles & Nurse, 2001). *S.pombe* cells have spherocylinder-like shape maintained by their bilayered cell wall. The cytoskeleton of fission yeast is mainly composed of actin and microtubule networks. Microtubules are organized in bundles preferentially oriented parallel to the main cell axis (**Figure 1.1**). Filamentous actin is organized into actin patches and actin cables. Fission yeast divides by medial fission. After cytokinesis, the two daughter cells initiate growth from the old ends inherited from the mother cell. In the G2 phase of the cell cycle, new end take-off (NETO) occurs. After this event, the cells grow at both cell ends (bipolar growth) until mitosis (phase M) (Mitchison & Nurse, 1985).

1.3 Actin cytoskeleton of fission yeast

1.3.1 Actin cytoskeleton organization

Actin is present in eukaryotes in two forms: monomeric (globular, G-actin) and polymerized (filamentous, F-actin). Due to the asymmetry in the structure of G-actin, each actin filament is oriented and has a barbed end and a pointed end (Holmes et al., 1990). F-actin is organized in two distinct ways in *S.pombe*. Firstly, parallel (bundled) organization of actin filaments is found in actin cables. Secondly, a network of branching F-actin is present within actin patches (Pelham & Chang, 2001). The localization of actin structures within cells is associated with the sites of active growth (**Figure 1.1**) (Marks, Hagan & Hyams, 1986). Actin network is involved in endocytosis (Section 1.3.4) and cell growth. The latter is also mediated by actin cables that serve as tracks for the delivery of the material required for growth to the cell ends (Lo Presti & Martin, 2011; Motegi, Arai & Mabuchi, 2001; Win et al., 2001).

1.3.2 Localization and functions of For3

The actin network is highly dynamic. A range of factors controlling actin polymerization dynamics is present in fission yeast, including the protein family of formins. Members of this protein family are known to play a role in actin polymerization and regulation of both actin and microtubule cytoskeletons. There are three formins in fission yeast: Cdc12, Fus1, and For3. Cdc12 acts during

cytokinesis (Section 1.5.4). Fus1 is involved in cell fusion and nuclear migration during mating, and does not seem to play a role in cell polarity during vegetative growth (Petersen et al., 1995).

For3 is involved in several cell processes. Firstly, it is required for the formation of actin cables: in cells lacking the *for3* gene (*for3*Δ cells) actin cables are absent in interphase. Instead, abnormal short and curled F-actin structures are observed in most *for3*Δ cells (Nakano et al., 2002). This leads to the mislocalization of the actin patches and of the type V myosin Myo52. Cell morphology of *for3*Δ cells is relatively normal. This indicates that neither actin cables nor the correct localization of actin patches is essential for maintaining cell polarity. Secondly, For3 is required for symmetric cell divisions. Most *for3*Δ cells have an abnormal pattern of cell growth: after division, one daughter cell starts to grow monopolarly (at one cell end), and the other – bipolarly (**Figure 1.2**). The cell growing bipolarly is the cell that inherited the birth scar from the mother cell (from the previous cell division). Thirdly, For3 plays a role in microtubule organization. The number of microtubule bundles is higher in *for3*Δ than in wild type cells (Feierbach & Chang, 2001). Overexpression of For3, on the other hand, leads to the thickening of microtubule bundles, although the effect is probably indirect (Nakano et al., 2002).

For3 is found in small dots that initially appear at the cell end cortex. The N-terminal region of For3 is responsible for its localization there (Nakano et al., 2002). For3 dots then move along the actin cables, away from the plasma membrane, at the speed of 0.3 μm/s. The polymerization of actin within the actin cables and For3 binding to actin (through its FH2 domain) are required for the movement of For3 dots. The current model describing actin cable internal dynamics is the following. After For3 activation at a cell end region, For3 initiates the polymerization of an actin filament, which is then transported together with For3 along the existing actin cable (Martin & Chang, 2006). As the result of this mode of actin polymerization, actin cables contain actin filaments that have their barbed ends oriented towards the cell ends. During cell division, For3 is localized to the site of cytokinesis. It requires F-actin for correct localization (Feierbach & Chang, 2001).

Several proteins bind to For3 and regulate its activity. One of them is profilin, it promotes For3 activity. Others are Pob1 and the Rho-GTPase Rho3; both are important for For3 localization to the cell ends (Nakano et al., 2002; Rincon et al., 2009). Also, there is the protein Rax2 that controls For3 localization during vegetative growth (Choi, Lee & Song, 2006). For3 is randomly distributed at the

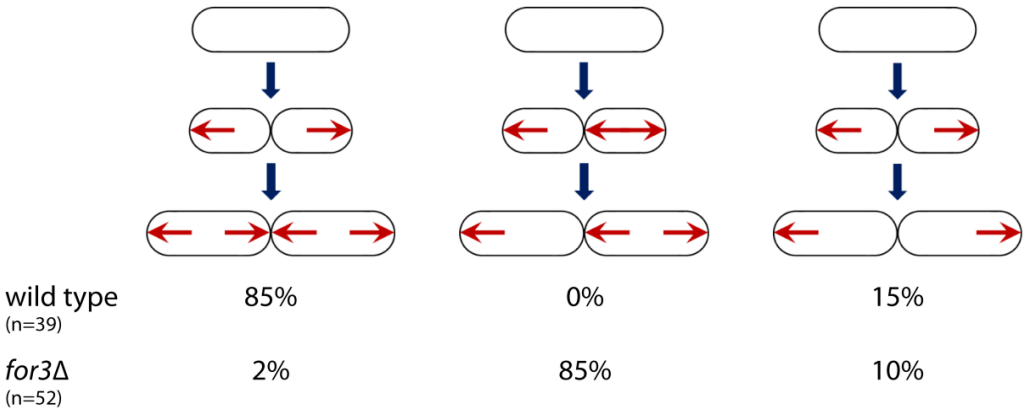

Figure 1.2. Growth patterns of wild type and *for3*Δ cells after cell division. Figure adapted from (Feierbach & Chang, 2001).

cell cortex in *rax2*Δ cells, and these cells lack actin cables. The rate of cell growth is reduced in *rax2*Δ cells. Rax2 is localized at the cell cortex at the growing cell ends only. During cytokinesis, Rax2 is present at the septum. There are two predicted transmembrane domains in Rax2, and they might be involved in its localization. The presence of both actin and microtubule cytoskeletons is required for the correct localization of Rax2.

1.3.3 Localization and functions of Bud6

Bud6 is the *S.pombe* homolog of the *S.cerevisiae* actin-binding protein Bud6/Aip3. The cell polarity factor Bud6/Aip3 is involved in the control of *S.cerevisiae* polarized growth *via* its role in the activation of one of *S.cerevisiae* formin proteins, Bni1, in the growing bud (Moseley & Goode, 2005). *S.pombe* Bud6 is localized to the cell end regions of the cortex during interphase. This localization pattern requires the presence of F-actin structures, but not of microtubules. During cytokinesis, Bud6 is localized to the actomyosin ring. *Bud6*Δ cells have a NETO defect: growth at the new end is not initiated properly. In the *cdc11* genetic background, these cells adopt branching or bent morphology (*cdc11* background is characterized by the accumulation of multiple nuclei due to defective cytokinesis) (Glynn et al., 2001).

Bud6 binds to the formin For3 when the latter is localized in the cell end regions, but does not move along actin cables with For3. The effect of Bud6 on For3 is the promotion of For3 activity (Martin & Chang, 2006). The mechanism of For3 activation by Bud6 consists in the reduction of For3 autoinhibition (Martin et al., 2007). Both localization and activity of For3 is regulated *via* the autoinhibitory

mechanism that is common for formins. An important role in this mechanism is played by the interaction of the DAD-like sequence located close to the C-terminus of the formin and the DID-like sequence located at its N-terminus. Bud6 acts in concert with the Rho GTPase Cdc42 in controlling the level of For3 activity. Bud6 binds at the DAD-like sequence in the C-terminal region of For3, and Cdc42 binds in the N-terminal region of For3. These protein interactions are required for counteracting For3 autoinhibition, and hence for its correct localization and proper level of activity. *Bud6*Δ cells with a mutation in the DAD-like region of For3 do not have the NETO defect observed in *bud6*Δ cells without this mutation. The counteraction of For3 autoinhibition by Cdc42 is facilitated by the protein Pob1 (Rincon et al., 2009) that was also shown to be involved in cell morphogenesis *via* its control of exocytosis (Nakano et al., 2011).

1.3.4 Endocytosis and exocytosis

The actin cytoskeleton is essential for cell growth, as it is involved in the transport of new cell wall material to the growth sites. Endocytosis and exocytosis are particularly important in this process. Endocytosis is the process by which cells engulf molecules from the region outside the plasma membrane. This process is also essential for recycling the plasma membrane and its associated proteins. The sequence of events leading to the internalization of an endocytic vesicle in fission yeast has a precise timing (Sirotkin et al., 2010). Initially, clathrin molecules organize at the plasma membrane to form a hemisphere-like invagination (**Figure 1.3**). Then, sequentially, the endocytic adaptor proteins End4 and Pan1, Arp2/3 complex activators Wsp1 and Myo1, and finally the Arp2/3 complex itself become recruited to this site. Arp2/3 complex triggers actin polymerization that generates the force for inward movement of the vesicle. The actin filaments are capped with the capping proteins and cross-linked with fimbrin. When the vesicle becomes internalized, the aforementioned actin patch components start leaving the vesicle, while coronin is being recruited there. Mathematical modeling of the endocytic process was performed (Berro, Sirotkin & Pollard, 2010). It showed that the branched network of actin filaments formed at the actin patch during the polymerization step can be disassembled within the time range observed experimentally only if the actin filaments are severed into fragments, and not simply depolymerized at their pointed ends. Electron microscopy data showed that the subsequent transport of endocytic vesicles does not seem to involve microtubules (Hoog et al., 2007).

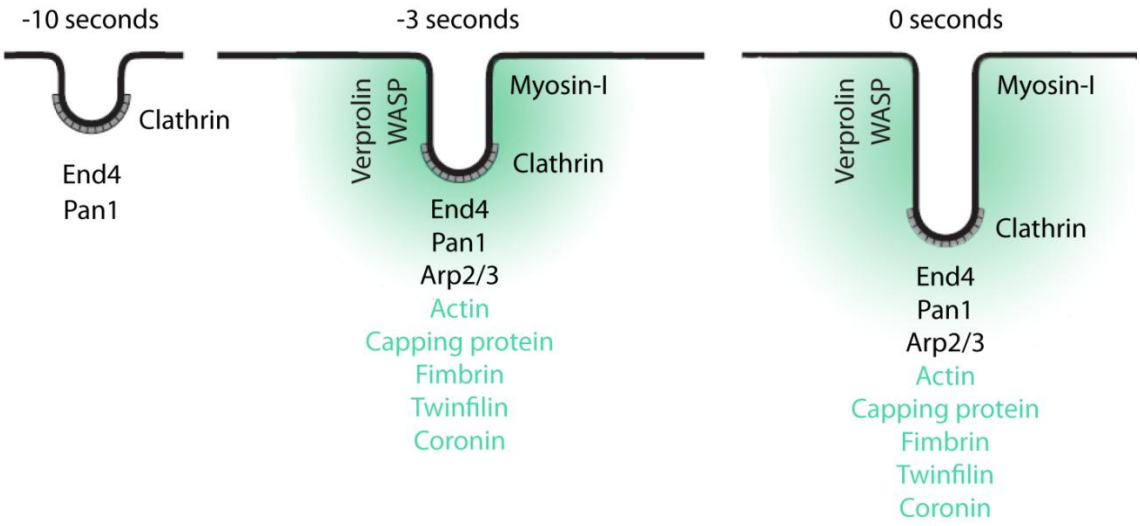

Figure 1.3. Schematic representation of the sequence of events leading to the internalization of an endocytic vesicle in fission yeast. Green zone – region of localization of the actin network and of the proteins listed in green. Figure adapted from (Sirotkin et al., 2010).

Polarized exocytosis is the process consisting of secretory vesicle transport to a particular region of the plasma membrane that is defined by landmark proteins, and subsequent vesicle fusion there. Polarized exocytosis is required for correct cell morphogenesis. In fission yeast, there are two independent morphogenetic pathways: actin cable-dependent and exocyst-dependent (Bendezu & Martin, 2011; Nakano et al., 2011; Snaith et al., 2011). Both pathways are downstream of Cdc42 and may be coupled by Pob1. Polarized growth takes place (although inefficiently) when either of the two pathways is perturbed, but does not if both pathways are not functional. Actin cables act as tracks for the transport of the secretory vesicles. For3 is required for actin cable formation, and Myo52 – for the transport of the vesicles. The eight-subunit protein complex exocyst is required for tethering of exocytic vesicles at the plasma membrane, which facilitates exocytic fusion (He & Guo, 2009).

1.4 Microtubule cytoskeleton of fission yeast

Besides their essential role in forming the mitotic spindle, fission yeast microtubules and their associated proteins are involved in cell polarity control, especially at cell cycle transition points, such as NETO (Brunner & Nurse, 2000b; Sawin & Nurse, 1998). More precisely, microtubules are required for the positioning of growth zones, but not for cell growth *per se* (Siegrist & Doe, 2007).

1.4.1 Microtubule cytoskeleton organization

Fission yeast cells have two genes encoding α-tubulin: *atb2* and *nda2*, and one gene encoding β-tubulin: *nda3* (Yanagida, 1987). Microtubules form by polymerization of α-tubulin and β-tubulin heterodimers into protofilaments. The majority of microtubules *in vivo* consist of 13 protofilaments forming a tube 25 nm in diameter (Downing & Nogales, 1998). Microtubules are polarized and have a plus and a minus end. This allows directional movement of molecular motors along microtubules. A very important property of microtubules is their capacity to undergo dynamic instability: they often switch between growing and shrinking modes (Howard & Hyman, 2009). The dynamic nature of microtubules allows them to exert pushing or pulling forces on any encountered obstacle, such as the plasma membrane. These forces are essential for intracellular positioning of various structures, such as the nucleus or mitotic spindle (Dogterom et al., 2005). *In vivo* microtubules act with a large set of associated molecules, such as molecular motors and cross-linking proteins. The interaction between microtubules and diverse microtubule-associated proteins leads to the establishment of self-organizing microtubule networks (Karsenti, Nedelec & Surrey, 2006).

For many years, immunofixation was the method of choice to study microtubule organization in fission yeast, and a substantial body of knowledge was produced using this method (Hagan, 1998). Then, the field was revolutionized by the use of GFP constructs that allowed studying the dynamics of microtubules and of a whole range of microtubule-associated proteins. After the first report on the use of GFP constructs in fission yeast (Nabeshima, Saitoh & Yanagida, 1997), this technology was used to study microtubule dynamics during meiosis (Ding et al., 1998), during interphase, and in mitosis (Tran et al., 1999). GFP labeling of microtubules and microtubule-associated proteins soon became a widely used and well-developed technique (Tran, Paoletti & Chang, 2004).

Microtubules in fission yeast are organized in bundles, with the plus ends of individual microtubules oriented towards the cell ends, and the minus end regions forming an overlap at the cell nucleus. Due to the constraints imposed by the cell shape, microtubule bundles are mainly oriented along the cell axis. Microtubule plus ends in fission yeast are dynamic and undergo catastrophes (switch from growth to shrinkage) at the cell cortex, preferentially at the cell ends (Drummond & Cross, 2000). When a microtubule reaches the cell cortex, the polymerization at its plus

end continues for 1.5 min on average before the catastrophe occurs. The pushing force produced by the polymerization is transferred along the microtubule to the nucleus that is connected with the central part of the microtubule bundle, in the anti-parallel microtubule overlap region. Since pushing forces are produced at both cell ends, they average out to center the nucleus within the cell (Tran et al., 2001). Compressive forces acting on microtubules while they are pushing against the cell cortex are the reason for microtubule catastrophes occurring preferentially in the cell end regions. The frequency of catastrophes depends on microtubule length: the longer a microtubule, the more microtubule-depolymerizing kinesin-8 proteins Klp5 and Klp6 accumulate at its plus end (Foethke et al., 2009; Tischer, Brunner & Dogterom, 2009). On the molecular level, catastrophes are thought to occur when the GTP-tubulin cap at the microtubule plus end is lost (Brun et al., 2009). Electron tomography results show that the contact with the plasma membrane is usually established by single microtubules, even if they are part of a multi-microtubule bundle (Hoog et al., 2007).

Fission yeast microtubules can be nucleated at different locations within the cell (Sawin & Tran, 2006). The most efficient microtubule nucleation or stabilization takes place at the fission yeast equivalent of the centrosome, the spindle pole body (SPB). The microtubule bundle associated with the SPB contains about two times as many microtubules as any other bundle within the cell (Hoog et al., 2007). For microtubule nucleation at other microtubule-organizing centers (MTOCs), γ-tubulin complexes (γ-TuCs) are essential. Microtubule nucleation at γ-TuCs requires the protein Mto2 (Janson et al., 2005). Such nucleation can occur not only at the nuclear membrane, but also along an already existing microtubule bundle.

Microtubule bundles in fission yeast contain 4.4 ± 2.6 microtubules. There are also individual microtubules in the cytoplasm (Hoog et al., 2007). Anti-parallel microtubule overlap regions at the nuclear membrane are stabilized by the bundling protein Ase1 (Loiodice et al., 2005). This protein is found along the overlaps and is highly dynamic in interphase. During mitosis, Ase1 is required for the stabilization of the spindle midzone. When a new microtubule is nucleated along an existing bundle, its transport to the anti-parallel microtubule overlap region is controlled by the balance of forces generated by the minus end-directed kinesin-14 motor protein Klp2 and the bundling protein Ase1 (Janson et al., 2007). An additional factor localized to the microtubule overlap regions was shown to be required for the stabilization of microtubule bundles: Dis1 (Roque et al., 2010). This protein

belongs to the conserved XMAP215 family of microtubule polymerases (Al-Bassam & Chang, 2011).

The mechanism of microtubule bundle formation is so robust that bundles self-organize correctly even in artificially enucleated cells. In the absence of nuclear MTOCs, the formation of functional interphase microtubule arrays is enabled by Ase1, Klp2, and the microtubule-nucleating protein Mto1 (Carazo-Salas & Nurse, 2006). The cytokinetic actomyosin ring can also assemble in the absence of the nucleus and nuclear MTOCs, although ring assembly is not robust in this case (Huang et al., 2007).

Microtubule plus end tracking proteins (termed +TIPs) are a subgroup of microtubule-associated proteins. +TIPs play important roles in regulating microtubule dynamics, they serve as linkers between microtubules and other cytoplasmic structures, and they affect cell division, morphogenesis, and motility in a range of cell types (Akhmanova & Hoogenraad, 2005).

1.4.2 Localization and functions of Mal3

The +TIP Mal3 is the fission yeast representative of the highly conserved EB1 family of proteins. Mal3 is involved in the control of microtubule dynamics. The functions of Mal3 include the promotion of microtubule growth initiation and the protection of microtubules from catastrophes in the cytoplasm. Microtubule catastrophes occur shortly after Mal3 is lost from the microtubule plus ends at the cortex in the cell end regions (Busch & Brunner, 2004). *In vitro*, Mal3 was shown to control catastrophes by preventing microtubule depolymerization and increasing the rescue frequency (Katsuki et al., 2009).

In addition to localizing to microtubule plus ends, Mal3 was found to bind to and stabilize the microtubule lattice seam (Sandblad et al., 2006). The seam is formed along the microtubule at the location where the tubulin sheet (that normally consists of 13 protofilaments arranged into the so-called B-lattice configuration) closes into a tube. At this location, there is a mismatch of the lateral interaction of the neighboring protofilaments that results in the A-lattice configuration. An alternative study showed that Mal3 binds between the protofilaments that form the B-lattice and binds to the microtubule seam only occasionally (Maurer et al., 2012). *In vitro* reconstitution studies showed that Mal3 has higher affinity for polymerizing microtubule plus ends than for the microtubule lattice (Bieling et al., 2007).

1.4.3 Localization and functions of Tip1 and Tea2

Tip1 is the fission yeast homologue of the mammalian protein CLIP-170. Tip1 is localized at microtubule plus ends, along the microtubules, and at the cortex in the cell end regions. Tip1 plays a role in the regulation of microtubule dynamics. It restricts microtubule catastrophes to the cell end regions of the cell cortex and prevents catastrophes elsewhere. This allows microtubule alignment along the main cell axis. In this configuration, the microtubule plus ends can reach the cell ends and deliver their cargo there. Due to the uncontrolled localization of microtubule catastrophes in *tip1*Δ cells, the microtubule bundles in these cells are shorter than in wild type cells (Brunner & Nurse, 2000a).

The importance of Tip1 regulation of microtubule dynamics is demonstrated in the process of nuclear centering. In *tip1*Δ cells, the microtubule plus end contact time with the cell cortex is shorter than in wild type cells. In *tip1*Δ cells with the nucleus displaced by centrifugation, these transient contacts do not allow efficient nucleus pushing towards the cell center. A slight nuclear positioning defect is also observed in non-centrifuged *tip1*Δ cells (Daga, Yonetani & Chang, 2006).

Tip1 interacts directly with Mal3 *in vitro*. Mal3 is essential for Tip1 localization at microtubule plus ends. On the other hand, Tip1 is not required for Mal3 localization to microtubules. However, in *tip1*Δ cells, Mal3 removal from microtubule plus ends prior to microtubule catastrophes can occur at any location at the cell cortex (rather than preferentially in the cell end regions, as in wild type cells) (Busch & Brunner, 2004).

Another protein required for Tip1 localization is the dimeric kinesin protein Tea2. It is localized to microtubule plus ends and to the cell cortex in the cell end regions. One of the functions of Tea2 is the promotion of microtubule growth; it also plays a role in maintaining cell polarity. *Tea2*Δ cells have shorter microtubule bundles than wild type cells. A subset of exponentially growing *tea2*Δ cells is bent. Upon the exit from the stationary phase, a large proportion of *tea2*Δ cells adopt the branching morphology (Browning et al., 2000).

Tea2 is loaded onto microtubules in the perinuclear region. As Tea2 is a plus end-directed molecular motor, it moves on microtubules towards their growing plus ends and accumulates there until it gets unloaded at the cell cortex. Functional Tea2 is required for the microtubule-based delivery of Tip1 to the cell ends (Browning,

Hackney & Nurse, 2003). This is due to the interaction between Tea2 and Tip1 that leads to Tea2 transporting Tip1 to microtubule plus ends. The association of both proteins with the ends of polymerizing microtubules requires Mal3 (both Tip1 and Tea2 interact with Mal3). Ultimately, Tip1 and Tea2 are unloaded at the cell end cortex. Tea2-based transport of Tip1, which has a microtubule-stabilizing function, explains the effect of *tea2* deletion on the length of microtubule bundles (Busch et al., 2004). Biochemical studies show that Mal3 and Tea2 recruit each other to the microtubules by increasing each other's affinity for microtubules (Browning & Hackney, 2005). The mechanism of interaction of Mal3, Tip1, and Tea2 at the microtubule plus ends was confirmed by an *in vitro* study. This study showed that these proteins form the minimal microtubule plus end tracking system (Bieling et al., 2007).

1.4.4 Localization and functions of Tea1

Tea1 is a protein with six kelch repeats at its N-terminus and alpha-helical coiled-coils at its C-terminus. Kelch repeats are known to be involved in protein-protein interactions in various organisms (Prag & Adams, 2003). Tea1 has limited homology to the ezrin-radixin-moesin protein family that is involved in linking the plasma membrane to the underlying cell cortex (Bretscher, Edwards & Fehon, 2002; Vega & Solomon, 1997). Tea1 accumulates at the growing microtubule plus ends and is deposited at the cell cortex in the cell end regions. There, Tea1 performs the role of a polarity marker by being involved in the recruitment of the growth machinery to the cell ends. Correct localization of the growth machinery at the cell ends is essential for maintaining straight cell shape. *Tea1*Δ cells have abnormal morphology with a high proportion of bent and branching cells. Tea1 was also thought to have an inhibitory effect on microtubule growth, based on the curling of microtubule bundles at the cell ends in *tea1*Δ cells (Behrens & Nurse, 2002; Mata & Nurse, 1997). However, we have shown that this curling can be explained by the influence of the cell geometry on the microtubules: *tea1*Δ cells are wider than wild type cells on average (Foethke et al., 2009). Another property of *tea1*Δ cells is their exclusively monopolar growth and the absence of NETO. Also, in the majority of *tea1*Δ cells, a growth pattern defect is observed. After cell division, the daughter cell that inherited the growing end of the mother cell starts growing at that end, while the other daughter cell starts growing at its new end (Glynn et al., 2001).

Tea1 is involved in both polarity establishment and maintenance. If the microtubule

network is artificially perturbed in a cell with established Tea1 localization to the cell ends, growth continues at the cell ends independently of microtubules, and cell polarity is maintained. The microtubule network is, however, required for the establishment of a new growth site. In this situation, microtubules deliver Tea1 to the ectopic growth site, and the growth machinery is recruited there. Thus, new cell morphology is established (Sawin & Snaith, 2004; Terenna et al., 2008). In the absence of microtubules, Tea1 accumulates in the vicinity of the nucleus, and an ectopic growth site is often established there. Microtubule-based transport of Tea1 away from the perinuclear region towards the cell ends is thus required to avoid the formation of branched cells (Castagnetti, Novak & Nurse, 2007). Mathematical modeling suggested that Tea1 acts within the positive feedback loop of actin polymerization, not being directly involved in the *de novo* F-actin nucleation (Csikasz-Nagy et al., 2008). In addition to that, Tea1 interacts with Mug33. Mug33 is a transmembrane protein localized to the cell end regions of the plasma membrane and to tubulovesicular elements within the cytoplasm. Mug33 was shown to be involved in regulating exocyst function (Snaith et al., 2011).

Tea2 is required for proper Tea1 localization (Browning et al., 2000). The transport of Tea1 along microtubules is not observed in cells with non-functional Tea2. At the cell ends, Tea1 is required for Tea2 and Tip1 anchoring (Browning et al., 2003). The coiled-coil domain of Tea1 is essential for its anchoring at the cell ends. Interestingly, a few Tea1 particles are not transferred from microtubules to the cell cortex, and are transported back to the perinuclear region at the depolymerizing microtubule ends (Behrens & Nurse, 2002). Tea1 directly interacts with Tip1, which is thought to retain Tea1 at the growing microtubule plus ends (Brunner & Nurse, 2000a; Feierbach, Verde & Chang, 2004).

1.4.5 Tea1 anchoring at cell ends: roles of Tea3 and Mod5

Tea1 has a homologue in fission yeast: the cell end marker Tea3. This protein has homology to the ezrin-radixin-moesin protein family, similarly to Tea1 (Gautreau, Louvard & Arpin, 2002). Tea3 is essential for efficient NETO: *tea3*Δ cells mainly grow monopolarly. Tea3 is also involved in the placement of the septum. The protein is localized to the cell ends *via* a mechanism dependent on microtubules and Tea1 (Arellano, Niccoli & Nurse, 2002). The microtubule network is almost unaffected in *tea3*Δ cells. These cells show no bending or branching that are typical of *tea1*Δ cells. Although Tea3 is not essential for the cell to identify its ends, it does

have a minor function in the mechanism of cell end definition (Niccoli, Arellano & Nurse, 2003). This is likely due to Tea3 being required for efficient accumulation of Tea1 in the cell end regions, particularly at the non-growing ends. Tea1 is, in turn, required for Tea3 localization at the cell ends (Snaith, Samejima & Sawin, 2005).

Another protein involved in the regulation of Tea1 localization is Mod5. Mod5 does not affect the microtubule-based transport of Tea1 to the cell ends. Instead, it is thought to enhance the anchoring of Tea1 at the cell cortex. Mod5 molecular association with the plasma membrane is dependent on C-terminal prenylation. Cell end specificity of Mod5 localization is dependent on Tea1: in *tea1*Δ cells, Mod5 is distributed homogeneously over the plasma membrane (Snaith & Sawin, 2003). Mod5 is also involved in Tea3 localization to the cell ends. Mod5 interacts directly with both Tea1 and Tea3. Different regions of the latter two proteins are involved in the interaction with the central region of Mod5: the N-terminal kelch repeat region of Tea1 and the C-terminal coiled coil region of Tea3 (Snaith et al., 2005).

1.4.6 Links between microtubule and actin cytoskeletons

The microtubule-associated protein Tea1 interacts physically with the actin-associated protein Bud6. Bud6 localization depends on Tea1. Tea1 localization, however, is independent of Bud6. Tea1 and Bud6 are thought to act in the same pathway, with Bud6 functioning downstream of Tea1 (Glynn et al., 2001). Together with Bud6 and For3, Tea1 was proposed to be one of the components of the polarisome complex (described in budding yeast). Tea1 and Bud6 are thought to regulate the localization of For3, and thus the process of actin cable formation. However, since *tea1*Δ *bud6*Δ *for3*Δ triple mutant cells are not polarized, it is likely that the three proteins function redundantly in cell polarity establishment (Feierbach et al., 2004).

The SH3 domain-containing protein Tea4 is a homologue of the *S.cerevisiae* Bud14p, a protein involved in bud site selection (Ni & Snyder, 2001). Tea4 has similar localization to Tea1. It was suggested to be transported to the cell end regions at microtubule plus ends. Proper localization of Tea4 is achieved only in the presence of Tea1. Tea4 is involved in the positioning of For3 to the new cell end and in the activation of For3-dependent F-actin nucleation. Tea4 is required for the establishment of the bipolar growth pattern: *tea4*Δ cells have similar NETO defect to *tea1*Δ cells. Tea4 binds directly to Tea1 and to For3, and was proposed to serve as

a bridge between the two proteins. Thus, Tea4 acts as a link between microtubule and actin cytoskeletons. The presence of the Tea1-Tea4 complex at the new cell end is required for NETO to take place (Martin et al., 2005; Snaith & Sawin, 2005; Tatebe et al., 2005). In addition to Tea4, Rax2 (Section 1.3.2) was also proposed to link Tea1 and For3. Rax2 is also thought to affect cell polarity *via* its interaction with Tea1 and to be part of the complex that recruits For3 to the cell ends (Choi et al., 2006).

Yet another protein was suggested to contribute to the linking of Tea1 and the growth machinery: End4/Sla2, a homologue of *S.cerevisiae* SLA2 (Castagnetti, Behrens & Nurse, 2005). End4/Sla2 is thought to act downstream of Tea1 and to be involved in the organization of the cortical actin cytoskeleton and in the establishment of cell polarity. *End4/sla2*Δ cells are not polarized and have an endocytic defect (Iwaki et al., 2004). Interestingly, the deletion of the actin-binding talin-like domain at the C-terminus of End4/Sla2 leads to a NETO defect (Castagnetti et al., 2005). Cell wall integrity is also affected in *end4/sla2*Δ cells (Ge et al., 2005).

End4/Sla2 is enriched at cell ends in interphase and at the septum during cytokinesis. Its transport to the cell ends does not require intact microtubules or actin filaments, but requires functional vesicular trafficking. However, an intact actin cytoskeleton is required for continuous removal of End4/Sla2 from the cell end regions. Tea1 is involved in End4/Sla2 positioning at the new cell end (Castagnetti et al., 2005). Tea1 was proposed to localize to the new cell ends first and perform the initial recruitment, but not the retention, of End4/Sla2 there. End4/Sla2 might subsequently organize the cortical actin network that is required for growth initiation at the new cell end. End4/Sla2 might interact with Tea1 *via* Bud6, as End4/Sla2 and Bud6 have comparable localization mechanisms and deletion phenotypes.

A membrane-associated protein Pal1 is thought to act downstream of End4/Sla2 (Ge et al., 2005). It localizes to the growing cell ends in interphase and to the septum during cytokinesis. This pattern of Pal1 localization depends neither on microtubules nor on the actin cytoskeleton. End4/Sla2 interacts directly with Pal1 and is required for its proper localization. *Pal1*Δ cells have a morphological defect: the majority of the cells are pear-shaped. This partial polarization of *pal1*Δ cells requires the presence of Tea1 (*pal1*Δ *tea1*Δ cells are mostly spherical). Also, the cell wall is structurally defective in *pal1*Δ cells. Based on its importance for cell polarity

and on its partial association with the plasma membrane, Pal1 might function as the link between the plasma membrane and the molecular structures required for cell polarity.

1.5 Cell polarity control in fission yeast

1.5.1 Cell wall remodeling machinery

Cell morphology of fission yeast is defined by the 3D shape of the cell wall. The cell wall undergoes significant remodeling at the cell ends during cell growth. Thus, the mechanisms controlling fission yeast morphogenesis ultimately have to position the cell wall remodeling machinery. The fission yeast cell wall is composed mainly of (1,3)α-D-glucan and (1,3)β-D-glucan in the form of fibrils and amorphous material (Ishiguro, 1998; Kopecka, Fleet & Phaff, 1995).

Mok1 is the protein acting as (1,3)α-D-glucan synthase. It is essential for cell morphogenesis: the cell shape and the cell wall structure are perturbed in *mok1* mutant cells. Also, the F-actin network is affected in these cells. Mok1 localizes to growing cell ends in interphase and to the cell middle region during mitosis and cytokinesis. Proper localization of Mok1 requires an intact F-actin network (Katayama et al., 1999). The transmembrane protein Ags1 is also responsible for α-glucan synthesis and remodeling (Grun et al., 2005; Hochstenbach et al., 1998).

The multisubunit enzyme (1,3)β-glucan synthase is responsible for β-glucan synthesis at the growth sites in interphase and at the septum during cytokinesis. Localization of (1,3)β-glucan synthase to the plasma membrane is required for its enzymatic activity. Inhibition of the enzyme leads to cell cycle arrest. The subunits of (1,3)β-glucan synthase in fission yeast are: Bgs1, Bgs2, Bgs3, and Bgs4. These subunits play different roles in cell wall remodeling throughout the *S.pombe* life cycle. Bgs1 functions during cytokinesis, polarized cell growth, mating, and spore formation. During vegetative growth, Bgs1 is localized to the regions of cell wall synthesis (Cortes et al., 2002). Bgs2 is required for the correct formation of the cell walls of ascopores. *Bgs2* is expressed only during sporulation (Martin et al., 2000). *Bgs3* is an essential gene and is expressed throughout the *S.pombe* life cycle. Reduction of the level of *bgs3* expression leads to the reduction of the cell size and to

the cell wall thickening (Martin et al., 2003). Bgs4 is the catalytic subunit of (1,3)β-glucan synthase. It is essential for cell wall synthesis and repair at all stages of the *S.pombe* life cycle. In the absence of Bgs4, the cells lyse at active growth sites. Bgs4 localization to the site of cytokinesis occurs later than that of Bgs1, suggesting Bgs4 involvement at later stages of the process. A functional F-actin network is required for relocation of Bgs4 within the cell, but not for its retention at growth sites (Cortes et al., 2005).

1.5.2 Additional proteins affecting cell polarity

In Sections 1.3 and 1.4, the influence of cytoskeleton-associated proteins on cell polarity was considered. This section deals with the functions of other proteins, including the cell cycle-related proteins, in cell polarity establishment.

The 12 Orb proteins were identified in a genetic screen designed to isolate temperature-sensitive polarity mutants in fission yeast. At the restrictive temperature, the mutant cells acquire spherical cell morphology (Snell & Nurse, 1994). The functions of different Orb proteins at different stages of the cell cycle are summarized in **Figure 1.4** (Verde, Mata & Nurse, 1995).

The protein kinase Pak1/Shk1/Orb2 is a homolog of the mammalian PAK1 and of STE20 in budding yeast. It is required for NETO (Verde, Wiley & Nurse, 1998).

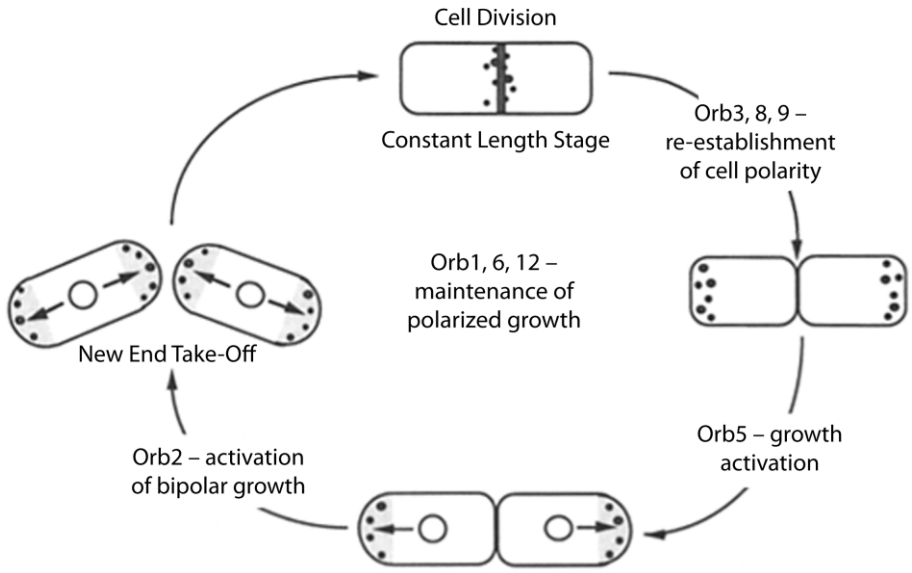

Figure 1.4. Roles of different Orb proteins in cell polarity. Figure adapted from (Verde et al., 1995).

The protein is part of the Ras1- and Cdc42-dependent signaling pathway (Marcus et al., 1995). Pak1/Shk1/Orb2 is thought to act in the recognition of cell ends as potential growth sites, similarly to Tea1, Tea3, and Tea4 (Sawin, Hajibagheri & Nurse, 1999). This mechanism of action is different from that in other mutants with the NETO defect that are unable to activate growth *per se* at the new end.

Orb5 is the fission yeast homolog of casein kinase IIα. Orb5 is essential for the establishment of polarized growth after cell division (Snell & Nurse, 1994). However, it is not required for the polarization of the actin cytoskeleton.

The Ndr kinase Orb6 is required for the maintenance of polarized growth in interphase. It also acts in the Ras1- and Cdc42-dependent signaling pathway that coordinates cell growth with cell cycle progression, downstream of Pak1/Shk1/Orb2. Orb6 localizes to the regions of cell growth: at the cell ends in interphase and at the septum during cytokinesis. *Orb6* and *orb2* interact genetically. Pak1/Shk1/Orb2 is required for the localization of Orb6 at the new cell end (Verde et al., 1998). Orb6 functions in concert with Mor2, a homolog of the *Drosophila* protein Furry. Mor2 is required for the polarization of the actin cytoskeleton and for restricting the size of the growth zones. Cells with mutated Mor2 are spherical and have a G2 delay. Mor2 localizes to the cell ends in interphase and to the site of cytokinesis. Its localization depends on the intact actin cytoskeleton. Mor2 and Orb6 localization is interdependent (Hirata et al., 2002).

Interestingly, it was suggested that the protein End4/Sla2, which is thought to contribute to the linking of Tea1 and the growth machinery (Section 1.4.6), might function downstream of the Orb pathway (Castagnetti et al., 2005).

Similarly to budding yeast, the proteins belonging to the Rho family of small GTPases regulate the glucan synthases involved in cell wall synthesis in fission yeast. The three most important protein family members are Rho1, Rho2, and Cdc42 (Perez & Rincon, 2010).

The essential protein Rho1 is required for cell integrity and for the polarization of the actin cytoskeleton. Rho1 localizes to growth zones both in interphase and during cytokinesis. It is predominantly membrane-bound (Arellano, Duran & Perez, 1997; Nakano, Arai & Mabuchi, 1997). Rho1 directly activates the (1,3)β-D-glucan synthase (**Figure 1.5**) and regulates the kinases Pck1 and Pck2 (Sayers et al., 2000).

Rho1 is regulated, among others, by the GTPase-activating proteins (GAPs) Rga1

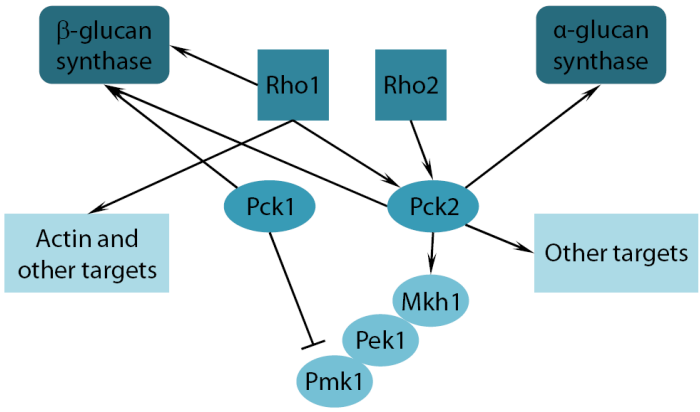

Figure 1.5. Schematic representation of the mechanism of action of Rho GTPases in fission yeast. Figure adapted from (Perez & Rincon, 2010).

and Rga5. Rga1 regulates the activity of Rho1 in the localization of actin patches at the cell ends and in the cell wall synthesis. Rga1 localizes to the cell ends in interphase and to the septum during cytokinesis (Nakano, Mutoh & Mabuchi, 2001). Rga5 is specific to Rho1. The role of Rga5 is to decrease the level of Rho1 activity in (1,3)-β-D-glucan synthase activation. Rga5 is localized to the cell growth regions (Calonge et al., 2003).

One of the functions of the GTPase Rho2 is to activate the kinase Pck2 (**Figure 1.5**). This protein is, in turn, involved in the control of the (1,3)α-D-glucan synthase Mok1 (Section 1.5.1) (Calonge et al., 2000).

The Rho-like GTPase Cdc42 (homolog of Cdc42p in budding yeast and in mammalian cells) is essential for cell growth in *S.pombe*. *Cdc42*Δ cells arrest growth and, as a consequence, are small and spherical. Cells with mutated Cdc42 GTP-binding domains (constitutively activated *cdc42* mutants) are large, with abnormal morphology. This shows the importance of Cdc42 for the establishment of polarized growth (Miller & Johnson, 1994). Cdc42 was also shown to be involved in membrane trafficking and fusion that are essential for polarized secretion and endosome recycling (Estravis et al., 2011). Neither actin cables nor the exocyst complex are required for Cdc42 activity and positioning at the cell ends (Bendezu & Martin, 2011).

Two guanine exchange factors (GEFs), Gef1 and Scd1, activate Cdc42 (**Figure 1.6**). Gef1 localizes mainly at the cell division site. However, it acts not only in cytokinesis, but also in the control of bipolar growth establishment. Gef1 is linked to the signaling pathway containing Pak1/Shk1/Orb2 and Orb6 (Coll et al., 2003).

Orb6, in particular, is required for the correct positioning of Gef1, and thus for the correct localization of Cdc42 activation (Das et al., 2009). Scd1, a homolog of Cdc24p in budding yeast, localizes to several sites in fission yeast cells, including the growing cell end regions (Hirota et al., 2003). Its interaction with Cdc42 is important for maintaining proper cell morphology (Chang et al., 1994). Mutant cells with *scd1* deleted are rounded and have mating defects. On the other hand, mutant cells with *gef1* deleted are slightly elongated and have defects in bipolar growth and in the formation of the septum. These differences in morphological defects of the two mutants show that Gef1 and Scd1 have different functions in cell polarity control (Coll et al., 2003).

Many of the proteins mentioned so far are involved in the formation and positioning of growth sites. In addition to that, there are proteins that are involved in the control of growth site size. Rga4 is a GAP specific for Rho-like GTPases that inactivates Cdc42 (Tatebe et al., 2008). Rga4 plays an important role in defining cell diameter: *rga4*Δ cells are wider and shorter than wild type cells. Rga4 localizes to the cell cortex in non-growing regions of the cell. In interphase, this is along the sides of the cell and, pre-NETO, at the new cell end (Das et al., 2007). Rga4 acts in concert with the Cdc42 GEF Scd1 to control the area of Cdc42 activation, and hence to define cell width (**Figure 1.6**) (Kelly & Nurse, 2011).

A protein regulating Rga4 localization, and thus influencing cell polarity, is Pom1 (Tatebe et al., 2008). The Dyrk-like protein kinase Pom1 was identified in mutant cells with abnormal cell shape and division (Bahler & Pringle, 1998). Pom1 is involved in the selection of the locations for functional growth sites. After cell division, *pom1* mutant cells initiate growth at either of the two cell ends, rather than exclusively at the old end, as in the wild type. Also, *pom1* mutant cells mostly do not perform NETO, and some cells adopt bent or branched cell morphology reminiscent of that of the *tea1*Δ cells (although the connection between Pom1 and Tea1 is not fully understood). However, unlike *tea1*Δ cells, *pom1* mutants frequently misplace their division septum. During mitosis, Pom1 is mostly found at the cell ends, but during cytokinesis it relocalizes to the septum (Bahler & Pringle, 1998; Niccoli et al., 2003). In interphase, Pom1 requires the Tea1-Tea4 complex for its positioning at the cell ends (Behrens & Nurse, 2002; Tatebe et al., 2005). A model was proposed in which Pom1 forms a "double concentration gradient" at the cortex. According to this model, Pom1 concentration decreases from both cell ends towards the cell center, the highest concentration being at the

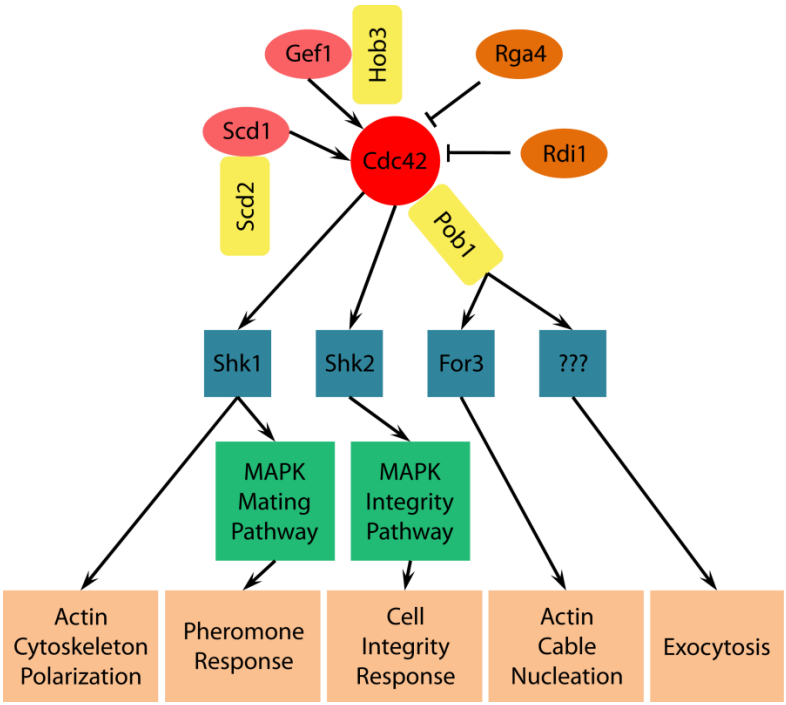

Figure 1.6. Proteins acting upstream and downstream of Cdc42, with their cellular functions. Figure adapted from (Perez & Rincon, 2010).

non-growing new cell end (Padte et al., 2006). The localization of Pom1 to the cell cortex is controlled by its non-catalytic domain, while its accumulation in the cell end regions requires the cell cycle-regulated kinase activity of Pom1 (Bahler & Nurse, 2001). Pom1 cortical gradient establishment involves a phosphorylation cycle. Pom1 associates with the plasma membrane *via* direct interaction with lipids. Tea4 increases Pom1 lipid affinity by facilitating its dephosphorylation, and thus strengthens Pom1 association with the cell ends. Pom1 molecules diffuse laterally along the plasma membrane. The release of Pom1 molecules from the membrane is achieved *via* the process of auto-phosphorylation that decreases lipid affinity (Hachet et al., 2011).

Another protein kinase controlling polarized cell growth is Ssp1. Ssp1 provides the condition necessary for NETO. It was proposed that this condition is an increased amount of free G-actin at the new cell end, required to organize the new growth zone. To locally increase the concentration of G-actin, Ssp1 promotes F-actin depolymerization. Under normal growth conditions, Ssp1 is found mainly in the cytoplasm. If the external osmolarity increases, Ssp1 relocates to the plasma membrane at the growing cell ends in interphase or at the septum during cell division. This relocalization reflects the role of Ssp1 in the stress-activated pathway (Rupes, Jia & Young, 1999).

1.5.3 Summary of cell morphogenesis mechanisms

The multiple proteins discussed in the previous sections can be divided into three groups: growth site positioning proteins, growth site confinement proteins, and proteins required for NETO (**Figure 1.7**) (Huisman & Brunner, 2011).

In short, the outline of the cell polarity maintenance mechanism is currently thought to be the following (**Figure 1.8**). The complex consisting of polarity factors Tea1 and Tea4 is transported on microtubules to the cell end regions. It is anchored to the plasma membrane *via* Mod5. Tea4 interacts with the actin polymerization promoter For3 that requires Cdc42 and Bud6 for its activation. The activity of Cdc42, in turn, is controlled by Tea1 *via* Pom1 and Rga4. Selective activation of For3 in the cell end regions makes them rich in F-actin that is required for localized cell growth *per se* (Chang & Martin, 2009; Huisman & Brunner, 2011; Martin, 2009; Perez & Rincon, 2010; Piel & Tran, 2009).

Many details concerning the molecular mechanism of fission yeast morphogenesis are still unclear. This may be partially due to the molecular elements still

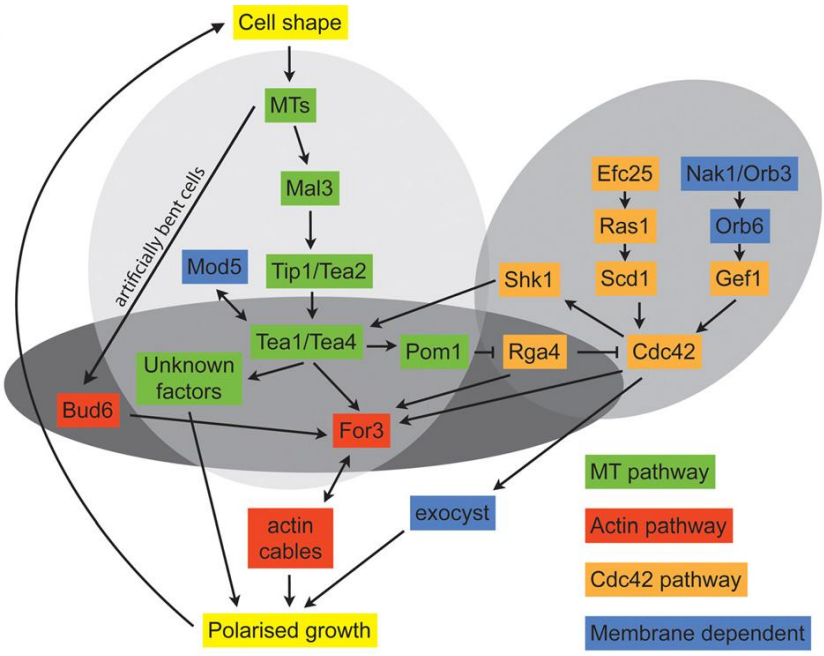

Figure 1.7. The network of the core proteins involved in cell polarity establishment and maintenance in fission yeast. The medium grey oval includes the proteins involved in growth site positioning, the light grey oval includes the proteins involved in growth site confinement, and the dark grey oval includes the proteins involved in NETO. Figure courtesy of (Huisman & Brunner, 2011).

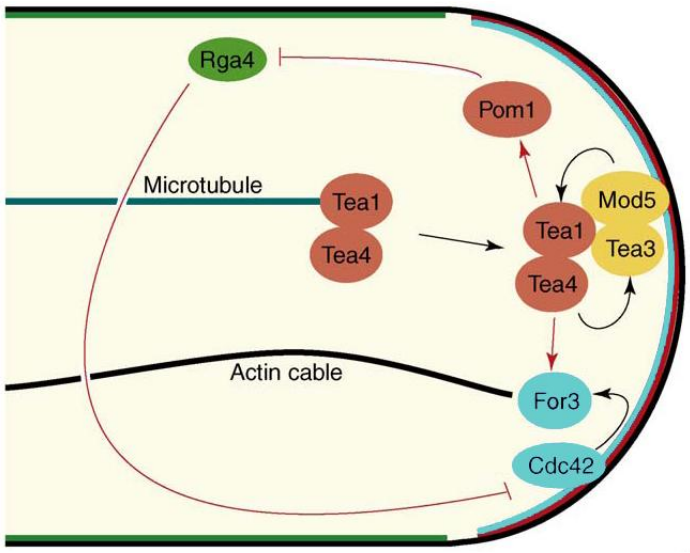

Figure 1.8. The scheme of the interactions of the core proteins involved in cell polarity (one cell end is considered). Figure adapted from (Martin, 2009).

missing from the picture, for example, in the domain of the interaction between the cell polarity markers and the cell wall synthesizing machinery that is directly responsible for localized cell growth. Another reason for the mechanism of fission yeast morphogenesis being not fully understood yet is a number of feedback loops acting in the process. An example of such a feedback loop is the complex interaction and localization interdependence of Mod5, Tea1, and Tea3 (**Figure 1.8**). Yet another reason for such complexity is the redundancy of the cell polarizing mechanisms, such as the parallel action of For3 and of the exocyst (**Figure 1.7**). In some cases, it was established that certain proteins interact, but the functional significance of this interaction for cell polarity is not yet fully understood (for example, the interaction of For3 with Tea1 *via* Tea4). In conclusion, a wealth of information concerning the functions and interactions of various proteins involved in fission yeast polarity control has already been gathered, but full understanding of the molecular details of this process has not yet been achieved.

1.5.4 Cytokinesis

Correct positioning of the site of cytokinesis has paramount importance for maintaining proper fission yeast polarity through consecutive cell divisions. This requires centering of the nucleus by interphase microtubules (Section 1.4.1). They position the nucleus, which is attached to central regions of the microtubule

bundles, by pushing against the cell cortex in the cell end regions (Tran et al., 2001). The position of the nucleus, in turn, defines the localization of the actomyosin ring in cytokinesis, and subsequently of the septum (Tran et al., 2000). The microtubular structure post-anaphase array nucleated at the actomyosin ring is essential for maintaining its localization in the cell middle region (Pardo & Nurse, 2003). The artificial displacement of the nucleus, either by centrifugation or by using optical tweezers, leads to the misplacement of the contractile ring (Daga & Chang, 2005; Tolic-Norrelykke et al., 2005). This effect is observed only when the nucleus is displaced during interphase or early prophase. After that, the division site is fixed.

The importance of the centering of the nucleus within the cell for the correct positioning of the cell division site is due to the role of the nucleus in positioning Mid1, an anillin-related protein. Mid1 is the key protein for the recruitment of the contractile actomyosin ring components. Incorrect Mid1 positioning leads to asymmetric cell division. During interphase and early mitosis, Mid1 shuttles between the nucleus and a broad band at the cell cortex around the nucleus. Then, before anaphase, the protein localization at the cell cortex becomes more compact: the diffuse band shrinks into a dense ring. This is preceded by Mid1 export from the nucleus. The cortical Mid1 band is overlying the nucleus even in cells with a displaced nucleus. In cells with multiple nuclei, there are multiple Mid1 bands. Mid1 localization is independent of the actin and microtubule cytoskeletons (Bahler et al., 1998a; Paoletti & Chang, 2000). There are two independent and spatially overlapping mechanisms for Mid1 localization at the medial cell cortex. The first mechanism involves the amphipathic helix at Mid1 C-terminus that can be inserted into the plasma membrane. This interaction with the plasma membrane is stabilized by Mid1 nuclear localization sequence located near the helix. The interaction with the plasma membrane allows the stable positioning of the Mid1 ring. The second mechanism of Mid1 localization involves its N-terminal region. In this case, Mid1 is anchored at the cortex by the kinase Cdr2 that is negatively regulated in the cell end regions by Pom1 (Celton-Morizur et al., 2004). The former mechanism is dominant over the latter, as illustrated by experiments in which the nucleus was displaced (Almonacid et al., 2009). The polo kinase Plo1 regulates Mid1 exit from the nucleus upon entry into mitosis, probably *via* Mid1 phosphorylation in the nucleus (Bahler et al., 1998a). Alternatively, it was proposed that Plo1 could have a role in stabilizing Mid1 association with the cell cortex (Celton-Morizur et al., 2004). The

role of Mid1 in actomyosin ring formation consists in the formation of "platforms" that recruit the other required components. The essential component of the actomyosin ring that Mid1 recruits directly is Rng2, an IQGAP-related protein. Rng2, in turn, is essential for the recruitment of the other components to the medial cortex (Padmanabhan et al., 2011). The interaction of Mid1 with Rng2 is controlled by Plo1 (Almonacid et al., 2011).

Another important regulator of Mid1 localization is Pom1. In addition to the growth defects mentioned in Section 1.5.2, *pom1* mutant cells often have functional, but misplaced, misoriented, or even multiple septa (Bahler & Pringle, 1998). This is due to Mid1 localization to the entire cell cortex in the half of the cell that contains the new cell end during interphase. This suggests that Pom1 excludes Mid1 from the new cell end region (Celton-Morizur et al., 2006; Padte et al., 2006).

Pom1 is not only involved in the positioning of the cell division site, but also in the timing of cell division. The cell end gradients of Pom1 allow coordinating progression through the cell cycle with cell length. This is achieved *via* the negative regulation of Cdr1 and Cdr2 (that control entry into mitosis) by Pom1. In interphase, Cdr1 and Cdr2 localize to the cell middle region. In short cells, Pom1 localization overlaps with that of Cdr1 and Cdr2. As cells elongate, the overlap, and with it Cdr1 and Cdr2 inhibition, gradually disappear. Hence, longer cells eventually can enter into mitosis (Martin & Berthelot-Grosjean, 2009; Moseley et al., 2009).

Another essential factor in cytokinesis is Cdc12. Cdc12 is one of three formins present in fission yeast, and it is required for the formation of the contractile ring in the cell middle region (Chang, Drubin & Nurse, 1997). Cdc12 is involved in cytokinesis initiation, downstream of the cell cycle machinery (Yonetani & Chang, 2010). The actin-polymerizing activity of Cdc12 is controlled by profilin. Different regions of Cdc12 are responsible for its localization in interphase and during cytokinesis. Cdc12 is present in a relatively low number of spot structures that move within the cytoplasm and are transported to the site where the contractile actomyosin ring forms (Yonetani et al., 2008). Cdc12 first localizes to 30 – 50 dynamic nodes that are arranged in a broad band in the cell middle region. These nodes nucleate randomly oriented actin filaments. Myosin motor proteins are thought to condense these actin filaments into a contractile ring (Coffman et al., 2009).

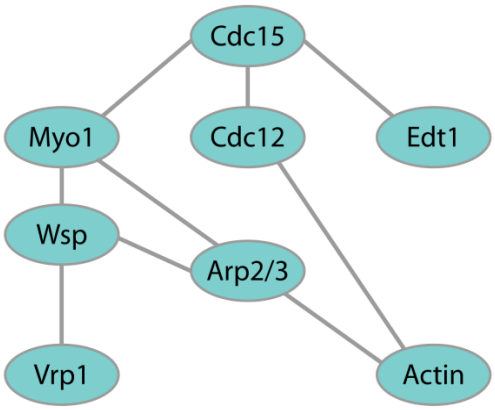

Figure 1.9. Regulatory pathway for the regulation of F-actin nucleation by Cdc15. Figure adapted from (Aspenstrom, Fransson & Richnau, 2006).

Yet another protein that is essential for cytokinesis is Cdc15. This protein is required for the relocation of actin patches, and thus endocytic sites, from the cell ends to the site of cell division at the beginning of cytokinesis. Cdc15 localizes to a cortical ring in the cell middle region (Balasubramanian et al., 1998; Fankhauser et al., 1995). Cdc15 controls F-actin nucleation *via* two independent mechanisms (**Figure 1.9**). It interacts with both the myosin Myo1 and the formin Cdc12. Myo1 is the activator of the Arp2/3 complex that is directly involved in F-actin nucleation within actin patches. This probably explains the importance of Cdc15 for actin patch relocalization at the beginning of cytokinesis. Cdc15 interaction with Cdc12 is required for the formation of the proper actomyosin ring (Carnahan & Gould, 2003). Cdc15 not only acts in organizing the actin cytoskeleton, but is also involved in organizing a specialized region of the plasma membrane at the site of cytokinesis (Section 1.6.3).

The temporal regulation of cytokinesis is performed by the septation initiation network (SIN) (Krapp, Gulli & Simanis, 2004; Wolfe & Gould, 2005). The SIN controls the transition from interphase to mitosis by activating the cytokinesis machinery and inhibiting components required for F-actin polarization at the cell ends (Ray et al., 2010).

1.6 Role of sterol-rich membranes (SRMs) in cell polarity

1.6.1 Composition and functions of lipid rafts and SRM domains

Studies of model membranes *in vitro*, their analysis *in silico* (Mouritsen & Jorgensen, 1997), and direct visualization *in vivo* (Duggan et al., 2008; Eggeling et al., 2009) showed that membranes with heterogeneous composition self-organize into regions with different properties. The plasma membrane is composed mainly of sterols, sphingolipids, and glycerophospholipids. The former two tend to form "lipid rafts" with tighter packing than the rest of the membrane. On the molecular level, this is due to the energetically favorable packing of the four-ring structure of sterols with the long saturated acyl chains of sphingolipids. Unsaturated side chains of glycerophospholipids prevent them from such tight packing (Alvarez, Douglas & Konopka, 2007). The diameter of lipid rafts was shown to be about 20 nm in mammalian cells (Eggeling et al., 2009). The functional importance of lipid rafts is mainly due to the existence of raftophilic proteins that preferentially associate with lipid rafts. Main classes of such proteins are GPI-anchored and palmitoylated proteins. Raftophilic proteins represent about 35% of plasma membrane proteins (Simons & Sampaio, 2011). In addition to diverse functions within cells, raftophilic proteins are involved in lipid raft stabilization (Hancock, 2006; Lingwood et al., 2009). In mammalian cells, lipid rafts were shown to be involved in cell signaling and membrane trafficking (Hanzal-Bayer & Hancock, 2007; Lingwood & Simons, 2010).

Lipid rafts were also identified in plant cells (Mongrand et al., 2010). In *Arabidopsis*, the core set of lipid raft-associated proteins contains cell wall-related proteins. Signaling proteins (receptor kinases, G-proteins, and calcium signaling proteins) were found to be among the variable members of lipid rafts (Kierszniowska, Seiwert & Schulze, 2009).

The analogue of lipid rafts in fungi are sterol-rich membrane (SRM) domains. They are significantly larger than typical lipid rafts, although it is not yet clear whether SRM domains are relatively homogeneous or whether they are aggregates of smaller domains. Similarly to lipid rafts, SRM domains are composed of sphingolipids and sterols (Bagnat et al., 2000). SRMs were identified in *S.cerevisiae* (Klose et al., 2010), *C.albicans,* and *A.nidulans* (Alvarez et al., 2007; Fischer, Zekert & Takeshita,

2008), among others. In the latter two organisms, SRMs were shown to be essential for growth.

1.6.2 Role of SRMs in fission yeast cell polarity

Sphingolipids in *S.pombe* contain ceramide with a longer fatty acid chain than that in mammalian cells. Ergosterol is the most common fission yeast sterol representing 70.6 ± 1.4% of the total amount of sterols. The precise molecular structures of the sphingolipids and ergosterol present in fission yeast ensure their association into SRM domains and are essential for their function *in vivo* (Eisenkolb et al., 2002; Iwaki et al., 2008). Ergosterol was shown to be significantly more domain-promoting than cholesterol *in vitro* (Xu et al., 2001). SRMs localize within the plasma membrane, with SRM domains centered at the growth sites. In wild type cells, these are the cell ends and the site of cytokinesis. SRM localization is coordinated with the cell cycle and was proposed to involve the secretory pathway (Wachtler, Rajagopalan & Balasubramanian, 2003). SRMs can be visualized with the fluorescent dye filipin that forms specific complexes with sterols (Drabikowski, Lagwinska & Sarzala, 1973). Cell cycle-dependent SRM localization was first observed indirectly using freeze-fracture electron microscopy on filipin-treated cells (Takeo, 1985).

In fission yeast, a range of proteins are SRM-associated. One of them is Bgs4, the catalytic subunit of (1,3)β-glucan synthase that is essential for cell wall synthesis (Section 1.5.1). Bgs4 stability was shown to depend on the presence of SRMs (Wachtler et al., 2003). SRMs are also involved in the maintenance and anchoring of the actomyosin ring at the plasma membrane in the cell middle region. It was suggested that SRM domains function as a structural framework for the cell growth and division machinery, including the proteins acting in cell wall and plasma membrane remodeling (Huisman & Brunner, 2011; Wachtler & Balasubramanian, 2006; Wachtler et al., 2003). Another role of SRM domains might be related to their biophysical properties being different from those of the rest of the plasma membrane. Tight packing of the SRM components leads to comparatively low deformability of the membrane (Alvarez et al., 2007). This may be important in the regions of active cell wall reorganization.

1.6.3 SRM positioning in fission yeast

Correct SRM positioning was proposed to require a functional secretory pathway. Microtubules are thought to be non-essential for SRM domain formation and positioning. In contrast, the disruption of the actin cytoskeleton leads to abnormal SRM distribution within the plasma membrane (Wachtler et al., 2003).

Several proteins were shown to influence the positioning of SRMs within the fission yeast plasma membrane. The type I myosin Myo1 is one of them. The protein is localized within SRM domains. Cells with *myo1* deletion, or expressing a mutant form of Myo1 lacking the TH1 domain, have SRMs distributed over the entire plasma membrane at all stages of the cell cycle. The Myo1 TH1 domain deletion also has an effect on the organization of F-actin, on the septation process, on cell polarity, but not on endocytosis. Thus, Myo1 is thought to influence SRM localization not *via* membrane trafficking, but *via* direct binding of the TH1 domain to acidic phospholipids. Overexpression of Myo1 leads to the formation of SRM domains at ectopic sites within the plasma membrane (Takeda & Chang, 2005; Toya et al., 2001).

Another protein, Btn1, was shown to affect the relocation of SRMs and Myo1 to the cell ends after cytokinesis and to affect polarized growth at 37°C. Btn1 is thought to affect SRM localization *via* its role in F-actin patch formation/polarization and endocytosis. Interestingly, this protein is also involved in vacuole pH homeostasis (Codlin, Haines & Mole, 2008).

Importantly, SRM localization at the site of cytokinesis was shown to be independent of Mid1 and of the actomyosin ring. However, Cdc15, which localizes within SRMs during cytokinesis and is required for the correct positioning of the contractile ring (Section 1.5.4), is also required for the positioning of SRMs at the contractile ring. In wild type cells, SRMs localize to the cell middle region after the actomyosin ring has formed and before it starts contracting. However, in the absence of the actomyosin ring, SRM positioning is not affected (Takeda, Kawate & Chang, 2004). Mutant Cdc15 causes a spiral-like cytokinetic SRM domain. This is different from the SRM distribution in *myo1* mutant cells, where SRMs are spread throughout the plasma membrane. Overexpression of Cdc15 also leads to the formation of SRM domains at ectopic sites. The mechanism of Cdc15 involvement in SRM positioning is thought to be *via* localizing Myo1 foci that, in turn, recruit SRMs to the site of cytokinesis (Takeda et al., 2004). It was suggested that SRM

domains form *via* protein-mediated clustering of much smaller lipid rafts. In this case, Myo1, Cdc15, and some other proteins could act as scaffolds for SRM stabilization (Alvarez et al., 2007).

Another protein involved in the positioning of SRMs is the kinase Kin1. In *kin1*Δ cells, SRMs are depolarized. Kin1 is anchored within the SRM domains. The molecular anchoring mechanism remains elusive. Functional vesicular trafficking and/or correct localization of SRM domains is required for Kin1 positioning at the growth sites (Cadou et al., 2010). Apart from its role in SRM localization, Kin1 is involved in positioning the cell wall-synthesizing proteins (β-glucan synthases). Consequently, *kin1*Δ cells have defective cell wall and abnormal morphology. As Kin1 also functions in F-actin positioning (La Carbona & Le Goff, 2006), it was proposed to be an essential linker between the cell cortex, the plasma membrane, and the cell wall (Cadou et al., 2010).

2 Aim

The aim of this project was to study the mechanisms of the localization and dynamics of sterol-rich membranes in *S.pombe*, as well as the link between the positioning of these membrane domains and cell growth. To achieve this, a detailed analysis of fission yeast morphogenesis and SRM dynamics was performed with unprecedented precision.

3 Materials and methods

3.1 Materials and methods used to study SRMs in *S.pombe* cells

For the part of the project consisting in the study of SRMs, *S.pombe* strain construction, cell culturing, and most of the imaging were performed by Paulo Alves.

3.1.1 Live marker for SRM visualization

Filipin is a widely used SRM marker (Drabikowski et al., 1973). Nevertheless, for this study of SRM dynamics a different SRM marker had to be chosen, since filipin disrupts the cell membrane and is not appropriate for *in vivo* observations (Bradley, Rayns & Forrester, 1980; Souto-Padron & de Souza, 1983). Paulo Alves selected a novel marker using a fission yeast protein localization database (Matsuyama et al., 2006). The selection criterion for the marker protein was that it should localize similarly to filipin. GFP-tagged Tna1 (spac1002.16c) with homology to the budding yeast Tna1p was chosen (Klebl, Zillig & Sauer, 2000; Llorente & Dujon, 2000). Control experiments performed by Paulo Alves showed that GFP-Tna1 fluorescence signal colocalizes with filipin signal at the cell membrane in all strains and for all conditions used in this study (**Figure 3.1**).

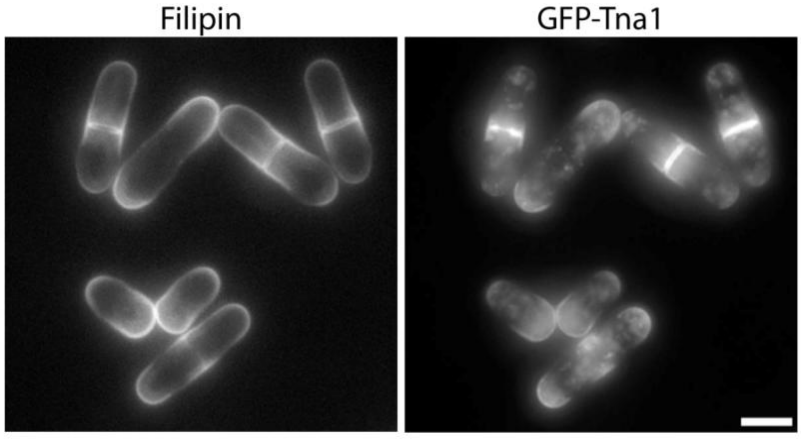

Figure 3.1. Comparison of the localization of filipin and GFP-Tna1 fluorescence signals. Scale bar: 5 µm. This figure was produced by Paulo Alves.

3.1.2 Yeast strains and cell culture

S.pombe strains used in this study are listed in **Table 3.1**. Standard procedures for handling fission yeast were employed (Moreno, Klar & Nurse, 1991). GFP-tagging was performed according to a previously described procedure (Bahler et al., 1998b). Exponentially growing cells were grown at 30°C in the synthetic medium EMM2 supplemented with the amino acids required for each strain.

Starved cell cultures were prepared by growing cells in EMM2 with 0.5% glucose for 2 days at 30°C (Zaitsevskaya-Carter & Cooper, 1997). For release from

Table 3.1. *S.pombe* strains used in the study of SRMs.

Strain	Genotype	Source
DB 643	*h- crn1-GFP::KanMX6*	D. Brunner lab
DB 797	*h+ tea1-GFP::KanMX6 leu1-32*	K. Sawin and P. Nurse labs
DB 1197	*h- lys1+::nmt1-GFP-atb2 ura4-D18*	D. Brunner lab
DB 1886	*h- Pnmt1-GFP-tna1::KanMX6*	P. Alves
DB 1936	*h- Pnmt1-GFP-tna1::KanMX6 tea1Δ::ura4⁺ ura4-D18*	P. Alves
DB 1970	*h- Pnmt1-GFP-tna1::KanMX6 tip1Δ::KanMX6*	P. Alves
DB 1974	*h- Pnmt1-GFP-tna1::KanMX6 mod5Δ::KanMX6*	P. Alves
DB 2390	*h+ bud6-3GFP::KanMX6 ade6-M216 leu1-32 ura4-D18*	S. Martin lab
DB 2396	*h+ for3-3GFP::ura4⁺ bud6::Kan MX6 ade6-M216 leu1-32 ura4-D18*	S. Martin lab
DB 2678	*h- for3::KanMX6 Pnmt1-GFP-tna1::KanMX6 ade6-M216 leu1-32 ura4-D18*	P. Alves
DB 2693	*h- Pnmt1-GFP-tna1::KanMX6 mal3::his3 ade6-M210 leu1-32 ura4-D18 his3-D1*	P. Alves
DB 2699	*h- Pnmt1-GFP-tna1::KanMX6 myo1::KanMX6 leu1-32*	P. Alves
DB 2703	*h- myo1::KanMX6 tea1-GFP::KanMX6 leu1-32*	P. Alves
DB 2711	*h- Pnmt1-GFP-tna1::KanMX6 tea4::KanMX6 ade6-M216*	P. Alves
DB 2774	*h- Pnmt1-GFP-tna1::KanMX6 bud6::KanMX6 ura4-D18*	P. Alves
DB 2804	*Pnmt1-GFP-tna1::KanMX6 myo1::KanMX6 tea1Δ::ura4+ ura4-D18*	P. Alves

starvation (RS), fresh EMM2 supplemented with adenine, leucine, and uracil (and histidine if needed) was added to the starved cell culture.

Prior to RS using EMM2 containing drugs, cells were pretreated with the same drugs. In such experiments, ketoconazole (Aldrich), latrunculin B (Calbiochem), and methyl-2-benzimidazolecarbamate (MBC, Aldrich) were added 30 min, 10 min, and 30 min before RS, respectively. Ketoconazole, latrunculin B, and MBC were dissolved in dimethyl sulfoxide (DMSO, Adrich) and used at the final concentration of 800 µM, 50 µM, and 25 µg/ml, respectively.

3.1.3 Imaging SRMs in cells recovering from starvation

Staining of cells with filipin (Aldrich) was performed as previously described (Takeda et al., 2004). Filipin was dissolved in DMSO and used at the final concentration of 5 µg/ml.

For still imaging, a 100x objective on an Axiovert 200M widefield fluorescence microscope (Zeiss) was used. Images were acquired with a Coolsnap HQ camera

Table 3.2. Lengths of the analyzed time-lapse movies for different *S.pombe* cell types (3 min time resolution).

Cell type	Time-lapse movie lengths
Wild type cells	7 movies: 2 of 2 h 33 min, 2 of 3 h 42 min, 2 of 6 h 30 min, 6 h
Ketoconazole-treated cells	2 movies of 6 h
DMSO-treated cells	4 movies: 2 of 2 h 33 min, 2 of 2 h
MBC-treated cells	5 movies: 2 of 3 h, 3 of 2 h 33 min
*Tea1*Δ cells	9 movies: 2 of 2 h 33 min, 4 h, 3 of 6 h, 7 h 12 min, 7 h 45 min, 8 h
*Tea4*Δ cells	2 movies: 4 h, 5 h
*Mod5*Δ cells	8 movies: 2 h, 4 of 2 h 33 min, 2 of 3 h, 5 h 36 min
*For3*Δ cells	11 movies: 4 of 2 h 30 min, 5 h 21 min, 4 of 6 h, 2 of 6 h 30 min
*Bud6*Δ cells	2 movies: 6 h, 6 h 21 min
*Bud6*Δ *tea1*Δ cells	3 movies: 3 h 42 min, 6 h 27 min, 7 h 15 min
*Myo1*Δ cells	7 movies: 3 h, 4 h, 5 h, 5 h 36 min, 5 h 48 min, 2 of 6 h
*Myo1*Δ *tea1*Δ cells	2 movies: 3 h 51 min, 2 h 27 min

(Roper Scientific) using MetaMorph software (Molecular Devices).

For live cell imaging during recovery from starvation, starved cell culture (15 µl) was spread on a glass bottom culture dish (MatTek) coated with lectin (Adrich). Supernatant (50 µl) from the centrifuged starved cell culture was added to the dish, which was then centrifuged at 300 rpm to force the cells into the horizontal position on the dish bottom. RS was performed by adding 2 ml of fresh EMM2 supplemented with adenine, leucine, and uracil (and histidine if needed) to the dish. Imaging was initiated 10 min after RS. Z-stacks were acquired every 3 min (1 min for some movies), with 0.25 µm z-spacing, in both fluorescence and phase contrast channels, using a 63x objective on an SP5 confocal microscope (Leica). Total movie lengths varied from 30 min to 7 hours (**Table 3.2**). The imaging was performed at 30°C.

3.1.4 Image analysis software

The image analysis software for this study was developed using MATLAB. The goal of the analysis of the time-lapse movies was to study SRM domain localization, size, and dynamics in correlation with cell growth.

3.1.4.1 Z-projections

The first step of the image analysis procedure is the creation of z-projections of the z-stacks acquired in phase contrast and fluorescence channels over time. The phase contrast average projection is performed with the three z-planes that are three, four, and five planes closer to the objective than the plane closest to the cell center (middle plane) (**Figure 3.2**, **D** and **E**). The fluorescence average projection is performed with seven z-planes: the middle plane, three planes above, and three planes below it (**Figure 3.2**, **F**). For strains with bent and branching cell morphology, all z-planes of a fluorescence z-stack are used to create the average projection.

The selection of the middle plane is based on the presence of rims around *S.pombe* cells on phase contrast images (**Figure 3.2**, **A**). Z-planes closer to the cell middle have narrower rims in comparison with farther z-planes. The middle plane was defined as the plane with the least number of pixels outside the range of intensities belonging to the image background. To select this plane, the histograms of

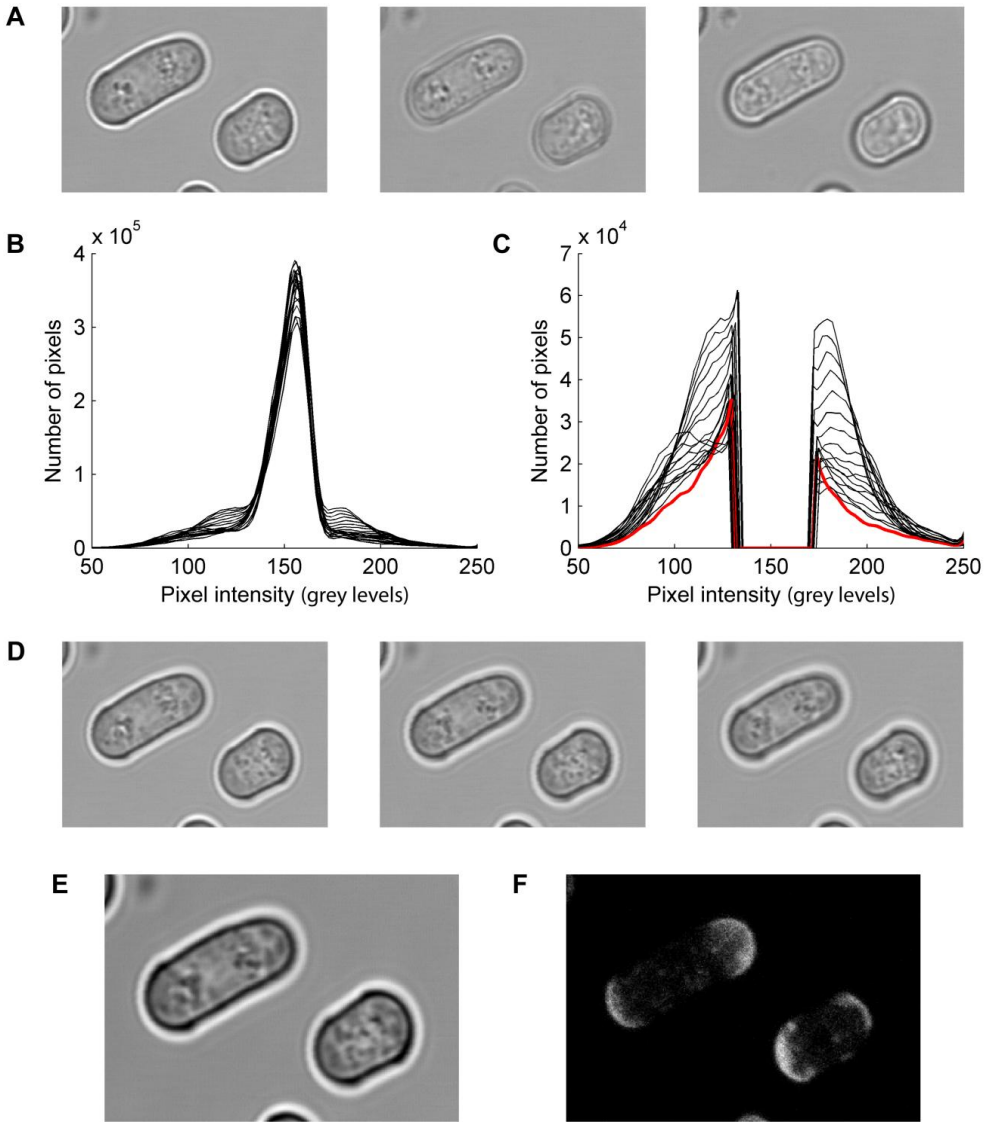

Figure 3.2. Procedure for creating z-projections of phase contrast and fluorescence images. Images A, D, E, F zoom in on two cells from a large field of view.

A – **Middle** – cell middle plane, **left** – z-plane two z-planes closer to the objective than the middle plane, **right** – z-plane two z-planes farther from the objective than the middle plane.

B – Envelopes of the image histograms of all z-planes of a z-stack (smoothed using smoothing spline).

C – Envelopes of the image histograms of all z-planes of a z-stack, central part of the curves removed. The red curve corresponds to the cell middle plane.

D – The three z-planes used to produce the phase contrast z-projection image. **Left to right**: z-planes that are three, four, and five z-planes farther from the objective than the middle plane.

E – The resulting phase contrast z-projection image.

F – The resulting fluorescence z-projection image.

individual z-planes from a z-stack (whole field of view with multiple cells) are compared (**Figure 3.2**, **B**). In each histogram, the central part of the distribution is removed, as it corresponds to the intensities of the image background (**Figure 3.2**, **C**). The part to be removed was defined by setting a threshold on the derivative of the smoothed histogram envelope (smoothing was performed using the smoothing spline method). The areas under the resulting histogram envelopes (after the removal of the central part) are compared for all z-planes of the stack, and the z-plane with the smallest value is used as the middle plane. The middle plane is selected for each z-stack of the time-lapse movie separately to take into account the possible gradual vertical shift in the imaging setup over time.

3.1.4.2 Registration

The registration of the phase contrast projection images is performed to compensate for the random horizontal shifts of the imaging setup. The registration algorithm used in this study is based on the software created by Manuel Guizar (http://www.mathworks.com/matlabcentral/fileexchange/18401-efficient-subpixel-image-registration-by-cross-correlation/content/dftregistration.m), which, in turn, is based on related previous work (Fienup & Kowalczyk, 1990). Fluorescence projection images are shifted using the values obtained for the corresponding phase contrast images.

3.1.4.3 Detecting the cell periphery and measuring cell properties

Cell peripheries are detected from the phase contrast projection images (**Figure 3.3**, **A and B**). First, the image background is corrected by subtracting from the original image the image obtained with morphological opening performed on the original image. Then, the image is filtered to reduce noise. Median and average filters are used sequentially (**Figure 3.3**, **C**). Then, contours are obtained using the Canny edge detection method (**Figure 3.3**, **D**). Short contours (corresponding to intensity inhomogeneity) are discarded (**Figure 3.3**, **E**). The remaining contours are processed individually. A contour is placed on a black background (**Figure 3.3**, **G**). After performing dilation to fill in eventual one or two pixel-wide gaps in the contour, holes in the resulting image are filled (**Figure 3.3**, **H**). Only the objects with an area that is reasonable for *S.pombe* cells are kept for subsequent analysis.

The cell length, width and orientation (**Figure 3.3**, **K**) are derived from the major and minor axis lengths and the orientation of the ellipse that has the same

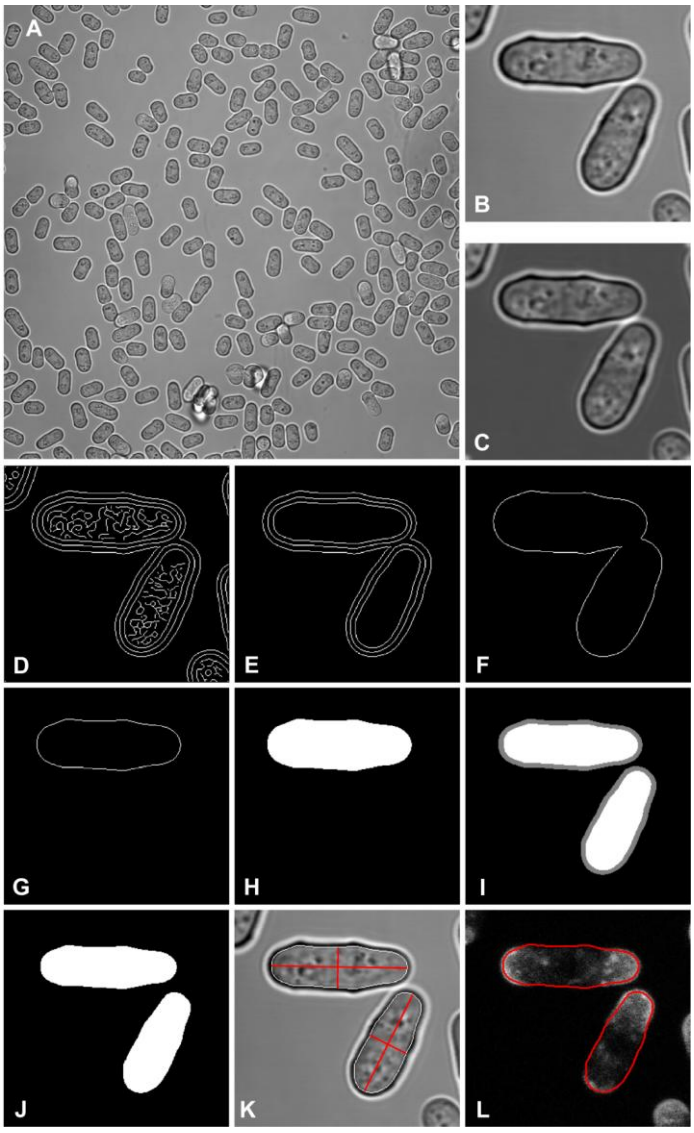

Figure 3.3. Cell periphery detection procedure.
A – Phase contrast z-projection image, whole field of view.
B – A zoom-in on two cells in the phase contract z-projection image.
C – Image after median and average filtering.
D – Edges detected using the Canny edge detection method.
E – Only contours longer than a threshold value are kept.
F – Contour surrounding two neighboring cells.
G – Individual cell contour.
H – Filled contour.
I – Multiple contours per cell.
J – Cell masks.
K – White outlines overlaid onto the phase contract z-projection image are the detected cell peripheries. Red lines represent cell length and cell width.
L – Red outlines overlaid onto the fluorescence z-projection image represent the detected cell peripheries.

normalized second central moments as the cell. As the shape of an *S.pombe* cell is not perfectly elliptical, a correction is required. The software developed in this study performs the correction by going from the ends of the major and minor ellipse axes towards the center, until the cell periphery is reached. The cell center is defined as the middle point between the cell ends. Again, only the objects with length and width values reasonable for *S.pombe* cells are kept for subsequent analysis.

Due to the rims around the cells that are characteristic of phase contrast images, three contours are detected per cell in the edge detection step (**Figure 3.3**, **D** and **E**). They correspond to the boundaries between the image background and the white rim around the cell (the outer contour), between the white rim and the black rim (the middle contour), and between the black rim and the cytoplasm (the inner contour). Out of the three contours, only the middle one can be used to reliably define the cell periphery, because both the inner and the outer contours can be open or imperfect. In addition, the outer contour can be shared by neighboring cells (**Figure 3.3**, **F**). In this case, the contour is discarded on the basis of the cell size, as described above.

The middle contour that represents the cell periphery was defined as the widest contour left after discarding the outer contour (**Figure 3.3**, **I**). To determine if a contour is the outer one, the mask corresponding to the filled contour is eroded with the structuring element of the size corresponding to half of the width of the white rim around the cell on the phase contrast projection image. If the contour is the outer one, the perimeter of the eroded mask is situated over the white rim when overlaid with the phase contrast image. To determine if this is the case, the median of the intensity taken from the phase contrast image along the perimeter is measured. If this value is above the background intensity (determined as the position of the maximum on the image histogram), then the contour is considered to be the outer contour and is discarded.

To adjust the cell periphery found from the phase contrast image to the fluorescence signal, erosion of the cell mask is performed (**Figure 3.3**, **J**). The size of the structuring element for the erosion was chosen so that the periphery of the resulting mask overlaps with the middle of the GFP-Tna1 signal at the plasma membrane (**Figure 3.3**, **L**).

To access the SRM dynamics and cell growth, each cell is tracked over time. The object in each movie frame closest to the initial center of a tracked cell was

considered to be that cell if its center was within 4 μm of the initial center of the tracked cell.

3.1.4.4 Construction of kymographs

To visualize SRM dynamics in individual cells (as seen on the 2D z-projection), kymographs representing the intensity along the cell membrane over time were created.

Kymographs are built by sequentially adding horizontal lines at the bottom of the nascent kymograph. One line represents one time point (**Figure 3.4**, **C**). To create a kymograph line, three steps are performed: extraction of fluorescence intensities along the cell periphery, followed by shifting and centering the array of these intensities.

Intensities are extracted along the detected cell periphery, starting from one of the cell ends. Each value is the result of averaging the intensities in the square of three-by-three pixels centered at the current position.

In order to define the shift and the centering position of the intensity array for the current time point, two steps are performed. Firstly, the line perpendicular to the cell axis that passes through the cell center is set on the image (movie frame) corresponding to the first time point. This line is fixed for this cell for all time points. Secondly, intersection points between this fixed line and the cell periphery at each time point are determined. These points were termed the opening point and the centering point (**Figure 3.4**, **A** and **B**).

The position of the opening point defines the shift of the intensity array. As a result of the shift, the intensity value corresponding to the opening point is placed at the right edge and the intensity of its neighboring point – at the left edge of the kymograph (both visualized with yellow dots in **Figure 3.4**).

The centering point defines the horizontal location where the shifted intensity array is placed on the kymograph: the intensity value corresponding to the centering point is placed on the vertical middle line of the kymograph. Centering individual kymograph lines in such a way leads to the visualization of SRM behavior and, indirectly, of growth separately for the two cell ends. The position of the cell ends over time is indicated on the kymograph with blue dots.

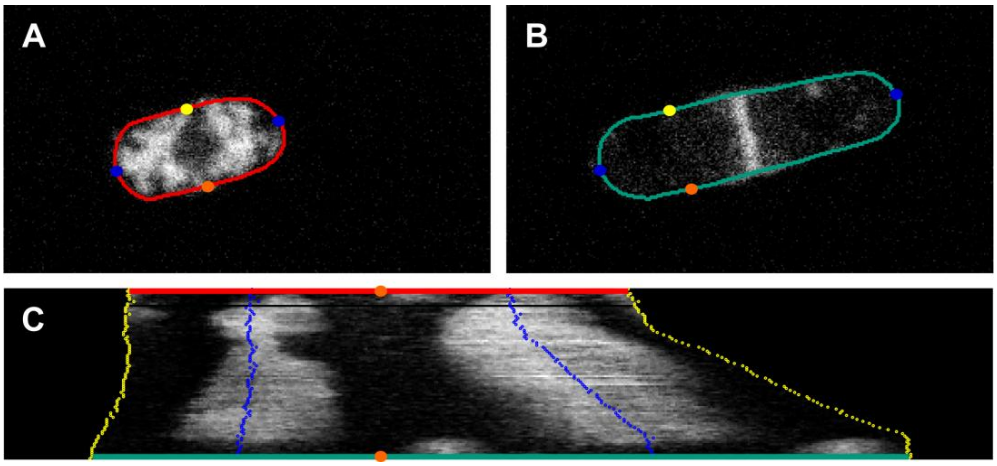

Figure 3.4. Kymograph construction principle. Blue – cell ends, yellow – opening point, orange – centering point.
A – Fluorescence z-projection of the first movie frame (zoom-in on one cell). Red – cell periphery.
B – Fluorescence z-projection of the last movie frame (zoom-in on the cell shown in panel A). Green – cell periphery.
C – Kymograph of the cell. Red – the line that corresponds to the first movie frame. Green – the line that corresponds to the last movie frame.

3.1.4.5 Quality control

Each detected cell was visually inspected using phase contrast projections and the time-lapse movies, where the detected cell periphery was overlaid onto the fluorescence signal of the cell for each time point. The cells falling into the following categories were discarded: non-horizontally positioned cells (common in the mutants with bent and branching cell morphology), strongly vacuolated cells, cells where cell periphery detection was imperfect, cells that moved in the horizontal plane under the influence of neighboring cells, cells with the plasma membrane detached from the cell wall at one of the cell ends, cells with very low total GFP-Tna1 signal. Only the cells that passed this quality control were analyzed further.

3.1.4.6 Analysis of cell growth

The analysis of cell growth is performed based on the information about the growth of each of the cell ends separately. The growth dynamics of a cell end is summarized in a growth curve (**Figure 3.5, B**). This curve represents the distance from the cell end to the initial cell center (position of the cell center at the first time point) over

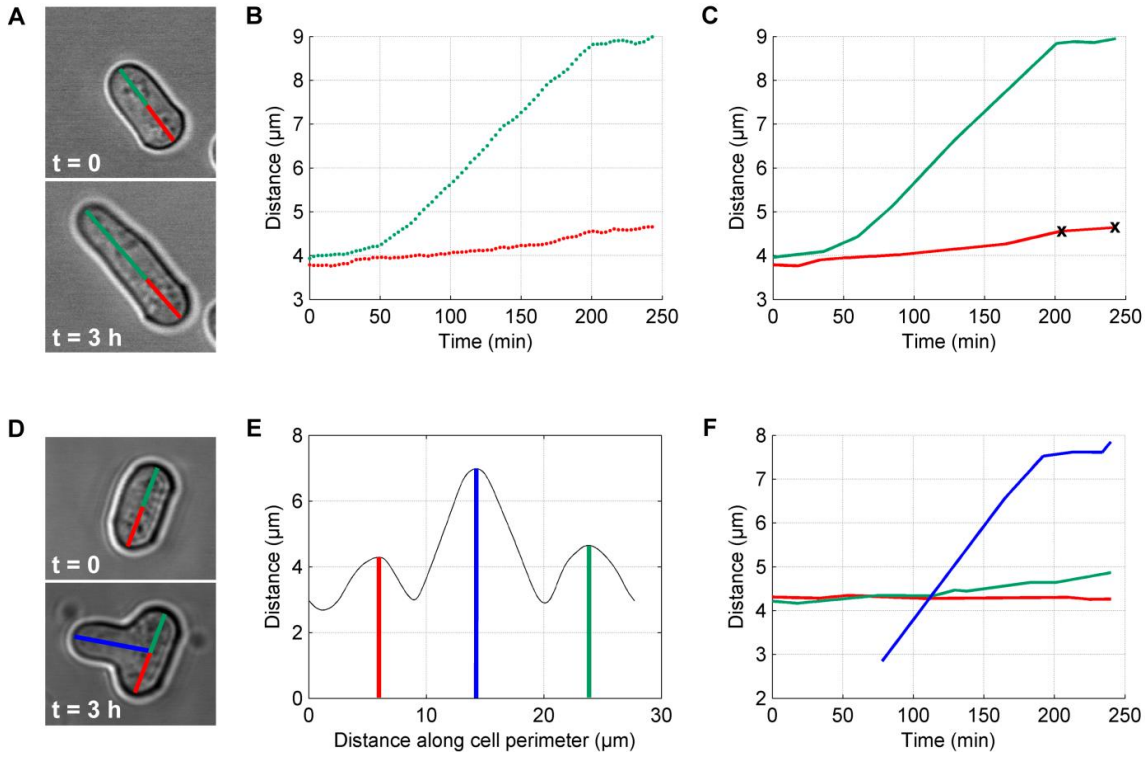

Figure 3.5. Analysis of growth of individual cell ends during the first cell cycle after RS. A, B, C – straight wild type cell. D, E, F – *tea1*Δ cell that becomes branching during the observation period.
A – Phase contrast projection image of a wild type cell at the first time point and after 3 hours of observation. Green and red lines – distances from the initial cell center to each of the cell ends.
B – Growth curves for both cell ends (color code as in A).
C – Growth curves fitted with MARS for both cell ends (color code as in A). Black crosses represent the ends of one of the growth phases (corresponding to the cell division phase).
D – Phase contrast projection image of a *tea1*Δ cell at the first time point and after 3 hours of observation. Green and red lines – distances from the initial cell center to each of the initial cell ends. Blue line – the distance from the initial cell center to the new cell end.
E – The distance curve that is used to determine the position of the cell ends. Vertical lines show which maximum corresponds to which cell end (color code as in D).
F – Growth curves fitted with MARS for the three cell ends (color code as in D). The blue curve starts when the new cell end is first detected.

time. For straight cells, cell ends were defined as the intersection points between the main cell axis and the cell perimeter (**Figure 3.5**, **A**). For the strains containing bent and branching cells (**Figure 3.5**, **D**), cell ends were defined as the positions on the

cell perimeter corresponding to the local maxima of the smoothed distance curve. This curve represents the distance between the initial cell center and each pixel on the cell perimeter at the current time point (**Figure 3.5**, **E**).

The growth curves are first smoothed using the sliding window average of size three and then fitted. The fitting is performed using the multivariate adaptive regression splines (MARS). This part of the software is based on Entool, a Matlab toolbox for regression, classification, and active learning developed by C. Merkwirth, J.D. Wichard, and M. Ogorzalek (http://www.j-wichard.de/entool/). The fitting is performed ten times for each growth curve, and the result corresponding to the minimal sum of squares of residuals (the closest to the initial curve) is kept (**Figure 3.5**, **C** and **F**). The information extracted from the fitting is: the time of the beginning and end of each growth phase, as well as the growth speed for each growth phase. A correction is made to ensure that growth analysis is not continued after cell division.

Automatic classification of growth patterns (*i.e.* whether cells initiate P4 or not) was performed for all cell types using only the cells that were followed until cell division (selected manually based on the kymographs).

3.1.4.7 Analysis of SRM dynamics

To correlate cell growth with SRM behavior, SRM dynamics was studied. The parameters measured over time were: the size of all SRM domains and the positions of the domain centers relative to the nearest cell end. These values were obtained

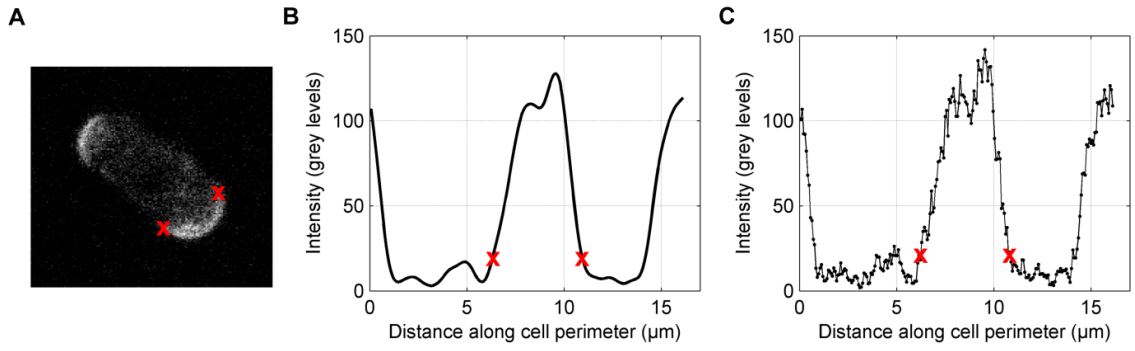

Figure 3.6. Measuring the SRM domain width. Red crosses – SRM domain edges.
A – Fluorescence projection image (zoom-in on one cell).
B – Smoothed intensity profile taken along the cell periphery.
C – Intensity profile taken along the cell periphery.

from projection images, so they describe the 2D dynamics of SRM domains in the planes neighboring the cell middle plane, not the overall 3D SRM behavior (**Figure 3.6**, **A**).

To determine the edges of an SRM domain located at a cell end, the intensity profile taken along the cell periphery is analyzed. The intensity profile is shifted, so that the position of the cell end is in the center of the profile. The profile is then smoothed using the running average of size three followed by a smoothing spline (**Figure 3.6**, **B**).

Then, a threshold is applied to the values of the smoothed intensity profile. The threshold was chosen so that the base intensity level (intensity in the absence of an SRM domain) and the noise are cut off. The limits of the region that is nearest to a cell end and has intensities above the threshold are then found. A correction is introduced to find the edges of the SRM domain on the initial, non-smoothed intensity profile (**Figure 3.6**, **C**). The coordinates of the domain edges allow determining the domain width and the position of the domain center relative to the nearest cell end. Both values are measured along the cell periphery.

3.2 Materials and methods used to study endocytosis in *S.pombe* cells

3.2.1 Creation of an endocytosis marker by GFP-tagging of Shd1

The gene *shd1* was endogenously C-terminally tagged with GFP. A linker sequence was introduced between *shd1* and the GFP sequence.

The tagging construct was obtained by the PCR performed according to the standard protocol (Bahler et al., 1998b) with the plasmid DL 191 (pFA6a-linker-GFP-kanMX6; linker sequence: ILGAPSGGGATAGAGGAGGPAGLI) (B. Hülsmann and D. Brunner, unpublished) and the primers DPE 895 and DPE 896 (sequences of all oligonucleotides mentioned can be found in **Table 3.3**). The PCR reaction was performed with the following composition in each tube (50 µl in total per tube): 31 µl of water, 10 µl of 5x HiFi buffer (Velocity), 1 µl of $MgCl_2$ (Velocity), 2 µl of the primer DPE 895 (10 µM), 2 µl of the primer DPE 896 (10 µM), 1 µl of dNTPs (20 mM), 2 µl of the template DL 191

(2.2 ng/µl), 1 µl of the polymerase (Velocity). The Velocity DNA polymerase kit was purchased from "Bioline". The following PCR program was used: (1) 97°C for 2 min, (2) 97°C for 30 sec, (3) 53°C for 30 sec, (4) 72°C for 1 min, (5) steps 2 to 4 repeated 32 times, (6) 72°C for 10 min, (7) finish at 4°C. The size of the PCR product was checked using the 0.8% agarose gel. The PCR product was purified using the QIAquick PCR Purification Kit purchased from "Qiagen".

The *S.pombe* strain DB 750 (h- ade6-M216 leu1 ura4-D18) was transformed with the tagging construct using the standard protocol (Keeney & Boeke, 1994). After two-day incubation at 30°C, the colonies growing on the selective replica-plates (YE5S + Geneticin) were isolated and tested for integration of the tagging construct with colony PCR.

The colony PCR was performed with the following composition in each tube (50 µl in total per tube): 38.5 µl of water, 0.5 µl of the primer DPL 890, 0.5 µl of the primer DPE 893, 1 µl of $MgSO_4$ (100 mM), 5 µl of 10x PCR buffer (AmpliTaq), 1 µl of dNTPs (20 mM), 0.5 µl of AmpliTaq polymerase, 3 µl of cell lysate. AmpliTaq DNA polymerase kit was purchased from "Applied Biosystems". Cell lysate was obtained as described in (Ling, Merante & Robinson, 1995). The following colony PCR program was used (with semi-hot start): (1) 95°C for 3 min, (2) 95°C for 30 sec, (3) 52°C for 30 sec, (4) 72°C for 3 min, (5) steps 2 to 4 repeated 35 times, (6) 72°C for 10 min, (7) finish at 4°C. The PCR product was checked using the 0.8% agarose gel. Out of the 84 colonies checked, only one colony integrated the tagging construct at the correct location. Imaging of the cells

Table 3.3. Sequences of the primers that were used to create the *S.pombe* strain DB 2567 with the endocytosis marker Shd1-GFP.

Primer	Sequence
DPE 888	ttggtggagcgcaaggtgcgaatgaagctggtaagaaagccagtatatatcaagcta ctccagacaatccttttggttttATCCTTGGAGCTCCTTCAGGA
DPE 889	caaatattattacgatttaaatgaaaagcagctttattaaagagcctaagggaagaatc aatgctccgaaaaaaaaagacGAATTCGAGCTCGTTTAAAC
DPE 890	Caaactctatcaatcatgaccg
DPE 893	Ctgaatatggctatgctcaacc
DPE 895	ttggtggagcgcaaggtgcgaatgaagctggtaagaaagccagtatatatcaagcta ctccagacaatccttttggttttATCCTTGGAGCTCCTTCAGGA (similar to the sequence of DPE 888)
DPE 896	gcgtaaactgtaacctaacgcagatgttatacctcaataattataccattttacacgag caaaatgaaaagacagaaaggGAATTCGAGCTCGTTTAAAC

obtained from that colony showed localization of the GFP signal to the expected endocytic sites. The resulting strain was given the number DB 2567 (the genotype of the strain can be found in **Table 3.4**).

Initially, the following primers, designed according to (Bahler et al., 1998b), were used to obtain the tagging construct: DPE 888 and DPE 889. The PCRs to obtain the tagging construct were performed two times, and the transformations were performed five times. No *shd1-GFP* recombinants were obtained using this pair of primers (about a hundred colonies were tested in total). To solve this problem, a new pair of primers was designed: DPE 895 and DPE 896. The sequence of DPE 895 is similar to that of DPE 888. The difference between the reverse primers DPE 896 and DPE 889 is in the distance between the end of the *shd1* open reading frame and the beginning of the 80 base pair sequence used to design the primers. For DPE 896, this distance is 48 base pairs, and for DPE 889 it is 142 base pairs. This distance being smaller for DPE 896 probably accounts for the success of the GFP tagging of Shd1 with the new pair of primers.

3.2.2 Crossing *S.pombe* strain containing endocytosis marker Shd1-GFP with mutant strains

The strain DB 2567 that contains the endocytosis marker Shd1-GFP was crossed with some of the mutant strains used in this study to analyze the SRM behavior in cells recovering from starvation. The crosses were performed following the standard protocols (Forsburg & Rhind, 2006). The resulting strains are listed in **Table 3.4**.

3.2.3 Imaging *S.pombe* cells with endocytosis marker Shd1-GFP

Cells containing the endocytosis marker Shd1-GFP were imaged with the PerkinElmer UltraView RS spinning disk microscope. The imaging conditions were: 200 ms, 250 ms, 300 ms, and 700 ms exposure time (depending on the total duration of image acquisition), binning 2, gain 200, AOTF set to 100%. The time resolution, the number of planes in a z-stack, and the spacing between the planes varied. These parameters are indicated in Sections 4.2.2 and 4.4.1.

The imaging of exponentially growing cells was performed at 25°C in EMM2 media supplemented with adenine, leucine, and uracil. The imaging of cells recovering from starvation was performed at 30°C and started 6 min after RS.

Table 3.4. Strains containing the endocytosis marker Shd1-GFP created in this study.

Strain	Genotype
DB 2567	*h- shd1- GFP::kanr ade6-M216 leu1 ura4-D18*
DB 2589	*h+ tip1Δ::kanr shd1- GFP::kanr ade6-M210*
DB 2592	*h- tea1Δ::ura4+ shd1- GFP::kanr ura4-D18 leu1*
DB 2594	*h- mod5Δ::kanMX shd1- GFP::kanr ade6-M216 leu1 ura4-D18*
DB 2596	*h- for3::kanMX6 shd1- GFP::kanr leu1-32 ura4D-18*

Opening and z-projection of z-stacks were performed using the ImageJ plugin for handling images saved in the PerkinElmer format. The kymographs for studying the dynamics of endocytosis were created using the ImageJ plugin "Kymograph".

4 Results

4.1 SRMs during recovery from starvation in wild type cells

4.1.1 Localization of SRMs and growth markers in starved wild type cells

To study *de novo* SRM formation and polarization at the plasma membrane and to observe the process of cell growth initiation, *S.pombe* cells were cultured for two days (for experimental procedures see Section 3.1.2). This time was sufficient for the cells to reach growth arrest; no filipin or GFP-Tna1 signal was detectable at the cell periphery (**Figure 4.1**). Then, nutrients were added, and SRM recovery and polarization were observed.

Apart from the absence of SRMs at the plasma membrane, starved cells were characterized by unpolarized localization of growth markers, such as actin patches, Bud6, and For3 (**Figure 4.2**).

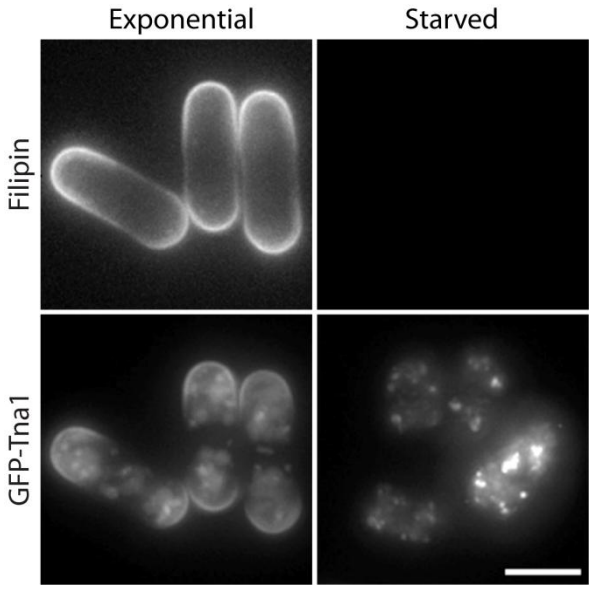

Figure 4.1. SRM localization at the cell membrane in exponentially growing and starved cells (filipin staining and GFP-Tna1 live marker images). Scale bar: 5 µm. Images were acquired by Paulo Alves.

4.1.2 SRMs and cell growth in post-starvation wild type cells

4.1.2.1 Four phases of the first post-starvation cell cycle

As starved cells don't have any detectable SRMs at the plasma membrane (**Figure 4.1**) and don't grow, they have to rebuild SRMs at the plasma membrane *de novo* and restart growth upon RS. This makes cells recovering from starvation the ideal system for studying the connection between SRMs and cell growth. In the following, the cells imaged during the first cell cycle after RS will be referred to as "post-starvation cells".

Time-lapse fluorescence microscopy was employed for imaging cells recovering from starvation. Custom automated image analysis software was developed to analyze this

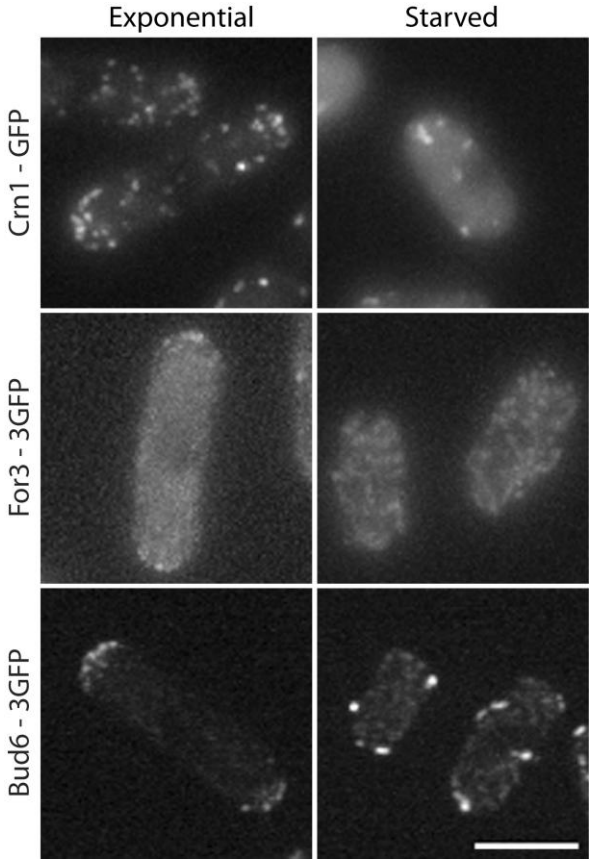

Figure 4.2. Localization of actin patches, For3, and Bud6 in exponentially growing and starved cells. Actin patches were visualized using the GFP-tagged actin-binding domain of coronin (Crn1-GFP). Localization of Bud6 and For3 was visualized using the markers Bud6-3GFP and For3-3GFP, respectively. Scale bar: 5 µm. Images were acquired by Paulo Alves.

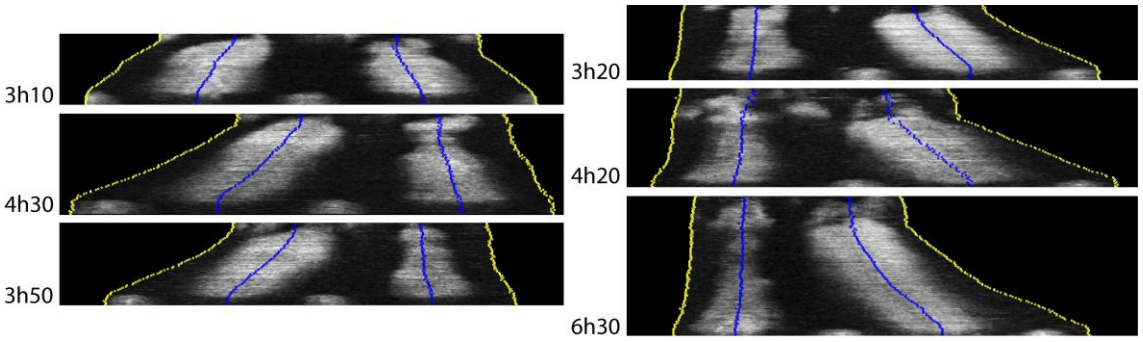

Figure 4.3. Kymographs of post-starvation wild type cells. All kymographs start 10 min after RS. The periods displayed on the kymographs are indicated at the bottom left.

data (Section 3.1.4). SRM dynamics at the cell periphery was visualized using kymographs (**Figure 4.3**). Each horizontal line on a kymograph shows the intensity along the cell periphery at a given time point. Yellow dots represent the borders of the kymograph, blue dots represent the position of the cell ends. The right and left halves of the kymograph visualize the SRM dynamics and growth of individual cell ends. A detailed description of the image analysis software (including kymograph generation procedure) can be found in Section 3.1.4.

The qualitative picture of SRM dynamics and cell growth in post-starvation cells can be seen in the kymographs (**Figure 4.3**). Several phases can be distinguished in the first cell cycle after RS.

Soon after nutrient addition, randomly distributed SRM domains appeared at the plasma membrane. The phase in which these domains were present at the cell periphery will be referred to as P1; cells were not growing during this phase.

The second phase (P2) started when SRMs began polarizing. During P2, SRM domains already present in the cell end regions started expanding, while the domains in the cell middle region started shrinking and then disappeared. Occasionally, new domains formed within the cell end regions and started to expand. During P2, slow cell growth was detected. Upon slow growth initiation, the shape of the cell ends became more pointed.

Eventually one of the cell ends increased its growth speed. This was considered the beginning of the third phase (P3). The cell end that increased its growth speed at that moment will be referred to as the "primary cell end", the other end will be referred to as the "secondary cell end". The beginning of P3 was accompanied by

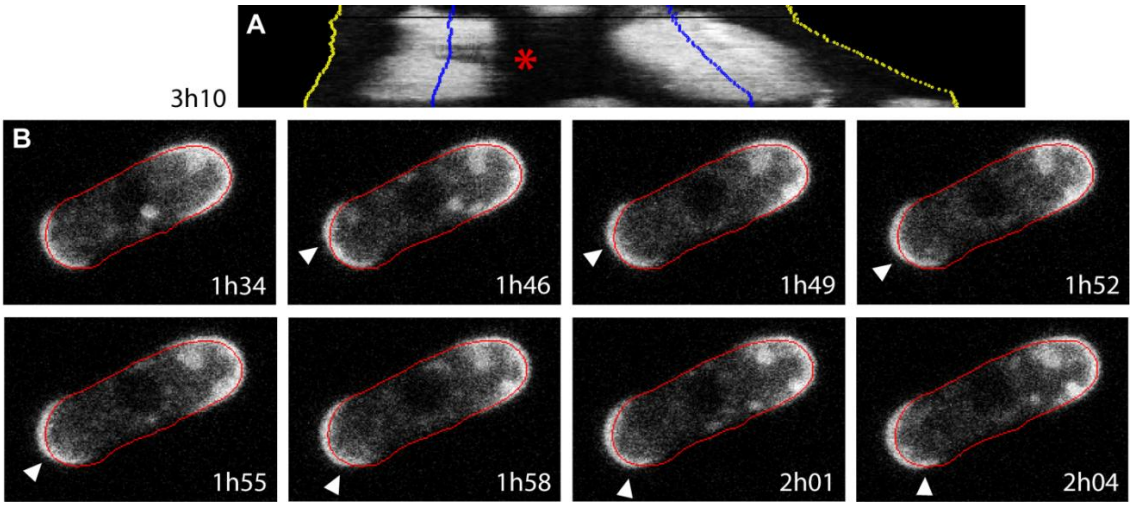

Figure 4.4. An example of a cell in which the plasma membrane (visualized with GFP-Tna1) locally detaches from the cell wall.
A – Kymograph of the cell. The red asterisk indicates the time when the plasma membrane comes in contact with the cell wall. The kymograph starts 10 min after RS. The period displayed on the kymograph is indicated at the bottom left.
B – Several movie frames of the cell corresponding to the kymograph in **A**. Red lines indicate the cell periphery over time, defined using the phase contrast images of the cell wall (not shown; Section 3.1.4.3). Arrows indicate the border between the region where there is contact between the plasma membrane and the cell wall, and the region with a gap between the two.

what seemed like SRM redistribution between the cell ends. While the SRM domain at the primary cell end continued expanding, the domain at the secondary cell end was shrinking in most cells. However, after some time the SRM domain at the secondary cell end expanded to approximately its original size. At the beginning of P3, the domain at the primary cell end expanded to a rather stable final width. Throughout P3, the SRM domain at the secondary cell end was generally narrower than at the primary cell end, and its width varied more over time.

In a subset of cells, the secondary cell end also increased its growth speed eventually. This was chosen as the beginning of the fourth post-starvation phase (P4).

An interesting observation was that in some cells the plasma membrane transiently lost contact with the cell wall in a cell end region. This was visualized using the SRM marker GFP-Tna1. Reestablishment of contact followed fast growth initiation at the respective cell end at the beginning of P3 or P4 (**Figure 4.4**).

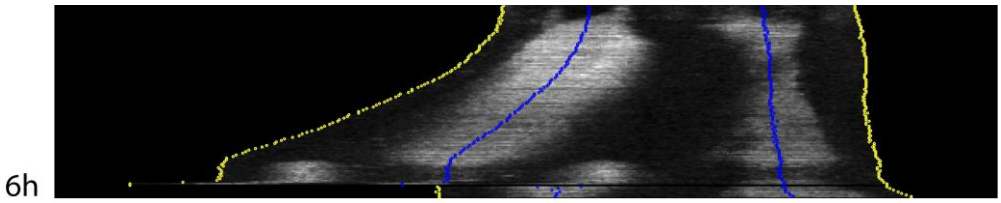

Figure 4.5. Kymograph of a post-starvation wild type cell, including cell division. At the bottom of the kymograph, the post-cytokinesis behavior of one of the daughter cells is visible. The shift of the GFP-Tna1 signal corresponding to the new end is due to the fast outward bulging of the new end after cell separation. The kymograph starts 10 min after RS. The period displayed on the kymograph is indicated at the bottom left.

The onset of the first mitosis after RS was accompanied by a drastic reorganization of SRMs (**Figure 4.3** and **Figure 4.5**). Domains at the cell ends disassembled, and strong SRM signal appeared at the site of cell division in the cell middle region. The reorganization was very fast (within about 10 min). After cell separation, SRMs covered the newly formed end of each daughter cell. Also, a new SRM domain rapidly formed at the old cell end of each daughter cell (**Figure 4.5**, bottom part of the kymograph).

4.1.2.2 Analysis of growth speed: introducing slow and fast growth

In the kymographs of wild type cells, a correlation between SRM dynamics and cell growth was observed (Section 4.1.2.1). To investigate this quantitatively, cell growth and SRM dynamics were first analyzed separately.

The quantitative description of cell growth was based on the analysis of growth profiles of individual cell ends (Section 3.1.4.6). The growth profile of a cell end was defined as the distance from the initial cell center to the cell end as a function of time. Linear segments in the growth profiles were detected automatically. These linear segments will be referred to as growth phases. The timing and speed of growth corresponding to individual growth phases are the basis for the analysis presented here.

Based on the growth profiles of both cell ends, cells can be broadly classified into the following categories: 1) one cell end initiates fast growth, the other end grows slowly until cell division (**Figure 4.6**, **A** and **B**), 2) both cell ends grow fast, initiating fast growth at different time points (**Figure 4.6**, **C**), 3) one cell end starts growing fast,

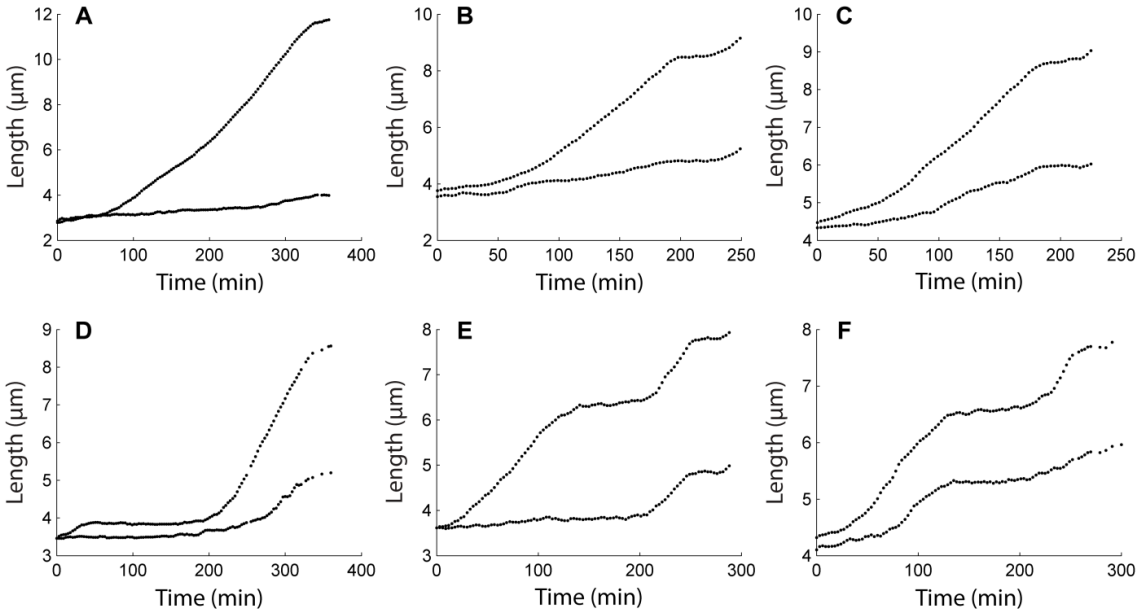

Figure 4.6. Typical growth profiles of post-starvation wild type cells. The two curves in each plot correspond to the two cell ends. The plateau at the right end of the curves corresponds to cell division. All plots start 10 min after RS.
A and **B** – Cells with a fast- and a slow-growing end.
C – A cell with two fast-growing ends, one of which initiates fast growth with a delay.
D and **E** – Cells with one end growing fast, then pausing growth; after the pause both cell ends grow fast.
F – A cell with two fast-growing ends that initiate fast growth at different time points, pause simultaneously, and then both restart growth.

then pauses, and then both cell ends start growing fast (**Figure 4.6**, **D** and **E**), 4) both cell ends start growing fast at different time points, then pause, and then restart growth (**Figure 4.6**, **F**). The plateau at the end of each growth profile corresponds to growth arrest during cell division.

To quantify the differences in wild type cell growth profiles, growth phase speeds were analyzed. As mentioned above, growth phases were defined for individual cell ends. The distribution of growth phase speeds is shown in **Figure 4.7**, **A**. It is evident that this distribution has two distinct maxima. Fitting the histogram with a double Gaussian located the minimum between the two peaks at 0.8 µm/hour. This value was set as a threshold for distinguishing two regimes of cell end growth: slow and fast growth. A cell end with growth speed above this threshold was considered

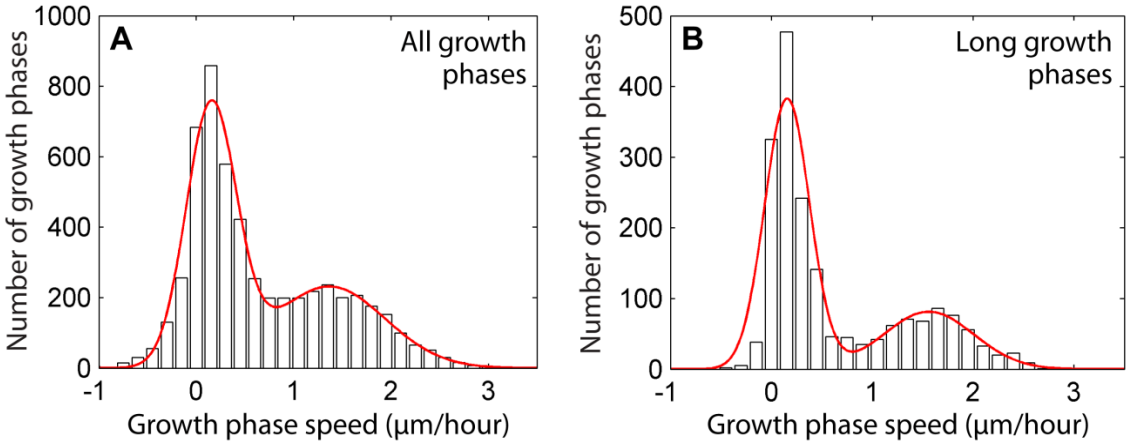

Figure 4.7. Distributions of growth phase speeds of individual cell ends for wild type cells: **A** – all detected growth phases, **B** – growth phases lasting longer than 30 min (10 time points). Red curves – double Gaussian fits.

fast-growing, otherwise it was considered slow-growing.

In the growth speed distribution, 14% of the values are negative (**Figure 4.7**, **A**). This can be due to several reasons. One obvious reason is the growth speed measurement error for short growth phases. To avoid this problem, the speed distribution of growth phases longer than 30 min, or 10 time points, was analyzed (**Figure 4.7**, **B**). This lowered the proportion of phases with negative speed to 8% and reduced the absolute values of their speeds. Another possible reason for the occurrence of negative speed values is that cells may transiently shrink, for example, due to cell wall remodeling. Finally, the resolution of the images used for analysis limits the precision of cell periphery detection.

In the speed distribution for long growth phases (**Figure 4.7**, **B**), the position of the minimum separating the peaks of slow and fast growth remains at 0.8 µm/hour, as in the distribution for all growth phases. This supports the choice of that value as the threshold separating slow and fast growth. The minimum between the two peaks is considerably more pronounced in the speed distribution for long growth phases than in that for all growth phases. This is due to most phases corresponding to growth acceleration being short and not contributing to the speed distribution for long growth phases. The presence of the minimum indicates that slow growth is a distinct regime and does not merely correspond to growth acceleration.

The distinction between slow and fast growth raised the question whether each cell end reaches the stage of fast growth. To answer this question, all growth phases of an

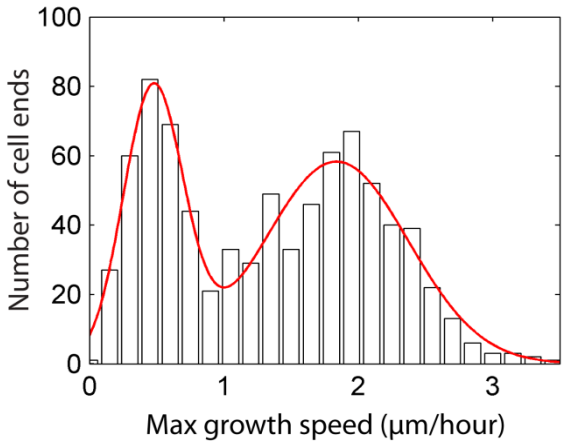

Figure 4.8. Maximal growth speed distribution for wild type cells. Red curve – double Gaussian fit.

individual cell end were compared and the phase with the maximal growth speed was determined. This was done for all wild type cells studied. The presence of two peaks in the distribution of maximal growth speeds (**Figure 4.8**) shows that a large proportion of cell ends remains below the threshold of 0.8 µm/hour and does not initiate fast growth (Section 4.1.2.3).

The maximal cell end growth speed that can be reached in post-starvation wild type fission yeast cells (termed "maximal detected growth speed") was also measured. The maximal detected growth speed depended on the set of growth phases analyzed. The sets in **Table 4.1** differed by the minimal duration of the growth phases included in the set. Selecting longer growth phases allows measuring the maximal detected growth speed more precisely, but reduces the number of growth phases considered. The maximal detected growth speed was smaller for sets of longer growth phases.

Table 4.1. Maximal detected growth speed of individual cell ends, for different minimal growth phase durations.

Minimal growth phase duration (min)	Maximal detected growth speed (µm/hour)	Number of cells considered	Number of growth phases considered
15	3.4	402	4339
21	3.3	402	3400
30	3.0	402	2212
45	2.6	355	1032
60	2.4	250	479

The highest growth speed measured was 3.4 μm/hour, for growth phases at least 15 min long (5 time points).

4.1.2.3 Classification of growth patterns

Based on the dynamics of the two ends of wild type cells considered conjointly, a classification of growth patterns was introduced.

To study cell growth patterns, the moments of fast growth initiation for the two cell ends had to be determined. In the automated image analysis software, the moment of fast growth initiation was defined as the beginning of the first growth phase with a growth speed above 0.8 μm/hour. This growth phase had to last for at least 15 min (5 time points) to be considered. The moments of fast growth initiation determined automatically and by visual inspection of the kymographs coincided (**Figure 4.9**). This confirms that the speed threshold for fast growth was chosen well.

Automated determination of the fast growth initiation moments for both ends of all wild type cells analyzed enabled a quantitative study of cell growth patterns. Only cells imaged up to the first cell division were used for growth pattern classification. Cells were classified into those that eventually initiated fast growth 1) at both cell ends ("fast-bipolar") and 2) at one cell end with the other growing slowly until cell division ("fast-monopolar"). 34% of cells (out of 102) fell into the category of fast-bipolar, 66% were fast-monopolar. No cells were found that did not initiate fast growth at at least one cell end during the first cell cycle after RS. Visual inspection of the kymographs confirmed the automated classification of growth patterns.

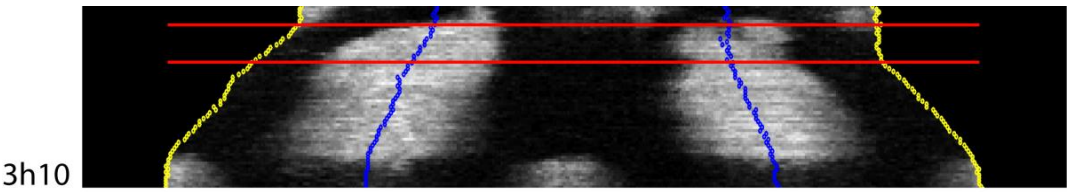

Figure 4.9. A kymograph of a wild type post-starvation cell. Red lines indicate the moments of fast growth initiation found by the automated image analysis software. The upper line corresponds to fast growth initiation of the left cell end, the lower line – to that of the right cell end.
The kymograph starts 10 min after RS. The period displayed on the kymograph is indicated at the bottom left.

4.1.2.4 Timing of the four post-starvation phases

The quantitative analysis of the four post-starvation phases included defining their starting time and measuring their duration. P1 lasted from RS to the beginning of P2. The beginning of P2 was detected from the kymographs as the moment when SRM domains started expanding at the two cell ends (independently of whether other SRM domains were still present in the cell middle region). The beginning of P3 was detected automatically as the moment when a cell initiated fast growth at one of the slowly growing cell ends (Section 4.1.2.3). Notably, the SRM expansion at the cell end switching from slow to fast growth continued for some time (see below). The beginning of P4 was detected automatically as the moment when a cell initiated fast growth at the secondary cell end, thus switching to fast-bipolar growth. In cells that did not initiate P4, P3 lasted until the beginning of cell division, which was defined as the moment when SRMs appeared at the cell division site in the kymographs and both cell ends stopped growing (these two events occurred simultaneously within the time resolution of this study). In cells that did initiate P4, P4 lasted until the beginning of cell division. Starting times and durations of the four phases are summarized in **Table 4.2**. The first two phases, P1 and P2, were shorter than the following two phases, P3 and P4, corresponding to fast-monopolar and fast-bipolar growth.

As mentioned above, the end of SRM polarization and the beginning of fast-monopolar growth did not necessarily occur simultaneously. To characterize SRM dynamics at the P2/P3 transition, the actual end of SRM polarization was determined. It was defined as the moment when all SRM domains in the cell middle region disappeared in the kymographs, and only SRM domains at the cell ends remained. SRM polarization was completed 50 ± 30 min after RS (n = 433). The period of time between the end of SRM polarization and the beginning of P3 was 10 ± 23 min (n = 275). In a significant proportion of cells (41%, n = 275), P3 started before SRM polarization was completed. These results imply that, although

Table 4.2. Timing of the four post-starvation phases.

Phase	Starting time (min after RS)	Duration (min)
P1	0	34 ± 18 (n = 269)
P2	34 ± 18 (n = 269)	30 ± 22 (n = 262)
P3	63 ± 33 (n = 394)	170 ± 71 (n = 108)
P4	165 ± 85 (n = 40)	82 ± 40 (n = 35)

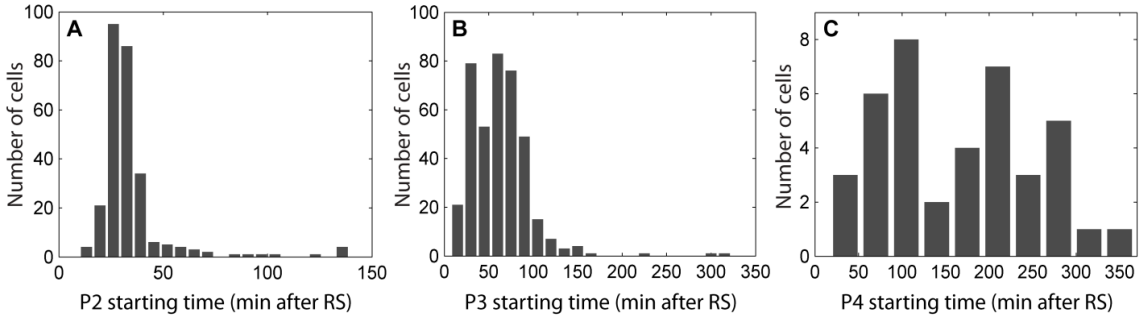

Figure 4.10. Distributions of starting times of P2 (**A**), P3 (**B**), P4 (**C**).

the completion of SRM polarization and the initiation of fast growth are very close in time, no strict regulation exists between the two processes.

Starting times of the post-starvation phases showed high variability (**Figure 4.10**). The distributions of P2 and P3 starting times had pronounced peaks, but in a small number of cells phase initiation was significantly delayed. To confirm that this delay did not result from an automated analysis error, the kymographs of corresponding cells were controlled visually. The distribution of P4 starting times was wide, with some cells initiating bipolar growth soon after RS and others doing so only shortly

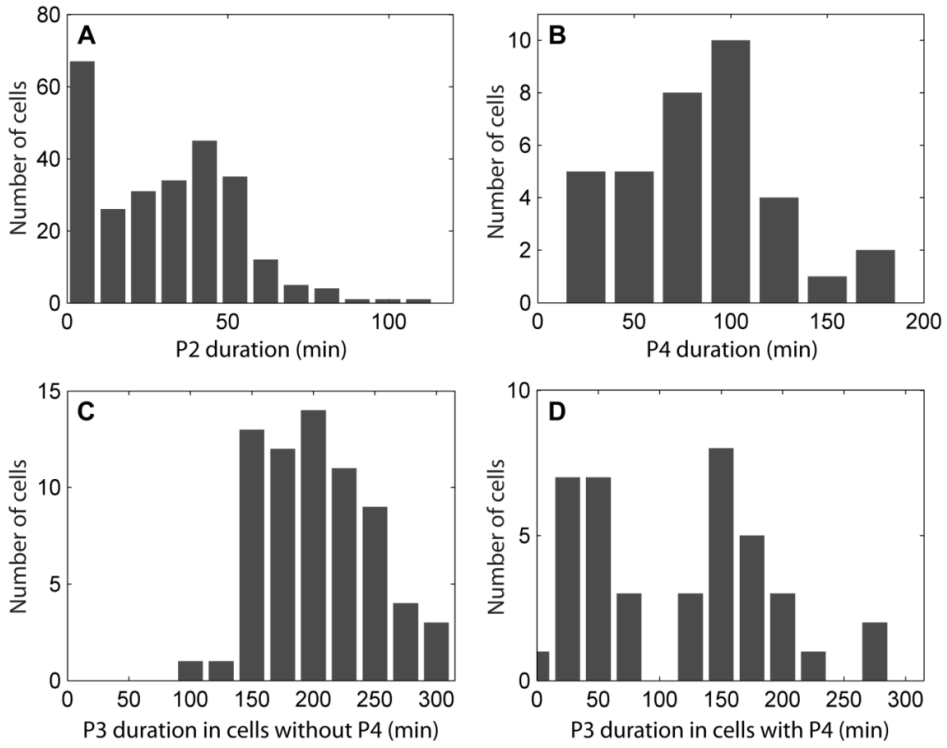

Figure 4.11. Phase duration distributions for P2 (**A**), P4 (**B**), P3 (in cells that did not initiate P4) (**C**), P3 (in cells that initiated P4) (**D**).

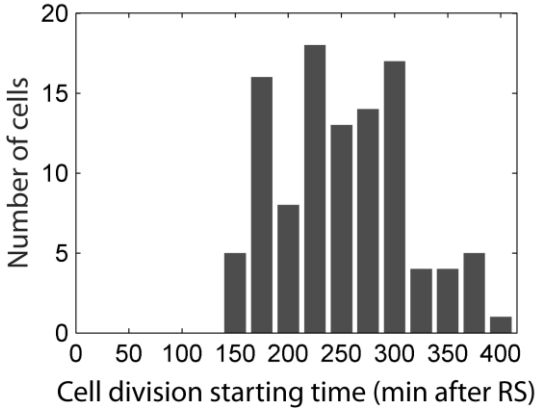

Figure 4.12. Distribution of cell division phase starting times.

before cell division. In this context, the cells never initiating P4 could be viewed as cases where cell division occurred before P4 could start.

The distribution of P1 durations coincides with the distribution of P2 starting times (**Figure 4.10**, **A**). The distributions of P2, P3, and P4 durations are shown in **Figure 4.11**. For P3, two distributions are presented: one for cells that later initiated P4 and one for those that did not. P3 duration was 116 ± 76 min (n = 40) for cells that initiated P4 and 202 ± 43 min (n = 68) for cells that did not.

The starting time of the first cell division after RS was determined for all wild type cells that were imaged until cell division. The time on a kymograph when SRMs became detectable at the division site was considered the beginning of cell division. This coincided with growth arrest at both cell ends. The beginning of cell division occurred 252 ± 60 min (n = 105) after RS (**Figure 4.12**). The time during which SRMs were present at the cell division site was about 30 min and showed little variation between cells.

4.1.2.5 Correlation between SRM dynamics and cell growth

The description of SRM remodeling and cell growth initiation presented in Sections 4.1.2.1 – 4.1.2.4 allows the analysis of the putative links between SRM domain formation and cell growth. SRM distribution at the cell membrane was characterized by the position of the center and the width of each SRM domain detected at the cell periphery (based on the 2D projection images). The position of the SRM domain center was defined relative to the closest cell end and measured along the detected cell periphery (Section 3.1.4.7).

As mentioned in Section 4.1.2.1, during P1, narrow SRM domains randomly

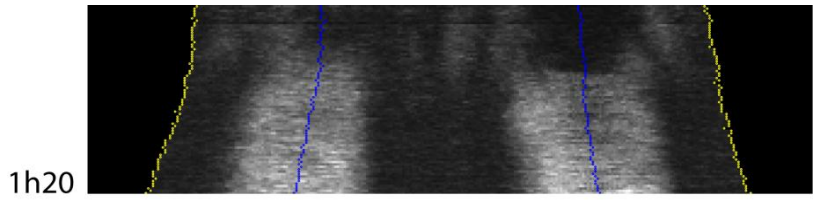

Figure 4.13. Kymograph of a cell imaged with increased time resolution (1 min intervals, rather than 3 min, as for all other kymographs), showing a more detailed view of phase transitions. The kymograph starts 3 min after RS. The period displayed on the kymograph is indicated at the bottom left.

distributed within the plasma membrane were seen on 2D projections. This SRM distribution underwent drastic changes at the P1/P2 transition. The initial SRM domains gradually shrank, two broad SRM domains formed and covered the cell ends (**Figure 4.13**).

Importantly, all the cells analyzed initiated slow or fast growth only if an SRM domain was present at the corresponding cell end. This indicates that SRMs might be a prerequisite for growth initiation. At the time of P3 initiation, the SRM domain width at the primary cell end was 4.6 ± 1.3 µm (n = 384). At the onset of P4, the SRM domain width at the secondary cell end was 4.9 ± 1.2 µm (n = 82). There was no statistically significant difference between SRM domain widths at the primary and secondary cell ends initiating fast growth.

One hour after RS, the width of wild type *S.pombe* cells was 3.5 ± 0.3 µm (n = 636). This value was measured based on the membrane signal, and thus does not include the thickness of the cell wall. Assuming the cell end to be a half sphere, the cell end arc length for a cell 3.5 µm wide would be approximately 5.5 µm. The comparison of this value to the widths of the SRM domains given in the previous paragraph shows that the cell end is mostly covered by an SRM cap at fast growth initiation. Later during P3 or P4, SRM domain width could reach about 10 µm (**Figure 4.14**), meaning that they not only covered the actual cell end regions, but also expanded into the cylindrical part of the cell.

At P3 and P4 initiation, the SRM domain was very well centered at the cell end initiating fast growth. This was quantified by determining the distance (D) from the SRM domain center to the tip of the closest cell end, measured along the cell periphery. The value of D at the beginning of P3 was 0.5 ± 0.5 µm, at the beginning of P4 it was only 0.3 ± 0.3 µm.

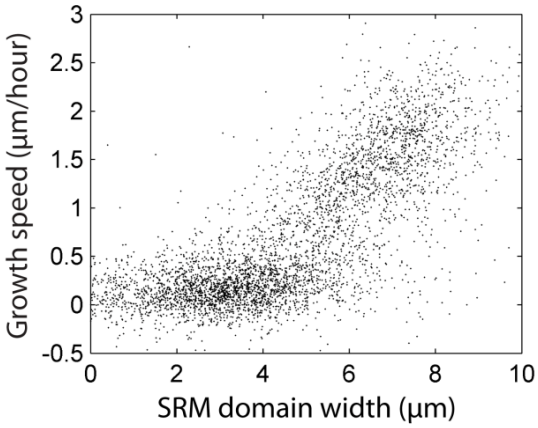

Figure 4.14. Growth phase speed *vs* SRM domain width (averaged over the growth phase) for post-starvation wild type cells. Each point corresponds to a single growth phase. Only phases longer than 15 min (5 time points) were considered.

Once a cell end had initiated fast growth, its SRM domain continued expanding until reaching a defined width. Thereafter, its width remained stable. This stability might be associated with fast growth, since during P3 the SRM domain at the secondary cell end was very dynamic. In 79% of the cells (n = 227) it was shrinking at the beginning of P3, while the domain at the primary cell end was expanding. In such cells, the SRM domain at the secondary cell end started expanding again 29 ± 15 min after P3 initiation (n = 179).

Visual inspection of kymographs indicated that the fast-growing cell ends generally had wider SRM domains than the slow-growing cell ends. To confirm this observation, the correlation between the growth speed and the width of SRM domains was studied quantitatively. A plot of growth phase speed *vs* SRM domain width (averaged over the growth phase) is shown in **Figure 4.14**. Two populations of data points can be clearly distinguished in the plot. The population of data points with growth speeds corresponding to slow growth (below 0.8 µm/hour) showed statistically significant weak correlation between domain width and growth speed (correlation coefficient R = 0.3). Linear regression of the points corresponding to slow growth gave a line with a slope of 0.05 $hour^{-1}$. The population of data points with growth speeds corresponding to fast growth also showed statistically significant weak correlation between domain width and growth speed (R = 0.3). Linear regression of these points gave a line with a slope of 0.29 $hour^{-1}$, greater than what was found for slow growth. Thus, the connection between growth speed and SRM domain width is more pronounced for fast growth. Also, the presence of two distinct

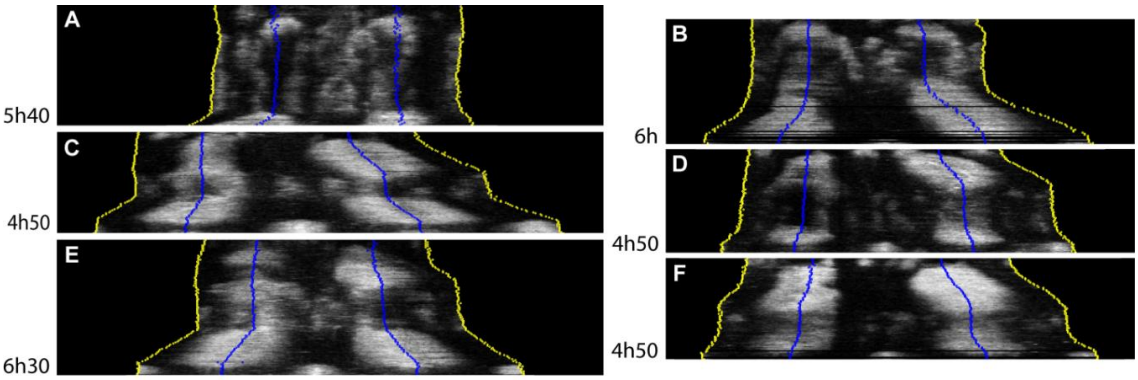

Figure 4.15. Kymographs of post-starvation wild type cells pausing at the P1/P2 transition (**A**), during P2 (**B**), during P3 (**C**, **D**, **E**), during P4 (**F**). All kymographs start 10 min after RS. The periods displayed on the kymographs are indicated at the bottom left.

populations of data points further confirms that slow and fast growth are two distinct types of fission yeast growth.

4.1.2.6 Loss of SRM polarization in pausing cells

The analysis of post-starvation wild type cells revealed a class of cells that paused SRM polarization/cell growth for up to several hours ("pausing cells"). The proportion of such cells in the population was 15.4% (n = 143). The following four subclasses were distinguished.

The first subclass paused SRM polarization at the P1/P2 transition. SRM polarization was initiated, and centrally located SRM domains started shrinking. However, this process was not completed, and SRMs returned to a random distribution at the cell periphery, characteristic of P1 (**Figure 4.15**, **A**). After some time, these cells entered P2 again and subsequently initiated fast growth.

The second subclass paused during P2 (**Figure 4.15**, **B**). These cells disorganized SRM domains at the cell ends and stopped slow growth, while SRMs reappeared at random positions in the cell middle region. After some time, these cells reinitiated normal P2 and later initiated fast growth.

The third (**Figure 4.15, C, D, E**) and fourth (**Figure 4.15, F**) subclasses paused during P3 and P4, respectively. In both cases, the pause started when cells stopped growth and lost SRM polarization, returning to a random distribution of SRMs in the cell middle region. Ultimately, these cells resumed growth.

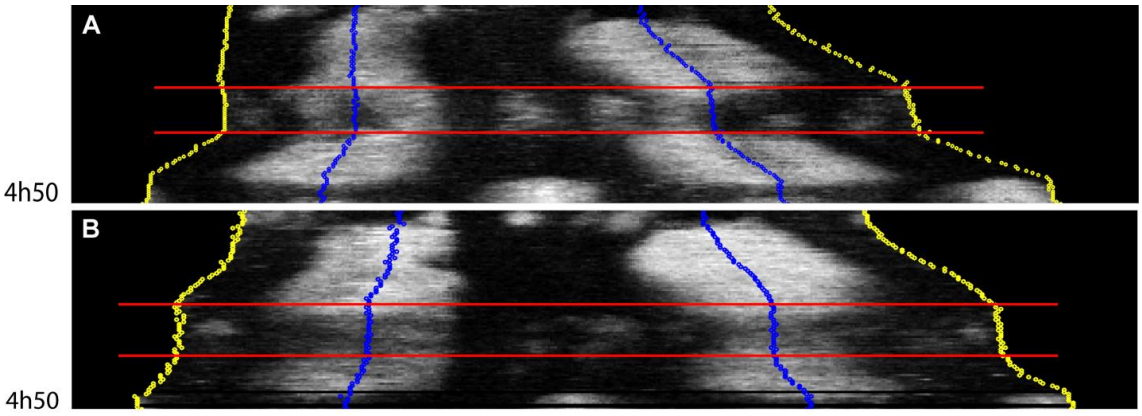

Figure 4.16. Kymographs of cells pausing in P3 (**A**) and P4 (**B**). Red lines indicate the beginning and end of the pause. The kymographs start 10 min after RS. The periods displayed on the kymographs are indicated at the bottom left.

To establish the sequence of events associated with the pause for cells pausing in P3 and P4, their kymographs were analyzed in more detail (**Figure 4.16**). Growth arrest occurred after SRM domains at the cell ends started shrinking, but before shrinkage was completed. Shortly after growth arrest, SRM domains appeared randomly at the cell periphery. At the end of the pause, cell growth restarted only after SRMs had re-polarized (broad domains formed at the cell ends, other domains disappeared from the cell middle region).

Pause duration in cells that paused in P3 and P4 was 130 ± 79 min (n = 23). The time from the beginning of P3 to the beginning of the pause was 79 ± 31 min (n = 21). The time from the beginning of P4 to the beginning of the pause was 44 ± 17 min (n = 3).

Table 4.3. Changes in cell growth pattern occurring at the pause.

Change in growth pattern	Proportion of cells
MFG to BFG	50.0%
Slow growth at both ends to MFG	13.5%
MFG (fast & no growth) to MFG (fast at the same end & slow growth)	9.1%
BFG to MFG	9.1%
MFG before and after, did not change growing end	9.1%
MFG before and after, changed growing end	4.6%
BFG to cell division phase	4.6%
Total number of pausing cells	**22**

Interestingly, a variety of growth pattern changes occurred at the pause (**Table 4.3**). Most prominently, 50% of pausing cells switched from monopolar fast growth (MFG) before the pause to bipolar fast growth (BFG) after the pause, indicating that pausing might preferentially occur at growth pattern transitions.

4.1.3 Importance of SRMs for cell growth

To establish whether SRMs play a role in *S.pombe* growth, SRMs had to be perturbed. The strongest perturbation possible is to affect the production of the lipids that constitute SRMs, so that SRM domains can't even be formed. Paulo Alves created *S.pombe* strains carrying deletions of the genes encoding the key enzymes of the ergosterol and the sphingolipid biosynthesis pathways (*erg1* and *lcb2,* respectively). These deletions resulted in cell lethality, showing that ergosterol and sphingolipids that form SRMs are essential in fission yeast.

As *erg1*Δ and *lcb2*Δ cells were not viable, pharmacological treatment was chosen as the method for perturbing SRMs. Paulo Alves released wild type cells from starvation in the presence of ketoconazole, the drug that interferes with the synthesis of ergosterol *in vivo* (Venkateswarlu & Kelly, 1996). Under these conditions, there was no apparent cell growth. Small regions of both filipin staining and GFP-Tna1 signal were present at random locations at the cell periphery. Bud6-3GFP and Crn1-GFP signals partly co-localized with these SRM domains.

The next stage of the experiment was to perform the washout of ketoconazole and study the recovery of the cells from the drug treatment. The cells were starved using the standard procedure used in this study and released from starvation in the presence of ketoconazole. After two hours, during which the cells remained in a quiescent state, the ketoconazole-containing medium was replaced with fresh, ketoconazole-free medium. With a short delay, the cells exited from their quiescent state and thereafter behaved very similarly to untreated cells released from starvation. They polarized their SRMs and initiated fast growth. All types of behaviors present in untreated cells were also found in the ketoconazole-treated cells after the drug washout: cells initiating bipolar fast growth (**Figure 4.17, A**), cells with monopolar fast growth and a stable (**Figure 4.17, B**) or an unstable (**Figure 4.17, C**) SRM domain at the secondary cell end, cells pausing growth (**Figure 4.17, D**), cells with the plasma membrane detached from the cell wall at the secondary cell end (**Figure 4.17, E**), cells with strongly delayed fast growth initiation (**Figure 4.17, F**).

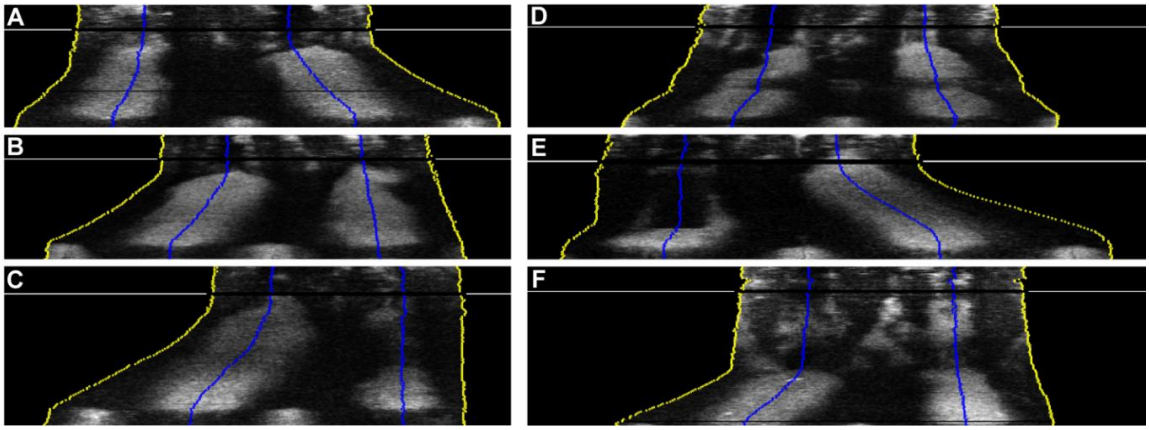

Figure 4.17. Kymographs of cells recovering from starvation in the presence of ketoconazole for two hours, then in the medium without ketoconazole. Horizontal white lines indicate the moment of ketoconazole washout. The time resolution before ketoconazole washout is 6 min, after ketoconazole washout – 3 min. All kymographs start 10 min after RS.
A – A bipolar cell. The kymograph displays a period of 6 h 30 min.
B – A monopolar cell with stable SRM domain at the secondary cell end. The kymograph displays a period of 6 h 30 min.
C – A monopolar cell with unstable SRM domain at the secondary cell end. The kymograph displays a period of 7 h 30 min.
D – A pausing cell. The kymograph displays a period of 6 h 40 min.
E – A cell with the plasma membrane temporarily detached from the cell wall at the secondary cell end. The kymograph displays a period of 6 h 10 min.
F – A cell with strongly delayed fast growth initiation. The kymograph displays a period of 8 h 10 min.

These results suggest that SRM polarization requires *de novo* SRM formation, and that it is the key initial process driving polarized growth.

Quantitative analysis of post-starvation cell behavior starting from the moment of ketoconazole washout was performed. The distribution of growth speeds was not affected by the ketoconazole treatment (**Figure 4.18**).

Fast growth initiation in ketoconazole-treated cells was delayed relative to untreated cells (**Table 4.4**; **Figure 4.19**, **A** and **B**). There was no significant difference in P3 duration in ketoconazole-treated and untreated cells that didn't initiate P4 (**Figure 4.19**, **C** and **D**). At the moment of P3 initiation, the width of the polar SRM domain at the primary cell end was not affected by the prior ketoconazole

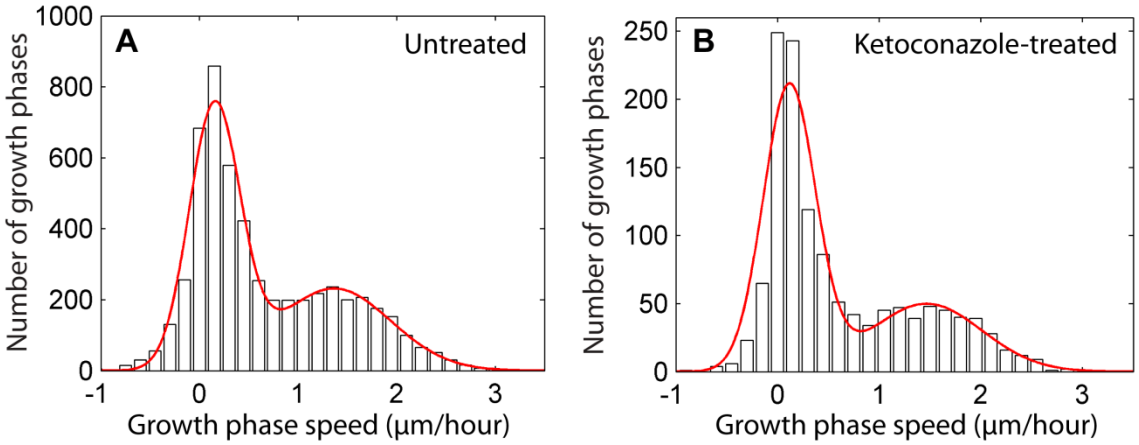

Figure 4.18. Distributions of growth phase speeds of individual cell ends for untreated (**A**) and ketoconazole-treated (**B**) post-starvation wild type cells. The latter dataset only covers the period of recovery from starvation starting at the ketoconazole washout.

treatment. The proportion of ketoconazole-treated cells with unstable SRM domains at the secondary cell ends during P3 (**Figure 4.17**, **C**) was higher than for untreated cells (**Table 4.4**). An unstable SRM domain was defined as a domain that was not detectable for at least 9 ± 3 min (3 time points).

The proportion of cells initiating P4 was lower in ketoconazole-treated cells (**Table 4.4**). The number of cells pausing growth was also reduced in the ketoconazole treatment experiment. Finally, there was a delay in the onset of cell division in ketoconazole-treated cells, as compared to untreated cells (**Figure 4.19**, **E** and **F**). This delay resulted in ketoconazole-treated cells being slightly longer by the beginning of the cell division phase (**Table 4.4**).

The analysis of ketoconazole-treated post-starvation cells showed that SRMs are essential for cell polarization and initiation of fast growth. A possible explanation of this fact is that SRMs may be necessary for the localization of proteins required for growth. To verify this, Paulo Alves correlated the localization of Bud6-3GFP and Crn1-GFP with SRMs in untreated post-starvation wild type cells. He showed that the signal of both proteins mostly co-localized with the SRMs. This includes the domains initially forming at random positions within 10 min after RS (the earliest time point acquired) and the domains observed during SRM polarization. It follows that SRMs could be functioning as essential platforms used for the assembly of the growth machinery, thus controlling the polar growth.

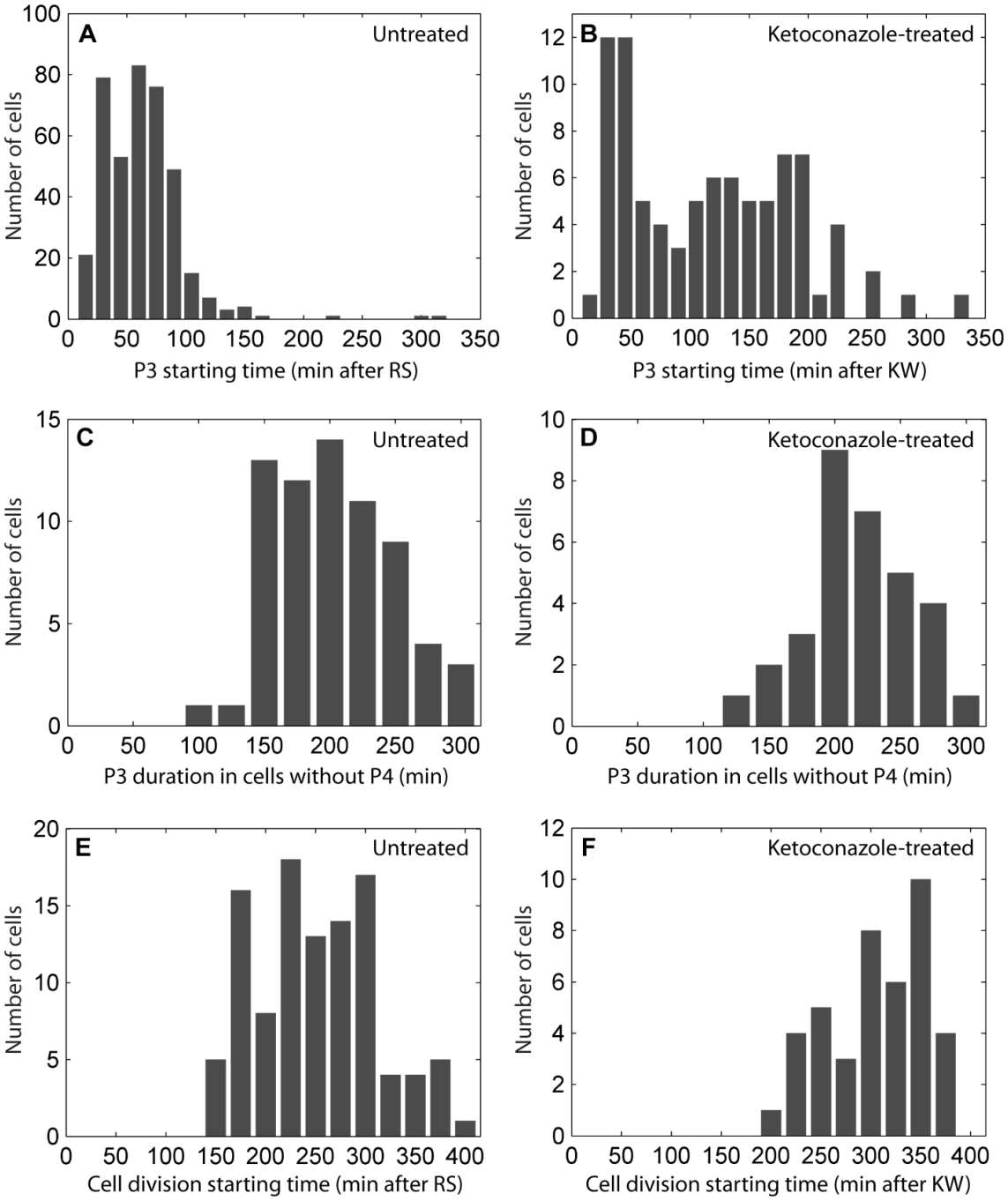

Figure 4.19. Phase timing in untreated and ketoconazole-treated post-starvation wild type cells. Distributions of P3 starting times for untreated wild type cells (time measurement started at RS) (**A**) and ketoconazole-treated wild type cells (time measurement started at ketoconazole washout, KW) (**B**). Distributions of P3 durations in untreated (**C**) and ketoconazole-treated (**D**) wild type cells without P4. Distributions of cell division starting times in untreated cells (time measurement started at RS) (**E**) and ketoconazole-treated cells (time measurement started at KW) (**F**).

Table 4.4. Comparison of ketoconazole-treated and untreated wild type cells.

Parameter	Untreated cells	Ketoconazole-treated cells
P3 starting time	63 ± 33 min after RS (n = 394) *	119 ± 72 min after KW (n = 87) *
Width of SRM domain at primary cell end at P3 initiation (µm)	4.6 ± 1.3 (n = 384)	4.9 ± 1.4 (n = 86)
Cells with unstable domain at secondary cell end	6.8% (n = 411) **	40% (n = 89) **
P3 duration in cells without P4 (min)	202 ± 43 (n = 68)	219 ± 43 (n = 32)
P3 duration in cells with P4 (min)	116 ± 76 (n = 40)	91 ± 22 (n = 5)
Cells with P4	34% (n = 102) ***	13% (n = 38) ***
P4 starting time	165 ± 85 min after RS (n = 40)	164 ± 51 min after KW (n = 5)
P4 duration (min)	82 ± 40 (n = 35)	91 ± 22 (n = 5)
Cells pausing growth	15.4% (n = 143) ***	3% (n = 89) ***
Cell division phase starting time	252 ± 60 min after RS (n = 105) *	305 ± 50 min after KW (n = 41)*
Cell length at division (µm)	13.4 ± 0.9 (n = 95) *	13.9 ± 0.8 (n = 41) *

Notes:
* numbers with a statistically significant difference (1% significance level, both the nonparametric Wilcoxon rank sum test and the two-sample t-test were used).
** the 99% confidence intervals of untreated and ketoconazole-treated cells do not overlap for the respective parameter.
*** the 90% confidence intervals of untreated and ketoconazole-treated cells do not overlap for the respective parameter.
"KW" indicates the moment of ketoconazole washout.

In summary, to study the link between SRMs and cell polarity, post-starvation wild type cells were imaged and analyzed automatically. The results revealed four phases describing de novo *SRM localization within the plasma membrane and cell growth initiation. The detailed analysis of individual cell end growth revealed the existence of two distinct types of growth: slow and fast growth. In cells released from starvation, SRM domains first formed at random locations at the plasma membrane. Then, SRMs started polarizing, and slow growth was initiated. Importantly, neither slow nor fast growth was initiated without an SRM domain at the corresponding cell end. When the SRM domain at a cell end reached a certain width, fast growth was initiated at that end. A redistribution of SRMs between the two cell ends was observed after that moment. In a subset of cells, fast growth was later initiated at the secondary cell end (covered with a broad SRM domain). During the cell division phase, SRMs formed a band at the site of cytokinesis. Growth pausing was observed in a subset of cells. This pause was accompanied by depolarization of SRMs and followed by a change in cell growth pattern (for example, a switch from fast-monopolar growth before the pause to fast-bipolar after the pause). A range of parameters describing the localization of SRMs, the timing of the phases, and the dynamics of cell growth was measured. This set the reference for the analysis of post-starvation cells in different environments and in different mutant backgrounds.*

Post-starvation cells treated with ketoconazole to disrupt SRMs neither initiated cell growth nor polarized their SRMs. After ketoconazole washout, the initiation of fast growth and the start of cell division were delayed, probably due to the time needed for the recovery from ketoconazole treatment (elimination of residual ketoconazole in the cells and ergosterol production). Thereafter, cells mostly behaved similarly to untreated post-starvation cells, except that the proportion of cells with unstable SRM domains at the secondary cell end was higher in ketoconazole-treated cells. These results, together with the study of the localization of growth machinery components under different conditions, suggest that SRMs are essential and fundamental to the establishment of cell polarity, to the formation of growth sites, and thus – to growth initiation in the first cell cycle after RS.

4.2 Role of F-actin and endocytosis in SRM dynamics

4.2.1 Role of F-actin in SRM polarization and cell growth

4.2.1.1 SRM dynamics in cells treated with latrunculin B

It is known that the localization of SRMs in both exponentially growing and post-starvation cells correlates with the localization of proteins involved in cell growth (Section 1.6.3). In addition, F-actin is known to be present at growth sites (Section 1.3.1). For this reason the role of F-actin in SRM positioning was studied. The experimental procedure consisted in imaging post-starvation cells in a medium containing Latrunculin B. This drug binds to G-actin and prevents its polymerization (Spector et al., 1989; Spector et al., 1983). Cells treated with latrunculin B are thus depleted of F-actin.

Of the phases described in Section 4.1.2.1 for untreated wild type cells, only P1 was observed in the kymographs of wild type cells released from starvation in the presence of latrunculin B (**Figure 4.20**). During P1, two differences in the behavior of untreated wild type cells and those treated with latrunculin B should be noted. Firstly, in untreated cells, most of the initial randomly distributed SRM domains had a stable width; in cells treated with latrunculin B, however, the domains were expanding already within 10 min following RS (start of the imaging). Also, when an SRM domain formed after imaging started, it was expanding without any lag time,

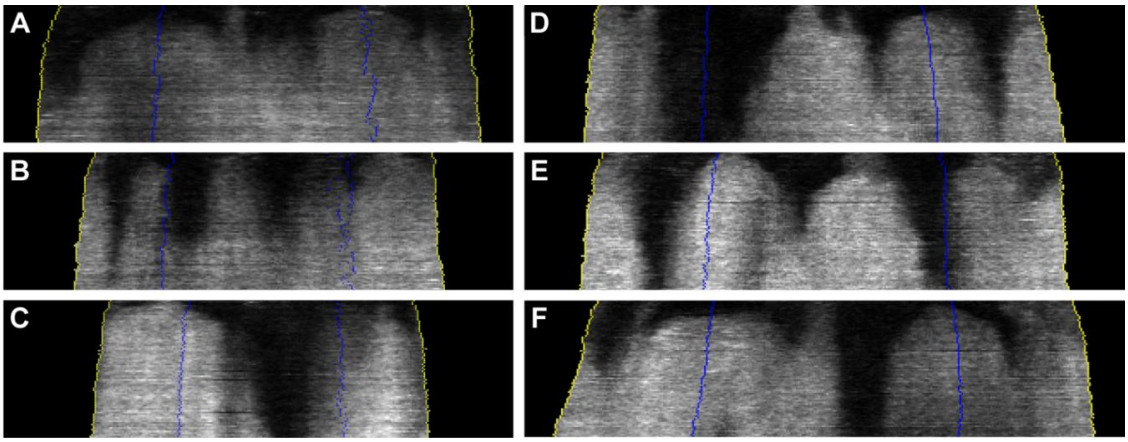

Figure 4.20. Kymographs of post-starvation wild type cells treated with latrunculin B with full (**A** and **B**) and partial (**C** to **F**) SRM coverage of the cell periphery by the end of the observation period. All kymographs start 10 min after RS and display a period of 4 hours.

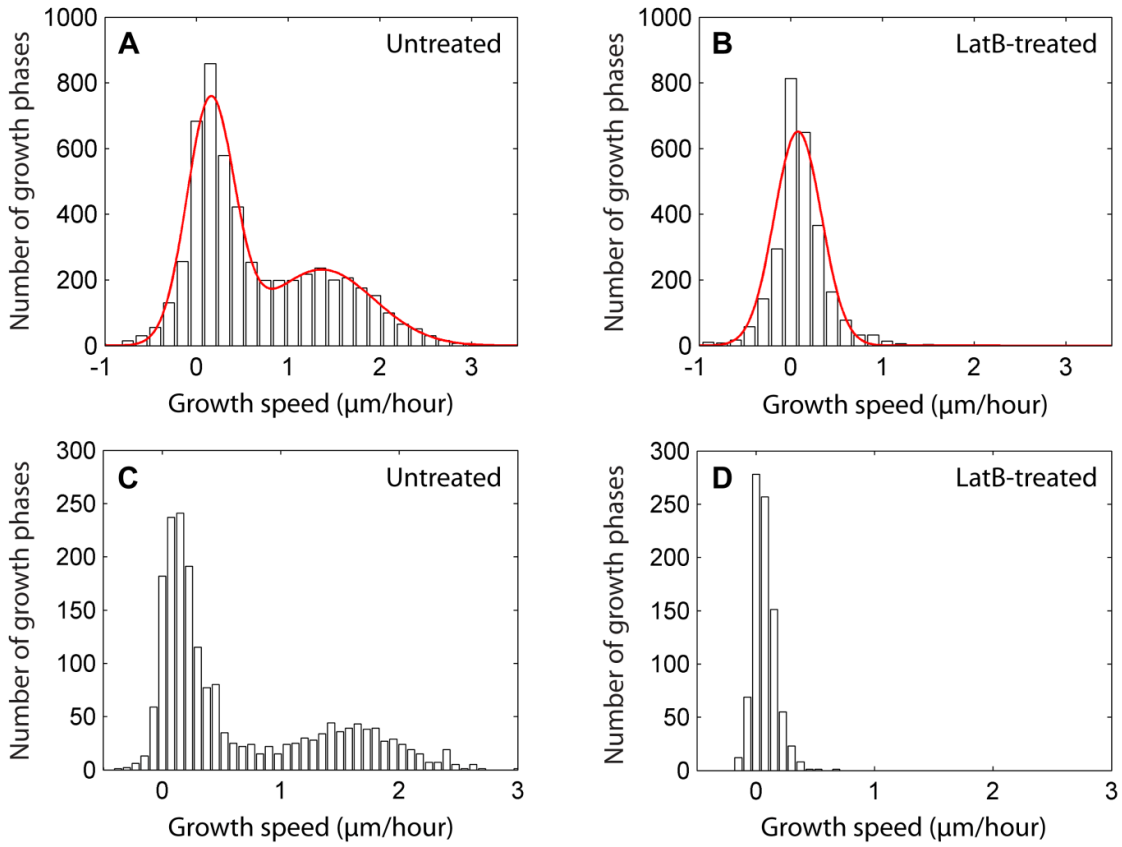

Figure 4.21. Distributions of growth phase speeds of individual ends of post-starvation wild type cells.
A – Untreated cells, all detected growth phases (red curve – double Gaussian fit).
B – Cells treated with latrunculin B, all detected growth phases (red curve – Gaussian fit).
C – Untreated cells, growth phases lasting at least 33 min (11 time points).
D – Cells treated with latrunculin B, growth phases lasting at least 33 min (11 time points).

wherever it formed (**Figure 4.20**, **D** and **F**). Secondly, in cells treated with latrunculin B, all the initial SRM domains expanded, unlike in untreated cells, where only the initial SRM domains near the cell end regions expanded. From these observations one can conclude that F-actin is involved neither in the formation nor in the expansion of SRM domains at the plasma membrane. However, F-actin is essential for the polarization of SRMs: it somehow mediates the disappearance of SRM domains in the cell middle region.

Within the four-hour observation period, the expansion of SRM domains resulted

in full SRM coverage of the cell periphery in some post-starvation cells treated with latrunculin B (as seen on the 2D projection images used in this study) (**Figure 4.20**, **A** and **B**). However, in other cells this was not the case, and low-intensity regions remained at the cell periphery throughout the observation period (**Figure 4.20**, **C** to **F**). In post-starvation wild type cells treated with latrunculin B, widths of different SRM domains varied greatly. In untreated cells, on the contrary, the width of the SRM domain at the fast-growing cell end was rather well-defined. One possible explanation for this observation would be the stabilization of domain width by the process of growth itself (discussed in Section 5.2).

Also, there does not seem to be any lateral movement of SRMs within the plasma membrane of cells treated with latrunculin B (**Figure 4.20**). This shows that the positioning of SRMs within the plasma membrane is stable, even when the SRM polarization mechanism is not functional.

4.2.1.2 Growth of cells treated with latrunculin B

Slow growth was observed in the kymographs of post-starvation wild type cells treated with latrunculin B (**Figure 4.20**). It was studied quantitatively by analyzing the growth speed distributions of all growth phases of individual cell ends. Cells treated with latrunculin B didn't initiate fast growth along the main cell axis within the four-hour observation period (**Figure 4.21**). No cell division was observed during this period either.

In addition to growth speeds of individual cell ends along the cell axis, the overall cell growth was analyzed. In the control wild type cells treated with DMSO (used as the solvent for latrunculin B), growth was highly polarized (**Table 4.5**). In cells

Table 4.5. Total cell growth over the period of 2 hours after RS for cells treated with latrunculin B and DMSO-treated control cells (n – number of cells).

	Length increase (%)	Length increase (µm)	Width increase (%)	Width increase (µm)
DMSO-treated control cells	25.0 ± 12.8 (n = 236)	1.8 ± 1.1 (n = 236)	-0.4 ± 4.1 (n = 236)	-0.02 ± 0.15 (n = 236)
Cells treated with latrunculin B	5.4 ± 1.5 (n = 225)	0.4 ± 0.1 (n = 225)	10.6 ± 3.5 (n = 225)	0.4 ± 0.1 (n = 225)

treated with latrunculin B, however, the values of the increase in cell length and cell width over two hours were similar (**Table 4.5**). This means that growth was not polarized in these cells, which correlates well with SRMs covering most of the cell periphery.

4.2.2 Role of endocytosis in SRM dynamics

4.2.2.1 Differences in endocytosis dynamics between *S.pombe* and *S.cerevisiae*

In Section 4.2.1.1 it was shown that F-actin is essential for SRM polarization. One possible mechanism for F-actin involvement in SRM polarization could be *via* endocytosis, which could be locally activated to remove SRM domains from the cell middle region. To study whether endocytosis plays a role in SRM repositioning during the recovery from starvation, endocytosis was imaged in both exponentially growing and post-starvation wild type cells. Shd1 was tagged with GFP at its C-terminus (Shd1-GFP) and used as the marker of endocytosis in fission yeast (experimental procedures can be found in Section 3.2).

Shd1 was chosen as the marker of endocytosis based on its homology to the *S.cerevisiae* endocytic marker Sla1p (Ayscough et al., 1999). Sla1p interacts with the proteins regulating actin dynamics and the proteins belonging to the endocytic machinery, acting as a link between actin cytoskeleton and endocytosis (Warren et al., 2002). It also links the endocytic cargo and actin dynamics (Mahadev et al., 2007). Sla1p is a good endocytic marker in *S.cerevisiae*, because it is present at endocytic sites throughout their lifetime. Initially, Sla1p participates in the formation of a non-motile complex at the plasma membrane. At a later stage, it is part of the complex that is moved from the plasma membrane inwards at the tip of the tubular membrane invagination. The complex is then disassembled (Kaksonen, Sun & Drubin, 2003).

The dynamics of Shd1 in *S.pombe* was similar to the reported dynamics of Sla1p in *S.cerevisiae*. In an exponentially growing cell, an Shd1 dot first appeared at the cell periphery. After some time, the dot moved away from the plasma membrane into the cytoplasm (underwent internalization) and disappeared (**Figure 4.22**). The similarity between the dynamics of Shd1 and of Sla1p indicates that Shd1-GFP is a good endocytic marker in *S.pombe*.

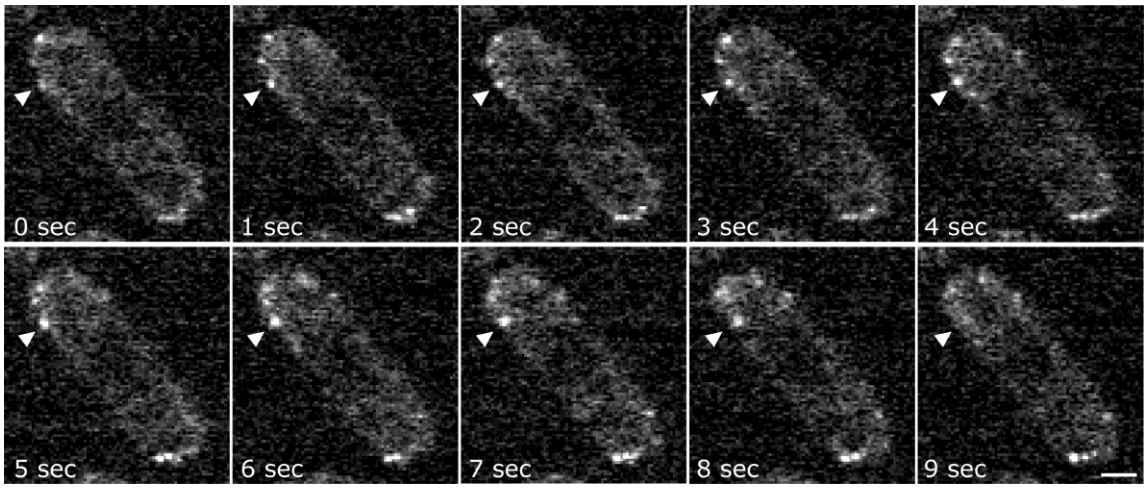

Figure 4.22. Individual frames from a time-lapse movie visualizing the dynamics of an Shd1 dot (indicated with an arrow) in an exponentially growing cell. A single z-plane was imaged. Scale bar represents 2 µm.

The overall distribution of the endocytic activity in exponentially growing cells is shown in **Figure 4.23**. In interphase, Shd1 dots that visualize endocytic sites were distributed randomly at the cell cortex with a higher density at the cell ends. In dividing cells, endocytic sites were denser at the site of cytokinesis with some endocytic sites also distributed randomly at the cell periphery. After the two daughter cells had separated, endocytic sites reorganized to a random distribution with a higher density at the cell ends.

To measure the lifetime of Shd1 dots, the kymographs of individual dots were

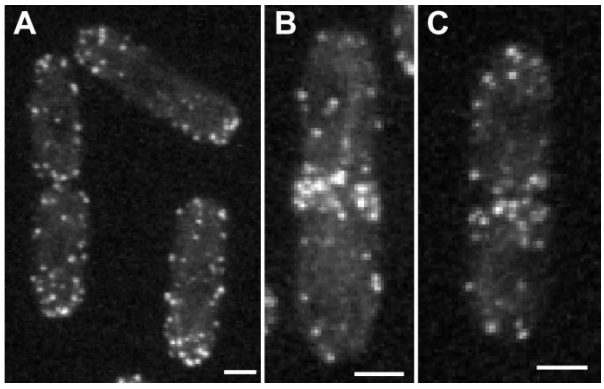

Figure 4.23. Localization of endocytic sites (visualized with Shd1-GFP) in exponentially growing cells in interphase (**A**), during cytokinesis (**B**), at the end of cytokinesis (**C**). The images are maximum projections of 17 z-planes acquired with 0.5 µm z-spacing. Scale bars represent 2 µm.

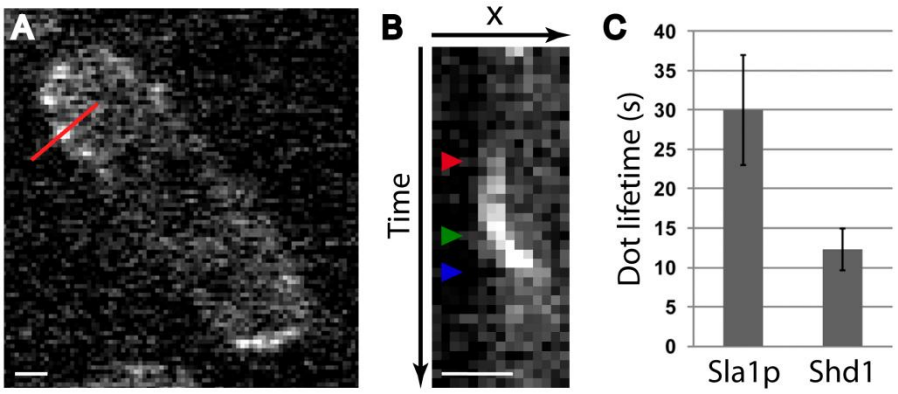

Figure 4.24. The lifetime of individual Shd1 dots. Scale bars represent 1 μm.
A – The intensity profiles for the construction of the kymograph, used for measuring the lifetime of an individual Shd1 dot, were extracted along the red line over time.
B – The appearance of an Shd1 dot (red arrow), the beginning of its internalization (green arrow), and its disappearance (blue arrow). Each pixel along the time axis corresponds to 1 s.
C – Comparison of lifetimes of Sla1p dots in *S.cerevisiae* and Shd1 dots in *S.pombe*.

analyzed. The kymograph of an Shd1 dot was produced using the intensity profiles taken at successive time points along the line passing through the dot and perpendicular to the cell periphery (**Figure 4.24, A**). The lifetime of an Shd1 dot was measured as the time span between the dot appearance and disappearance in the kymograph (**Figure 4.24, B**). The lifetime of Shd1 dots was found to be 12.3 ± 2.6 s (**Figure 4.24, C**). This value is smaller than the published lifetime of Sla1p dots (30 ± 7 s) in budding yeast (Kaksonen et al., 2003). This cannot be accounted for by the difference in the measurement methods used (Sla1p dot lifetimes were measured by direct tracking of the dots over time). This result shows that Shd1 in *S.pombe* is present at endocytic sites for a shorter time than its homolog Sla1p in *S.cerevisiae*. This observation complements a study of the dynamics of a range of proteins localized at endocytic sites in *S.pombe* (Sirotkin et al., 2010), in which Shd1 dynamics was not considered.

4.2.2.2 Endocytosis and SRM polarization

In Section 4.1.2.1 it was shown that SRMs polarized in post-starvation wild type cells. Before the beginning of the polarization, SRM domains were randomly distributed at the cell periphery. When polarization was completed, SRMs were

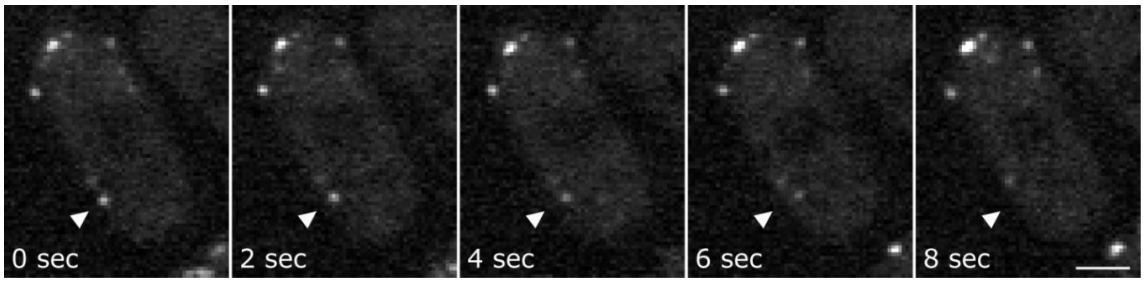

Figure 4.25. Individual frames from a time-lapse movie visualizing the internalization of an Shd1 dot (indicated with an arrow) in a cell in starvation. A single z-plane was imaged. Scale bar represents 2 µm.

covering both cell ends, and there were no SRM domains in the cell middle region. A qualitative analysis of the kymographs did not reveal any lateral movement of SRMs within the plasma membrane during the polarization. This indicates that SRMs are polarized *via* the removal of the initial SRM domains from the cell periphery and the transport of SRMs to the cell ends. A logical mechanism for the removal of the initial SRM domains would be endocytosis. In this case, it would be expected that during P2 there would be an increase in endocytic activity at the disappearing SRM domains. To study the potential role of endocytosis in SRM polarization, Shd1 dots were imaged over time in starved and post-starvation cells.

In starved cells, endocytic activity was strongly reduced in comparison with exponentially growing cells, as visualized by the reduced density of Shd1 dots at the cell periphery (**Figure 4.25**).

In post-starvation wild type cells, two distinct phases of endocytosis recovery were observed (**Figure 4.26**). The first phase was characterized by a gradual increase in the number of endocytic sites. Within about half an hour after RS, their number increased to the value typical for exponentially growing cells. This timing roughly corresponds to the beginning of SRM polarization (Section 4.1.2.4). The second phase was characterized by the gradual polarization of endocytic sites. In starvation and during the initial period after RS, endocytic sites were randomly distributed at the cell cortex. Within about an hour after RS, the distribution of endocytic sites at the cell cortex reached the situation typical for exponentially growing cells: their density was higher at the cell ends. The end of the partial polarization of endocytic sites correlated in time with the end of SRM polarization and the moment of fast growth initiation in post-starvation wild type cells (Section 4.1.2.4).

The qualitative analysis of the time-lapse movies (3 hours long, 3 min time

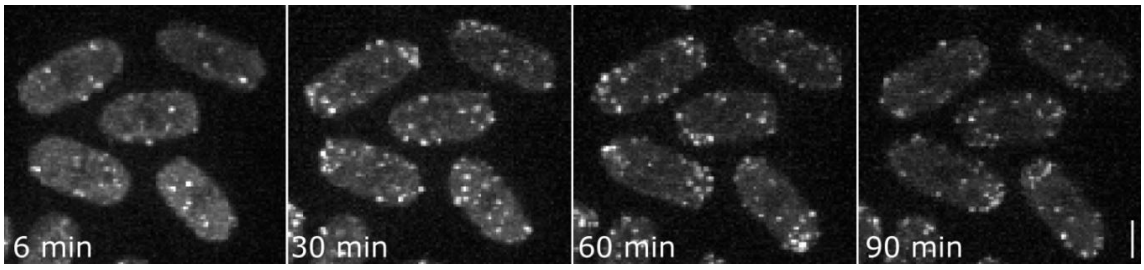

Figure 4.26. Localization of endocytic sites (visualized with Shd1-GFP) in post-starvation wild type cells. Time measurement started at RS. Time resolution of the imaging was 3 min. Images represent maximal projections of 18 z-planes acquired with 0.5 µm z-spacing. Scale bar represents 2 µm.

resolution) showed no sudden burst in endocytic activity at any time. This suggests that endocytosis is not the main process responsible for the quick internalization of the SRM domains located in the cell middle region at the P1/P2 transition.

Although the data presented above suggest that endocytosis is not directly responsible for the quick internalization of the SRM domains located in the cell middle region, the timing of endocytic site polarization correlates with the timing of SRM polarization. Furthermore, Paulo Alves showed that actin patches mostly colocalized with the SRM domains during P1. As actin patches are believed to form at endocytic sites, this partial colocalization indicates that the positioning of endocytic sites and of SRMs may be linked.

In summary, the results on the role of F-actin and endocytosis in SRM polarization were presented in this section. It was concluded that F-actin is essential for SRM polarization, because when F-actin was depleted pharmacologically in post-starvation cells, all initial SRM domains expanded, leading to the coverage of a large part of the cell periphery with SRMs. Post-starvation wild type cells where F-actin was depleted grew slowly and nearly isotropically. This is in agreement with the coverage of the greater part of the cell periphery with SRMs, as well as with the random distribution of the proteins involved in growth in these cells.

A likely mechanism for the control of SRM polarization by F-actin would be by means of endocytosis that could be responsible for the removal of the initial SRM domains from the middle part of the plasma membrane. However, endocytosis does not seem to be directly responsible for the SRM polarization, as there was no sudden burst of endocytic activity at the locations where SRMs were rapidly disappearing during SRM polarization. Instead, endocytic sites and SRMs were polarizing in parallel in post-starvation cells. By the typical SRM polarization starting time, endocytic activity reached its normal level after having a decreased level in starvation. Endocytic sites were partially polarizing simultaneously with the SRMs: the density of endocytic sites at both cell ends was increasing.

4.3 Role of microtubule cytoskeleton in SRM dynamics

4.3.1 Microtubule-mediated SRM stabilization

In Section 4.2.1, it was shown that F-actin is essential for SRM polarization. When F-actin was depleted in post-starvation wild type cells, all initial SRM domains expanded, and most of the cell periphery became covered with SRMs. Thus, F-actin is involved in SRM removal from the plasma membrane. This removal would have to be counteracted by an SRM stabilization mechanism acting specifically at the cell ends in wild type cells. Microtubules are known to target cell ends very efficiently with their plus ends. Some of the proteins transported on microtubules could be involved in SRM stabilization at the cell ends. Also, some of these proteins are known to be essential for defining growth sites (Section 1.4). Elucidating the role of such proteins with respect to SRMs would allow the study of the link between the positioning of SRMs and of growth sites.

To study the role of microtubules in SRM positioning, microtubules were depolymerized pharmacologically. Starved wild type cells were pre-treated with MBC, resulting in the absence of microtubules in these cells at RS. The cells were released from starvation with fresh medium containing MBC, and their recovery from starvation was imaged (Section 3.1.2). Paulo Alves showed that MBC treatment worked efficiently: microtubules were depolymerized throughout the first cell cycle after RS.

As MBC was dissolved in DMSO, control cells were treated with DMSO alone, following the same protocol. The kymographs showed no obvious differences in SRM dynamics (including SRM polarization) between DMSO-treated and untreated wild type cells. In some DMSO-treated cells, there was fast-bipolar growth with stable SRM domains at both cell ends (**Figure 4.27**, **A**). In other cells, there was fast-monopolar growth within the observation period with a stable (**Figure 4.27**, **B** to **D**) or unstable (**Figure 4.27**, **E**) SRM domain at the secondary cell end. In some cells, fast growth initiation was strongly delayed (**Figure 4.27**, **F**). In such cells, SRM domains were not properly polarized during the growth delay. Even if they were localized mostly to the cell end regions, SRM domains were not properly formed, similarly to those in untreated wild type cells with delayed fast growth initiation. In conclusion, the similarity of the kymographs of DMSO-treated cells to those of untreated cells confirms the possibility of using the results obtained

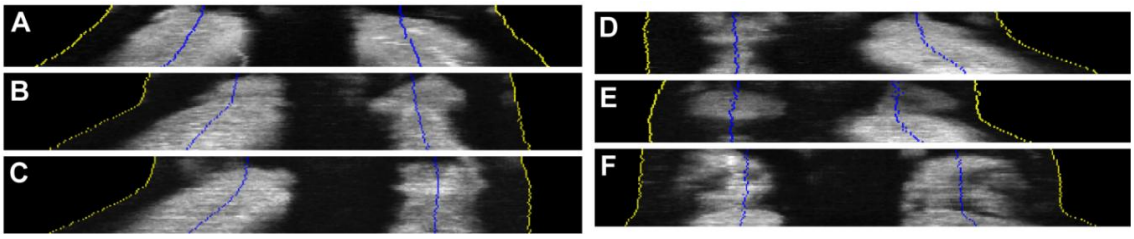

Figure 4.27. Kymographs of DMSO-treated post-starvation wild type cells. All kymographs start 10 min after RS. The periods displayed on the kymographs are: A, D, and E – 2 hours; B, C, and F – 2 hours 30 min.
A – A cell with fast-bipolar growth and stable SRM domains at both cell ends.
B, **C**, **D** – Cells with fast-monopolar growth and stable SRM domains at the secondary cell ends.
E – A cell with fast-monopolar growth and an unstable SRM domain at the secondary cell end.
F – A cell with delayed initiation of fast growth.

for DMSO-treated cells as a reference for MBC-treated cells.

The kymographs of MBC-treated post-starvation cells showed no noticeable difference with the kymographs of DMSO-treated or untreated wild type cells during P1 and P2 (**Figure 4.27** and **Figure 4.28**). Initial SRM domains formed at the cell periphery and polarized normally in cells with depolymerized microtubules. This suggests that microtubules are not involved in either of the two processes.

The differences between MBC-treated and control cells became noticeable during P3 and P4. SRM and growth dynamics in MBC-treated and control cells showed both some similarities and some differences. Similarly to control cells, MBC-treated cells were of the following types: cells with fast-bipolar growth and stable SRM domains at both cell ends (**Figure 4.28**, **A**), cells with fast-monopolar growth and stable SRM domains at the secondary cell ends (**Figure 4.28**, **F**), and cells with strongly delayed fast growth initiation (**Figure 4.28**, **D**).

A much higher proportion of cells with fast-monopolar growth and unstable SRM domains at the secondary cell ends was found in MBC-treated than in control cells. There were different degrees of SRM domain instability: from short (**Figure 4.28**, **G**) to extended periods of domain absence (**Figure 4.28**, **H** to **J**). The SRM domain at the secondary cell end was disappearing at the beginning of P3, shortly after fast growth initiation at the primary cell end, while the domain at the

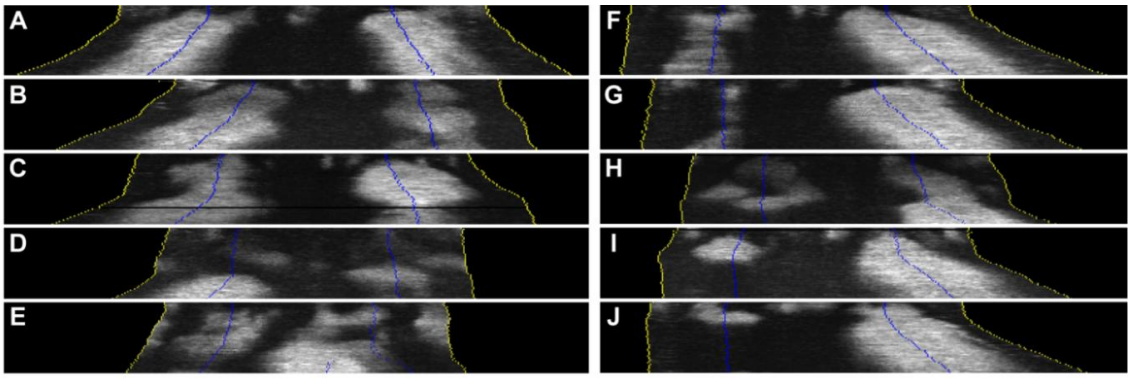

Figure 4.28. Kymographs of MBC-treated post-starvation wild type cells. All kymographs start 10 min after RS and display a period of 2 hours 30 min.
A – A cell with fast-bipolar growth and stable SRM domains at both cell ends.
B and **C** – Cells with a growth slowdown (right side of the kymographs). The slowdown was followed by the shrinkage of the corresponding SRM domain.
D – A cell with delayed initiation of fast growth.
E – A branching cell with a new end forming in the cell middle region. The formation of the new cell end is visualized by the line of blue dots at the bottom center of the kymograph. A large SRM domain is present at the newly forming end.
F – A cell with fast-monopolar growth and a stable SRM domain at the secondary cell end.
G to **J** – Cells with fast-monopolar growth and unstable SRM domains at the secondary cell ends.

primary cell end was expanding. Importantly, in the absence of an SRM domain at the secondary cell end, no growth was detected at that end. During SRM domain shrinkage, slow growth at the secondary cell end stopped (**Figure 4.28**, **I** and **J**).

A special class of MBC-treated cells was that of branching cells. These were rare: they represented only about 1% of the cell population (n = 234). Branching cells had a distinctive pattern of SRM distribution at their surface (**Figure 4.28**, **E**). At the end of P2, SRMs were absent from the two cell ends in these cells. Instead, a well-formed SRM domain was positioned in the cell middle region, at the location of the newly forming cell end. The time point when the new cell end became prominent enough to be detected corresponds to the appearance of a new line of blue dots in the kymograph (**Figure 4.28**, **E**).

Another class of MBC-treated cells includes cells with a slowdown of secondary cell

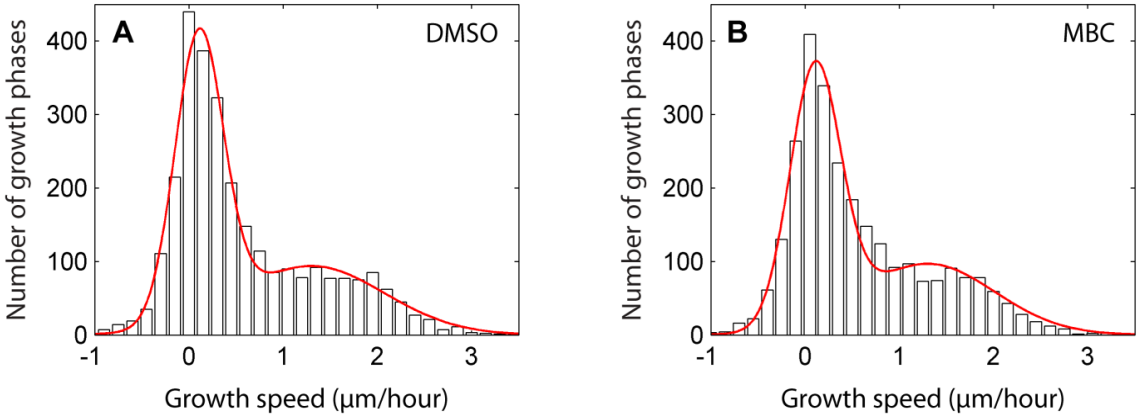

Figure 4.29. Distributions of growth phase speeds of individual cell ends of DMSO-treated control wild type cells (**A**) and MBC-treated wild type cells (**B**). Red curves – double Gaussian fits.

end growth (**Figure 4.28**, **B** and **C**). While growth at the secondary cell end was slowing down, the corresponding SRM domain was shrinking. This occurred nearly simultaneously with the speedup of primary cell end growth and the expansion of the SRM domain at that end.

Despite the important differences in cell behavior observed in the kymographs of MBC-treated cells and DMSO-treated control cells, there were no major differences in their growth phase speed distributions (**Figure 4.29**). Both distributions show the presence of slow growth and fast growth regimes that correspond to the two peaks on the double Gaussian fit.

Post-starvation phase timing and SRM domain stability in MBC-treated and control cells are compared in **Table 4.6**. There was no significant difference in the starting times of P3 and P4 between MBC- and DMSO-treated cells. The duration of P3 in cells that had P4 did not differ significantly between MBC- and DMSO-treated cells either. These results could not be directly compared to the values for untreated wild type cells, because the time-lapse movies for MBC- and DMSO-treated cells were shorter than for untreated wild type cells (**Table 3.2**).

There was a clear difference between the numbers of MBC-treated and control cells with unstable SRM domains at the secondary cell end. As for the other cell types analyzed in this study, an SRM domain at a cell end was considered unstable if it was not detected for at least 9 ± 3 min (3 time points). SRM instability was detected in almost half of the population of MBC-treated cells, and in a much smaller

Table 4.6. Comparison of MBC-treated and DMSO-treated (control) wild type cells.

Parameter	DMSO-treated cells	MBC-treated cells
P3 starting time (min after RS)	60 ± 27 (n = 201)	62 ± 31 (n = 234)
P3 duration in cells with P4 (min)	41 ± 22 (n = 26)	37 ± 29 (n = 39)
P4 starting time (min after RS)	73 ± 21 (n = 26)	83 ± 31 (n = 39)
Cells with unstable domain at secondary cell end	11.4% (n = 245) *	49.0% (n = 239) *

Notes:
* the 99% confidence intervals of DMSO- and MBC-treated cells do not overlap for the respective parameter.

There was no statistically significant difference between the values for MBC-treated and DMSO-treated cells in the first three rows of the table (at the 10% significance level, both the nonparametric Wilcoxon rank sum test and the two-sample t-test were used).

proportion of control cells (**Table 4.6**). This suggests that microtubule function is essential for SRM stability at the secondary cell end. At the primary cell end, no SRM instability was detected in MBC-treated cells.

There was no major difference in the P3 starting time distributions for MBC- and DMSO-treated cells (**Figure 4.30**). The distributions are rather broad. The right tails of the distributions might be truncated due to the limited length of the analyzed movies (**Table 3.2**).

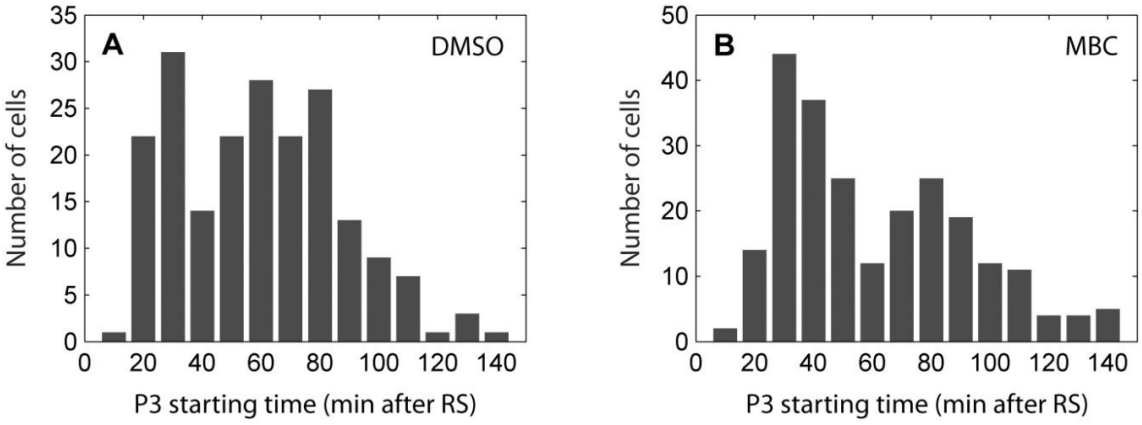

Figure 4.30. Distributions of P3 starting times for DMSO-treated (**A**) and MBC-treated (**B**) post-starvation wild type cells.

4.3.2 Influence of reduced microtubule length on SRM positioning

In Section 4.3.1, the importance of microtubules for correct positioning of SRMs was demonstrated using microtubule depolymerization experiments. To further study the role of microtubules, a mutant strain with the *mal3* gene deleted (*mal3*Δ) was analyzed. In this mutant, microtubules are shorter than in the wild type, and they do not reach the cell ends and do not deliver their cargo to the cell ends efficiently (Section 1.4.2).

The kymographs of post-starvation *mal3*Δ cells were reminiscent of the kymographs of MBC-treated post-starvation wild type cells. The two cell types had similar SRM dynamics and cell growth during the first cell cycle after RS. Some *mal3*Δ cells had fast-monopolar growth with stable (**Figure 4.31**, **A**, **B**, **E**, and **F**) and unstable (**Figure 4.31**, **C** and **D**) SRM domains at the secondary cell ends. There were also cells with fast-bipolar growth and stable SRM domains at both cell ends (**Figure 4.31**, **G**). Some cells slowed down growth at one of the cell ends (**Figure 4.31**, **E**).

In addition to straight cells, there were bent and branching *mal3*Δ cells. In bent cells, the SRM domain at a cell end was shifted sideward, and the growth direction was shifted accordingly, resulting in growth at an angle to the main cell axis and a bent cell shape. In the kymographs of such cells, this resulted in a characteristic kink of the line of blue dots indicating the position of the cell end (**Figure 4.31**, **H** and **I**). The distance between the cell end and the center of the corresponding SRM domain (which was also the center of the active growth site) varied from small (**Figure 4.31**, **H**) to larger values (**Figure 4.31**, **I**). If this distance reached a certain value, the new growth region and the cell end became separated, resulting in the formation of a new cell end. In branching cells, formation of an SRM domain in the cell middle region preceded growth initiation there (**Figure 4.31**, **J**). The proportion of branching and strongly bent cells was higher in post-starvation *mal3*Δ cells than in MBC-treated post-starvation wild type cells (**Table 4.7**).

A large proportion of *mal3*Δ cells had unstable SRM domains at the secondary cell ends during P3, although this proportion was smaller than for MBC-treated cells (**Table 4.7**). SRM domains seem more dynamic in *mal3*Δ cells (**Figure 4.31**) than in MBC-treated wild type cells (**Figure 4.28**), the main SRM domain associated with fast growth being the exception. This further confirms the importance of full-length microtubules for SRM positioning.

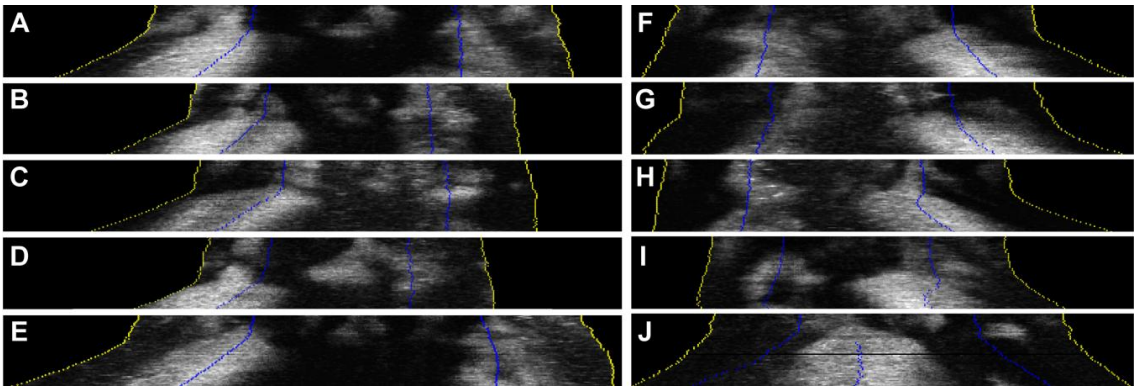

Figure 4.31. Kymographs of post-starvation *mal3*Δ cells. All kymographs start 10 min after RS and display a period of 2 h 30 min.
A to **F** – Cells with fast-monopolar growth. Cells **A**, **B**, **E**, and **F** have stable SRM domains at the secondary cell ends. Cells **C** and **D** have unstable SRM domains at the secondary cell ends. Cell **E** slowed down growth at the secondary cell end.
G – A cell with fast-bipolar growth and stable SRM domains at both cell ends.
H and **I** – Bent cells. Kinks in the lines of blue dots at the right side of the kymographs indicate that growth occurs on the side of the existing cell ends.
J – A branching cell. The formation of the new cell end can be seen in the middle of the kymograph.

Table 4.7. Comparison of untreated wild type, MBC-treated wild type, and *mal3*Δ cells.

Parameter	Untreated wild type cells	MBC-treated wild type cells	*Mal3*Δ cells
Cells with unstable SRM domain at secondary cell end	6.8% (n = 411) *	49.0% (n = 239)	30% (n = 30)
Branching cells	0 (n = 411) *	1% (n = 234) *	15% (n = 61)

Note:
* the 99% confidence intervals of the parameter for the corresponding cell type and for *mal3*Δ cells do not overlap.

In summary, in post-starvation cells with pharmacologically depolymerized microtubules, SRM polarization occurred as in control cells. The timing of P3 and P4 was also not affected.

The first striking effect that was observed in MBC-treated cells was the strongly increased instability of SRM domains at secondary cell ends during P3, as compared to control cells. This suggests that microtubules play an important role in stabilizing SRMs at the secondary cell end. The SRM domain was lost from the secondary cell end at the beginning of P3, when the primary cell end initiated fast growth, and while the domain at the primary cell end was expanding. This suggests that there may be a mechanism of SRM redistribution between the cell ends. No growth was detectable at the secondary cell end while the SRM domain was absent from that end. This provides further evidence for the requirement of SRMs for cell growth.

The second difference between MBC-treated and control cells was the presence of bent and branching cells in the population of MBC-treated cells. If the center of an SRM domain was shifted to the side of an existing cell end, the cell grew in the direction defined by the domain, at an angle to the main cell axis. This resulted in bent cells. If an SRM domain formed in the cell middle region, then cell growth occurred exclusively at that site, and a new cell end formed, leading to branching cell morphology. In branching cells, SRMs were localized at the new cell end, and no detectable SRM domains were present at the initial cell ends. These observations suggest that the localization of SRM domains dictates the positioning of growth sites in fission yeast.

The analysis of post-starvation mal3Δ *cells revealed the importance of full-length microtubules for the proper positioning of SRMs. These mutant cells are known to have short microtubules. This defect resulted in a high proportion of bent and branching cells during the first cell cycle after RS. The localization of SRMs in* mal3Δ *cells was similar to that in MBC-treated wild type cells of similar shapes and corresponded to the localization of growth sites. Importantly, in both bent and branching* mal3Δ *cells, an SRM domain was formed at a certain location, and only then growth became detectable at that site.*

In conclusion, the analysis of both MBC-treated and mal3Δ *cells revealed the importance of full-length microtubules for two aspects of SRM positioning: 1) localization of properly formed SRM domains and growth sites specifically at the cell ends; 2) SRM stability at the secondary cell end during P3.*

4.4 Role of growth markers in positioning SRMs and growth sites

4.4.1 Role of Tea1 in microtubule-mediated SRM positioning

The importance of full-length microtubules for the positioning of SRMs and of growth sites was shown in Section 4.3. The positioning of growth sites is also known to depend on the protein Tea1 that is transported to the cell ends on growing microtubule plus ends (Section 1.4.4). Since microtubules have normal length and dynamics in the absence of Tea1, Tea1 may be the link between microtubules and the SRM positioning machinery. Therefore, the role of Tea1 in SRM localization was analyzed to further study the nature of the connection between microtubules and growth site positioning. The polarization of *tea1*Δ cells during the first cell cycle after RS was imaged and analyzed.

*Tea1*Δ cells are known to have a strong morphological defect: in exponentially growing cell cultures, 37% of cells are bent or branching (Behrens & Nurse, 2002). Post-starvation *tea1*Δ cells in the present study had an even stronger morphological defect, with the following distribution of cell shapes: branching – 76%, bent – 22%, straight – 2% (total number of cells – 423). Accordingly, the kymographs of post-starvation *tea1*Δ cells fall into two categories: kymographs of cells bent to various degrees (**Figure 4.32**, **A** to **D**) and kymographs of branching cells (**Figure 4.32**, **E** to **H**). Similarly to exponentially growing *tea1*Δ cells (Mata & Nurse, 1997), post-starvation *tea1*Δ cells grew monopolar (**Table 4.9**).

Significant instability of the SRM domains at secondary cell ends can be seen in the kymographs of both bent and branching *tea1*Δ cells. Most cells lost all SRM domains not associated with the primary cell end at the beginning of P3 (**Table 4.9**). All such cells followed until division recovered some SRM domains later during P3. The recovered SRM domains were dimmer than the domain associated with the primary cell end and were not properly formed, sometimes covering a large portion of the cell periphery (**Figure 4.32**). Importantly, no detectable growth was associated with these dim SRM domains. The time during which the SRMs not associated with the growth site were absent from the plasma membrane varied greatly (70 ± 30 min from the start of P3 to SRM reappearance, n = 47).

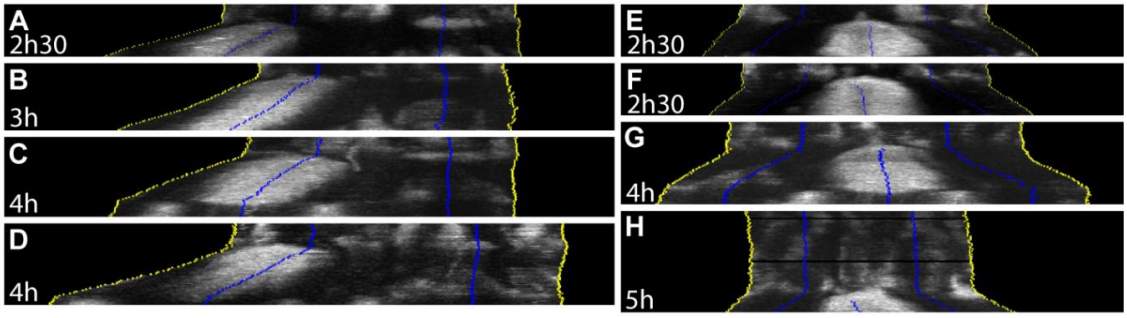

Figure 4.32. Kymographs of post-starvation *tea1*Δ cells. All kymographs start 10 min after RS. The periods displayed on the kymographs are indicated at the bottom left. The cells C, D, and G were followed until division.
A to **D** – Cells with bent morphology.
E to **G** – Cells with branching morphology.
H – A cell with strongly delayed growth initiation and branching morphology.

The dynamics of the SRM domain at the primary cell end in *tea1*Δ cells was similar to that in *mal3*Δ and MBC-treated wild type cells. Fast growth was initiated in *tea1*Δ cells almost simultaneously with the end of SRM polarization and the formation of the SRM domain at the primary cell end. The SRM domain at the primary cell end was formed directly at the site of fast growth, and no lateral movement of the domain was observed. In branching cells, the SRM domain formed in the cell middle region, defining the position of the new cell end (**Figure 4.32**, **E** to **H**).

The growth speed distribution for *tea1*Δ cells was also studied (**Figure 4.33**). The two peaks on this distribution correspond to slow and fast growth. The position of the minimum between the peaks is similar for wild type and *tea1*Δ cells (**Figure 4.33**, **A** and **B**). This justifies the usage of the same threshold for fast growth (0.8 μm/hour) for both types of cells.

A difference in the growth speed distributions of wild type and *tea1*Δ cells was observed in their fast growth regions. The position of the second maximum in the double Gaussian fit of the distribution for *tea1*Δ cells was shifted to higher speeds by 0.5 μm/hour relative to the wild type (**Figure 4.33**, **A** and **B**; **Table 4.8**). Also, the second peak of the distribution was broader for *tea1*Δ cells than for wild type cells (**Table 4.8**).

In addition to the distributions of all growth phase speeds (**Figure 4.33**, **A** and **B**),

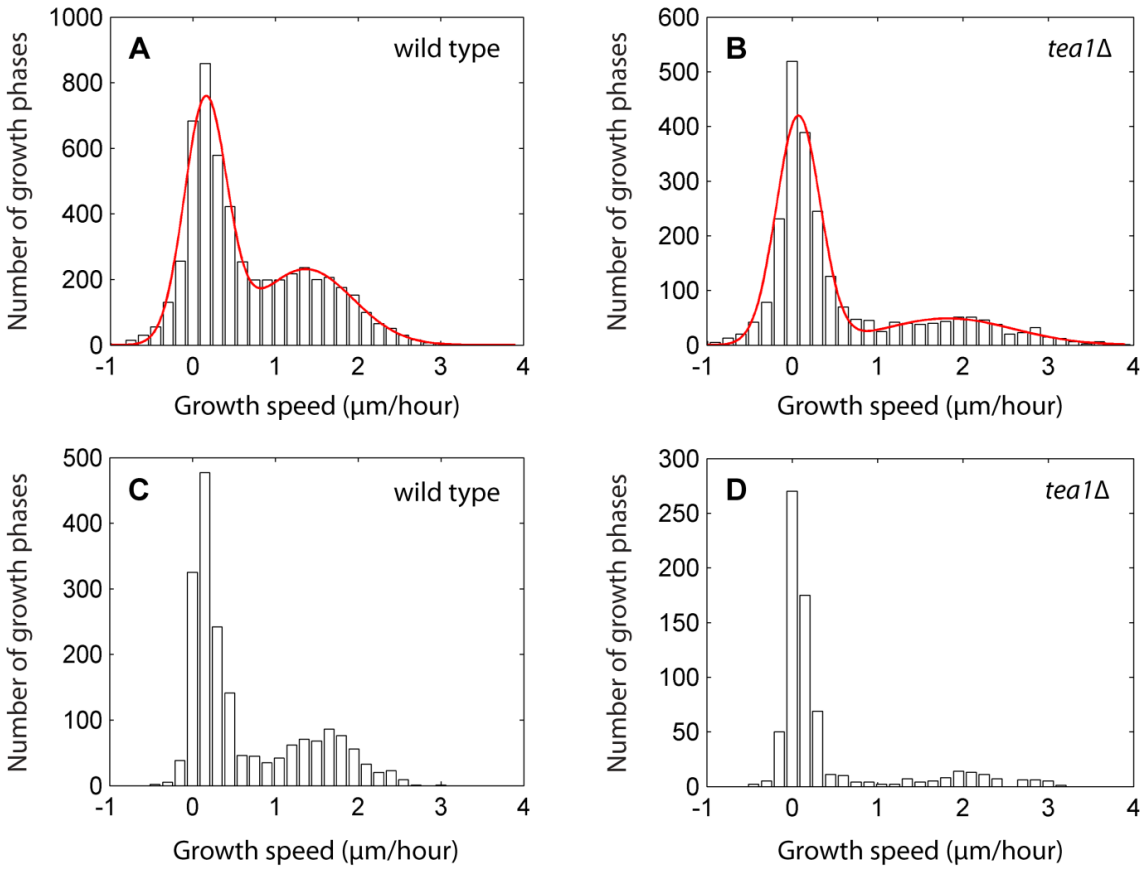

Figure 4.33. Distributions of growth phase speeds of individual cell ends. Red curves – double Gaussian fits.
A – Wild type cells, all growth phases.
B – *Tea1*Δ cells, all growth phases.
C – Wild type cells, only growth phases longer than 30 min.
D – *Tea1*Δ cells, only growth phases longer than 30 min.

the distributions corresponding to growth phases lasting longer than 30 min (10 time points) were considered for both wild type and *tea1*Δ cells (**Figure 4.33**, **C** and **D**). These distributions do not contain data from intermediate growth phases that correspond to cell end growth acceleration or deceleration. The fast growth region of the distribution of long phases in *tea1*Δ cells is shifted to higher speeds in comparison with the fast growth region of the distribution of long phases in the wild type. This is similar to what is seen in the distributions for all growth phases. This might be explained by the monopolar growth of *tea1*Δ cells: the growth machinery is concentrated at a single growth site, rather than being distributed among cell ends, as in wild type cells.

To further investigate the higher fast growth speeds in *tea1*Δ cells, the maximal growth speeds were analyzed (**Figure 4.34**). The maximal growth speed was defined

Table 4.8. Parameters of the second peaks in Figure 4.33, A and B.

Parameter	Wild type	*Tea1Δ*
Position of the maximum (μm/h)	1.3	1.8
Variance ($\mu m^2/h^2$)	0.7	1.1

for individual cells as the highest among the speeds of all growth phases of all cell ends. Similarly to the growth speed distributions of all growth phases, a shift to higher speeds is evident for the maximal growth speeds in *tea1*Δ cells, as compared to wild type. The maximum of the wild type distribution is located at 1.9 μm/hour, while for *tea1*Δ cells the maximum is at 2.4 μm/hour. It can be concluded from these results that individual cell ends generally grow faster in *tea1*Δ than in wild type cells.

Comparison of post-starvation wild type and *tea1*Δ cells revealed a delay of about half an hour in P3 initiation for *tea1*Δ cells (**Table 4.9**). This can also be seen from the distributions of P3 starting times for wild type and *tea1*Δ cells (**Figure 4.35**). A reduction in P3 duration in *tea1*Δ cells relative to wild type was also observed (**Table 4.9**). As mentioned earlier, the proportion of cells with unstable SRM domains at secondary cell ends was higher in *tea1*Δ than in wild type cells (**Table 4.9**).

Despite the difference in P3 starting times for *tea1*Δ and wild type cells, the cell division phase started at similar times in both cell types (**Table 4.9**). The beginning of this phase was defined as the moment when the SRM ring at the site of cytokinesis was first detectable. The distributions of cell division phase starting times

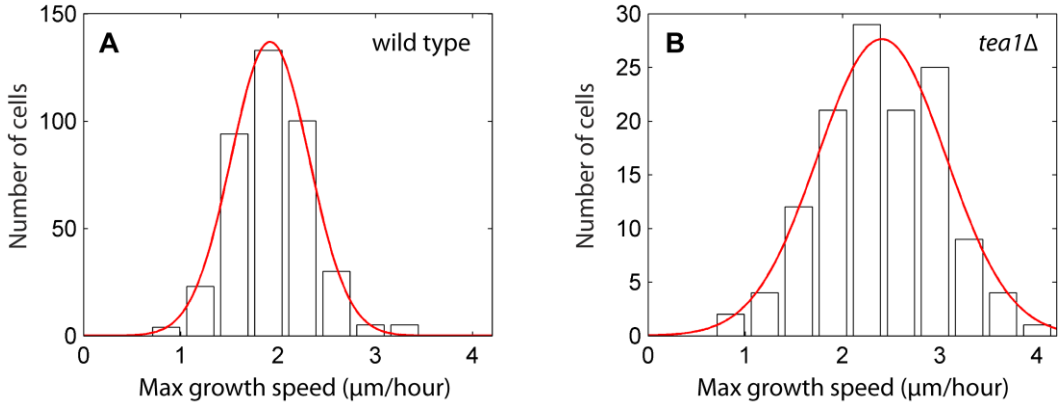

Figure 4.34. Maximal growth speed distributions for wild type (**A**) and *tea1*Δ cells (**B**). Red curves – Gaussian fits. Only growth phases at least 12 min long (4 time points) were considered.

Table 4.9. Comparison of post-starvation wild type and *tea1*Δ cells.

Parameter	Wild type cells	*Tea1*Δ cells
P3 starting time (min after RS)	63 ± 33 (n = 394) *	97 ± 37 (n = 118) *
P3 duration (min)	202 ± 43 (n = 68) * (for cells without P4)	161 ± 38 (n = 20) *
Cells with unstable domain at secondary cell end	6.8% (n = 411) **	95.7% (n = 47) **
Cells with P4	34% (n = 102) **	0 (n = 118) **
Cell division phase starting time (min after RS)	252 ± 60 (n = 105)	263 ± 50 (n = 51)

Notes:
* numbers with a statistically significant difference (1% significance level, both the nonparametric Wilcoxon rank sum test and the two-sample t-test were used).
** the 99% confidence intervals of wild type and *tea1*Δ cells do not overlap for the respective parameter.

in wild type and *tea1*Δ cells are shown in **Figure 4.36**. These distributions are rather broad and are limited at their right tails by the length of the time-lapse movies used in the analysis (**Table 3.2**).

Paulo Alves observed the presence of microtubules and the localization of Tea1 to the cell ends in starved wild type cells. As SRMs were undetectable at the plasma membrane of starved cells, this suggests that SRMs do not control the positioning of Tea1. On the other hand, the observations presented above suggest that Tea1 affects

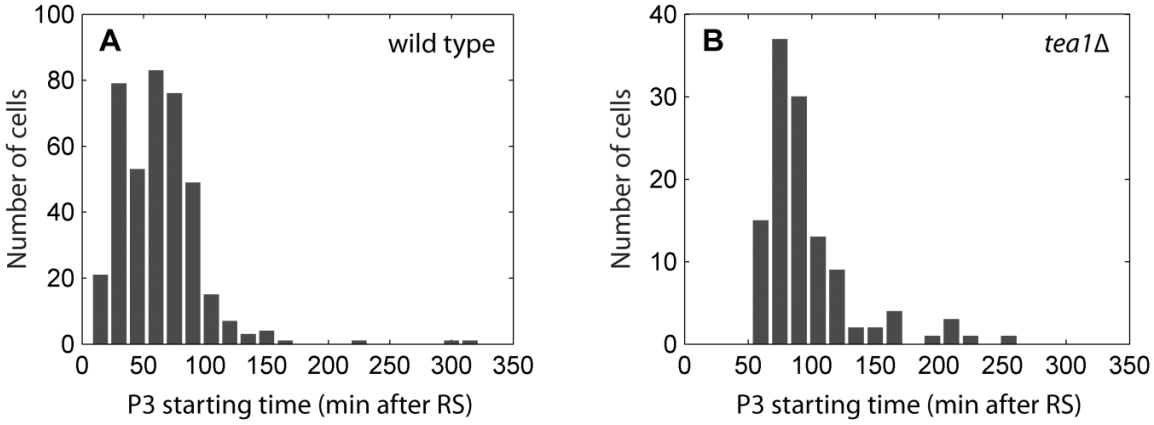

Figure 4.35. Distributions of P3 starting times of post-starvation wild type (**A**) and *tea1*Δ cells (**B**).

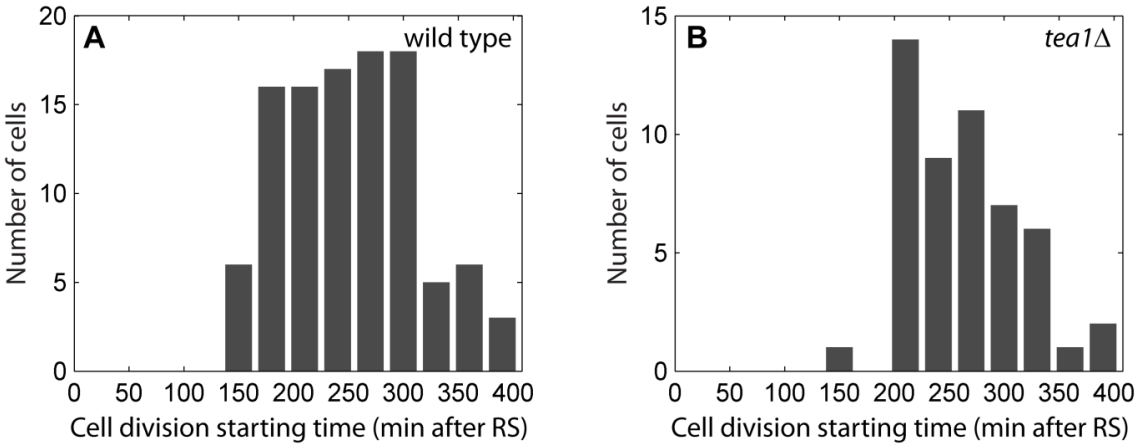

Figure 4.36. Distributions of cell division phase starting times of post-starvation wild type (**A**) and *tea1*Δ cells (**B**).

the localization of SRMs.

Based on the analysis of endocytosis in post-starvation wild type cells, it was suggested that the positioning of endocytosis and of SRMs may be linked (Section 4.2.2.2). The possibility of such a link was further analyzed by studying the dynamics of Shd1 dots in post-starvation *tea1*Δ cells, where SRM polarization was delayed.

Endocytosis recovery in post-starvation *tea1*Δ cells (**Figure 4.37**) followed the same pattern as in post-starvation wild type cells (**Figure 4.26**). First, the density of endocytic sites gradually increased from its lowered value in starvation to the density typical for exponentially growing cells. Second, endocytic sites gradually polarized. The polarization was not complete in *tea1*Δ cells: only preferential localization of endocytic sites to the cell ends was achieved, as in the wild type. Two important differences with wild type cells were observed. Firstly, *tea1*Δ cells reached the partial polarization of endocytic sites later than wild type cells (**Figure 4.37**). This correlates well with SRM polarization and growth initiation being delayed in *tea1*Δ cells. Secondly, the partial polarization of endocytic sites was monopolar in *tea1*Δ cells, instead of bipolar, as in wild type cells. *Tea1*Δ cells are known to grow monopolarly. Accordingly, endocytic sites localized preferentially to the growing end, including in branching cells. Such localization of endocytic sites correlates with SRMs being preferentially localized to the growing end in *tea1*Δ cells. Together, these results suggest that endocytosis is not the main factor responsible for localizing SRMs, but rather the preferential localization of endocytic sites coincides with SRM domains.

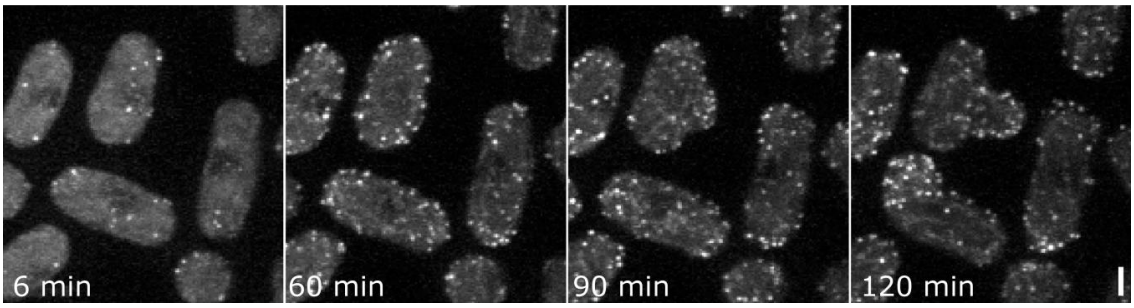

Figure 4.37. Localization of endocytosis (visualized with Shd1-GFP) in post-starvation *tea1*Δ cells. Time was measured from RS. Time resolution of the imaging was 3 min. Images represent maximal projections of 18 z-planes acquired with 0.5 µm z-spacing. Scale bar represents 2 µm.

4.4.2 Role of Tip1 in SRM dynamics

In Section 4.4.1, it was shown that Tea1 is essential for SRM localization to the cell ends. This, together with the requirement of full-length microtubules for proper SRM localization (Section 4.3), indicates that the correct localization of Tea1 is critical for SRM positioning. The protein Tip1 is known to be essential for correct Tea1 delivery to the cell ends by microtubules due to its role in anchoring of Tea1 to microtubule plus ends (Section 1.4.3). To study the role of Tip1 in SRM positioning, cells in which the gene *tip1* was deleted (*tip1*Δ cells) were imaged during the first cell cycle after RS. To visualize SRM dynamics in these cells, kymographs were created for individual cells using custom automated image analysis software (Section 3.1.4).

Kymographs revealed many similarities in SRM dynamics between post-starvation *tip1*Δ and *tea1*Δ cells. Firstly, most *tip1*Δ cells were either bent (**Figure 4.38**, **A** to **E**) or branching (**Figure 4.38**, **F** to **H**). Secondly, there was a well-formed SRM domain at the fast-growing cell end in *tip1*Δ cells. The fast-growing cell end was either one of the previously existing cell ends (bent cells) or a newly formed cell end (branching cells). Thirdly, SRM domains not associated with the primary cell end were highly unstable in *tip1*Δ cells. The time of domain absence varied from short (**Figure 4.38**, **A** and **B**) to much longer times (**Figure 4.38**, **D**).

The difference between *tip1*Δ and *tea1*Δ cells with respect to SRM dynamics was subtle. In *tip1*Δ cells, the SRM domains present during P1 (before SRM polarization) and the domains not associated with the primary cell end during P3

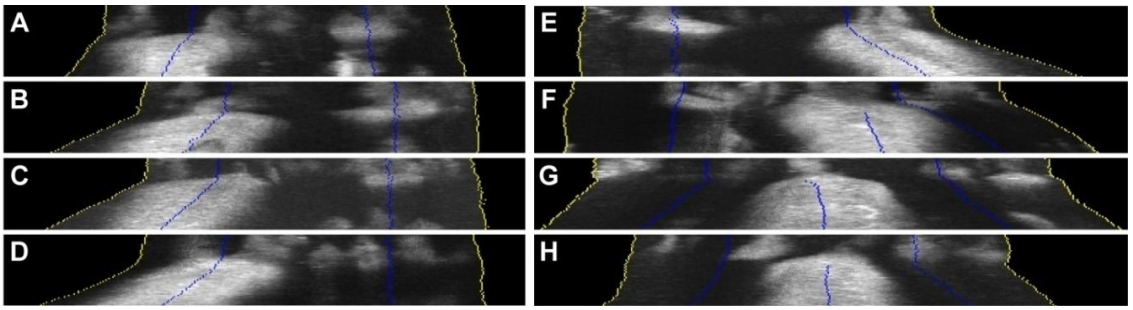

Figure 4.38. Kymographs of post-starvation *tip1*Δ cells. All kymographs start 10 min after RS and display a period of 2 h 30 min.
A to **E** – Cells with bent morphology.
F to **H** – Cells with branching morphology.

had intensities comparable to those of the SRM domains at the primary cell ends (**Figure 4.38**), while in *tea1*Δ cells they were often dimmer (**Figure 4.32**).

To study whether the effect of *tip1* deletion on SRM dynamics was due to the role of Tip1 in Tea1 localization, the mutant *tip1*Δ299 was studied. In this mutant, the carboxy-terminal third of the *tip1* gene was deleted. Although microtubules in *tip1*Δ299 cells have similar length to wild type, Tea1 is mislocalized in these cells (Brunner & Nurse, 2000a).

Kymographs representing post-starvation *tip1*Δ299 cells (**Figure 4.39**) did not reveal significant differences with *tip1*Δ cells. This confirms that the mislocalization of Tea1, and not the reduced length of microtubules, is responsible for the defects observed in *tip1*Δ cells.

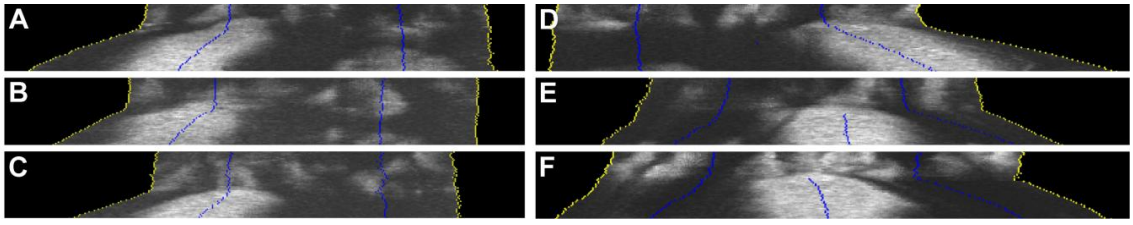

Figure 4.39. Kymographs of post-starvation *tip1*Δ299 cells. All kymographs start 10 min after RS and display a period of 2 h 30 min.
A to **D** – Cells with bent morphology.
E and **F** – Cells with branching morphology.

4.4.3 Role of Mod5 in SRM dynamics

It was shown above that SRM dynamics was affected in cells with mislocalized Tea1 (*mal3*Δ, *tip1*Δ, *tip1*Δ299, and MBC-treated wild type cells). Apart from Tea1 delivery to the cell ends, Tea1 anchoring to the plasma membrane is required for retaining Tea1 at the cell ends. Plasma membrane anchoring of Tea1 is known to involve Mod5 (Section 1.4.5). To study the role of Mod5 in Tea1-mediated SRM positioning, post-starvation cells lacking the *mod5* gene (*mod5*Δ cells) were imaged and analyzed.

Kymographs of *mod5*Δ cells (**Figure 4.40**) revealed SRM dynamics with certain similarities to that of MBC-treated wild type cells (**Figure 4.28**). SRM domains formed similarly to wild type cells during P1, and SRMs polarized during P2. During P3, almost half of *mod5*Δ cells had unstable SRM domains at the secondary cell ends (**Table 4.10**), with the SRM domains absent for various time periods (**Figure 4.40**, **A** to **E**). The proportion of *mod5*Δ cells with unstable SRM domains

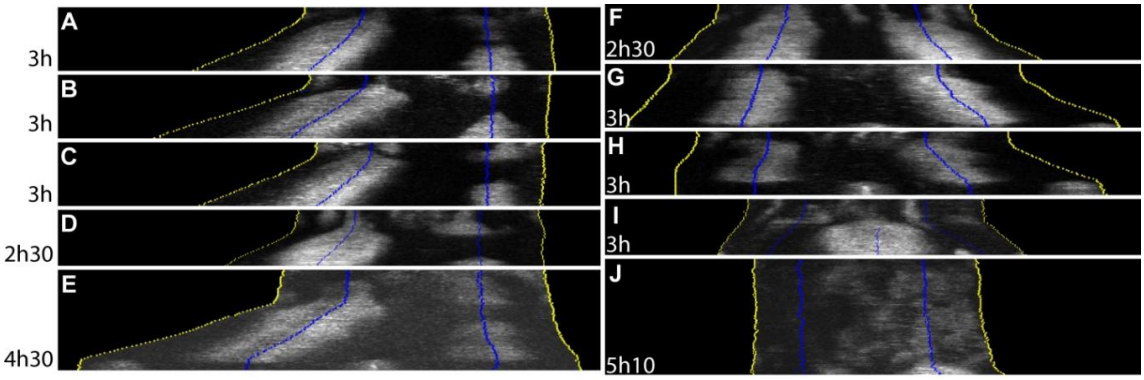

Figure 4.40. Kymographs of post-starvation *mod5*Δ cells. All kymographs start 10 min after RS. The periods displayed on the kymographs are indicated at the bottom left.
A to **D** – Cells with fast-monopolar growth (during the observation period) and an unstable SRM domain at the secondary cell end.
E – A cell with fast-bipolar growth and an unstable SRM domain at the secondary cell end during P3.
F and **G** – Cells with fast-bipolar growth and stable SRM domains at both cell ends.
H – A cell with one of the cell ends slowing down during P4 (left side of the kymograph).
I – A branching cell with the new cell end forming in the cell middle region (central part of the kymograph).
J – A cell with strongly delayed initiation of fast growth.

was comparable to that of MBC-treated wild type cells. Importantly, no growth was detectable at the secondary cell ends when SRM domains were absent from those ends. Seven cells with unstable SRMs at the secondary cell ends were imaged until the first cell division after RS. Two of these cells initiated P4 after SRM domains reappeared at the secondary cell ends (**Figure 4.40**, **E**).

Interestingly, the proportion of cells that initiated P4 was about two times higher for *mod5*Δ than for wild type cells (**Table 4.10**). Strikingly, 67% (n = 24) of *mod5*Δ cells that initiated P4 returned to fast-monopolar growth before the first cell division after RS (**Figure 4.40**, **H**). The SRM domain at the cell end that was slowing down did not shrink significantly in these cells.

There was only 0.5% of branching cells in the population of post-starvation *mod5*Δ cells (n = 415). This is comparable to the low number of branching cells in the population of MBC-treated wild type cells (Section 4.3.1). In branching *mod5*Δ cells, a broad SRM domain covered the fast-growing newly formed cell end (**Figure 4.40**, **I**).

As for most other cell types analyzed in this study, cell growth was strongly delayed in a few *mod5*Δ cells (**Figure 4.40**, **J**). During the time preceding growth initiation, SRMs were randomly distributed within the plasma membrane.

There were several differences between wild type and *mod5*Δ cells with respect to the timing of cell growth. P3 starting times were similar in the two cell types (**Table 4.10**). However, P3 was significantly shorter in *mod5*Δ cells in comparison to wild type cells. This was the case both in cells with and without P4. P4 started significantly earlier in *mod5*Δ cells, but had approximately the same duration as in wild type cells. The cell division phase also started significantly earlier in *mod5*Δ cells than in wild type cells. *Mod5*Δ cell length at the initiation of the cell division phase was higher than that for wild type cells. This seems to be in contradiction with the shorter duration of the first cell cycle after RS for *mod5*Δ cells. A possible explanation for the greater length of *mod5*Δ cells at cell division is related to the higher proportion of *mod5*Δ cells initiating P4: more cells grow at both cell ends, thus achieving greater length than wild type cells in shorter time. The differences in the timing of phases could potentially be affected by the shorter length of most *mod5*Δ movies, as compared to wild type (**Table 3.2**).

Table 4.10. Comparison of post-starvation wild type and *mod5*Δ cells.

Parameter	Wild type cells	*Mod5*Δ cells
P3 starting time (min after RS)	63 ± 33 (n = 394) *	57 ± 17 (n = 386) *
Cells with unstable domain at secondary cell end	6.8% (n = 411) **	46% (n = 415) **
P3 duration in cells without P4 (min)	202 ± 43 (n = 68) *	122 ± 30 (n = 6) *
P3 duration in cells with P4 (min)	116 ± 76 (n = 40) *	27 ± 34 (n = 83) *
Cells with P4	34% (n = 102) **	77.4% (n = 31) **
P4 starting time (min after RS)	165 ± 85 (n = 40) *	79 ± 37 (n = 83) *
P4 duration (min)	82 ± 40 (n = 35)	81 ± 22 (n = 24)
Cell division phase starting time (min after RS)	252 ± 60 (n = 105) *	179 ± 49 (n = 45) *
Cell length at division (μm)	13.4 ± 0.9 (n = 95) *	14.3 ± 1.3 (n = 45) *

Notes:
* numbers with a statistically significant difference (1% significance level, both the nonparametric Wilcoxon rank sum test and the two-sample t-test were used).
** the 99% confidence intervals of wild type and *mod5*Δ cells do not overlap for the respective parameter.

In summary, the link between SRMs and Tea1, the protein involved in growth site positioning, was studied. Based on the analysis of starved cells, it was shown that the localization of Tea1 is independent of SRMs. However, SRM localization is dependent on Tea1, as it was strongly perturbed in post-starvation tea1Δ *cells. In these cells, the main SRM domain was forming simultaneously with fast growth initiation at the unique growth site. The growth site was either at one of the initial cell ends (resulting in straight or bent cells) or in the cell middle region (resulting in branching cells). SRMs not associated with the growth site were highly unstable in* tea1Δ *cells, and they were dimmer than the main SRM domain. The part of the growth speed distribution corresponding to fast growth in* tea1Δ *cells was shifted to higher values and was broader than for wild type cells. This may be related to the different number of growth sites in wild type and* tea1Δ *cells. P3 initiation was delayed in* tea1Δ *cells, but the cell division phase starting time was not significantly different from that in wild type cells. Endocytic sites were partially polarizing simultaneously with the SRMs in post-starvation* tea1Δ *cells. The monopolar partial polarization of endocytic sites was in agreement with the monopolar pattern of growth in these cells.*

The nature of the SRM-Tea1 link was further studied by analyzing the role of the protein Tip1 in SRM positioning. Tip1 is known to be essential for correct Tea1 positioning. Post-starvation tip1Δ *and* tea1Δ *cells had many similarities in both cell morphology and SRM dynamics. However, SRM domains during P1 and SRMs not associated with the growth site during P3 in* tip1Δ *cells seemed to be better formed than in* tea1Δ *cells, as they had intensities similar to that of the main SRM domain. The study of* tip1Δ299 *cells showed that the phenotype of* tip1Δ *cells with respect to SRMs was due to Tip1 interaction with Tea1 and not to reduced microtubule length.*

The role that Mod5, the protein involved in the anchoring of Tea1 to the plasma membrane, plays in SRM positioning was also studied. The phenotypes of mod5Δ *and MBC-treated wild type cells had many similarities with respect to both cell morphology and SRM dynamics. In both cell types, about half of the cells had unstable SRM domains at the secondary cell ends. Importantly, no growth was detectable at a cell end when an SRM domain was absent from that end. Similarly to MBC-treated wild type cells, P3 initiation in* mod5Δ *cells was not delayed relative to untreated wild type cells. Unexpectedly, the proportion of* mod5Δ *cells with P4 was about twice as high as that of wild type cells. After the initiation of P4, the majority of these cells underwent the transition back to fast-monopolar growth.*

4.5 Link between SRMs and cell growth

4.5.1 Role of Tea4 in Tea1-mediated SRM positioning

In Section 4.4.1, the central role of Tea1 in SRM positioning was shown. To further explore the mechanism by which Tea1 affects SRM positioning, the protein Tea4 was considered. Tea4 is known to act as a linker between Tea1 and the formin For3 (Section 1.4.6). For3, in turn, is known to play a role in cell polarity (Section 1.3.2). To test if the Tea1-Tea4-For3 interaction is responsible for the SRM positioning defects observed in *tea1*Δ cells, post-starvation cells with the gene *tea4* deleted (*tea4*Δ cells) were analyzed.

The kymographs of post-starvation *tea4*Δ cells (**Figure 4.41**) and *tea1*Δ cells (**Figure 4.32**) have many similarities. During P1, dynamic SRM domains were present at the cell periphery in *tea4*Δ cells. By the end of P2, one broad SRM domain formed either at a cell end (**Figure 4.41**, **A** to **D**) or at a location in the cell middle region (**Figure 4.41**, **E** to **G**). Simultaneously with the expansion of this SRM domain, fast growth was initiated at its location. In cells where the SRM domain was at a cell end, but not centered well, growth was directed at an angle to the main cell axis, and the cells became bent (**Figure 4.41**, **C**). 4% of *tea4*Δ cells (n = 47) changed the position of their growth site (**Figure 4.41**, **H**). Growth

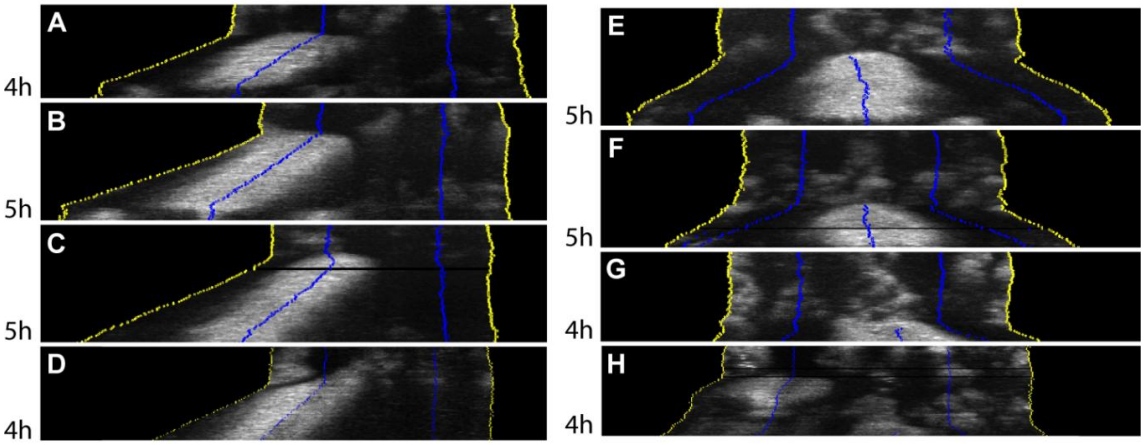

Figure 4.41. Kymographs of post-starvation *tea4*Δ cells. All kymographs start 10 min after RS. The periods displayed on the kymographs are indicated at the bottom left.
A to **D** – Straight and bent cells.
E to **G** – Branching cells.
H – A cell that changed the growth site position.

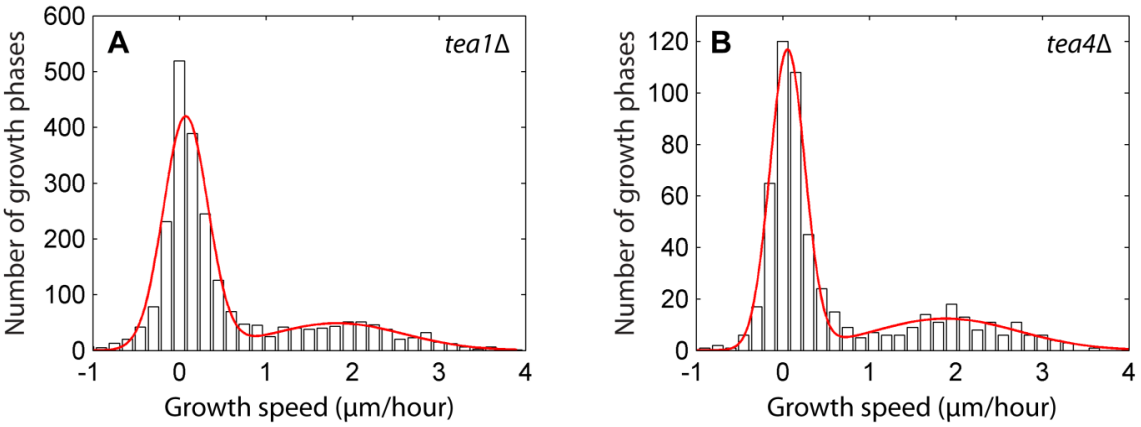

Figure 4.42. Distributions of growth phase speeds of individual cell ends for *tea1*Δ (**A**) and *tea4*Δ cells (**B**).

slowdown was followed by the shrinkage of the corresponding SRM domain in these cells.

SRM domains at the secondary cell ends were highly unstable in *tea4*Δ cells: they disappeared at the beginning of P3 in all cells. In all *tea4*Δ cells imaged until cell division (n = 12), SRM domains appeared at random locations at the plasma membrane later in P3 (**Figure 4.41**). These SRMs were not associated with detectable growth and were much dimmer than the SRM domain associated with the growth site.

Growth speeds were comparable in *tea1*Δ and *tea4*Δ cells: there were no major differences in the growth phase speed distributions for the two cell types (**Figure 4.42**).

Table 4.11. Comparison of post-starvation *tea1*Δ and *tea4*Δ cells.

Parameter	*Tea1*Δ cells	*Tea4*Δ cells
P3 starting time (min after RS)	97 ± 37 (n = 118) *	124 ± 57 (n = 33) *
P3 duration (min)	161 ± 38 (n = 20)	157 ± 26 (n = 5)
Cell division phase starting time (min after RS)	263 ± 50 (n = 51)	256 ± 29 (n = 12)

Note:
* numbers with a statistically significant difference (1% significance level, both the nonparametric Wilcoxon rank sum test and the two-sample t-test were used).

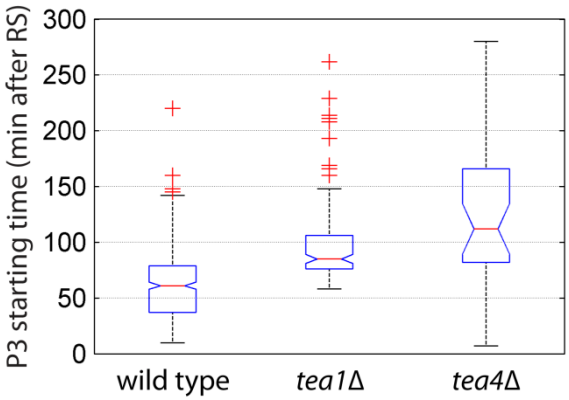

Figure 4.43. Box plots of P3 starting times for wild type, *tea1*Δ, and *tea4*Δ cells. Horizontal red lines represent the median value of the P3 starting time for the corresponding cell type. The lines at the bottom of the box plots correspond to the 25th percentile (q_{25}), the lines at the top – to the 75th percentile (q_{75}). The width of the notches is calculated so that the box plots whose notches do not overlap have different medians at the 5% significance level. Individual crosses represent the outlier data points (larger than $q_{75} + 1.5(q_{75} - q_{25})$ or smaller than $q_{25} - 1.5(q_{75} - q_{25})$). The whiskers are plotted to the extreme data values that were not considered as outliers.

In *tea4*Δ cells, P3 was initiated approximately half an hour later than in *tea1*Δ cells (**Table 4.11**) that, in turn, had a delay in P3 initiation in comparison with wild type cells (**Figure 4.43**). There was no significant difference in P3 duration and the starting time of cell division between *tea1*Δ and *tea4*Δ cells. However, the values of these two parameters might be underestimated for *tea4*Δ cells, as about half of them did not undergo cell division within the observation period.

4.5.2 Role of For3 in SRM dynamics

In Section 4.5.1, Tea4 was shown to be essential for SRM positioning. Tea4 is thought to act as the linker protein between Tea1 and the formin For3 (Section 1.4.6). For3 is a protein involved in the formation of actin cables. It is also known to affect cell growth patterns (monopolar *vs* bipolar growth) (Section 1.3.2). For this reason, the role of For3 in SRM positioning was studied. Cells with *for3* deleted (*for3*Δ cells) were imaged during the first cell cycle after RS; SRM dynamics and cell growth were analyzed.

In the kymographs of post-starvation *for3*Δ cells, P1 was similar to that of wild type

cells (**Figure 4.44**). P2, however, was very long in some *for3*Δ cells (**Figure 4.44**, **M**). This resulted in delayed P3 initiation in *for3*Δ cells relative to wild type (**Table 4.12**).

*For3*Δ cells were divided into two groups based on SRM dynamics during P3 and P4. The first group consisted of cells with stable SRM domains at both cell ends and represented 78% of *for3*Δ cells (n = 117) (**Figure 4.44**, **A** to **F**). Stable SRM domains are also typical for wild type cells, but cell growth in this group of *for3*Δ cells was strongly affected. The shape of blue lines that represent the positions of cell ends on the kymographs indicates that growth speed varied in *for3*Δ cells with stable SRM domains. In many cells, the cell ends that initiated fast growth slowed down later (**Figure 4.44**, **C** to **F**). In some cases, growth slowdown at a cell end was associated with the narrowing of its SRM domain (**Figure 4.44**, **C** and **F**).

The second group was formed by *for3*Δ cells that had an unstable SRM domain at the secondary cell end during P3 (**Figure 4.44**, **G** and **I** to **M**). These cells represented 22% of the cell population (n = 117; **Table 4.12**). This proportion is significantly higher than for wild type cells, but almost two times lower than for *mod5*Δ or MBC-treated wild type cells. The duration of SRM domain absence at the secondary cell end varied from short (**Figure 4.44**, **G**) to much longer periods (**Figure 4.44**, **M**). In *mod5*Δ and MBC-treated wild type cells with an unstable SRM domain at the secondary cell end, the domain disappeared at the beginning of P3, and then reappeared at the cell end after some time. The sequence of events was different in *for3*Δ cells. In many cells, the SRM domain at the secondary cell end underwent several rounds of shrinking and reforming during P3 (**Figure 4.44**, **J** to **L**). Importantly, no fast growth was detected at a cell end when an SRM domain was absent from that end.

In the mutants and pharmacologically treated cells described in the previous sections, the SRM domain at the secondary cell end became unstable at the beginning of P3, when the primary cell end was initiating fast growth. However, in some *for3*Δ cells, the SRM domain at the secondary cell end became unstable before the growth speed of the primary cell end reached the fast growth threshold (**Figure 4.44**, **J**). In some other *for3*Δ cells, the SRM domain at the secondary cell end became unstable later in P3, prior to growth acceleration at that end (**Figure 4.44**, **H** and **I**).

There were two important differences in SRM dynamics between *for3*Δ and *tea4*Δ

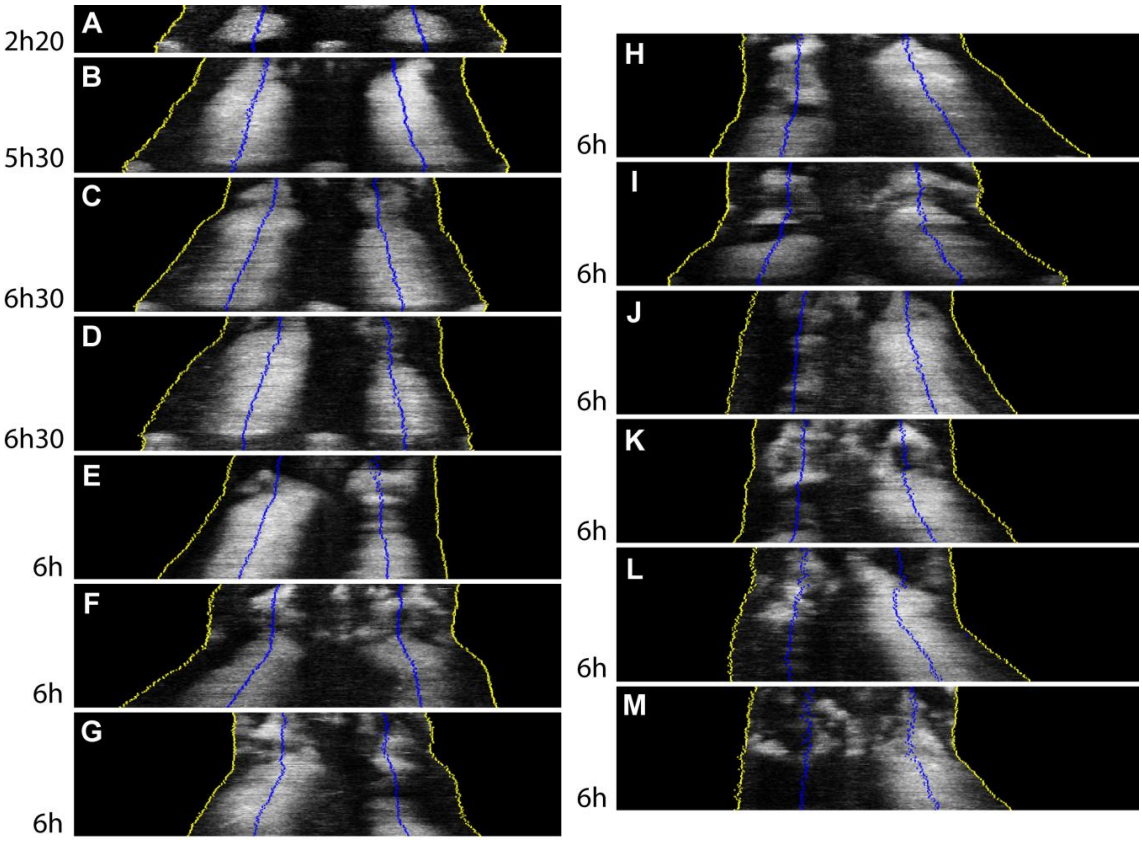

Figure 4.44. Kymographs of post-starvation *for3*Δ cells. All kymographs start 10 min after RS. The periods displayed on the kymographs are indicated at the bottom left.
A to **F** – Cells with stable SRM domains at both cell ends after SRM polarization.
G – A cell that lost the SRM domain at the cell end that decreased its growth speed.
H – A cell with partial loss of the SRM domain at the secondary cell end prior to growth acceleration at that end.
I – A cell where the SRM domain at the secondary cell end is lost prior to growth acceleration at that end.
J to **M** – Cells with an unstable SRM domain at the secondary cell end.

cells. Firstly, by the end of P2, SRM domains were present at both cell ends in most *for3*Δ cells (**Figure 4.44**), rather than only at one of the cell ends, as in *tea4*Δ cells (**Figure 4.41**). Secondly, there were no *for3*Δ cells that formed an SRM domain in the cell middle region. Accordingly, there were no branching *for3*Δ cells: all cells were straight or slightly bent.

The distribution of growth speeds of individual cell end growth phases of *for3*Δ cells was different from that of any other cell type analyzed in this study, including wild

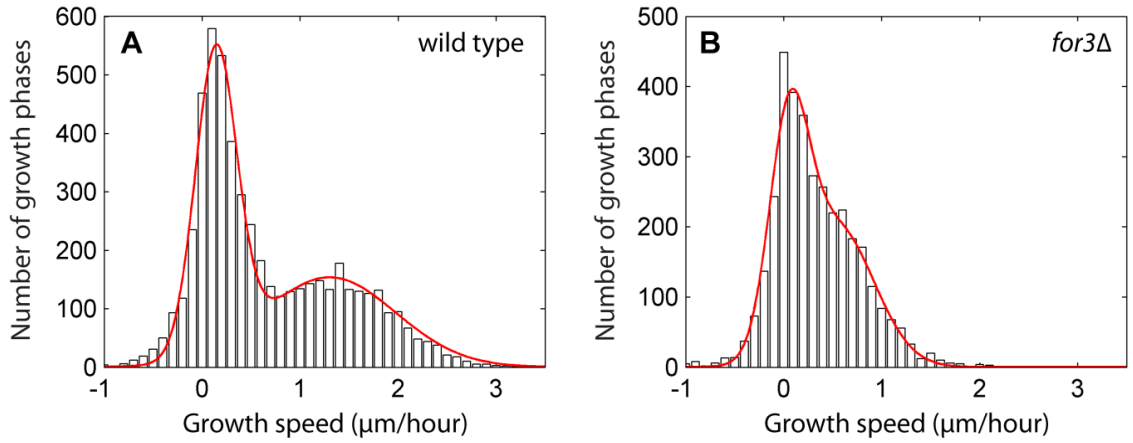

Figure 4.45. Distributions of growth phase speeds of individual cell ends for wild type (**A**) and *for3*Δ cells (**B**). Red curves – double Gaussian fits.

type (**Figure 4.45**). The proportion of growth phases falling into the category of fast growth (growth speed above 0.8 µm/hour) was significantly lower for *for3*Δ than for wild type cells. Importantly, however, all *for3*Δ cells followed until cell division initiated fast growth at least at one cell end, and about half of the cells initiated P4 (**Table 4.12**).

To further analyze the differences in growth speed between wild type and *for3*Δ cells, distributions of the maximal growth speeds were analyzed (**Figure 4.46**). This parameter was measured for individual cells as the highest speed of all growth phases of both cell ends. For *for3*Δ cells, the maximum of the distribution was shifted to lower speeds by 0.8 µm/hour relative to wild type. The highest growth speed of

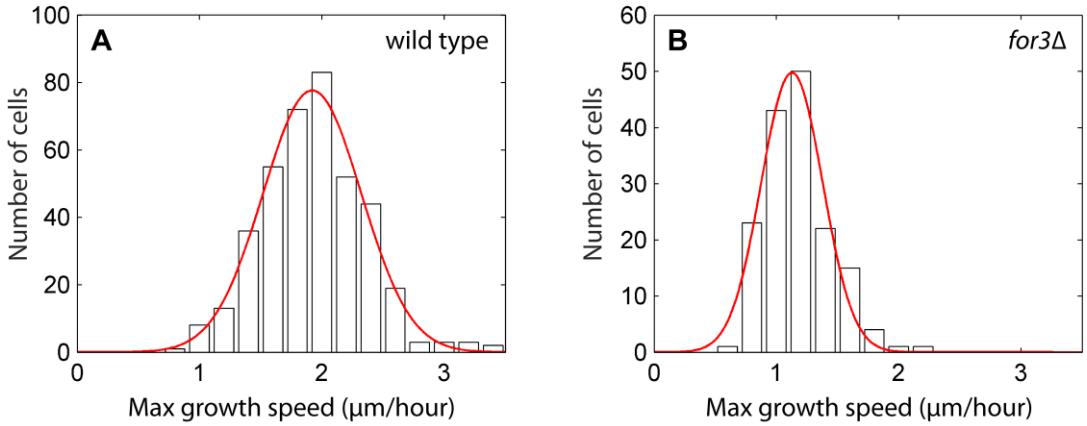

Figure 4.46. Maximal growth speed distributions for wild type (**A**) and *for3*Δ cells (**B**). Red curves – Gaussian fits. Only growth phases at least 12 min long (4 time points) were considered.

Table 4.12. Comparison of post-starvation wild type and *for3*Δ cells.

Parameter	Wild type cells	*For3*Δ cells
P3 starting time (min after RS)	63 ± 33 (n = 394) *	142 ± 75 (n = 160) *
Width of SRM domain at primary cell end at P3 initiation (µm)	4.6 ± 1.3 (n = 384)	4.6 ± 2.1 (n = 141)
Cells with unstable domain at secondary cell end	6.8% (n = 411) ***	22% (n = 117) ***
P3 duration in cells without P4 (min)	202 ± 43 (n = 68)	173 ± 77 (n = 24)
P3 duration in cells with P4 (min)	116 ± 76 (n = 40) *	75 ± 54 (n = 57) *
Cells with P4	34% (n = 102)	49% (n = 49)
P4 starting time (min after RS)	165 ± 85 (n = 40) **	202 ± 82 (n = 57) **
P4 duration (min)	82 ± 40 (n = 35)	84 ± 52 (n = 23)
Cell division phase starting time (min after RS)	252 ± 60 (n = 105)	254 ± 99 (n = 51)

Notes:
* numbers with a statistically significant difference (1% significance level, both the nonparametric Wilcoxon rank sum test and the two-sample t-test were used).
** numbers with a statistically significant difference (5% significance level, both the nonparametric Wilcoxon rank sum test and the two-sample t-test were used).
** the 99% confidence intervals of wild type and *for3*Δ cells do not overlap for the respective parameter.

a cell end was also lower in *for3*Δ cells, by about 1 µm/hour. These results show that growth is less efficient in the absence of For3, as *for3*Δ cells in general grow slower than wild type cells during the first cell cycle after RS.

The comparison of the timing of post-starvation phases revealed that *for3*Δ cells initiated fast growth significantly later than wild type cells (**Table 4.12**). The distribution of P3 starting times was significantly broader for *for3*Δ than for wild type cells (**Figure 4.47**). There was no statistically significant difference in P3 duration between wild type and *for3*Δ cells without P4. In such cells, P3 lasted until cell division. P3 starting time and duration might be underestimated for *for3*Δ cells, since most cells did not divide within the observation period. In *for3*Δ cells with P4, P3 was shorter than in wild type cells. The proportion of cells with P4 was higher in *for3*Δ than in wild type cells, but the difference was not statistically significant. Out

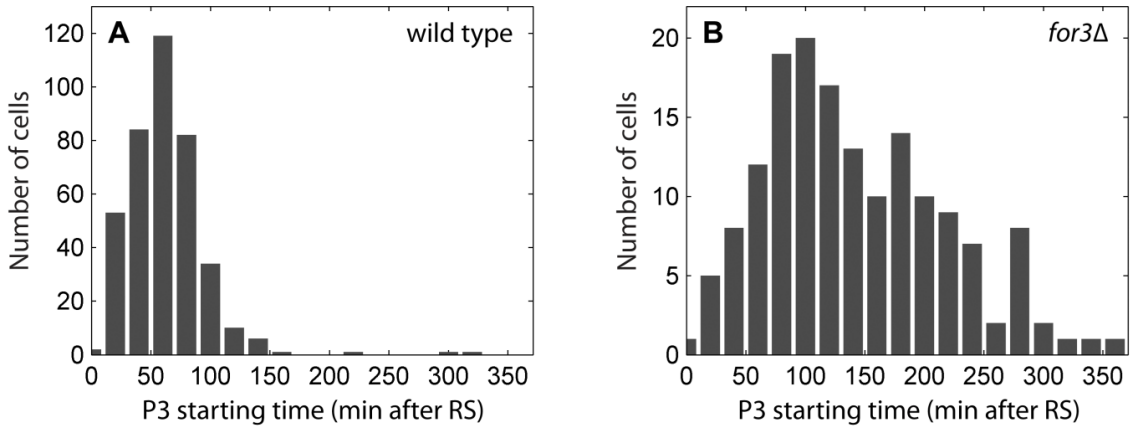

Figure 4.47. Distributions of P3 starting times for post-starvation wild type (**A**) and *for3*Δ cells (**B**).

of 24 *for3*Δ cells with P4 that were followed until cell division, 25% underwent the transition to fast-monopolar growth during P4. P4 was initiated later in *for3*Δ than in wild type cells. There was no statistically significant difference between *for3*Δ and wild type cells in either P4 duration or cell division phase starting time. However, most *for3*Δ cells did not divide within the observation period. As the movies acquired for wild type and *for3*Δ cells were of comparable lengths (**Table 3.2**), it can be concluded that the first cell cycle after RS was longer in *for3*Δ cells.

Despite the high level of SRM instability in *for3*Δ cells, the average width of the SRM domain at the primary cell end at P3 initiation was similar to that in wild type cells (**Table 4.12**).

4.5.3 Role of Bud6 in SRM dynamics

Both For3 and Tea1 interact with Bud6, and the three proteins were suggested to function in the same pathway. Bud6 is thought to act downstream of Tea1 and to be one of the activators of For3 (Sections 1.3.3 and 1.4.6). To study whether Tea1 affects SRM positioning *via* Bud6, post-starvation cells with the gene *bud6* deleted (*bud6*Δ) were imaged and analyzed quantitatively.

Qualitative kymograph inspection showed that P1 and P2 in *bud6*Δ cells were similar to those in wild type cells (**Figure 4.48**). By the end of P2, both cell ends were covered with SRM domains, with some rare exceptions (**Figure 4.48**, **L**). Starting from the beginning of P3, *bud6*Δ cells exhibited a range of interesting behaviors in both SRM dynamics and cell growth. Based on these, *bud6*Δ cells can

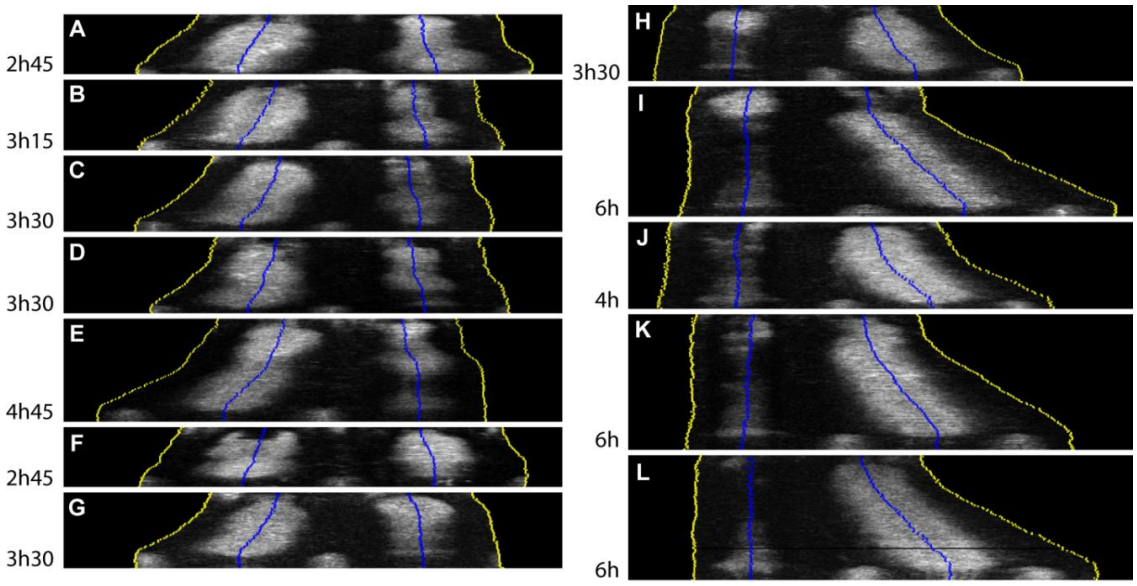

Figure 4.48. Kymographs of post-starvation *bud6*Δ cells. All kymographs start 10 min after RS. The periods displayed on the kymographs are indicated at the bottom left.
A – A cell with P4 and stable SRM domains at both cell ends.
B and **C** – Cells returning to fast-monopolar growth during P4.
D to **G** – Cells swapping fast-growing ends.
H and **I** – Cells with fast-monopolar growth and well-formed SRM domains at their secondary cell ends by the end of P2.
J to **L** – Cells with fast-monopolar growth and narrow SRM domains at their secondary cell ends during P2.

be divided into five classes.

One cell out of the 69 *bud6*Δ cells classified belonged to the first class: it initiated P4 and had stable SRM domains at both cell ends (**Figure 4.48**, **A**). Such behavior was also observed in wild type cells.

The second class consisted of *bud6*Δ cells that returned to fast-monopolar growth after initiating P4 (**Figure 4.48**, **B** and **C**). This occurred in 4% of *bud6*Δ cells (n = 69). The return to fast-monopolar growth was due to growth slowdown at the secondary cell end, the growth speed of the primary cell end was not affected. The width of the SRM domain at the secondary cell end decreased upon return to fast-monopolar growth. Nevertheless, the SRM domain did not entirely disappear in any of the *bud6*Δ cells analyzed. The return to fast-monopolar growth during P4 was also observed in *mod5*Δ cells (Section 4.4.3). However, in those cells it was not accompanied by significant shrinkage of the SRM domain at the secondary cell end.

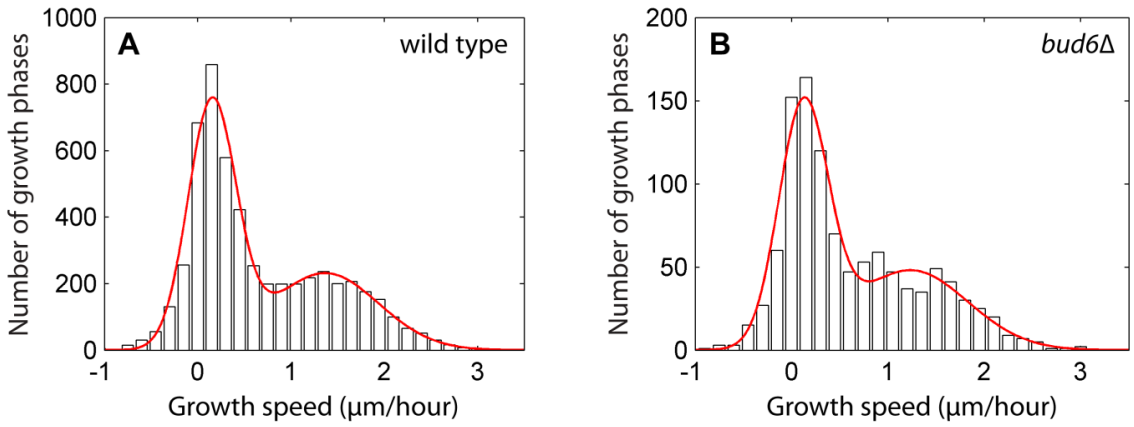

Figure 4.49. Distributions of growth phase speeds of individual cell ends for wild type (**A**) and *bud6*Δ (**B**) cells. Red curves – double Gaussian fits.

The third class consisted of *bud6*Δ cells that swapped fast-growing cell ends (**Figure 4.48**, **D** to **G**). In these cells, fast growth was initiated at the primary cell end, then growth at that end slowed down, while the secondary cell end initiated fast growth. Thus, these cells never entered P4. The proportion of such cells in the *bud6*Δ population was 22% (n = 69), while they were not observed in any of the other cell types analyzed in this study. In some cells, swapping of the fast-growing end even occurred twice. Whenever there was a slowdown in the growth of a cell end, it was accompanied by a decrease in the width of the corresponding SRM domain. The SRM domain shrinkage could occur either after (9 cells), during (5 cells), or before (1 cell) the change in growth speed. Importantly, for all *bud6*Δ cells observed, the SRM domain at a cell end that was growing fast at some point in time remained stable even if the growth speed at that cell end decreased.

The fourth class consisted of *bud6*Δ cells with a distinctive SRM dynamics at the secondary cell end. Initially, a broad SRM domain was formed at the slowly growing secondary cell end. At the onset of P3, when the primary cell end initiated fast growth, the secondary cell end slowed down. The SRM domain at that end decreased in width (**Figure 4.48**, **H**) or even transiently disappeared (**Figure 4.48**, **I**). 49% of *bud6*Δ cells (n = 69) belonged to this class.

Finally, *bud6*Δ cells of the fifth class did not have a broad SRM domain at the secondary cell end by the end of P2. During P3, the domain at the secondary cell end was either stable (**Figure 4.48**, **J**) or unstable (**Figure 4.48**, **K** and **L**). 23% of *bud6*Δ cells (n = 69) belonged to this class.

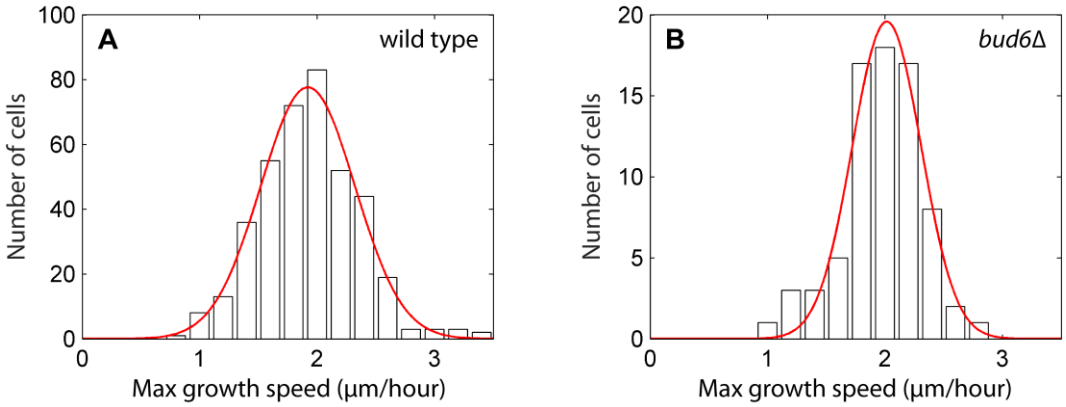

Figure 4.50. Maximal growth speed distributions for wild type (**A**) and *bud6*Δ cells (**B**). Red curves – Gaussian fits. Only growth phases at least 12 min long (4 time points) were considered.

In contrast to *for3*Δ, *bud6*Δ cells did not show significant differences to wild type cells with respect to growth speed distributions for the growth phases of individual cell ends (**Figure 4.49**). The positions of the maxima on the distributions of maximal cell end growth speeds (determined for individual cells) were similar for *bud6*Δ and wild type cells (**Figure 4.50**). This suggests that the speed of fast growth was generally unaffected in *bud6*Δ cells. Nevertheless, the distribution of *bud6*Δ maximal growth speeds was narrower than for wild type, indicating some effect of Bud6 on growth speed variability.

P3 initiation was slightly delayed in *bud6*Δ cells, as compared to the wild type (**Table 4.13**). However, the delay was much smaller than that of *tea4*Δ and *for3*Δ cells. P3 duration in cells with P4 was substantially smaller for *bud6*Δ than for wild type cells. Cells swapping fast-growing ends were included neither in the category of cells with P4, nor in the category of cells without P4. Out of the six *bud6*Δ cells initiating P4 that were followed until cell division, three returned to fast-monopolar growth during P4. There was no statistically significant difference between wild type and *bud6*Δ cells in the values of P3 duration (for cells without P4), of P4 starting times, of P4 duration, and of the cell division phase starting time. On the other hand, the proportion of cells with P4 was significantly lower for *bud6*Δ than for wild type cells.

SRM domains at the secondary cell ends were highly unstable in *bud6*Δ cells (**Table 4.13**). The proportion of cells with unstable secondary cell end domains was comparable to that of *mod5*Δ and ketoconazole- and MBC-treated wild type cells. However, the duration of SRM absence from the secondary cell ends of *bud6*Δ cells

Table 4.13. Comparison of post-starvation wild type and *bud6*Δ cells.

Parameter	Wild type cells	*Bud6*Δ cells
P3 starting time (min after RS)	63 ± 33 (n = 394) *	73 ± 39 (n = 75) *
Cells with unstable domain at secondary cell end	6.8% (n = 411) **	55% (n = 69) **
P3 duration in cells without P4 (min)	202 ± 43 (n = 68)	200 ± 47 (n = 37)
P3 duration in cells with P4 (min)	116 ± 76 (n = 40) *	41 ± 21 (n = 6) *
Cells with P4	34% (n = 102) **	8% (n = 73) **
P4 starting time (min after RS)	165 ± 85 (n = 40)	113 ± 33 (n = 6)
P4 duration (min)	82 ± 40 (n = 35)	77 ± 17 (n = 6)
Cell division phase starting time (min after RS)	252 ± 60 (n = 105)	250 ± 59 (n = 53)

Notes:
* numbers with a statistically significant difference (5% significance level, both the nonparametric Wilcoxon rank sum test and the two-sample t-test were used).
** the 99% confidence intervals of wild type and *bud6*Δ cells do not overlap for the respective parameter.

was twice that of *mod5*Δ cells (72 ± 50 min (n = 35) for *bud6*Δ cells *vs* 36 ± 18 min (n = 116) for *mod5*Δ cells). This suggests that Bud6 plays a more important role in stabilizing SRM domains at the secondary cell ends than Mod5.

4.5.4 Combined effect of *bud6* and *tea1* deletion on SRM positioning and cell growth

As shown in Section 4.5.3, *bud6*Δ cells had defects in both SRM stability and cell growth. However, the phenotype of these cells did not have many similarities with the phenotype of *tea1*Δ cells. To further study whether Tea1 and Bud6 functions in the control of SRM localization are coordinated, the double mutant *bud6*Δ *tea1*Δ was studied.

Similarly to *tea1*Δ cells, *bud6*Δ *tea1*Δ cells had severe morphological defects: the majority of these cells was either bent or branching. The pattern of SRM localization in *bud6*Δ *tea1*Δ cells had similarities to that in *tea1*Δ cells. *Bud6*Δ *tea1*Δ cells were growing at a single growth site, which was covered with a broad SRM domain in both bent and branching cells (**Figure 4.51**).

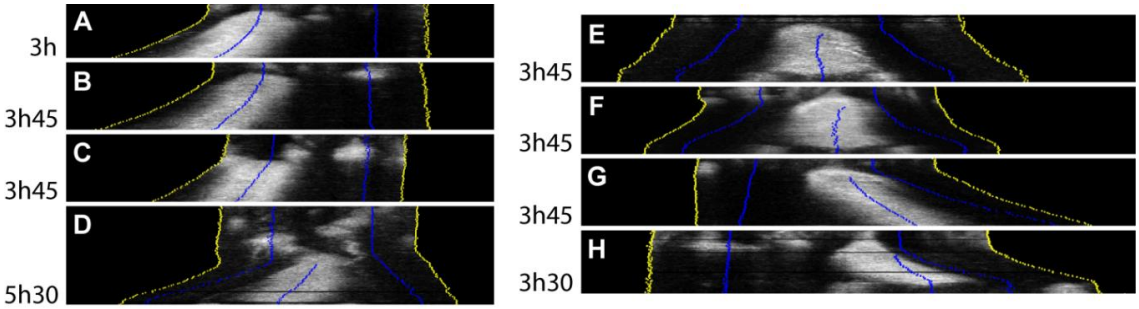

Figure 4.51. Kymographs of post-starvation *bud6*Δ *tea1*Δ double mutant cells. All kymographs start 10 min after RS. The periods displayed on the kymographs are indicated at the bottom left.
A to **C** – Straight cells.
D to **H** – Branching cells.

There were three differences between *bud6*Δ *tea1*Δ (**Figure 4.51**) and *tea1*Δ cells (**Figure 4.32**) with respect to SRM localization. Firstly, the SRM domains that were not associated with the growth site and that appeared at the cell periphery during P3 in all *tea1*Δ cells were not observed in the majority of *bud6*Δ *tea1*Δ cells. Secondly, the SRM domains present during P1 were fewer and brighter in *bud6*Δ *tea1*Δ cells than in *tea1*Δ cells. Thirdly, in some *bud6*Δ *tea1*Δ cells, an SRM domain formed during P2 and was accompanied by slow growth, but fast growth was then initiated at a different location. At fast growth initiation, a broad SRM domain was formed at that location. At the same time, all other SRM domains disappeared (**Figure 4.51**, **B** to **D** and **H**).

The fast growth part of the *bud6*Δ *tea1*Δ growth speed distribution (growth phases with speeds above 0.8 µm/hour) was shifted to higher speeds in comparison to wild type and *bud6*Δ (**Figure 4.52**, **Table 4.14**). However, this shift was smaller than in the *tea1*Δ distribution. The variance associated with the fast growth part of the *bud6*Δ *tea1*Δ distribution was higher than that for wild type and *bud6*Δ cells, but slightly lower than that for *tea1*Δ cells (**Table 4.14**). These results suggest that the deletion of *bud6* partially suppresses the fast growth phenotype of *tea1*Δ cells.

To study the effect of the double deletion on fast growth in *bud6*Δ *tea1*Δ cells in more detail, the distributions of maximal cell end growth speeds for wild type, *bud6*Δ, *tea1*Δ, and *bud6*Δ *tea1*Δ cells were compared (**Figure 4.53**). The *bud6*Δ *tea1*Δ distribution was shifted to higher growth speeds, as compared to the wild type and *bud6*Δ distributions. The positions of the maxima on the Gaussian fits of the *bud6*Δ *tea1*Δ and *tea1*Δ distributions were close. However, the *bud6*Δ *tea1*Δ

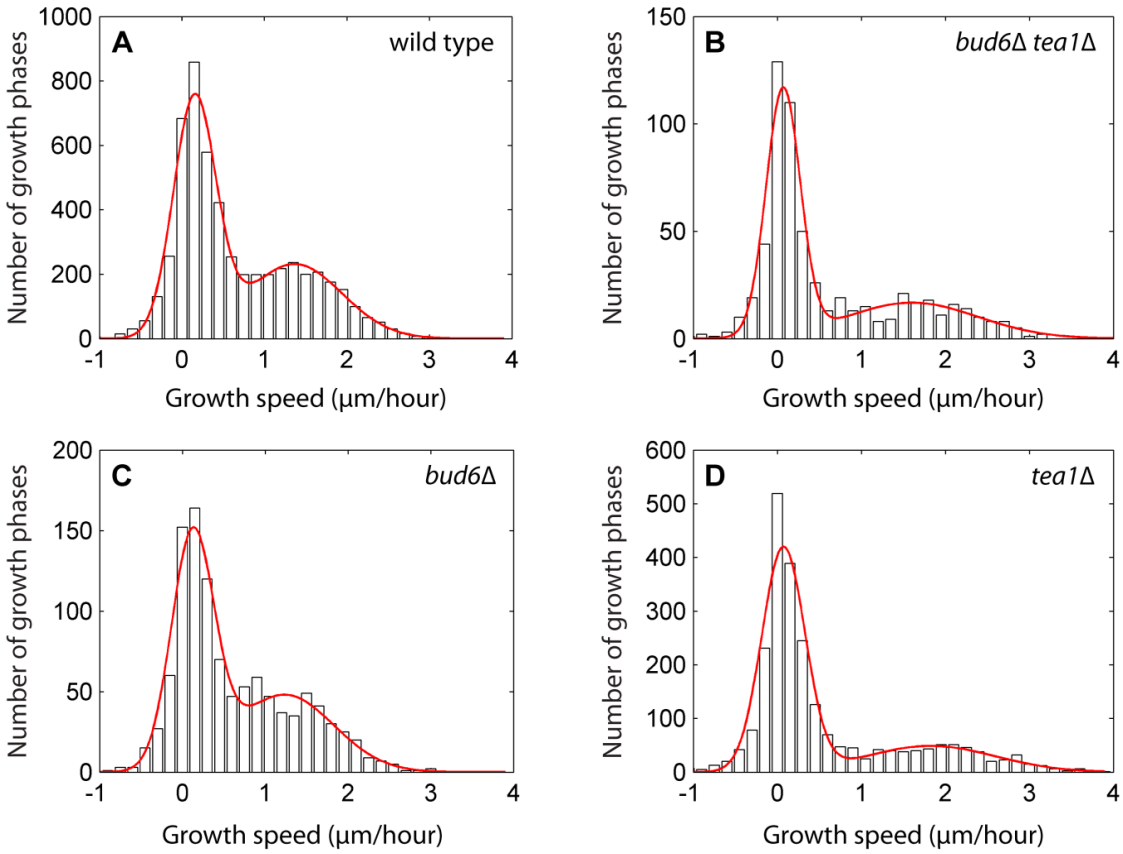

Figure 4.52. Distributions of growth phase speeds of individual cell ends for wild type cells (**A**), *bud6*Δ *tea1*Δ cells (**B**), *bud6*Δ cells (**C**), and *tea1*Δ cells (**D**). Red curves – double Gaussian fits.

distribution was narrower than the *tea1*Δ distribution. This could be explained by the influence of the *bud6* deletion on the growth speed phenotype of the double mutant.

The comparison of P3 starting times in wild type, *bud6*Δ, *tea1*Δ, and *bud6*Δ *tea1*Δ cells is presented in **Table 4.15**. There was no statistically significant difference in this parameter between *bud6*Δ *tea1*Δ and *bud6*Δ cells. P3 in *bud6*Δ *tea1*Δ cells was

Table 4.14. Parameters of the second peaks in Figure 4.52.

Cell type	Position of the maximum (μm/h)	Variance (μm²/h²)
Wild type	1.3	0.7
*Bud6*Δ *tea1*Δ	1.5	1.0
*Bud6*Δ	1.2	0.7
*Tea1*Δ	1.8	1.1

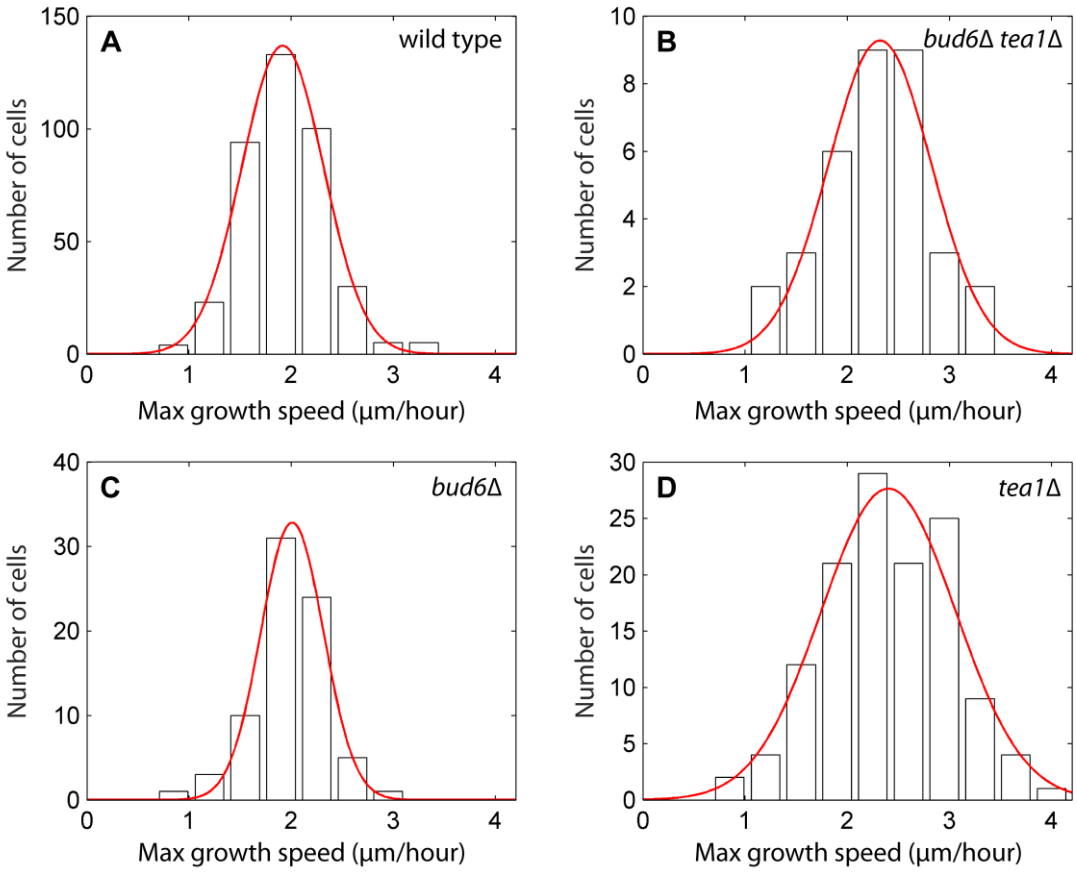

Figure 4.53. Maximal growth speed distributions for wild type cells (**A**), *bud6*Δ *tea1*Δ cells (**B**), *bud6*Δ cells (**C**), and *tea1*Δ cells (**D**). Red curves – Gaussian fits. Only growth phases at least 12 min long (4 time points) were considered.

Table 4.15. Comparison of the post-starvation wild type, *bud6*Δ, *tea1*Δ, and *bud6*Δ *tea1*Δ cells.

Parameter	Wild type cells	*Bud6*Δ cells	*Tea1*Δ cells	*Bud6*Δ *tea1*Δ cells
P3 starting time (min after RS)	63 ± 33 (n = 394) *	73 ± 39 (n = 75)	97 ± 37 (n = 118) *	79 ± 21 (n = 29)
P3 duration in cells without P4 (min)	202 ± 43 (n = 68)	200 ± 47 (n = 37)	161 ± 38 (n = 20)	158 ± 49 (n = 4)

Note:
* numbers with a statistically significant difference to the corresponding *bud6*Δ *tea1*Δ number (5% significance level, both the nonparametric Wilcoxon rank sum test and the two-sample t-test were used).

initiated later than in wild type and earlier than in *tea1*Δ cells (in both cases, the differences were small, but statistically significant). The number of *bud6*Δ *tea1*Δ cells that could be followed until the first cell division after RS was not high enough to determine whether there were statistically significant differences in P3 durations between *bud6*Δ *tea1*Δ and the other three strains. However, P3 duration in the *bud6*Δ *tea1*Δ cells available for analysis was closer to that in *tea1*Δ than in *bud6*Δ cells (**Table 4.15**).

In summary, the deletion of the tea4 *gene, encoding a protein known to mediate the interaction between Tea1 and For3, resulted in a post-starvation phenotype similar to that of* tea1Δ *cells with respect to cell morphology, SRM dynamics, and cell growth speed. This suggests that all functions of Tea1 in cell polarization are mediated by Tea4.*

The post-starvation phenotype of for3Δ *cells was generally similar to the wild type and differed greatly from the* tea4Δ *phenotype with respect to both cell morphology and SRM dynamics. There were, however, interesting differences between wild type and* for3Δ *cells. Firstly, cell growth was affected in* for3Δ *cells: cell end growth speeds were, on average, significantly lower than in wild type cells. Also, in many* for3Δ *cells, growth speed was not stable: it decreased after a period of fast growth. Secondly,* for3Δ *cells had differences in SRM dynamics with the other cell types analyzed in this study. The proportion of unstable SRM domains at the secondary cell ends was higher than in the wild type, but lower than in* mod5Δ *cells or MBC-treated wild type cells. Importantly, this SRM instability was observed in* for3Δ *cells under conditions different than those for the other strains, where SRM domains at the secondary cell ends were lost at P3 initiation and reappeared after variable periods of time. In* for3Δ *cells, on the contrary, the timing of SRM domain loss was not directly linked to P3 initiation: the domain could be lost either prior to this moment or much later. Also, multiple rounds of SRM domain loss and recovery at the secondary cell ends were observed in many cells. Thirdly, the timing of post-starvation phases was affected in* for3Δ *cells: P3 and P4 were significantly delayed in comparison with wild type cells.*

The post-starvation phenotype of bud6Δ *cells was closer to that of wild type than of* for3Δ *cells. Fast growth speeds were not affected in* bud6Δ *cells. However, in some* bud6Δ *cells, growth patterns were not stable: cells switched growing ends, or returned to fast-monopolar growth after initiating P4. In these cells, the decrease of growth speed at a cell end was accompanied by SRM domain shrinkage. P3 initiation was slightly delayed in* bud6Δ *cells in comparison with wild type cells. The proportion of* bud6Δ *cells initiating P4 was significantly lower than in the wild type. The proportion of* bud6Δ *cells with unstable SRM domains at the secondary cell ends was comparable to that of* mod5Δ *cells, as well as ketoconazole- and MBC-treated wild type cells.*

The post-starvation phenotype of bud6Δ tea1Δ *double mutant cells had a combination of features observed in* bud6Δ *and in* tea1Δ *cells. The cell morphology and the positioning of the main SRM domain seem to be the contribution of* tea1 *deletion.* Bud6 *deletion manifested itself in SRM domains being narrower and brighter in* bud6Δ tea1Δ *than in* tea1Δ *cells during P1. Strikingly, SRM domains not associated with the growth site that*

were observed in all tea1Δ *cells during P3 were not observed in* bud6Δ tea1Δ *cells. The distribution of cell maximal growth speeds for* bud6Δ tea1Δ *cells was shifted to higher values relative to the wild type, as in the case of* tea1Δ *cells. The delay of P3 initiation in* bud6Δ tea1Δ *cells was similar to that in* bud6Δ *cells (P3 was initiated later than in wild type, but earlier than in* tea1Δ *cells).*

4.6 Tea1- and Myo1-mediated SRM confinement to cell ends

4.6.1 Role of myosin Myo1 in SRM dynamics

As mentioned in Section 1.6.3, SRMs in *myo1*Δ cells cover most of the plasma membrane. Yet, these cells have spherocylinder morphology similar to the wild type, which seems to contradict the model stating that SRMs define growth zones. Starvation recovery experiments in general allow the analysis of the link between SRM dynamics and cell growth. However, in *myo1*Δ cells, SRMs were not removed from the plasma membrane during starvation: the whole cell periphery was covered with SRMs. This made the study of *de novo* SRM domain formation at the plasma membrane impossible. Nevertheless, interesting SRM dynamics was observed in *myo1*Δ cells during the first cell cycle after RS.

SRMs were present throughout the plasma membrane in post-starvation *myo1*Δ cells. There were, however, regions of increased GFP-Tna1 signal intensity, referred to as "bright regions" in the following (**Figure 4.54**). In most cells, such bright regions were formed at the cell ends during P2. When fast growth was initiated at a cell end, the bright region moved with the tip of that end with a delay. This resulted in the formation of a ring with increased GFP-Tna1 signal intensity at the base of

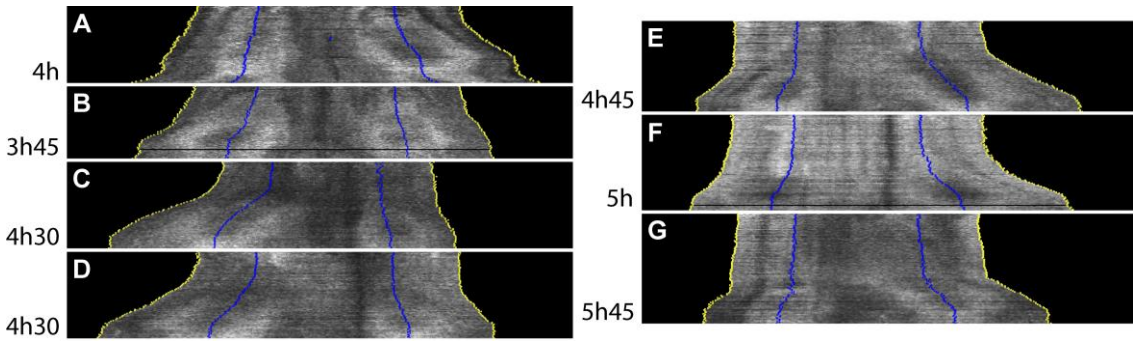

Figure 4.54. Kymographs of post-starvation *myo1*Δ cells. All kymographs start 10 min after RS. The periods displayed on the kymographs are indicated at the bottom left.
A – A cell followed beyond cell division. The distribution of SRMs within the plasma membrane and the initiation of cell growth at the beginning of the second cell cycle after RS can be seen at the bottom of the kymograph.
B to **G** – Cells followed until cell division.

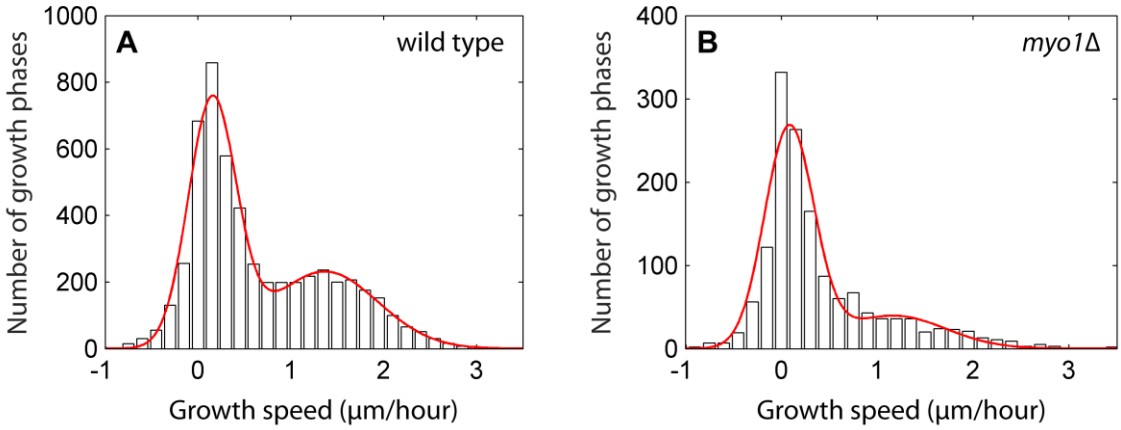

Figure 4.55. Distributions of growth phase speeds of individual cell ends for wild type (**A**) and *myo1*Δ cells (**B**). Red curves – double Gaussian fits.

the growing cell end. The signal intensity at the tip of the growing cell end was comparable to that in the cell middle region.

Surprisingly, bright regions appeared at the two cell ends during cell division in *myo1*Δ cells, but there was no increase of GFP-Tna1 signal at the site of cytokinesis in the cell middle region (**Figure 4.54**). This is different from all *S.pombe* strains described so far in this study, where SRMs disappeared from the cell ends at the beginning of the cell division phase and formed a ring at the site of cytokinesis. At the beginning of the second cell cycle after RS, the daughter cells initiated fast growth, and ring-shaped bright regions formed around the growing cell ends, as was the case during the first cell cycle after RS (**Figure 4.54**, **A**).

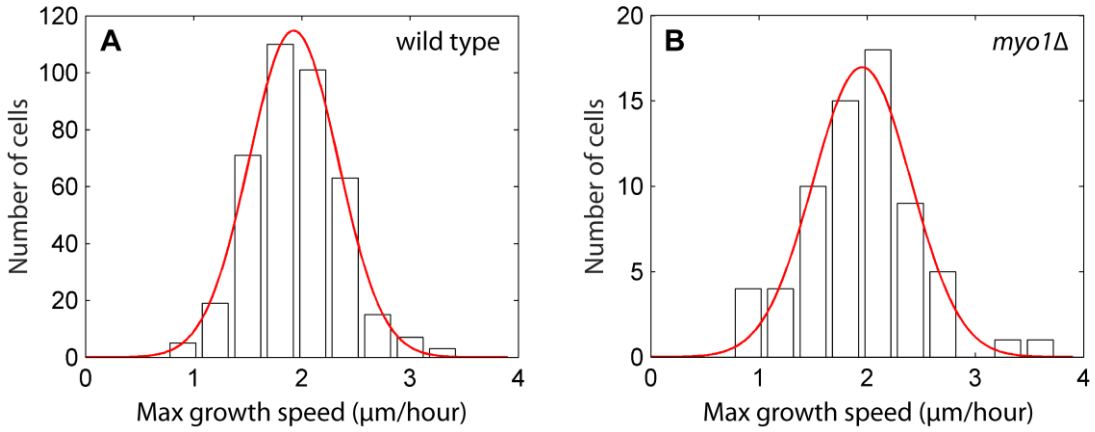

Figure 4.56. Maximal growth speed distributions for wild type (**A**) and *myo1*Δ cells (**B**). Red curves – Gaussian fits. Only growth phases at least 12 min long (4 time points) were considered.

Table 4.16. Comparison of post-starvation wild type and *myo1*Δ cells.

Parameter	Wild type cells	*Myo1*Δ cells
P3 starting time (min after RS)	63 ± 33 (n = 394) *	142 ± 58 (n = 67) *
P3 duration in cells without P4 (min)	202 ± 43 (n = 68) *	140 ± 43 (n = 5) *
P3 duration in cells with P4 (min)	116 ± 76 (n = 40) *	65 ± 37 (n = 40) *
P4 starting time (min after RS)	165 ± 85 (n = 40) **	202 ± 56 (n = 40) **
P4 duration (min)	82 ± 40 (n = 35)	64 ± 33 (n = 17)
Cell division phase starting time (min after RS)	252 ± 60 (n = 105)	248 ± 47 (n = 29)

Notes:
* numbers with a statistically significant difference (1% significance level, both the nonparametric Wilcoxon rank sum test and the two-sample t-test were used).
** numbers with a statistically significant difference (5% significance level, both the nonparametric Wilcoxon rank sum test and the two-sample t-test were used).

The proportion of fast growth phases (growth speeds above 0.8 μm/hour) in the distribution of growth phase speeds was lower for *myo1*Δ than for wild type cells (**Figure 4.55**). This was due to the delay in fast growth initiation in *myo1*Δ cells. To investigate the effect of *myo1* deletion on fast growth, the distribution of maximal growth speeds (determined for individual cells) was analyzed (**Figure 4.56**). The position of the maximum on the fit for *myo1*Δ cells was very close to the position of the maximum on the fit for wild type cells. This shows that *myo1* deletion did not affect maximal growth speeds. When only *myo1*Δ cells followed until division were considered, the maximal cell end growth speed was 2.0 ± 0.4 μm/hour (number of cells: 23; only growth phases at least 18 min long, 6 time points, were considered). All of these cells initiated fast growth.

In *myo1*Δ cells, both P3 and P4 were delayed in comparison with wild type cells (**Table 4.16**). In addition, the durations of P3 and P4 were shorter in *myo1*Δ cells. This correlated with cell division starting at similar times in *myo1*Δ and wild type cells. About a third of *myo1*Δ cells did not initiate P3 during the observation period (31%, n = 113). These cells might have initiated fast growth outside the observation

time window, which means that the timings presented in **Table 4.16** might be underestimated for *myo1*Δ cells.

4.6.2 Combined effect of *myo1* and *tea1* deletion on SRM positioning and cell growth

In Section 4.6.1 it was shown that SRMs were distributed almost homogeneously throughout the plasma membrane of post-starvation *myo1*Δ cells during P1. Then, during P2, regions with increased GFP-Tna1 signal intensity appeared at the cell ends. During P3 and P4, these bright regions were in the shape of rings around the fast-growing ends. Despite only partial SRM polarization, *myo1*Δ cells grew polarized, without major morphological defects, suggesting that proper SRM polarization is not essential for restricting growth to the cell ends. However, in Section 4.4.1, Tea1 was shown to be essential for the correct localization of SRM domains to the cell ends during P2. This suggests that Tea1 ensures polarized growth in *myo1*Δ cells, despite the presence of SRMs throughout the plasma membrane of these cells. To explore this possibility, the double deletion mutant strain *myo1*Δ *tea1*Δ was studied. Paulo Alves created this strain and showed that this double deletion had a severe effect on cell viability and morphology.

Similarly to *myo1*Δ cells, SRMs in starved *myo1*Δ *tea1*Δ cells were spread nearly homogeneously within the plasma membrane. This SRM distribution did not change during P1 (**Figure 4.57**). However, at P3 initiation, SRMs underwent a drastic reorganization and adopted a *tea1*Δ-like localization pattern. A broad SRM domain was present at the unique growth site. This was the case for straight (**Figure 4.57**, **A** and **C**), bent (**Figure 4.57**, **B**), and branching (**Figure 4.57**, **D**) *myo1*Δ *tea1*Δ cells. The removal of SRMs not associated with the fast-growing cell

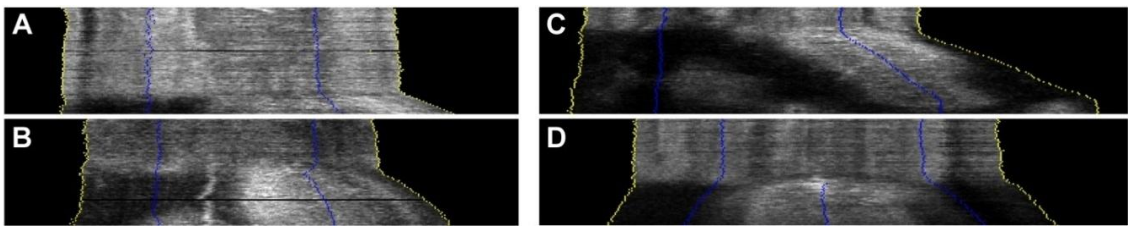

Figure 4.57. Kymographs of post-starvation *myo1*Δ *tea1*Δ double mutant cells. All kymographs start 10 min after RS and display a period of 4 hours. **A** and **C** – straight cells; **B** – a bent cell; **D** – a branching cell.

end from the plasma membrane occurred at the initiation of fast growth. In *myo1*Δ *tea1*Δ cells, SRM domains reappeared outside of the growth site later during P3 (**Figure 4.57**, **B** and **C**), similarly to what was observed in *tea1*Δ cells (**Figure 4.32**).

There was a significant delay in P3 initiation in *myo1*Δ *tea1*Δ cells in comparison with both wild type and *tea1*Δ cells, while in *myo1*Δ and *myo1*Δ *tea1*Δ cells there was no statistically significant difference in P3 starting times (**Table 4.17**). Most *myo1*Δ *tea1*Δ cells (80%, n = 46) did not initiate P3 within the observation period (about 4 hours), but might have done so later. This means that P3 starting time could be underestimated for *myo1*Δ *tea1*Δ cells.

Table 4.17. Comparison of post-starvation wild type, *myo1*Δ, *tea1*Δ, and *myo1*Δ *tea1*Δ cells.

	Wild type cells	***Myo1*Δ cells**	***Tea1*Δ cells**	***Myo1*Δ *tea1*Δ cells**
P3 starting time (min after RS)	63 ± 33 (n = 394) *	142 ± 58 (n = 67)	97 ± 37 (n = 118) *	149 ± 47 (n = 7)

Note:
* numbers with a statistically significant difference from the value of the parameter for *myo1*Δ *tea1*Δ cells (1% significance level, both the nonparametric Wilcoxon rank sum test and the two-sample t-test were used).

In summary, the nearly homogeneous distribution of SRMs within the plasma membrane in myo1Δ *cells during starvation, and then during P1, indicated that Myo1 is essential for the removal of SRMs from the plasma membrane. SRM dynamics in* myo1Δ *and wild type cells during subsequent post-starvation phases had three major differences. Firstly, in* myo1Δ *cells, SRMs were spread throughout the plasma membrane during the first post-starvation cell cycle. Since no distinct SRM domains formed in* myo1Δ *cells (as was the case in the other cell types analyzed in this study), the dynamics of regions with increased GFP-Tna1 intensity was studied in these cells. Secondly, the region with increased GFP-Tna1 intensity that formed at a cell end during P2 did not move with the tip of that cell end upon fast growth initiation. Instead, it transformed into a ring around the cell end, and the ring then followed the growing end. The intensity at the tip of the growing cell end was comparable to that in the cell middle region. Thirdly, during cell division, regions with increased GFP-Tna1 intensity formed at the cell ends in* myo1Δ *cells, rather than at the cytokinetic ring in the cell middle region, as in wild type cells. The speed of fast growth was not affected in* myo1Δ *cells, but P3 and P4 were strongly delayed in comparison with wild type cells.*

To study whether Tea1 might be responsible for the polarized growth of myo1Δ *cells, the* myo1Δ tea1Δ *double mutant was studied. These cells combined the post-starvation phenotypes of both* myo1Δ *and* tea1Δ *cells. During P1, SRMs were distributed nearly homogeneously within the plasma membrane of* myo1Δ tea1Δ *cells (the contribution of* myo1 *deletion to the phenotype). At P3 initiation, SRMs were removed from the plasma membrane, except for the SRM domain associated with the unique growth site (the contribution of* tea1 *deletion to the phenotype). Later during P3, additional SRM domains formed in some cells. P3 starting times were comparable in* myo1Δ *and* myo1Δ tea1Δ *cells.*

5 Discussion

This section starts by considering cell growth and the differences in growth-related phenotypes of the various mutant strains analyzed in this study. Then, the roles of cytoskeleton-associated proteins in SRM positioning and the functions of SRMs are examined. This is followed by the discussion of the correlation between SRM dynamics and cell growth. Finally, possible future research directions are outlined.

5.1 Growth of post-starvation cells

The analysis of cell growth carried out in this study had two main objectives. Firstly, the role of various proteins in growth control was studied. For this purpose, growth patterns and the timing of cell growth were analyzed. Secondly, cell growth was correlated with SRM dynamics. This was achieved by introducing four post-starvation phases. These phases were also used to compare SRM dynamics in untreated and pharmacologically treated wild type cells, as well as various mutant strains.

All the imaging in this study was performed on post-starvation cells attached to lectin-coated glass surfaces. Thus, cells were not floating randomly in the medium, and the visualized displacement of the cell ends was due to growth. In this configuration, the distance from the initial cell center to each of the cell ends was measured and plotted over time. The growth dynamics observed on such growth profiles of individual cell ends was more complex than previously thought. Commonly, only the presence or absence of cell growth are distinguished. In this study, however, phases of slow and fast growth, as well as growth acceleration, deceleration, and pausing were detected. A special technique of curve fitting allowed extracting information on growth speeds and the timing of individual growth phases with unprecedented precision (Section 3.1.4.6).

Histograms showing the distributions of growth phase speeds for most *S.pombe* strains and drug-treated cells analyzed in this study are presented side-by-side in **Figure 5.1** for comparison. The general feature of all distributions is the presence of two modes of growth that were named “slow growth” and “fast growth” in this study. Slow growth corresponds to the first peak of the distributions, fast growth – to the second peak.

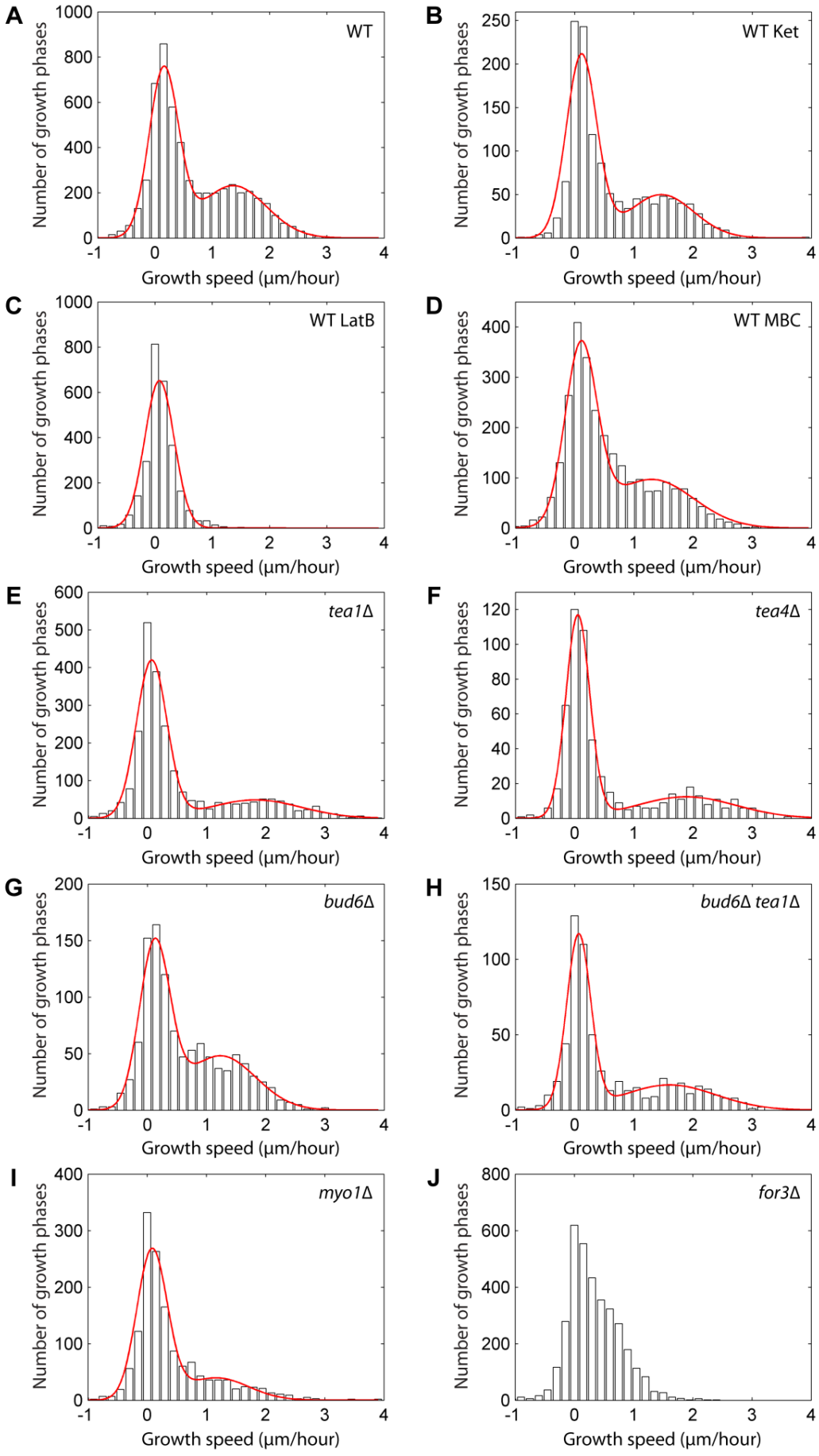
A
WT
B
WT Ket
C
WT LatB
D
WT MBC
E
tea1Δ
F
tea4Δ
G
bud6Δ
H
bud6Δ tea1Δ
I
myo1Δ
J
for3Δ
Number of growth phases
Growth speed (μm/hour)

Figure 5.1. Distributions of growth speeds of individual growth phases of individual cell ends for post-starvation wild type cells (**A**), ketoconazole-treated wild type cells (growth analyzed from the moment of ketoconazole washout) (**B**), wild type cells treated with latrunculin B (**C**), MBC-treated wild type cells (**D**), *tea1*Δ cells (**E**), *tea4*Δ cells (**F**), *bud6*Δ cells (**G**), *bud6*Δ *tea1*Δ cells (**H**), *myo1*Δ cells (**I**), *for3*Δ cells (**J**).

Wild type cells that were released from starvation in the presence of ketoconazole (**Figure 5.1**, **B**) did not differ in growth speeds after the drug washout from untreated cells (**Figure 5.1**, **A**). Thus, temporary perturbation of SRM domains did not affect cell growth speeds following the drug washout. However, the ketoconazole treatment led to the reduction of NETO occurrence after the drug washout (**Table 5.1**). The disruption of F-actin structures in post-starvation wild type cells by latrunculin B treatment led to a drastic reduction in growth speeds (**Figure 5.1**, **C**). However, slow isotropic growth was still present in these cells. Microtubule depolymerization did not have a significant effect on growth speeds (**Figure 5.1**, **D**). Interestingly, the fast growth parts of the distributions for *tea1*Δ and *tea4*Δ cells are broader than for the wild type and shifted to higher speeds (**Figure 5.1**, **E** and **F**). A possible explanation for this is the exclusively monopolar growth of these cells. The single growth site might recruit all of the growth machinery that is normally spread between the two cell ends, thus leading to increased growth efficiency and faster growth. This may also explain why *tea1*Δ cells grow with a larger diameter than wild type, as previously shown (Foethke et al., 2009). *Bud6*Δ cells had growth speed distribution (**Figure 5.1**, **G**) similar to the wild type. However, *bud6*Δ distribution of maximal cell end growth speeds was narrower than that for wild type (**Figure 4.50**). This result suggests that the cell end growth speed is more tightly controlled in the absence of Bud6. In view of the main function of Bud6 known to date, the promotion of For3 activity (Martin & Chang, 2006), the growth phenotype of *bud6*Δ cells is intriguing. Combining *bud6*Δ and *tea1*Δ, two mutations with opposite effects on the fast growth part of the distribution, gives an intermediate growth phenotype that, however, is different from the wild type (**Figure 5.1**, **H**).

In *myo1*Δ cells, fast growth is affected (**Figure 5.1, I**), but not as strongly as in *for3*Δ cells, where only a small proportion of growth phases corresponds to fast growth (**Figure 5.1, J**). The growth phenotype of *for3*Δ cells is consistent with For3 being essential for the formation of actin cables (Nakano et al., 2002) that are important

for the transport of the material required for cell growth to the cell ends (Lo Presti & Martin, 2011). In *myo1*Δ cells, the organization of F-actin is affected (actin patches are delocalized in one third of the cells in interphase), but actin cables are present (Toya et al., 2001). This may account for the less severe growth phenotype of *myo1*Δ cells. The growth phenotype of *for3*Δ cells, in turn, is less severe than that of cells treated with latrunculin B. This is most probably due to the absence of all F-actin structures in cells treated with latrunculin B, which is not the case in *for3*Δ cells.

All growth speed distributions, except those for wild type cells treated with latrunculin B and *for3*Δ cells, show two peaks corresponding to slow and fast growth (**Figure 5.1**). When considering the growth profiles of individual cell ends fitted with linear segments, a clear transition from slow growth to fast growth can be observed for most cell ends. To detect this transition automatically, a threshold for fast growth was chosen to be 0.8 μm/hour. The transition from slow growth to fast growth at one of the cell ends was chosen as the beginning of the phase P3. Fast growth initiation at the second cell end was chosen as the beginning of the phase P4.

Cell growth speeds were previously analyzed in exponentially growing cells (Mitchison & Nurse, 1985; Miyata, Miyata & Johnson, 1988; Miyata, Miyata & Johnson, 1990). The total cell length growth profiles analyzed in these publications have phases of growth at constant growth rates, rate change points, and a constant-length stage during mitosis and cytokinesis (starting just after the anaphase and lasting for about the last 20% of the cycle). More recently, there has been a controversy over exponential *vs* bilinear models of fission yeast growth. Currently, the bilinear model of fission yeast growth (increase in the total cell length over time) is generally accepted (Baumgartner & Tolic-Norrelykke, 2009; Buchwald & Sveiczer, 2006; Goranov & Amon, 2010; Mitchison, 2003). This model involves three rate change points: at the beginning of the cell cycle (RCP1), in mid-G2 (RCP2), and at the beginning of the constant-length stage.

There was also significant controversy on whether RCP2 and NETO coincide in exponentially growing cells (reviewed in (Mitchison, 2003)). It was proposed that under normal growth conditions this is the case in wild type cells. In some cell types, however, RCP2 takes place while NETO does not. Examples are the *cdc* mutants at the restrictive temperature and *wee1* mutant cells. The mean growth rates of the two cell ends after RCP2 were shown to be similar in wild type cells. In these cells, the total cell length growth rate was shown to increase by 30% on average at RCP2. As

this number was smaller than expected, it was suggested that in the majority of cells the old end slowed down at the time when the new end increased its growth rate (Mitchison, 2003). However, the authors of a recent publication performed more accurate growth measurements and arrived at the opposite conclusion: they found an increase in growth rate of the old end at RCP2 (Baumgartner & Tolic-Norrelykke, 2009). In addition, these authors disagreed with the claim in (Mitchison, 2003) that NETO and RCP2 coincide. They reported that NETO was only observed in a subset of cells and did not correspond to RCP2 in these cells. They also found that the total cell length growth rate increased by 60% at RCP2, which is two times the value stated in (Mitchison, 2003). This discrepancy might be due to differences in culturing conditions. The results of both studies pertain to cells cultured at 25°C. Interestingly, it was claimed that the growth rate prior to RCP2 is independent of temperature, while the mean growth rate after RCP2 increases with temperature. Also, the completion of DNA synthesis was shown to be essential for RCP2. It was suggested that the material required for faster growth is synthesized during the period of time between the end of DNA synthesis and RCP2 (Baumgartner & Tolic-Norrelykke, 2009).

The software developed in the present study offers many advantages in comparison with the methods of growth analysis used previously. Firstly, in prior publications, the rate change points were usually defined based on measurements of the total cell length as a function of time. In the present study, however, the growth of the individual cell ends was analyzed. This allowed automatic detection of rate change points with unprecedented precision and led to the conclusion that the P3/P4 transition detected in post-starvation cells corresponds to NETO for all mutants and growth conditions analyzed here. Secondly, the definition of fast growth chosen in this study allows unambiguously classifying cells into those performing and those not performing NETO, based on clear criteria and in an automated way. Thirdly, the precision of growth analysis in the present study allowed distinguishing additional growth phases, not defined by the major rate change points (P3 and P4 starting times). Fourthly, the method of cell periphery detection developed in this study allows cell end tracking, and hence – fully automated cell growth analysis. This further improves precision and allows analyzing many more cells within the same time range in comparison with semi-manual analysis. Finally, as cells are detected based on the phase contrast images, no GFP labeling is needed for growth studies. Thus, the method developed here can be used for studying cell growth of different *S.pombe* strains without concerns about possible effects of fluorescent tags.

The data related to growth of post-starvation cells collected in this study can be compared with the data available for exponentially growing cells, to analyze the effects of starvation on subsequent growth. The most detailed study of growth in exponentially growing wild type cells so far was presented in (Baumgartner & Tolic-Norrelykke, 2009). The main features of growth rate dynamics observed for the individual cell ends of exponentially growing cells are similar to those observed for post-starvation wild type cells studied here. This suggests that the growth dynamics of post-starvation cells does not differ significantly from that of exponentially growing cells.

The length of exponentially growing wild type cells starts to increase immediately following cell division. When sister cells separate, the new cell ends that are initially flat become rounded rapidly, probably due to the turgor pressure inside the cells. This increases the cell length by about 1 μm in the first 5 min after division (Baumgartner & Tolic-Norrelykke, 2009). A similar process was observed in the present study in cells released from starvation. Although the ends of starved cells are not as flat as the new ends of daughter cells at separation, they are flatter than in exponentially growing cells. The initial growth of post-starvation cells studied here was due to cell ends becoming more pointed.

In wild type cells growing exponentially at 32°C, RCP2 was detected at 37 ± 15 min (n = 40) after cell division (Baumgartner & Tolic-Norrelykke, 2009). In the post-starvation wild type cells analyzed here, the transition from slow growth at both cell ends to P3 occurred 63 ± 33 min after RS (n = 394) at 30°C. This difference in the timing is unlikely to be accounted for by the small difference in the cell culturing temperature or the different wild type strains used in the two studies. Most likely, the difference in the timing of the rate change points is due to the time required for the polarization of cells recovering from starvation prior to growth initiation. Accordingly, when the P3 starting time was measured from the moment when SRMs were already polarized, its value (30 ± 22 min, n = 262) was close to the RCP2 time previously reported for exponential cells (37 ± 15 min, n = 40). This suggests that the RCP2 measured in (Baumgartner & Tolic-Norrelykke, 2009) corresponds to the transition from slow growth at both cell ends to P3 in post-starvation cells. The growth before RCP2, termed “basal growth”, was shown to be independent of temperature and DNA synthesis (Baumgartner & Tolic-Norrelykke, 2009). This “basal growth” corresponds to the term “slow growth” used in this

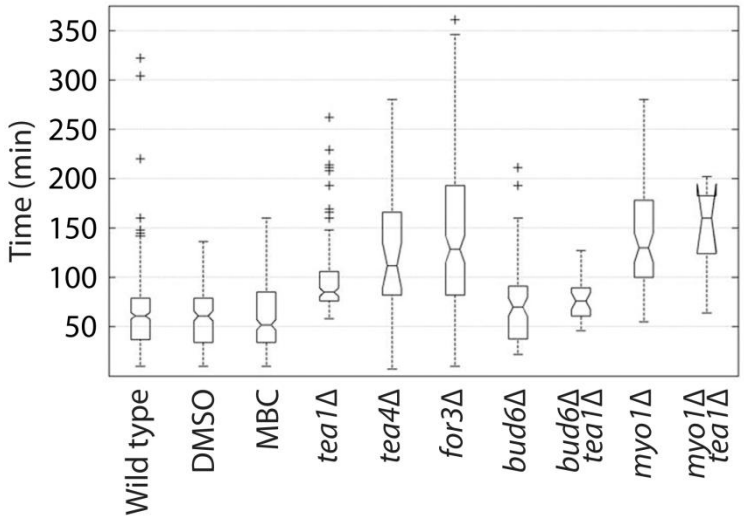

Figure 5.2. Box plots of P3 starting times for most cell types analyzed. The number and length of the movies used for the analysis are given in Table 3.2. The lines in the middle of the box plots represent the median value of the P3 starting time for the corresponding cell type. The lines at the bottom of the box plots correspond to the 25th percentile (q_{25}), the lines at the top – to the 75th percentile (q_{75}). The width of the notches is calculated so that the box plots whose notches do not overlap have different medians at the 5% significance level. Individual crosses represent the outlier data points (larger than $q_{75} + 1.5(q_{75} - q_{25})$ or smaller than $q_{25} - 1.5(q_{75} - q_{25})$). The whiskers are plotted to the extreme data values that were not considered as outliers.

study. However, the two terms differ in that "basal growth" was introduced on the basis of measuring the total cell length increase over time, while "slow growth" refers to the growth of individual cell ends.

P3 starting times for different *S.pombe* strains and for pharmacologically treated wild type cells are summarized in **Figure 5.2**. *Tea1*Δ cells initiated fast growth significantly later than wild type cells. In *tea4*Δ, *for3*Δ, *myo1*Δ, and *myo1*Δ *tea1*Δ double mutant cells fast growth initiation was delayed even more severely.

It has been reported that only a subset of exponentially growing wild type cells performs NETO (Baumgartner & Tolic-Norrelykke, 2009; Miyata et al., 1990). The proportion of such cells was 75% (n = 44), while 23% of cells initiated bipolar growth right after cell division, and 1 cell was found to initiate growth at the new end prior to the old end (Miyata et al., 1990). In the analysis of post-starvation cells performed in this study, NETO was defined as the P4 starting time. The proportion

of post-starvation wild type cells performing NETO was found to be 34% (n = 102) (**Table 5.1**). However, this number should not be compared with the numbers obtained for exponentially growing cells. Firstly, the three categories introduced for exponentially growing cells fall into the category of cells performing NETO in the present study. Cells initiating bipolar growth shortly after RS are considered a special case of cells performing NETO, with NETO occurring very early in the first cell cycle after RS. Also, because the experimental procedures in this study were based on RS, the distinction between new and old cell ends was not made. Secondly, the classifications of growth patterns of exponentially growing and post-starvation cells were performed according to different algorithms. The classification of exponentially growing cells was based on the comparison of growth speeds of the two cell ends (Miyata et al., 1990). This automatically leads to 100% of the cells falling into one of the categories defined for exponentially growing cells. The classification of growth patterns of post-starvation cells performed in the present study, on the other hand, was based on the threshold growth speed that was chosen to determine whether a cell end initiated fast growth. Thus, the proportion of post-starvation cells having NETO did not reach 100% of the cells followed until division for any of the mutants or pharmacologically treated cells analyzed (**Table 5.1**).

The proportion of cells performing NETO was the highest for post-starvation *mod5*Δ cells (**Table 5.1**). This may be related to Mod5 involvement in Tea1 anchoring at the plasma membrane. In *mod5*Δ cells, Tea1 is transported on microtubules to the cell end regions, but is not properly anchored at the plasma membrane (Snaith & Sawin, 2003). The resulting diffuse localization of Tea1 at the cell ends might be responsible for the high rate of NETO occurrence in post-starvation *mod5*Δ cells.

The proportion of *for3*Δ cells performing NETO was lower than for *mod5*Δ cells, but higher than for the wild type (**Table 5.1**). 49% (n = 49) of post-starvation *for3*Δ cells performed NETO, which agrees very well with the growth phenotype reported for exponentially growing *for3*Δ cells: following cell division, one daughter cell grows monopolar, the other – bipolar (Feierbach & Chang, 2001). Besides the large proportion of post-starvation *for3*Δ cells performing NETO, the growth phenotype of these cells is also characterized by a less stable growth speed in comparison with the other cell types studied here. The growth speed of individual cell ends changes several times during the first cell cycle after RS. The main effect of *for3* deletion is

Table 5.1. Proportion of cells performing NETO.

Wild type cells	Ketocona-zole-treated	*Mod5*Δ cells	*For3*Δ cells	*Bud6*Δ cells
34% (n = 102)	13% (n = 38)	77.4% (n = 31)	49% (n = 49)	8% (n = 73)

the disruption of actin cables in the mutant cells. This suggests that actin cables are essential for the stability of growth and for negative control of NETO triggering.

Only 8% of post-starvation *bud6*Δ cells (n = 73) performed NETO (**Table 5.1**). This low number contrasts with about 50% (n = 479) of the exponentially growing *bud6*Δ cells that were reported to perform NETO (Glynn et al., 2001). The definition of NETO for exponentially growing cells (total growth at the new cell end over the whole cell cycle being above 0.5 µm, as measured from the newest birth scar) was different from the one used in the present study that imposes stricter requirements on the cells to be classified as performing NETO. This may explain the difference in the proportion of cells performing NETO in exponentially growing and post-starvation cells. However, the other possibility is that the difference is due to the effect of starvation on the growth patterns of *bud6*Δ cells during the first cell cycle after RS. Further studies are needed to establish the reason for the difference between exponentially growing and post-starvation *bud6*Δ cells.

It has been shown that the oscillations of the concentration of the active Rho GTPase Cdc42 and its regulators between the cell ends are required for NETO to take place (Das et al., 2012). It would be interesting to study how starvation affects these oscillations. If they are perturbed during starvation, the recovery of the oscillations after RS could be analyzed in wild type cells to study whether the perturbation is responsible for the relatively low proportion of post-starvation cells performing NETO. It would also be interesting to study the oscillations of Cdc42 and its regulators in all cell types analyzed here to determine whether potential differences in oscillation recovery in different cell types can explain their different levels of NETO occurrence during the first cell cycle after RS.

In *tea1*Δ, *tea4*Δ, *bud6*Δ *tea1*Δ, and *myo1*Δ *tea1*Δ mutants, NETO was not detected during the first cell cycle after RS. This is in agreement with the previously established monopolarity of exponentially growing *tea1*Δ and *tea4*Δ cells (Glynn et al., 2001; Tatebe et al., 2005). It was suggested that in these mutants growth at one location inhibits growth elsewhere. A possible molecular mechanism for that is the

sequestration of critical growth machinery proteins to the first growth site. The signal for NETO might facilitate the interaction between Tea1 and For3 *via* Tea4. This was proposed to explain the absence of NETO in *tea1*Δ and *tea4*Δ cells (Snaith & Sawin, 2005), although it remained unclear why *for3*Δ cells do not show the same NETO defect. Another explanation of the importance of Tea1 and Tea4 for NETO is related to their role in localizing Rga4 (Cdc42 GAP) to the cell ends *via* Pom1 kinase. Rga4 is required for the activation of Cdc42 and thus controls the positioning of growth sites, including at the new cell end (Tatebe et al., 2008). This study suggests an alternative model. In *tea1*Δ, *tea4*Δ, *bud6*Δ *tea1*Δ, and *myo1*Δ *tea1*Δ mutants, a broad SRM domain is positioned at a single growth site. Paulo Alves showed that SRM domains recruit growth machinery. Thus, the monopolar polarization of SRMs in these mutants may lead to the recruitment of the growth machinery to the unique growth site, not allowing NETO to take place.

It would be interesting to apply the methods of growth analysis developed in this study to exponentially growing cells with the various mutations studied here to see if the growth phenotypes of post-starvation cells discussed in this section are also present in exponential growth. In principle, the methodology of cell growth analysis developed in this study can be used for any kind of growth studies performed with fission yeast cells.

5.2 Regulation of SRM dynamics and its connection to cell growth

Filipin has long been used for SRM visualization. However, this dye is incompatible with live imaging. Lipid-modified (acylated) monomeric CFP and YFP were shown to function as lipid raft markers for live imaging in mammalian cells (Zacharias et al., 2002); in fission yeast, acylated GFP was used (Takeda & Chang, 2005). In the present study, the novel SRM marker Tna1, tagged with GFP, was used. This construct localized to the same plasma membrane regions as filipin and was suitable for live cell imaging, enabling the study of SRM dynamics in fission yeast. Because SRMs are absent from the plasma membrane in starved cells, the imaging of cells recovering from starvation using the live marker is a good way to study *de novo* SRM localization to the plasma membrane. Studying SRM localization *de novo* is essential, because it allows avoiding the feedback loops governing the localization of SRMs and of polarity markers in exponentially growing cells. *De novo* formation of SRM domains within the plasma membrane (rather than their maintenance and dynamics during the cell cycle) was analyzed for the first time in the present study.

To study SRM dynamics in detail, kymographs of the total cell periphery were combined with direct detection of SRM domain positions within the plasma membrane. The analysis of SRM dynamics was performed jointly with the analysis of cell growth, revealing five phases of post-starvation cell behavior in wild type cells. These phases were used as the basis for the description of the phenotypes of various mutants and pharmacologically treated wild type cells.

The first post-starvation phase (P1) was characterized by the presence of SRM domains at random locations within the plasma membrane. The formation of these domains was completed within 10 min after RS (starting time of the imaging). The initial SRM domains were detected in all cell types analyzed in the present study. This suggests that neither the microtubules nor the actin cytoskeleton are responsible for the formation of these initial SRM domains. No cell growth was detected during P1, showing that SRM domain formation within the plasma membrane is independent of cell growth, contrary to what was previously assumed.

During the second post-starvation phase (P2), SRMs became polarized, and slow growth was initiated in most cell types studied here, including the wild type. In wild type cells, SRMs polarized to form a broad domain at each cell end. In some of the mutants, for instance in *tea1*Δ cells, a single SRM domain was formed by the end of

SRM polarization. It could be positioned at any location within the plasma membrane.

The start of the third post-starvation phase (P3) was defined as the moment of the transition from slow growth at both cell ends to fast growth at one of the cell ends (or at the newly-forming end in some of the mutant cells). This phase was detected in all cell types and pharmacological treatment experiments studied here, except for the wild type cells treated with latrunculin B (with F-actin depolymerized).

The beginning of the fourth post-starvation phase (P4) was detected when the secondary cell end initiated fast growth. It is likely that the beginning of this phase corresponds to New End Take-Off (NETO), which is well-established in fission yeast. P4 was detected for most cell types and growth conditions studied. The following cell types, however, did not initiate P4: wild type cells treated with latrunculin B, *tea1*Δ and *tea4*Δ mutants, as well as *tea1*Δ *bud6*Δ and *tea1*Δ *myo1*Δ double mutants.

The fifth post-starvation phase was the constant cell length phase. The beginning of this phase coincided with the beginning of SRM relocation from the cell ends to the cell division site. When this process was completed, SRMs formed a band in the cell middle region. The duration of the constant cell length phase was about 30 min in wild type cells and did not differ significantly in the other cell types analyzed in this study. After daughter cell separation, SRMs redistributed between the new and the old cell ends in both daughter cells (at least in the case of wild type cells).

This basic information on the five post-starvation phases is used in the following to discuss the roles played by the proteins studied in this work with respect to SRMs and cell growth.

The initial SRM domains appear at random locations at the plasma membrane within the first minutes of P1. Such a short time period is most probably not sufficient for the *de novo* synthesis of ergosterol and sphingolipids. Instead, the initial SRM domains at the plasma membrane seem to originate, at least in part, from a preexisting pool, where they were stored during starvation. This is supported by the results obtained in ketoconazole-treated wild type cells. In these cells, randomly distributed SRM domains still appeared upon RS, even though ergosterol production was blocked. However, subsequent SRM polarization and growth initiation did not take place in ketoconazole-treated cells until the drug washout, showing that these steps depend on ergosterol synthesis.

An initial phase characterized by the lack of cell growth, which would correspond to P1, was not described in the previously published analyses of exponentially growing wild type cells (Baumgartner & Tolic-Norrelykke, 2009; Mitchison & Nurse, 1985; Miyata et al., 1988; Miyata et al., 1990). Thus, P1 is most probably specific to post-starvation cells. A possible explanation for the existence of P1 follows from the results obtained for post-starvation wild type cells where F-actin was disrupted with latrunculin B. In these cells, all initial SRM domains started to expand right after RS (rather than staying relatively constant in width during P1, as in the control cells with unperturbed F-actin). In addition, the SRM domains in the cell middle region were not removed in cells treated with latrunculin B, as opposed to control cells, where they were removed at the P1/P2 transition. This suggests that F-actin is required for selective removal of SRM domains outside of the cell end regions. It is likely that P1 in post-starvation fission yeast cells with unperturbed F-actin corresponds to the time necessary for the actin network to recover from starvation.

The P1/P2 transition corresponds to the beginning of SRM domain expansion in cell end regions and gradual shrinkage of the domains in the cell middle region. The mechanism of such SRM redistribution is intriguing. Paulo Alves showed good colocalization of actin patches, which are thought to correspond to endocytic sites, with randomly distributed SRM domains present during P1. However, in Section 4.2.2 it was shown that the fast removal of the SRM domains in the cell middle region at the P1/P2 transition is not due to locally increased endocytic activity, as no such increase was observed. Yet, F-actin is essential for the removal of SRM domains in the cell middle region. Further studies are required to unravel the molecular mechanism of SRM domain removal from the plasma membrane. Interestingly, the study of endocytic dynamics showed that the polarization of endocytic sites was completed roughly by the end of P2. This reveals a link between SRM and endocytic site polarization.

The expansion of cell end SRM domains occurs during P2, in parallel with SRM domain removal from the middle region of the plasma membrane. The analysis of the SRM polarization process did not reveal any lateral movement of SRMs within the plasma membrane. This suggests exocytosis as a possible mechanism of SRM domain expansion in the cell end regions. Additional studies are required to establish the link between SRM dynamics and exocytosis.

In the majority of the cell types studied here, interesting SRM dynamics was observed at the beginning of P3. While the SRM domain at the primary cell end was

expanding, the domain at the secondary cell end was shrinking in many cells. There seemed to be a redistribution of SRMs between the two cell ends. In the majority of wild type cells, the shrinking of the SRM domain associated with the secondary (slowly growing) cell end was partial and transient. However, some cell types showed high SRM instability at the secondary cell end. **Table 5.2** lists the proportion of cells where the SRM domain completely disappeared from the secondary cell end for at least 10 min (judging by the absence of GFP-Tna1 signal) for various cell types and growth conditions.

In *tea1*Δ and *tea4*Δ mutants, as well as *bud6*Δ *tea1*Δ and *myo1*Δ *tea1*Δ double mutants, SRM domain instability at the secondary cell end was observed in the majority of the cells. This shows that Tea1 and Tea4 are essential for the retention of SRMs at the secondary cell ends. Accordingly, when microtubules (that deliver Tea1 to the cell ends) were disrupted by MBC treatment, SRM domains at the secondary cell ends became highly unstable (**Table 5.2**). As shown by Paulo Alves, SRM domains present during P1 recruit components of the growth and polarity machinery independently of growth *per se*. This suggests a simple model explaining the absence of NETO in *tea1*Δ and *tea4*Δ cells, since in the absence of properly formed SRM domains at secondary cell ends the growth and polarity factors are not present there either. Consequently, these cell ends cannot activate a secondary growth site when required. In other words, SRMs at secondary cell ends serve to maintain these ends as putative future growth sites by accumulating the components required for growth initiation. This explains the importance of the microtubule cytoskeleton and of the Tea1-Tea4 complex for SRM positioning and NETO. The less severe SRM stability phenotype of MBC-treated wild type cells than that of *tea1*Δ cells can be explained by the presence of Tea1 in MBC-treated cells. Tea1 performs its functions at the cell ends in these cells, even though it is not properly localized when microtubules are depolymerized.

Although Mal3 localizes to the microtubules, and is not present at the cell ends, the deletion of *mal3* has a dramatic effect on SRM domain stability at the secondary cell ends (**Table 5.2**). A possible explanation for the effect of *mal3* deletion on SRMs is related to the function of Mal3 in microtubule stabilization. In *mal3*Δ cells, microtubules are shorter than in the wild type, and the efficiency of the microtubule-based delivery of polarity markers, such as Tea1, to the cell ends is reduced. This may be the reason for the decreased stability of SRM domains at the secondary cell ends, as in *tea1*Δ cells these domains are not stable. Accordingly, the

Table 5.2. Proportion of cells with unstable SRM domains at secondary cell ends.

Cell type	Proportion of cells
Wild type	6.8% (n = 411)
DMSO-treated wild type	11.4% (n = 245)
Ketoconazole-treated wild type	40% (n = 89)
MBC-treated wild type	49% (n = 239)
*mal3*Δ	30% (n = 30)
*mod5*Δ	46% (n = 415)
*for3*Δ	22% (n = 117)
*bud6*Δ	55% (n = 69)

proportion of *mal3*Δ cells with unstable SRM domains at the secondary cell ends was higher than that of untreated (normal microtubule length) and lower than that of MBC-treated (depolymerized microtubules) wild type cells.

The level of SRM domain instability at the secondary cell end in *mod5*Δ cells was comparable to that in MBC-treated wild type cells (**Table 5.2**). Most probably, Mod5 acts on SRMs through its role in Tea1 positioning. In *mod5*Δ cells, Tea1 is transported on microtubules to the cell end regions, but its anchoring at the cell cortex does not take place (Snaith & Sawin, 2003). Thus, in this case, Tea1 does not perform its role in SRM domain stabilization at the secondary cell end as efficiently as in wild type cells. An alternative possibility is that Mod5 directly interacts with SRMs and stabilizes them *via* its C-terminal prenylation (Snaith & Sawin, 2003). If a mechanism of SRM stabilization mediated by Mod5 were determined experimentally, this would have an interesting consequence. In *tea1*Δ cells, Mod5 is distributed homogeneously over the plasma membrane, instead of being localized at the cell ends (Snaith & Sawin, 2003). Thus, in *tea1*Δ cells, Mod5 activity in SRM domain stabilization might explain the presence of SRM domains not associated with the unique growth site during P3.

For3 also plays a role in maintaining SRM domains at the secondary cell ends (**Table 5.2**). As For3 is known to be required for actin cable formation (Nakano et al., 2002), actin cables may be required for SRM domain stability. The level of SRM domain instability in *for3*Δ cells is significantly lower than in MBC-treated wild type cells (**Table 5.2**). This implies that actin cables are less important for SRM domain stability than microtubules. An alternative mechanism of For3 action with respect to SRM domain stability might be related to its interaction with Tea1 *via*

Tea4. For3 is not merely acting downstream of Tea1, as was previously suggested (Martin et al., 2005), because the phenotype of *for3*Δ cells is less severe than that of *tea1*Δ cells with respect to both cell morphology and SRM domain stability at the secondary cell ends. However, the interaction between For3 and Tea1 might have an indirect effect on SRM domains.

The effect of *bud6* deletion on SRM domain stability is stronger than that of *for3* deletion (**Table 5.2**). This is intriguing, as the main function of Bud6 is thought to be the reduction of For3 autoinhibition (Martin et al., 2007). The level of SRM instability at the secondary cell end in *bud6*Δ cells is slightly higher than in *mod5*Δ cells (**Table 5.2**). Also, the duration of SRM absence at the secondary ends of *bud6*Δ cells is twice that for *mod5*Δ cells. This suggests that Bud6 plays a more important role in maintaining SRM domains at the secondary cell ends than Mod5, which is involved in the anchoring of Tea1 at the cell ends (Snaith & Sawin, 2003). As Bud6 and Tea1 are known to interact (Glynn et al., 2001), their combined effect on SRM stability was studied. In *bud6*Δ *tea1*Δ double mutant cells, the SRM domains not associated with the unique growth site were not observed in most cells during P3, while they were present in all *tea1*Δ cells. This suggests that, in the absence of Tea1, Bud6 might be responsible for the partial stabilization of SRM domains not associated with the growth site. Thus, it can be inferred that Tea1 acts in SRM domain stabilization at the secondary cell end *via* Bud6. On the other hand, the function of Tea1 related to the positioning of the growth sites (and their associated SRM domains) is not mediated by Bud6, as in *bud6*Δ cells growth sites are positioned at the cell ends (there are no branching cells). In *bud6*Δ *tea1*Δ double mutant cells, only the SRM domain associated with the unique growth site is present during P3, which implies that the domain might be stabilized by some growth machinery-related proteins in the absence of both Bud6 and Tea1.

The SRM domain instability discussed above concerns the slowly growing or non-growing cell end at the beginning of P3. Instability of the SRM domain at the cell end that already initiated fast growth was not observed in any of the cell types analyzed. This suggests that once the growth machinery network is properly established at a cell end, it provides feedback to maintain the SRM domain. Importantly, this is independent of the presence of Tea1. Furthermore, once stabilized by such feedback, the SRM domain remains stable, even if growth slows down, as seen in *bud6*Δ cells. SRM domain loss was not observed at any of the *bud6*Δ cell ends that were growing fast and then slowed down.

Ketoconazole treatment experiments showed that SRMs are essential for fission yeast growth. The logical explanation for this would be that SRMs perform a role analogous to that of the lipid rafts described in other model systems (Simons & Sampaio, 2011): recruiting a set of proteins to a particular location and thus facilitating their interaction and regulation. In particular, SRMs may organize the proteins required for cell growth. It would be interesting to study in detail the molecular mechanism of the localization of the cell wall remodeling machinery within SRMs.

Apart from the functions of Tea1 already discussed, it might have an additional function in the structuring of SRM domains. This function is proposed based on the analysis of the SRM domains not associated with the unique fast-growing end in *tea1*Δ cells. There are two types of such domains: the randomly distributed SRM domains present during P1 and the SRM domains not associated with the growth site observed during P3. The domains of both types are dimmer relative to the intensity of the SRM domain associated with the growth site within the same *tea1*Δ cell. This is not the case in other cell types studied here, for example, in *tip1*Δ cells. The absence of growth (even slow growth) associated with such dim SRM domains in *tea1*Δ cells suggests that only properly formed SRM domains can be associated with growth. This may explain the observed delay in fast growth initiation in *tea1*Δ cells. In these cells, neither slow growth nor polarized SRMs were observed before the initiation of P3. It is possible that without these two factors (that are present in wild type cells) the set-up of the growth machinery required for fast growth initiation takes more time. Similar considerations might be true for *tea4*Δ cells, which have a delay in P3 initiation as well.

In wild type cells that undergo the P3/P4 transition (*i.e.* initiate fast growth at the secondary cell end), SRM domains are reorganized again. During P3, the SRM domain at the fast-growing cell end is typically larger than at the secondary cell end. During P4, however, there is no obvious difference in the size of SRM domains at the two cell ends. Also, the width of the SRM domain at a cell end initiating fast growth is not significantly different whether it is the primary cell end at the beginning of P3 or the secondary cell end at the beginning of P4. At the P3/P4 transition, the SRM domain associated with the secondary cell end expands. In some cases, this is accompanied by a slight shrinking of the other SRM domain, indicating that SRMs may be redistributed between the two cell ends at the P3/P4 transition. As previously discussed, SRM redistribution may also occur at the beginning of P3.

No lateral movement of SRMs within the plasma membrane was observed during this process, suggesting other mechanisms orchestrating SRM domain dynamics at the cell ends. This could involve competition for SRM material between the cell ends.

Fast growth correlated with the presence of a broad SRM domain at the growth site in all cells of all cell types analyzed in this study. The question of how the size of SRM domains associated with fast-growing ends is defined is intriguing. None of the proteins studied here were essential for the stability of the SRM domains at the fast-growing cell ends. A possible explanation is that the SRM domain stability depends on the fast growth *per se*. This idea is based on the results obtained in the latrunculin B treatment experiment. There was no fast growth in the post-starvation wild type cells treated with latrunculin B, and the multiple SRM domains at the plasma membrane of these cells were of various sizes.

A possible mechanism of fast growth-related SRM domain size control is *via* localized exocytosis combined with the endocytic recycling. It is possible to suggest a model where the polarity markers localized at the cell ends would preferentially direct the exocytosis-based delivery of SRMs to the growing cell end region of the plasma membrane. Endocytosis would, on the other hand, be responsible for the removal of SRMs from the plasma membrane. Thus, the size of the SRM domain at a fast-growing cell end would be defined by the equilibrium between the rate of cell growth at that end and the rate of endocytosis-based internalization of SRMs.

Myo1 was shown to be essential for the restriction of SRM domain size, since SRMs were reported to uniformly cover the perimeter of exponentially growing *myo1*Δ cells. It was also shown that such homogeneous distribution of SRMs within the plasma membrane was not merely due to an endocytic defect (Takeda & Chang, 2005). SRM dynamics in post-starvation *myo1*Δ cells differed greatly from that in the other cell types studied here (Section 4.6.1). Regions of increased intensity of the SRM marker GFP-Tna1 were observed at the cell ends in post-starvation *myo1*Δ cells. Interestingly, an increase in intensity was observed at a cell end when that end switched to fast growth. Once the cell end was growing fast, the region of increased GFP-Tna1 intensity remained at its initial position. Consequently, this region transformed into a ring around the cell end. This suggests that the mechanism recruiting SRMs to the ends of *myo1*Δ cells in preparation for fast growth is partly functional, while the mechanism relocalizing SRMs to the tip of the growing cell end is not functional.

Partial SRM polarization in *myo1*Δ cells can be explained by the presence of the other SRM-polarizing proteins in these cells. As discussed above, Tea1 plays a central role in coordinating SRM polarization. In *myo1*Δ *tea1*Δ double mutant cells, SRMs are not polarized until the initiation of fast growth at a certain location. In agreement with the model presented above, the established site of fast growth might recruit the SRMs from the cell periphery to form a proper SRM domain associated with that unique growth site. The strongly reduced viability of *myo1*Δ *tea1*Δ cells and their weak polarization suggest that Tea1 and Myo1 are part of redundant mechanisms acting at fast-growing cell ends. Myo1 would serve to restrict the size of SRMs, and thus of the growth platforms, while Tea1 would focus critical growth factors to the cell ends. In the absence of one mechanism, the other would maintain growth. Since even in *myo1*Δ *tea1*Δ cells there is a good degree of polarization in surviving cells, one would have to propose a third mechanism that can polarize fission yeast cells in the absence of Myo1 and Tea1, although less efficiently.

In conclusion, a complex feedback loop regulates the link between SRMs and cell growth. SRMs are essential for the polarization of the growth machinery that, in turn, stabilizes SRMs at the cell ends once fast growth is initiated. Most importantly, though, the results presented here show that SRMs are a critical factor for *de novo* cell polarization, and not merely a player in its maintenance, as was previously thought.

5.3 Outlook

The in-depth analysis of SRM domain dynamics performed in this study in the context of fission yeast morphogenesis suggests a range of interesting follow-up studies.

The role of SRMs as platforms for the recruitment of the growth machinery to the cell ends and to the cell division site should be studied in more detail. The proteins of prime interest are the proteins with localization patterns similar to that of SRMs. Particularly interesting are the proteins with plasma membrane anchors, because they might preferentially localize to SRMs and recruit other proteins there. Mac1 is one of these proteins: it colocalizes with SRM domains *via* its transmembrane domain at the N-terminus. Mac1 does not simply colocalize with growth sites: it is present at both cell ends during interphase, even in mutant cells growing monopolarly (for example, in *pom1*Δ cells). Preferential localization within SRM domains is a possible mechanism for Mac1 positioning. Mac1 was shown to be involved in the cell separation process in cells cultured at 34 – 36°C (Grandin & Charbonneau, 2002). It would be interesting to study if Mac1 is required, directly or indirectly, for the recruitment of other proteins to the regions of SRM localization. Another protein of potential interest is Mug33. It is a transmembrane protein found in the cell end regions of the plasma membrane and within cytoplasmic structures. Mug33 was shown to interact with Tea1, to affect the function of the exocyst, and to have a minor role in cell polarity establishment (Snaith et al., 2011). It would be interesting to study whether Mug33 preferentially localizes to SRMs and whether it is involved in the anchoring of other proteins in the cell end regions.

A range of exciting questions related to the links between SRMs and the cell cycle proteins or cell polarity proteins was beyond the scope of the present study. These proteins include Cdc42 and its effectors, Pom1 (Section 1.5.2), and Kin1 (that was shown to affect SRM localization, Section 1.6.3). The molecular signals responsible for the timing of the post-starvation phases, introduced in this study based on cell growth and SRM dynamics, should also be studied further.

Future studies should test the model for the mechanism of SRM localization proposed here. A detailed analysis of SRM intra-domain dynamics, combined with genetic and pharmacological studies, would generate insights into the role of endocytosis and exocytosis in SRM positioning in fission yeast cells.

In conclusion, studies of SRMs should lead to better understanding of the complex and fascinating processes taking place in the cell end regions in fission yeast. This knowledge could initiate new directions of research in other organisms as well.

References

AKHMANOVA, A. & HOOGENRAAD, C. C. (2005). Microtubule plus-end-tracking proteins: mechanisms and functions. *Curr Opin Cell Biol* **17,** 47-54.

AL-BASSAM, J. & CHANG, F. (2011). Regulation of microtubule dynamics by TOG-domain proteins XMAP215/Dis1 and CLASP. *Trends Cell Biol* **21,** 604-14.

ALMONACID, M., CELTON-MORIZUR, S., JAKUBOWSKI, J. L., DINGLI, F., LOEW, D., MAYEUX, A., CHEN, J. S., GOULD, K. L., CLIFFORD, D. M. & PAOLETTI, A. (2011). Temporal control of contractile ring assembly by Plo1 regulation of myosin II recruitment by Mid1/anillin. *Curr Biol* **21,** 473-9.

ALMONACID, M., MOSELEY, J. B., JANVORE, J., MAYEUX, A., FRAISIER, V., NURSE, P. & PAOLETTI, A. (2009). Spatial control of cytokinesis by Cdr2 kinase and Mid1/anillin nuclear export. *Curr Biol* **19,** 961-6.

ALVAREZ, F. J., DOUGLAS, L. M. & KONOPKA, J. B. (2007). Sterol-rich plasma membrane domains in fungi. *Eukaryot Cell* **6,** 755-63.

ARELLANO, M., DURAN, A. & PEREZ, P. (1997). Localisation of the Schizosaccharomyces pombe rho1p GTPase and its involvement in the organisation of the actin cytoskeleton. *J Cell Sci* **110 (Pt 20),** 2547-55.

ARELLANO, M., NICCOLI, T. & NURSE, P. (2002). Tea3p is a cell end marker activating polarized growth in Schizosaccharomyces pombe. *Curr Biol* **12,** 751-6.

ASPENSTROM, P., FRANSSON, A. & RICHNAU, N. (2006). Pombe Cdc15 homology proteins: regulators of membrane dynamics and the actin cytoskeleton. *Trends Biochem Sci* **31,** 670-9.

AYSCOUGH, K. R., EBY, J. J., LILA, T., DEWAR, H., KOZMINSKI, K. G. & DRUBIN, D. G. (1999). Sla1p is a functionally modular component of the yeast cortical actin cytoskeleton required for correct localization of both Rho1p-GTPase and Sla2p, a protein with talin homology. *Mol Biol Cell* **10,** 1061-75.

BAGNAT, M., KERANEN, S., SHEVCHENKO, A. & SIMONS, K. (2000). Lipid rafts function in biosynthetic delivery of proteins to the cell surface in yeast. *Proc Natl Acad Sci U S A* **97,** 3254-9.

BAHLER, J. & NURSE, P. (2001). Fission yeast Pom1p kinase activity is cell cycle regulated and essential for cellular symmetry during growth and division. *EMBO J* **20,** 1064-73.

BAHLER, J. & PRINGLE, J. R. (1998). Pom1p, a fission yeast protein kinase that provides positional information for both polarized growth and cytokinesis. *Genes Dev* **12,** 1356-70.

BAHLER, J., STEEVER, A. B., WHEATLEY, S., WANG, Y., PRINGLE, J. R., GOULD, K. L. & MCCOLLUM, D. (1998a). Role of polo kinase and Mid1p in determining the site of cell division in fission yeast. *J Cell Biol* **143,** 1603-16.

BAHLER, J., WU, J. Q., LONGTINE, M. S., SHAH, N. G., MCKENZIE, A., 3RD, STEEVER, A. B., WACH, A., PHILIPPSEN, P. & PRINGLE, J. R. (1998b). Heterologous modules for efficient and versatile PCR-based gene targeting in Schizosaccharomyces pombe. *Yeast* **14,** 943-51.

BALASUBRAMANIAN, M. K., MCCOLLUM, D., CHANG, L., WONG, K. C., NAQVI, N. I., HE, X., SAZER, S. & GOULD, K. L. (1998). Isolation and characterization of new fission yeast cytokinesis mutants. *Genetics* **149,** 1265-75.

BAUMGARTNER, S. & TOLIC-NORRELYKKE, I. M. (2009). Growth pattern of single fission yeast cells is bilinear and depends on temperature and DNA synthesis. *Biophys J* **96,** 4336-47.

BEHRENS, R. & NURSE, P. (2002). Roles of fission yeast tea1p in the localization of polarity factors and in organizing the microtubular cytoskeleton. *J Cell Biol* **157,** 783-93.

BENDEZU, F. O. & MARTIN, S. G. (2011). Actin cables and the exocyst form two independent morphogenesis pathways in the fission yeast. *Mol Biol Cell* **22,** 44-53.

BERRO, J., SIROTKIN, V. & POLLARD, T. D. (2010). Mathematical modeling of endocytic actin patch kinetics in fission yeast: disassembly requires release of actin filament fragments. *Mol Biol Cell* **21,** 2905-15.

BIELING, P., LAAN, L., SCHEK, H., MUNTEANU, E. L., SANDBLAD, L., DOGTEROM, M., BRUNNER, D. & SURREY, T. (2007). Reconstitution of a microtubule plus-end tracking system in vitro. *Nature* **450,** 1100-5.

Bornens, M. (2008). Organelle positioning and cell polarity. *Nat Rev Mol Cell Biol* **9,** 874-86.

Bradley, M. P., Rayns, D. G. & Forrester, I. T. (1980). Effects of filipin, digitonin, and polymyxin b on plasma membrane of ram spermatozoa--an EM study. *Arch Androl* **4,** 195-204.

Bretscher, A., Edwards, K. & Fehon, R. G. (2002). ERM proteins and merlin: integrators at the cell cortex. *Nat Rev Mol Cell Biol* **3,** 586-99.

Browning, H. & Hackney, D. D. (2005). The EB1 homolog Mal3 stimulates the ATPase of the kinesin Tea2 by recruiting it to the microtubule. *J Biol Chem* **280,** 12299-304.

Browning, H., Hackney, D. D. & Nurse, P. (2003). Targeted movement of cell end factors in fission yeast. *Nat Cell Biol* **5,** 812-8.

Browning, H., Hayles, J., Mata, J., Aveline, L., Nurse, P. & McIntosh, J. R. (2000). Tea2p is a kinesin-like protein required to generate polarized growth in fission yeast. *J Cell Biol* **151,** 15-28.

Brun, L., Rupp, B., Ward, J. J. & Nedelec, F. (2009). A theory of microtubule catastrophes and their regulation. *Proc Natl Acad Sci U S A* **106,** 21173-8.

Brunner, D. & Nurse, P. (2000a). CLIP170-like tip1p spatially organizes microtubular dynamics in fission yeast. *Cell* **102,** 695-704.

Brunner, D. & Nurse, P. (2000b). New concepts in fission yeast morphogenesis. *Philos Trans R Soc Lond B Biol Sci* **355,** 873-7.

Buchwald, P. & Sveiczer, A. (2006). The time-profile of cell growth in fission yeast: model selection criteria favoring bilinear models over exponential ones. *Theor Biol Med Model* **3,** 16.

Busch, K. E. & Brunner, D. (2004). The microtubule plus end-tracking proteins mal3p and tip1p cooperate for cell-end targeting of interphase microtubules. *Curr Biol* **14,** 548-59.

Busch, K. E., Hayles, J., Nurse, P. & Brunner, D. (2004). Tea2p kinesin is involved in spatial microtubule organization by transporting tip1p on microtubules. *Dev Cell* **6,** 831-43.

CADOU, A., COUTURIER, A., LE GOFF, C., SOTO, T., MIKLOS, I., SIPICZKI, M., XIE, L., PAULSON, J. R., CANSADO, J. & LE GOFF, X. (2010). Kin1 is a plasma membrane-associated kinase that regulates the cell surface in fission yeast. *Mol Microbiol* **77,** 1186-202.

CALONGE, T. M., ARELLANO, M., COLL, P. M. & PEREZ, P. (2003). Rga5p is a specific Rho1p GTPase-activating protein that regulates cell integrity in Schizosaccharomyces pombe. *Mol Microbiol* **47,** 507-18.

CALONGE, T. M., NAKANO, K., ARELLANO, M., ARAI, R., KATAYAMA, S., TODA, T., MABUCHI, I. & PEREZ, P. (2000). Schizosaccharomyces pombe rho2p GTPase regulates cell wall alpha-glucan biosynthesis through the protein kinase pck2p. *Mol Biol Cell* **11,** 4393-401.

CARAZO-SALAS, R. E. & NURSE, P. (2006). Self-organization of interphase microtubule arrays in fission yeast. *Nat Cell Biol* **8,** 1102-7.

CARNAHAN, R. H. & GOULD, K. L. (2003). The PCH family protein, Cdc15p, recruits two F-actin nucleation pathways to coordinate cytokinetic actin ring formation in Schizosaccharomyces pombe. *J Cell Biol* **162,** 851-62.

CASTAGNETTI, S., BEHRENS, R. & NURSE, P. (2005). End4/Sla2 is involved in establishment of a new growth zone in Schizosaccharomyces pombe. *J Cell Sci* **118,** 1843-50.

CASTAGNETTI, S., NOVAK, B. & NURSE, P. (2007). Microtubules offset growth site from the cell centre in fission yeast. *J Cell Sci* **120,** 2205-13.

CELTON-MORIZUR, S., BORDES, N., FRAISIER, V., TRAN, P. T. & PAOLETTI, A. (2004). C-terminal anchoring of mid1p to membranes stabilizes cytokinetic ring position in early mitosis in fission yeast. *Mol Cell Biol* **24,** 10621-35.

CELTON-MORIZUR, S., RACINE, V., SIBARITA, J. B. & PAOLETTI, A. (2006). Pom1 kinase links division plane position to cell polarity by regulating Mid1p cortical distribution. *J Cell Sci* **119,** 4710-8.

CHANG, E. C., BARR, M., WANG, Y., JUNG, V., XU, H. P. & WIGLER, M. H. (1994). Cooperative interaction of S. pombe proteins required for mating and morphogenesis. *Cell* **79,** 131-41.

Chang, F., Drubin, D. & Nurse, P. (1997). cdc12p, a protein required for cytokinesis in fission yeast, is a component of the cell division ring and interacts with profilin. *J Cell Biol* **137,** 169-82.

Chang, F. & Martin, S. G. (2009). Shaping fission yeast with microtubules. *Cold Spring Harb Perspect Biol* **1,** a001347.

Choi, E., Lee, K. & Song, K. (2006). Function of rax2p in the polarized growth of fission yeast. *Mol Cells* **22,** 146-53.

Codlin, S., Haines, R. L. & Mole, S. E. (2008). btn1 affects endocytosis, polarization of sterol-rich membrane domains and polarized growth in Schizosaccharomyces pombe. *Traffic* **9,** 936-50.

Coffman, V. C., Nile, A. H., Lee, I. J., Liu, H. & Wu, J. Q. (2009). Roles of formin nodes and myosin motor activity in Mid1p-dependent contractile-ring assembly during fission yeast cytokinesis. *Mol Biol Cell* **20,** 5195-210.

Coll, P. M., Trillo, Y., Ametzazurra, A. & Perez, P. (2003). Gef1p, a new guanine nucleotide exchange factor for Cdc42p, regulates polarity in Schizosaccharomyces pombe. *Mol Biol Cell* **14,** 313-23.

Cortes, J. C., Carnero, E., Ishiguro, J., Sanchez, Y., Duran, A. & Ribas, J. C. (2005). The novel fission yeast (1,3)beta-D-glucan synthase catalytic subunit Bgs4p is essential during both cytokinesis and polarized growth. *J Cell Sci* **118,** 157-74.

Cortes, J. C., Ishiguro, J., Duran, A. & Ribas, J. C. (2002). Localization of the (1,3)beta-D-glucan synthase catalytic subunit homologue Bgs1p/Cps1p from fission yeast suggests that it is involved in septation, polarized growth, mating, spore wall formation and spore germination. *J Cell Sci* **115,** 4081-96.

Csikasz-Nagy, A., Gyorffy, B., Alt, W., Tyson, J. J. & Novak, B. (2008). Spatial controls for growth zone formation during the fission yeast cell cycle. *Yeast* **25,** 59-69.

Daga, R. R. & Chang, F. (2005). Dynamic positioning of the fission yeast cell division plane. *Proc Natl Acad Sci U S A* **102,** 8228-32.

Daga, R. R., Yonetani, A. & Chang, F. (2006). Asymmetric microtubule pushing forces in nuclear centering. *Curr Biol* **16,** 1544-50.

DAS, M., DRAKE, T., WILEY, D. J., BUCHWALD, P., VAVYLONIS, D. & VERDE, F. (2012). Oscillatory dynamics of Cdc42 GTPase in the control of polarized growth. *Science* **337,** 239-43.

DAS, M., WILEY, D. J., CHEN, X., SHAH, K. & VERDE, F. (2009). The conserved NDR kinase Orb6 controls polarized cell growth by spatial regulation of the small GTPase Cdc42. *Curr Biol* **19,** 1314-9.

DAS, M., WILEY, D. J., MEDINA, S., VINCENT, H. A., LARREA, M., ORIOLO, A. & VERDE, F. (2007). Regulation of cell diameter, For3p localization, and cell symmetry by fission yeast Rho-GAP Rga4p. *Mol Biol Cell* **18,** 2090-101.

DING, D. Q., CHIKASHIGE, Y., HARAGUCHI, T. & HIRAOKA, Y. (1998). Oscillatory nuclear movement in fission yeast meiotic prophase is driven by astral microtubules, as revealed by continuous observation of chromosomes and microtubules in living cells. *J Cell Sci* **111 (Pt 6),** 701-12.

DOGTEROM, M., KERSSEMAKERS, J. W., ROMET-LEMONNE, G. & JANSON, M. E. (2005). Force generation by dynamic microtubules. *Curr Opin Cell Biol* **17,** 67-74.

DOWNING, K. H. & NOGALES, E. (1998). Tubulin structure: insights into microtubule properties and functions. *Curr Opin Struct Biol* **8,** 785-91.

DRABIKOWSKI, W., LAGWINSKA, E. & SARZALA, M. G. (1973). Filipin as a fluorescent probe for the location of cholesterol in the membranes of fragmented sarcoplasmic reticulum. *Biochim Biophys Acta* **291,** 61-70.

DRUMMOND, D. R. & CROSS, R. A. (2000). Dynamics of interphase microtubules in Schizosaccharomyces pombe. *Curr Biol* **10,** 766-75.

DUGGAN, J., JAMAL, G., TILLEY, M., DAVIS, B., MCKENZIE, G., VERE, K., SOMEKH, M. G., O'SHEA, P. & HARRIS, H. (2008). Functional imaging of microdomains in cell membranes. *Eur Biophys J* **37,** 1279-89.

EGEL, R., ED. (2004). The Molecular Biology of Schizosaccharomyces pombe.

EGGELING, C., RINGEMANN, C., MEDDA, R., SCHWARZMANN, G., SANDHOFF, K., POLYAKOVA, S., BELOV, V. N., HEIN, B., VON MIDDENDORFF, C., SCHONLE, A. & HELL, S. W. (2009). Direct observation of the nanoscale dynamics of membrane lipids in a living cell. *Nature* **457,** 1159-62.

Eisenkolb, M., Zenzmaier, C., Leitner, E. & Schneiter, R. (2002). A specific structural requirement for ergosterol in long-chain fatty acid synthesis mutants important for maintaining raft domains in yeast. *Mol Biol Cell* **13,** 4414-28.

Estravis, M., Rincon, S. A., Santos, B. & Perez, P. (2011). Cdc42 regulates multiple membrane traffic events in fission yeast. *Traffic* **12,** 1744-58.

Fankhauser, C., Reymond, A., Cerutti, L., Utzig, S., Hofmann, K. & Simanis, V. (1995). The S. pombe cdc15 gene is a key element in the reorganization of F-actin at mitosis. *Cell* **82,** 435-44.

Feierbach, B. & Chang, F. (2001). Roles of the fission yeast formin for3p in cell polarity, actin cable formation and symmetric cell division. *Curr Biol* **11,** 1656-65.

Feierbach, B., Verde, F. & Chang, F. (2004). Regulation of a formin complex by the microtubule plus end protein tea1p. *J Cell Biol* **165,** 697-707.

Fienup, J. R. & Kowalczyk, A. M. (1990). Phase retrieval for a complex-valued object by using a low-resolution image. *J. Opt. Soc. Am. A* **7,** 450-458.

Fink, J., Carpi, N., Betz, T., Betard, A., Chebah, M., Azioune, A., Bornens, M., Sykes, C., Fetler, L., Cuvelier, D. & Piel, M. (2011). External forces control mitotic spindle positioning. *Nat Cell Biol* **13,** 771-8.

Fischer, R., Zekert, N. & Takeshita, N. (2008). Polarized growth in fungi--interplay between the cytoskeleton, positional markers and membrane domains. *Mol Microbiol* **68,** 813-26.

Foethke, D., Makushok, T., Brunner, D. & Nedelec, F. (2009). Force- and length-dependent catastrophe activities explain interphase microtubule organization in fission yeast. *Mol Syst Biol* **5,** 241.

Forsburg, S. L. & Rhind, N. (2006). Basic methods for fission yeast. *Yeast* **23,** 173-83.

Gautreau, A., Louvard, D. & Arpin, M. (2002). ERM proteins and NF2 tumor suppressor: the Yin and Yang of cortical actin organization and cell growth signaling. *Curr Opin Cell Biol* **14,** 104-9.

Ge, W., Chew, T. G., Wachtler, V., Naqvi, S. N. & Balasubramanian, M. K. (2005). The novel fission yeast protein Pal1p interacts with Hip1-related Sla2p/End4p and is involved in cellular morphogenesis. *Mol Biol Cell* **16,** 4124-38.

GIERER, A. & MEINHARDT, H. (1972). A theory of biological pattern formation. *Kybernetik* **12,** 30-9.

GLYNN, J. M., LUSTIG, R. J., BERLIN, A. & CHANG, F. (2001). Role of bud6p and tea1p in the interaction between actin and microtubules for the establishment of cell polarity in fission yeast. *Curr Biol* **11,** 836-45.

GORANOV, A. I. & AMON, A. (2010). Growth and division--not a one-way road. *Curr Opin Cell Biol* **22,** 795-800.

GRANDIN, N. & CHARBONNEAU, M. (2002). Mac1, a fission yeast transmembrane protein localizing to the poles and septum, is required for correct cell separation at high temperatures. *Biol Cell* **94,** 127-37.

GRUN, C. H., HOCHSTENBACH, F., HUMBEL, B. M., VERKLEIJ, A. J., SIETSMA, J. H., KLIS, F. M., KAMERLING, J. P. & VLIEGENTHART, J. F. (2005). The structure of cell wall alpha-glucan from fission yeast. *Glycobiology* **15,** 245-57.

HACHET, O., BERTHELOT-GROSJEAN, M., KOKKORIS, K., VINCENZETTI, V., MOOSBRUGGER, J. & MARTIN, S. G. (2011). A phosphorylation cycle shapes gradients of the DYRK family kinase Pom1 at the plasma membrane. *Cell* **145,** 1116-28.

HAGAN, I. M. (1998). The fission yeast microtubule cytoskeleton. *J Cell Sci* **111 (Pt 12),** 1603-12.

HANCOCK, J. F. (2006). Lipid rafts: contentious only from simplistic standpoints. *Nat Rev Mol Cell Biol* **7,** 456-62.

HANZAL-BAYER, M. F. & HANCOCK, J. F. (2007). Lipid rafts and membrane traffic. *FEBS Lett* **581,** 2098-104.

HAWKINS, R. J., BENICHOU, O., PIEL, M. & VOITURIEZ, R. (2009). Rebuilding cytoskeleton roads: active-transport-induced polarization of cells. *Phys Rev E Stat Nonlin Soft Matter Phys* **80,** 040903.

HAYLES, J. & NURSE, P. (2001). A journey into space. *Nat Rev Mol Cell Biol* **2,** 647-56.

HE, B. & GUO, W. (2009). The exocyst complex in polarized exocytosis. *Curr Opin Cell Biol* **21,** 537-42.

Hirata, D., Kishimoto, N., Suda, M., Sogabe, Y., Nakagawa, S., Yoshida, Y., Sakai, K., Mizunuma, M., Miyakawa, T., Ishiguro, J. & Toda, T. (2002). Fission yeast Mor2/Cps12, a protein similar to Drosophila Furry, is essential for cell morphogenesis and its mutation induces Wee1-dependent G(2) delay. *EMBO J* **21,** 4863-74.

Hirota, K., Tanaka, K., Ohta, K. & Yamamoto, M. (2003). Gef1p and Scd1p, the Two GDP-GTP exchange factors for Cdc42p, form a ring structure that shrinks during cytokinesis in Schizosaccharomyces pombe. *Mol Biol Cell* **14,** 3617-27.

Hochstenbach, F., Klis, F. M., van den Ende, H., van Donselaar, E., Peters, P. J. & Klausner, R. D. (1998). Identification of a putative alpha-glucan synthase essential for cell wall construction and morphogenesis in fission yeast. *Proc Natl Acad Sci U S A* **95,** 9161-6.

Holmes, K. C., Popp, D., Gebhard, W. & Kabsch, W. (1990). Atomic model of the actin filament. *Nature* **347,** 44-9.

Hoog, J. L., Schwartz, C., Noon, A. T., O'Toole, E. T., Mastronarde, D. N., McIntosh, J. R. & Antony, C. (2007). Organization of interphase microtubules in fission yeast analyzed by electron tomography. *Dev Cell* **12,** 349-61.

Howard, J. & Hyman, A. A. (2009). Growth, fluctuation and switching at microtubule plus ends. *Nat Rev Mol Cell Biol* **10,** 569-74.

Huang, Y., Tran, P. T., Oliferenko, S. & Balasubramanian, M. K. (2007). Assembly of microtubules and actomyosin rings in the absence of nuclei and spindle pole bodies revealed by a novel genetic method. *PLoS One* **2,** e618.

Huisman, S. M. & Brunner, D. (2011). Cell polarity in fission yeast: A matter of confining, positioning, and switching growth zones. *Semin Cell Dev Biol.*

Ishiguro, J. (1998). Genetic control of fission yeast cell wall synthesis: the genes involved in wall biogenesis and their interactions in Schizosaccharomyces pombe. *Genes Genet Syst* **73,** 181-91.

Iwaki, T., Iefuji, H., Hiraga, Y., Hosomi, A., Morita, T., Giga-Hama, Y. & Takegawa, K. (2008). Multiple functions of ergosterol in the fission yeast Schizosaccharomyces pombe. *Microbiology* **154,** 830-41.

IWAKI, T., TANAKA, N., TAKAGI, H., GIGA-HAMA, Y. & TAKEGAWA, K. (2004). Characterization of end4+, a gene required for endocytosis in Schizosaccharomyces pombe. *Yeast* **21,** 867-81.

JANSON, M. E., LOUGHLIN, R., LOIODICE, I., FU, C., BRUNNER, D., NEDELEC, F. J. & TRAN, P. T. (2007). Crosslinkers and motors organize dynamic microtubules to form stable bipolar arrays in fission yeast. *Cell* **128,** 357-68.

JANSON, M. E., SETTY, T. G., PAOLETTI, A. & TRAN, P. T. (2005). Efficient formation of bipolar microtubule bundles requires microtubule-bound gamma-tubulin complexes. *J Cell Biol* **169,** 297-308.

KAKSONEN, M., SUN, Y. & DRUBIN, D. G. (2003). A pathway for association of receptors, adaptors, and actin during endocytic internalization. *Cell* **115,** 475-87.

KARSENTI, E., NEDELEC, F. & SURREY, T. (2006). Modelling microtubule patterns. *Nat Cell Biol* **8,** 1204-11.

KATAYAMA, S., HIRATA, D., ARELLANO, M., PEREZ, P. & TODA, T. (1999). Fission yeast alpha-glucan synthase Mok1 requires the actin cytoskeleton to localize the sites of growth and plays an essential role in cell morphogenesis downstream of protein kinase C function. *J Cell Biol* **144,** 1173-86.

KATSUKI, M., DRUMMOND, D. R., OSEI, M. & CROSS, R. A. (2009). Mal3 masks catastrophe events in Schizosaccharomyces pombe microtubules by inhibiting shrinkage and promoting rescue. *J Biol Chem* **284,** 29246-50.

KEENEY, J. B. & BOEKE, J. D. (1994). Efficient targeted integration at leu1-32 and ura4-294 in Schizosaccharomyces pombe. *Genetics* **136,** 849-56.

KELLY, F. D. & NURSE, P. (2011). Spatial control of Cdc42 activation determines cell width in fission yeast. *Mol Biol Cell.*

KIERSZNIOWSKA, S., SEIWERT, B. & SCHULZE, W. X. (2009). Definition of Arabidopsis sterol-rich membrane microdomains by differential treatment with methyl-beta-cyclodextrin and quantitative proteomics. *Mol Cell Proteomics* **8,** 612-23.

KLEBL, F., ZILLIG, M. & SAUER, N. (2000). Transcription of the yeast TNA1 gene is not only regulated by nicotinate but also by p-aminobenzoate. *FEBS Lett* **481,** 86-7.

Klose, C., Ejsing, C. S., Garcia-Saez, A. J., Kaiser, H. J., Sampaio, J. L., Surma, M. A., Shevchenko, A., Schwille, P. & Simons, K. (2010). Yeast lipids can phase-separate into micrometer-scale membrane domains. *J Biol Chem* **285,** 30224-32.

Kopecka, M., Fleet, G. H. & Phaff, H. J. (1995). Ultrastructure of the cell wall of Schizosaccharomyces pombe following treatment with various glucanases. *J Struct Biol* **114,** 140-52.

Krapp, A., Gulli, M. P. & Simanis, V. (2004). SIN and the art of splitting the fission yeast cell. *Curr Biol* **14,** R722-30.

La Carbona, S. & Le Goff, X. (2006). Spatial regulation of cytokinesis by the Kin1 and Pom1 kinases in fission yeast. *Curr Genet* **50,** 377-91.

Ling, M., Merante, F. & Robinson, B. H. (1995). A rapid and reliable DNA preparation method for screening a large number of yeast clones by polymerase chain reaction. *Nucleic Acids Res* **23,** 4924-5.

Lingwood, D., Kaiser, H. J., Levental, I. & Simons, K. (2009). Lipid rafts as functional heterogeneity in cell membranes. *Biochem Soc Trans* **37,** 955-60.

Lingwood, D. & Simons, K. (2010). Lipid rafts as a membrane-organizing principle. *Science* **327,** 46-50.

Llorente, B. & Dujon, B. (2000). Transcriptional regulation of the Saccharomyces cerevisiae DAL5 gene family and identification of the high affinity nicotinic acid permease TNA1 (YGR260w). *FEBS Lett* **475,** 237-41.

Lo Presti, L. & Martin, S. G. (2011). Shaping fission yeast cells by rerouting actin-based transport on microtubules. *Curr Biol* **21,** 2064-9.

Loiodice, I., Staub, J., Setty, T. G., Nguyen, N. P., Paoletti, A. & Tran, P. T. (2005). Ase1p organizes antiparallel microtubule arrays during interphase and mitosis in fission yeast. *Mol Biol Cell* **16,** 1756-68.

Mahadev, R. K., Di Pietro, S. M., Olson, J. M., Piao, H. L., Payne, G. S. & Overduin, M. (2007). Structure of Sla1p homology domain 1 and interaction with the NPFxD endocytic internalization motif. *EMBO J* **26,** 1963-71.

Marcus, S., Polverino, A., Chang, E., Robbins, D., Cobb, M. H. & Wigler, M. H. (1995). Shk1, a homolog of the Saccharomyces cerevisiae Ste20 and

mammalian p65PAK protein kinases, is a component of a Ras/Cdc42 signaling module in the fission yeast Schizosaccharomyces pombe. *Proc Natl Acad Sci U S A* **92,** 6180-4.

MARKS, J., HAGAN, I. M. & HYAMS, J. S. (1986). Growth polarity and cytokinesis in fission yeast: the role of the cytoskeleton. *J Cell Sci Suppl* **5,** 229-41.

MARTIN, S. G. (2009). Microtubule-dependent cell morphogenesis in the fission yeast. *Trends Cell Biol* **19,** 447-54.

MARTIN, S. G. & BERTHELOT-GROSJEAN, M. (2009). Polar gradients of the DYRK-family kinase Pom1 couple cell length with the cell cycle. *Nature* **459,** 852-6.

MARTIN, S. G. & CHANG, F. (2006). Dynamics of the formin for3p in actin cable assembly. *Curr Biol* **16,** 1161-70.

MARTIN, S. G., MCDONALD, W. H., YATES, J. R., 3RD & CHANG, F. (2005). Tea4p links microtubule plus ends with the formin for3p in the establishment of cell polarity. *Dev Cell* **8,** 479-91.

MARTIN, S. G., RINCON, S. A., BASU, R., PEREZ, P. & CHANG, F. (2007). Regulation of the formin for3p by cdc42p and bud6p. *Mol Biol Cell* **18,** 4155-67.

MARTIN, V., GARCIA, B., CARNERO, E., DURAN, A. & SANCHEZ, Y. (2003). Bgs3p, a putative 1,3-beta-glucan synthase subunit, is required for cell wall assembly in Schizosaccharomyces pombe. *Eukaryot Cell* **2,** 159-69.

MARTIN, V., RIBAS, J. C., CARNERO, E., DURAN, A. & SANCHEZ, Y. (2000). bgs2+, a sporulation-specific glucan synthase homologue is required for proper ascospore wall maturation in fission yeast. *Mol Microbiol* **38,** 308-21.

MATA, J. & NURSE, P. (1997). tea1 and the microtubular cytoskeleton are important for generating global spatial order within the fission yeast cell. *Cell* **89,** 939-49.

MATSUYAMA, A., ARAI, R., YASHIRODA, Y., SHIRAI, A., KAMATA, A., SEKIDO, S., KOBAYASHI, Y., HASHIMOTO, A., HAMAMOTO, M., HIRAOKA, Y., HORINOUCHI, S. & YOSHIDA, M. (2006). ORFeome cloning and global analysis of protein localization in the fission yeast Schizosaccharomyces pombe. *Nat Biotechnol* **24,** 841-7.

Maurer, S. P., Fourniol, F. J., Bohner, G., Moores, C. A. & Surrey, T. (2012). EBs recognize a nucleotide-dependent structural cap at growing microtubule ends. *Cell* **149,** 371-82.

Meinhardt, H. & Gierer, A. (2000). Pattern formation by local self-activation and lateral inhibition. *Bioessays* **22,** 753-60.

Mellman, I. & Nelson, W. J. (2008). Coordinated protein sorting, targeting and distribution in polarized cells. *Nat Rev Mol Cell Biol* **9,** 833-45.

Miller, P. J. & Johnson, D. I. (1994). Cdc42p GTPase is involved in controlling polarized cell growth in Schizosaccharomyces pombe. *Mol Cell Biol* **14,** 1075-83.

Mitchison, J. M. (2003). Growth during the cell cycle. *Int Rev Cytol* **226,** 165-258.

Mitchison, J. M. & Nurse, P. (1985). Growth in cell length in the fission yeast Schizosaccharomyces pombe. *J Cell Sci* **75,** 357-76.

Miyata, H., Miyata, M. & Johnson, B. F. (1988). Pseudo-exponential growth in length of the fission yeast, Schizosaccharomyces pombe. *Can J Microbiol* **34,** 1338-43.

Miyata, H., Miyata, M. & Johnson, B. F. (1990). Pattern of end growth of the fission yeast Schizosaccharomyces pombe. *Can J Microbiol* **36,** 390-4.

Mongrand, S., Stanislas, T., Bayer, E. M., Lherminier, J. & Simon-Plas, F. (2010). Membrane rafts in plant cells. *Trends Plant Sci* **15,** 656-63.

Moreno, S., Klar, A. & Nurse, P. (1991). Molecular genetic analysis of fission yeast Schizosaccharomyces pombe. *Methods Enzymol* **194,** 795-823.

Moseley, J. B. & Goode, B. L. (2005). Differential activities and regulation of Saccharomyces cerevisiae formin proteins Bni1 and Bnr1 by Bud6. *J Biol Chem* **280,** 28023-33.

Moseley, J. B., Mayeux, A., Paoletti, A. & Nurse, P. (2009). A spatial gradient coordinates cell size and mitotic entry in fission yeast. *Nature* **459,** 857-60.

Motegi, F., Arai, R. & Mabuchi, I. (2001). Identification of two type V myosins in fission yeast, one of which functions in polarized cell growth and moves rapidly in the cell. *Mol Biol Cell* **12,** 1367-80.

MOURITSEN, O. G. & JORGENSEN, K. (1997). Small-scale lipid-membrane structure: simulation versus experiment. *Curr Opin Struct Biol* **7,** 518-27.

NABESHIMA, K., SAITOH, S. & YANAGIDA, M. (1997). Use of green fluorescent protein for intracellular protein localization in living fission yeast cells. *Methods Enzymol* **283,** 459-71.

NAKANO, K., ARAI, R. & MABUCHI, I. (1997). The small GTP-binding protein Rho1 is a multifunctional protein that regulates actin localization, cell polarity, and septum formation in the fission yeast Schizosaccharomyces pombe. *Genes Cells* **2,** 679-94.

NAKANO, K., IMAI, J., ARAI, R., TOH, E. A., MATSUI, Y. & MABUCHI, I. (2002). The small GTPase Rho3 and the diaphanous/formin For3 function in polarized cell growth in fission yeast. *J Cell Sci* **115,** 4629-39.

NAKANO, K., MUTOH, T. & MABUCHI, I. (2001). Characterization of GTPase-activating proteins for the function of the Rho-family small GTPases in the fission yeast Schizosaccharomyces pombe. *Genes Cells* **6,** 1031-42.

NAKANO, K., TOYA, M., YONEDA, A., ASAMI, Y., YAMASHITA, A., KAMASAWA, N., OSUMI, M. & YAMAMOTO, M. (2011). Pob1 ensures cylindrical cell shape by coupling two distinct rho signaling events during secretory vesicle targeting. *Traffic* **12,** 726-39.

NELSON, W. J. (2003). Adaptation of core mechanisms to generate cell polarity. *Nature* **422,** 766-74.

NI, L. & SNYDER, M. (2001). A genomic study of the bipolar bud site selection pattern in Saccharomyces cerevisiae. *Mol Biol Cell* **12,** 2147-70.

NICCOLI, T., ARELLANO, M. & NURSE, P. (2003). Role of Tea1p, Tea3p and Pom1p in the determination of cell ends in Schizosaccharomyces pombe. *Yeast* **20,** 1349-58.

PADMANABHAN, A., BAKKA, K., SEVUGAN, M., NAQVI, N. I., D'SOUZA, V., TANG, X., MISHRA, M. & BALASUBRAMANIAN, M. K. (2011). IQGAP-related Rng2p organizes cortical nodes and ensures position of cell division in fission yeast. *Curr Biol* **21,** 467-72.

Padte, N. N., Martin, S. G., Howard, M. & Chang, F. (2006). The cell-end factor pom1p inhibits mid1p in specification of the cell division plane in fission yeast. *Curr Biol* **16,** 2480-7.

Paoletti, A. & Chang, F. (2000). Analysis of mid1p, a protein required for placement of the cell division site, reveals a link between the nucleus and the cell surface in fission yeast. *Mol Biol Cell* **11,** 2757-73.

Pardo, M. & Nurse, P. (2003). Equatorial retention of the contractile actin ring by microtubules during cytokinesis. *Science* **300,** 1569-74.

Pelham, R. J., Jr. & Chang, F. (2001). Role of actin polymerization and actin cables in actin-patch movement in Schizosaccharomyces pombe. *Nat Cell Biol* **3,** 235-44.

Perez, P. & Rincon, S. A. (2010). Rho GTPases: regulation of cell polarity and growth in yeasts. *Biochem J* **426,** 243-53.

Petersen, J., Weilguny, D., Egel, R. & Nielsen, O. (1995). Characterization of fus1 of Schizosaccharomyces pombe: a developmentally controlled function needed for conjugation. *Mol Cell Biol* **15,** 3697-707.

Piel, M. & Tran, P. T. (2009). Cell shape and cell division in fission yeast. *Curr Biol* **19,** R823-7.

Prag, S. & Adams, J. C. (2003). Molecular phylogeny of the kelch-repeat superfamily reveals an expansion of BTB/kelch proteins in animals. *BMC Bioinformatics* **4,** 42.

Ray, S., Kume, K., Gupta, S., Ge, W., Balasubramanian, M., Hirata, D. & McCollum, D. (2010). The mitosis-to-interphase transition is coordinated by cross talk between the SIN and MOR pathways in Schizosaccharomyces pombe. *J Cell Biol* **190,** 793-805.

Rincon, S. A., Ye, Y., Villar-Tajadura, M. A., Santos, B., Martin, S. G. & Perez, P. (2009). Pob1 participates in the Cdc42 regulation of fission yeast actin cytoskeleton. *Mol Biol Cell* **20,** 4390-9.

Roque, H., Ward, J. J., Murrells, L., Brunner, D. & Antony, C. (2010). The fission yeast XMAP215 homolog Dis1p is involved in microtubule bundle organization. *PLoS One* **5,** e14201.

RUPES, I., JIA, Z. & YOUNG, P. G. (1999). Ssp1 promotes actin depolymerization and is involved in stress response and new end take-off control in fission yeast. *Mol Biol Cell* **10,** 1495-510.

SANDBLAD, L., BUSCH, K. E., TITTMANN, P., GROSS, H., BRUNNER, D. & HOENGER, A. (2006). The Schizosaccharomyces pombe EB1 homolog Mal3p binds and stabilizes the microtubule lattice seam. *Cell* **127,** 1415-24.

SAWIN, K. E., HAJIBAGHERI, M. A. & NURSE, P. (1999). Mis-specification of cortical identity in a fission yeast PAK mutant. *Curr Biol* **9,** 1335-8.

SAWIN, K. E. & NURSE, P. (1998). Regulation of cell polarity by microtubules in fission yeast. *J Cell Biol* **142,** 457-71.

SAWIN, K. E. & SNAITH, H. A. (2004). Role of microtubules and tea1p in establishment and maintenance of fission yeast cell polarity. *J Cell Sci* **117,** 689-700.

SAWIN, K. E. & TRAN, P. T. (2006). Cytoplasmic microtubule organization in fission yeast. *Yeast* **23,** 1001-14.

SAYERS, L. G., KATAYAMA, S., NAKANO, K., MELLOR, H., MABUCHI, I., TODA, T. & PARKER, P. J. (2000). Rho-dependence of Schizosaccharomyces pombe Pck2. *Genes Cells* **5,** 17-27.

SIEGRIST, S. E. & DOE, C. Q. (2007). Microtubule-induced cortical cell polarity. *Genes Dev* **21,** 483-96.

SIMONS, K. & SAMPAIO, J. L. (2011). Membrane organization and lipid rafts. *Cold Spring Harb Perspect Biol* **3,** a004697.

SIROTKIN, V., BERRO, J., MACMILLAN, K., ZHAO, L. & POLLARD, T. D. (2010). Quantitative analysis of the mechanism of endocytic actin patch assembly and disassembly in fission yeast. *Mol Biol Cell* **21,** 2894-904.

SNAITH, H. A., SAMEJIMA, I. & SAWIN, K. E. (2005). Multistep and multimode cortical anchoring of tea1p at cell tips in fission yeast. *EMBO J* **24,** 3690-9.

SNAITH, H. A. & SAWIN, K. E. (2003). Fission yeast mod5p regulates polarized growth through anchoring of tea1p at cell tips. *Nature* **423,** 647-51.

SNAITH, H. A. & SAWIN, K. E. (2005). Tea for three: control of fission yeast polarity. *Nat Cell Biol* **7,** 450-1.

Snaith, H. A., Thompson, J., Yates, J. R., 3rd & Sawin, K. E. (2011). Characterization of Mug33 reveals complementary roles for actin cable-dependent transport and exocyst regulators in fission yeast exocytosis. *J Cell Sci* **124,** 2187-99.

Snell, V. & Nurse, P. (1994). Genetic analysis of cell morphogenesis in fission yeast--a role for casein kinase II in the establishment of polarized growth. *EMBO J* **13,** 2066-74.

Souto-Padron, T. & de Souza, W. (1983). Freeze-fracture localization of filipin-cholesterol complexes in the plasma membrane of Trypanosoma cruzi. *J Parasitol* **69,** 129-37.

Spector, I., Shochet, N. R., Blasberger, D. & Kashman, Y. (1989). Latrunculins--novel marine macrolides that disrupt microfilament organization and affect cell growth: I. Comparison with cytochalasin D. *Cell Motil Cytoskeleton* **13,** 127-44.

Spector, I., Shochet, N. R., Kashman, Y. & Groweiss, A. (1983). Latrunculins: novel marine toxins that disrupt microfilament organization in cultured cells. *Science* **219,** 493-5.

Takeda, T. & Chang, F. (2005). Role of fission yeast myosin I in organization of sterol-rich membrane domains. *Curr Biol* **15,** 1331-6.

Takeda, T., Kawate, T. & Chang, F. (2004). Organization of a sterol-rich membrane domain by cdc15p during cytokinesis in fission yeast. *Nat Cell Biol* **6,** 1142-4.

Takeo, K. (1985). A correlation between mode of growth and regional ultrastructure of the plasma membrane of Schizosaccharomyces pombe as revealed by freeze-fracturing before and after filipin treatment. *J Gen Microbiol* **131,** 309-16.

Tatebe, H., Nakano, K., Maximo, R. & Shiozaki, K. (2008). Pom1 DYRK regulates localization of the Rga4 GAP to ensure bipolar activation of Cdc42 in fission yeast. *Curr Biol* **18,** 322-30.

Tatebe, H., Shimada, K., Uzawa, S., Morigasaki, S. & Shiozaki, K. (2005). Wsh3/Tea4 is a novel cell-end factor essential for bipolar distribution of Tea1 and protects cell polarity under environmental stress in S. pombe. *Curr Biol* **15,** 1006-15.

TERENNA, C. R., MAKUSHOK, T., VELVE-CASQUILLAS, G., BAIGL, D., CHEN, Y., BORNENS, M., PAOLETTI, A., PIEL, M. & TRAN, P. T. (2008). Physical mechanisms redirecting cell polarity and cell shape in fission yeast. *Curr Biol* **18,** 1748-53.

THERY, M. & BORNENS, M. (2006). Cell shape and cell division. *Curr Opin Cell Biol* **18,** 648-57.

TISCHER, C., BRUNNER, D. & DOGTEROM, M. (2009). Force- and kinesin-8-dependent effects in the spatial regulation of fission yeast microtubule dynamics. *Mol Syst Biol* **5,** 250.

TOLIC-NORRELYKKE, I. M., SACCONI, L., STRINGARI, C., RAABE, I. & PAVONE, F. S. (2005). Nuclear and division-plane positioning revealed by optical micromanipulation. *Curr Biol* **15,** 1212-6.

TOYA, M., MOTEGI, F., NAKANO, K., MABUCHI, I. & YAMAMOTO, M. (2001). Identification and functional analysis of the gene for type I myosin in fission yeast. *Genes Cells* **6,** 187-99.

TRAN, P. T., DOYE, V., CHANG, F. & INOUE, S. (2000). Microtubule-dependent nuclear positioning and nuclear-dependent septum positioning in the fission yeast Schizosaccharomyces [correction of Saccharomyces] pombe. *Biol Bull* **199,** 205-6.

TRAN, P. T., MADDOX, P., CHANG, F. & INOUE, S. (1999). Dynamic confocal imaging of interphase and mitotic microtubules in the fission yeast, S. pombe. *Biol Bull* **197,** 262-3.

TRAN, P. T., MARSH, L., DOYE, V., INOUE, S. & CHANG, F. (2001). A mechanism for nuclear positioning in fission yeast based on microtubule pushing. *J Cell Biol* **153,** 397-411.

TRAN, P. T., PAOLETTI, A. & CHANG, F. (2004). Imaging green fluorescent protein fusions in living fission yeast cells. *Methods* **33,** 220-5.

VEGA, L. R. & SOLOMON, F. (1997). Microtubule function in morphological differentiation: growth zones and growth cones. *Cell* **89,** 825-8.

VENKATESWARLU, K. & KELLY, S. L. (1996). Biochemical characterisation of ketoconazole inhibitory action on Aspergillus fumigatus. *FEMS Immunol Med Microbiol* **16,** 11-20.

Verde, F., Mata, J. & Nurse, P. (1995). Fission yeast cell morphogenesis: identification of new genes and analysis of their role during the cell cycle. *J Cell Biol* **131,** 1529-38.

Verde, F., Wiley, D. J. & Nurse, P. (1998). Fission yeast orb6, a ser/thr protein kinase related to mammalian rho kinase and myotonic dystrophy kinase, is required for maintenance of cell polarity and coordinates cell morphogenesis with the cell cycle. *Proc Natl Acad Sci U S A* **95,** 7526-31.

Wachtler, V. & Balasubramanian, M. K. (2006). Yeast lipid rafts?--an emerging view. *Trends Cell Biol* **16,** 1-4.

Wachtler, V., Rajagopalan, S. & Balasubramanian, M. K. (2003). Sterol-rich plasma membrane domains in the fission yeast Schizosaccharomyces pombe. *J Cell Sci* **116,** 867-74.

Warren, D. T., Andrews, P. D., Gourlay, C. W. & Ayscough, K. R. (2002). Sla1p couples the yeast endocytic machinery to proteins regulating actin dynamics. *J Cell Sci* **115,** 1703-15.

Wedlich-Soldner, R. & Li, R. (2003). Spontaneous cell polarization: undermining determinism. *Nat Cell Biol* **5,** 267-70.

Win, T. Z., Gachet, Y., Mulvihill, D. P., May, K. M. & Hyams, J. S. (2001). Two type V myosins with non-overlapping functions in the fission yeast Schizosaccharomyces pombe: Myo52 is concerned with growth polarity and cytokinesis, Myo51 is a component of the cytokinetic actin ring. *J Cell Sci* **114,** 69-79.

Wolfe, B. A. & Gould, K. L. (2005). Split decisions: coordinating cytokinesis in yeast. *Trends Cell Biol* **15,** 10-8.

Xu, X., Bittman, R., Duportail, G., Heissler, D., Vilcheze, C. & London, E. (2001). Effect of the structure of natural sterols and sphingolipids on the formation of ordered sphingolipid/sterol domains (rafts). Comparison of cholesterol to plant, fungal, and disease-associated sterols and comparison of sphingomyelin, cerebrosides, and ceramide. *J Biol Chem* **276,** 33540-6.

Yanagida, M. (1987). Yeast tubulin genes. *Microbiol Sci* **4,** 115-8.

YONETANI, A. & CHANG, F. (2010). Regulation of cytokinesis by the formin cdc12p. *Curr Biol* **20,** 561-6.

YONETANI, A., LUSTIG, R. J., MOSELEY, J. B., TAKEDA, T., GOODE, B. L. & CHANG, F. (2008). Regulation and targeting of the fission yeast formin cdc12p in cytokinesis. *Mol Biol Cell* **19,** 2208-19.

ZACHARIAS, D. A., VIOLIN, J. D., NEWTON, A. C. & TSIEN, R. Y. (2002). Partitioning of lipid-modified monomeric GFPs into membrane microdomains of live cells. *Science* **296,** 913-6.

ZAITSEVSKAYA-CARTER, T. & COOPER, J. A. (1997). Spm1, a stress-activated MAP kinase that regulates morphogenesis in S.pombe. *EMBO J* **16,** 1318-31.